



UNIVERSITÀ  
DEGLI STUDI  
DI PADOVA

Head Office: Università degli Studi di Padova

Department of Biology

---

Ph.D. COURSE IN: Biosciences

CURRICULUM: Biochemistry and Biotechnologies

SERIES XXXII

## **CALCINEURIN REGULATES PARKIN-TRANSLOCATION TO MITOCHONDRIA AND MITOPHAGY**

The work hereby described was supported by the research grant “Ricerca Finalizzata” (GR-2011-02351151; Italian Ministry of Health)

**Coordinator:** Prof. Ildikò Szabò

**Supervisor:** Prof. Elena Ziviani

**Ph.D. student:** Elena Marchesan

# INDEX

1. SUMMARY .....	3
2. INTRODUCTION .....	6
2.1. PARKINSON'S DISEASE .....	6
2.1.1. CLINICAL CHARACTERISTICS AND THERAPIES .....	6
2.1.2. THE PATHOPHYSIOLOGY OF PARKINSON'S DISEASE .....	8
2.1.3. SPORADIC FORMS OF PARKINSON'S DISEASE .....	9
2.1.4. FAMILIAL FORMS OF PARKINSON'S DISEASE AND THEIR GENETICS .....	10
Dominant genes .....	11
Recessive genes .....	11
2.1.5. PINK1: STRUCTURE AND FUNCTIONS .....	13
2.1.6. PARKIN STRUCTURE AND MECHANISM OF ACTIVATION .....	14
2.2. MITOCHONDRIA: BEYOND THE POWERHOUSE OF THE CELLS .....	18
2.2.1. MITOCHONDRIA STRUCTURE AND PHYSIOLOGY .....	18
Mitochondria dynamics: when shape meets function .....	19
Mitochondrial Calcium homeostasis: sinks or stores? .....	20
2.3. CALCINEURIN: CALCIUM-CALMODULIN PHOSPHATASE .....	22
2.3.1. CALCINEURIN STRUCTURE AND ROLE IN CELLULAR HOMEOSTASIS .....	22
2.3.2. CALCINEURIN ROLE IN NEURODEGENERATION .....	24
2.4. AUTOPHAGY .....	26
2.4.1. MECHANISM OF AUTOPHAGY IN MAMMALIAN .....	26
2.4.2. MITOPHAGY: SELECTIVE REMOVAL OF UNWANTED MITOCHONDRIA .....	28
The PINK1-Parkin pathway .....	31
3. AIM .....	34
4. RESULTS .....	35
5. ABBREVIATIONS .....	67
6. ANNEX .....	70

# 1. SUMMARY

Mitochondria are key organelles within the cellular environment. Beside ATP production these organelles also regulate calcium ( $\text{Ca}^{2+}$ ) homeostasis and programmed cell death<sup>1,2</sup>. Mitochondrial malfunctions can result in the release of reactive species of oxygen (ROS) that damages the cellular components or, more generally, activate pathways that are leading to cell death. It is therefore not surprising that in the course of evolution cells have developed finely regulated mechanisms to control mitochondria number and fitness. This process is made possible by the balanced activity of opposing forces that regulates mitochondria synthesis and mitochondrial degradation via mitochondria quality control. Mitophagy is a highly regulated process that involves the selective degradation of damaged or superfluous mitochondria via Autophagy<sup>3-6</sup>. Alterations in this process are associated with the onset of neurodegenerative diseases such as Alzheimer's (AD) and Parkinson's disease (PD)<sup>7-9</sup>. PD has a slow but progressive evolution. It is clinically characterized by resting tremor, postural instability and bradykinesia (difficulty in starting a muscular movement). At the cellular level, the symptomatology correlates to the loss of dopaminergic neurons of the *substantia nigra pars compacta*, formation of intracellular aggregates known as Levy Bodies, and mitochondria dysfunction. The current lack of a resolving therapy, makes PD one of the most important neurodegenerative diseases, even in the face of advancing life expectancy of the world population<sup>10</sup>. The disease may occur sporadically, for which it is not possible to identify a causal genetic inheritance, or in family form. Family cases have proved to be fundamental as a starting point for research to investigate the molecular mechanisms underlying the disease. In particular, mutations in PINK1 and Parkin genes are associated with early-onset forms, the so-called juvenile Parkinson's disease<sup>11,12</sup>. PINK1 is a Serine-Threonine kinase that is stabilized on the outer mitochondrial membrane of depolarized mitochondria. Parkin is an E3 ubiquitin ligase that translocates to depolarized mitochondria<sup>3,4</sup> to ubiquitinate mitochondrial resident proteins. In a remarkable set of studies, PINK1 and Parkin were found to act within the same signaling pathway that leads to the activation of mitophagy, with PINK1 being upstream of Parkin<sup>4,6,13</sup>. Studies in genetically modified model organisms such as PINK1 and Parkin KO flies (*Drosophila Melanogaster*), mouse and rat have provided key contributions for the dissection of the molecular pathways that leads to the degeneration of the dopaminergic neurons<sup>14-18</sup>. Based on these studies, a promising field of therapeutic application is

represented by the modulation of mitophagy, conducted by acting on proteins such as PINK1 and Parkin.

The work presented in this PhD thesis aims at studying the mechanisms that regulate PINK1-Parkin dependent mitophagy. It was previously found that PINK1 phosphorylates Parkin, an event that is required for Parkin mitochondrial recruitment and mitophagy<sup>3,4</sup>. The resolution of the crystallographic structure of Parkin allowed demonstrating that Parkin undergoes a conformational change as a result of PINK1 phosphorylation, which is required for Parkin translocation and activity<sup>19</sup>. It is well known that post-translational modifications (PTM) such as phosphorylation and dephosphorylation can affect protein conformation, activity and subcellular localization. Thus, we came up with the idea that dephosphorylation events might also contribute to Parkin translocation and regulate mitophagy. We focused on the potential role of Ca<sup>2+</sup>-calmodulin-dependent phosphatase Calcineurin (CaN) for three main reasons: firstly, CCCP treatment (perhaps the most consolidated stimulus to promote Parkin translocation and mitophagy) also promotes CaN activation by generating cytosolic Ca<sup>2+</sup> rise<sup>20</sup>; secondly CaN activation is required for Drp1 translocation to mitochondria to induce mitochondrial fission<sup>21</sup>, which is a fundamental prerequisite for mitophagy to occur<sup>22</sup>; thirdly, CaN can specifically be activated by lysosomal Ca<sup>2+</sup> release to promote the transcription of autophagy genes via TFEB<sup>23</sup>. Previous studies conducted in my laboratory found that Parkin recruitment required Ca<sup>2+</sup>. Intrigued by these findings, it was next tested the effect of CaN on Parkin translocation. In CCCP treated cells, the expression of a dominant form of CaN ( $\Delta$ CnAH151Q) significantly impaired Parkin recruitment to mitochondria. Interestingly, the expression of a constitutively active mutant ( $\Delta$ CnA), which is insensitive to Ca<sup>2+</sup> was sufficient to promote Parkin translocation even in the absence of CCCP intoxication.

Starting from these important findings, and considering the canonical “PINK1-Parkin axis”, I investigated the role of PINK1. PINK1 phosphorylates Parkin to control Parkin translocation and activity. Accordingly, in the absence of PINK1, Parkin translocation is inhibited. Surprisingly, the introduction of constitutive active CaN ( $\Delta$ CnA) was sufficient to promote Parkin translocation in PINK1 KO cells, supporting the hypothesis that CaN promotes Parkin translocation independently of PINK1 expression.

Because Parkin translocation precedes mitophagy, I next investigated the role of CaN in this context. I used different approaches to measure mitophagy namely (i) FACS and confocal analysis

of mitochondria-targeted fluorescent probe mitoKeima<sup>24</sup>, (ii) quantification of mitochondrial mass, estimated by western blotting analysis of matrix protein Cyclophilin D (CypD) and inner mitochondrial membrane protein ATP synthase (ATP5A), (iii) confocal analysis of LC3-decorated mitochondria, and (iv) electron microscopy (EM). The corroboration of these results led us to conclude that CaN is an absolute requirement for stress induced mitophagy. Importantly, expression of constitutive active CaN exacerbated basal mitophagy. This effect was dependent on the expression of Parkin, indicative of a functional interaction between Parkin and CaN in the activation of mitophagy.

Because my previous results showed that constitutive active CaN can induce Parkin translocation under basal conditions (i.e. non-intoxicated cells) and in the absence of PINK1, I investigated whether this was also paralleled by mitophagy induction. Importantly, in PINK1 KO cells constitutive active CaN failed to promote basal mitophagy, despite Parkin was efficiently recruited to mitochondria.

In summary, we identified CaN as a novel key player in the regulation of Parkin translocation, and PINK1/Parkin dependent mitophagy. CaN activation is sufficient to promote Parkin translocation and mitophagy under basal condition, and it appears to be an absolute requirement for stress-induced Parkin recruitment and mitophagy. Under this condition, PINK1 is dispensable for Parkin translocation but not for mitophagy.

## 2. INTRODUCTION

### 2.1. PARKINSON'S DISEASE

Parkinson's disease (PD) is the second most common neurodegenerative disorder after Alzheimer's disease, with a prevalence of approximately 1% at age 65, which rises to nearly 5% by the age of 85<sup>25</sup>. Considering the rising life expectancy within the older population, the prevalence of PD is anticipated to increase dramatically, which leads to increased urgency to identify therapies that delay progression and mitigate disability. At present, there is no cure for PD.

#### 2.1.1. CLINICAL CHARACTERISTICS AND THERAPIES

PD is a movement disorder characterized by resting tremor, bradykinesia (slowed movements), muscular rigidity, postural imbalance, and gait impairment<sup>25</sup>. The onset of symptoms may precede the clinical recognition by many years, due to the insidious nature of the disease. Symptoms are correlated to the degeneration of *substantia nigra pars compacta* (SNpc) dopaminergic neurons. In postmortem brain samples derived from PD patients, there is an evident depigmentation of the midbrain, caused by the loss of dopaminergic cells which contain neuromelanin, a dark pigment structurally related to melanin<sup>26</sup> (Figure 1A). Intracytoplasmic inclusions, termed Lewy bodies (LB), are typically observed in neurons of affected patients. LB look as eosinophilic cytoplasmic proteins aggregates, composed of numerous proteins, including  $\alpha$ -synuclein, ubiquitin, heat shock proteins, neurofilaments and Parkin, and they are found in all affected brain regions<sup>26</sup> (Figure 1B).

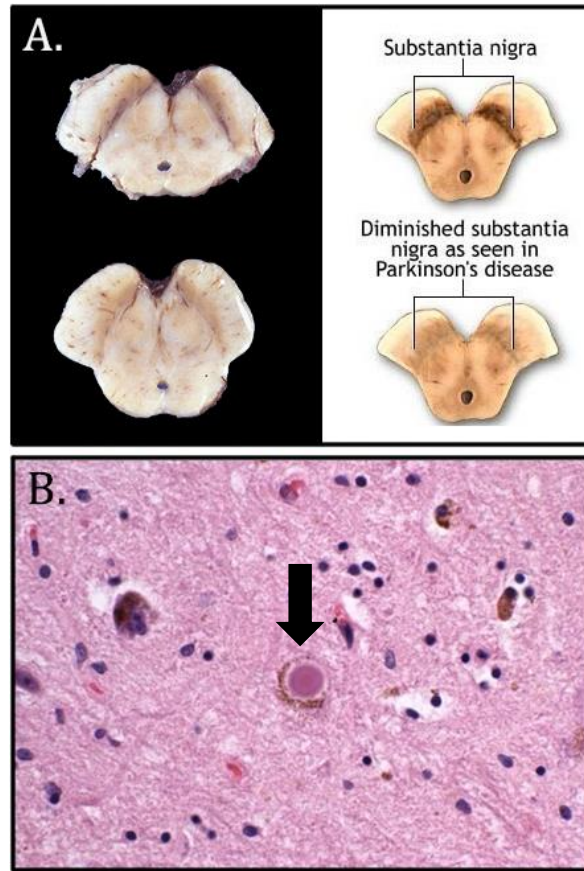


**Figure 1:** (A) Midbrain section showing normal *substantia nigra* (on the top); midbrain section showing loss of pigmented cells of the *substantia nigra* in Parkinson's disease (on the bottom). From: *CNS Pathology* (B) Round eosinophilic inclusions (arrowhead) are Lewy bodies in post-mortem midbrain section of Parkinson's disease patient From: *CNS Pathology*.

PD motor manifestations are the consequence of dopamine (DA) neurons loss within the SNc<sup>27</sup>. DA is an important endogenous catecholamine, which exerts widespread effects both in neuronal (as a neurotransmitter) and non-neuronal tissues (as an autocrine or paracrine agent)<sup>28</sup>. The factors causing specific loss of DA neurons are subject of continuous speculation and experimental studies. An interesting work by the group of Surmeier proposed an unusual reliance of SNc dopaminergic neurons on L-type  $Ca_v1.3$   $Ca^{2+}$  channels to drive their essential pacemaking activity. This reliance increases with age, making SNc dopaminergic neurons more susceptible to stressors inducing  $Ca^{2+}$  rise, as we age. By blocking L-type  $Ca_v1.3$   $Ca^{2+}$  channels, it is possible to induce a homeostatic reversion of SNc dopaminergic neurons to the  $Ca^{2+}$  - independent pacemaking mechanisms, thus, diminishing the vulnerability of SNc dopaminergic neurons<sup>29</sup>.

Motor features remain the essential criteria for a clinical diagnosis of the disease and they represent the major source of disability. The pathologic involvement is not only limited to SNc, but spreads beyond the basal ganglia, a cluster of deep nuclei that participate in the initiation and execution of movements<sup>30</sup>. Thus, as PD progresses, other motor and neurological hallmarks become prominent, such as frequent motor freezing and falls, pain and sensory complaints, autonomic dysfunction (urinary incontinence and orthostatic intolerance), depression, hallucinations, and dementia<sup>31</sup>.

At present the main approach for medical intervention is the control of symptoms for as long as possible while minimizing side effects. Thus, most treatment strategies aim at compensating for the loss of DA by administering L-DOPA, a direct precursor of DA<sup>32,33</sup>. Upon administration of the drug, L-DOPA is converted into DA by the enzyme aromatic L-amino acid decarboxylase (DOPA decarboxylase). However, L-DOPA administration often generates adverse side effects in patients, due to excessive peripheral dopamine signaling<sup>34</sup>. To prevent the peripheral synthesis of dopamine from L-DOPA, the administration of the drug is usually coupled with a peripheral DOPA decarboxylase inhibitor (DDCI) such as carbidopa or benserazide<sup>35</sup>. Other strategies involve the inhibition of dopamine catabolism. These include inhibition of Monoamine Oxidase B (MAO-B) or of Catechol-O-methyl-transferase (COMT)<sup>36</sup>. MAO-B inhibitors can be used as treatment during the early stages of the disease. It prevents DA conversion into DOPAC (3,4-Dihydroxyphenyl acetic acid), so DA concentration increases. Conversely, COMT inhibitors (Entacapone) are given together with L-DOPA to treat severe stages of the disease<sup>36</sup>. COMT reduces DA levels by methylating DA to 3-Methoxytyramine, and it also acts in the peripheric region of the brain, thus preventing excessive L-DOPA concentrations peripherally. In some other more severe cases, tremor is treated with anticholinergics<sup>33</sup>. Although the currently available PD therapies delay disability and prolong life expectancy, none of them has been proved to significantly stop the ongoing neurodegenerative process and, at present there is no cure for PD.

### 2.1.2. THE PATHOPHYSIOLOGY OF PARKINSON'S DISEASE

The selective loss of DA neurons in *substantia nigra* is the basis of PD's pathophysiology. Over the years, several mechanisms were proposed for neuronal death, including changes in



mitochondria homeostasis and protein aggregation in Lewy bodies. Mitochondrial dysfunction is associated with oxidative stress, which contributes to the onset of PD. Another hypothesis suggests misfolding and aggregation of proteins as the primary cause<sup>37</sup>. The two theories are not mutually exclusive, rather they should be considered interconnected. The first of the two hypothesis is based on the evidence that chemical inhibition of mitochondrial Complex I in the electron transport chain reproduces parkinsonism, including selective dopaminergic neuron loss<sup>38</sup>. A line of evidence for mitochondrial dysfunction related to oxidative stress and dopaminergic cell damage also comes from the findings that genes which mutations that are linked to familiar forms of PD, like Parkin, DJ-1, and PINK, encode for proteins that have mitochondria-related functions<sup>11,12,39</sup>. Cells derived from patients with mutations in these genes exhibit increased oxidative stress<sup>40</sup>, impaired activity of Complex I<sup>41,42</sup>, and mitochondrial dysfunction<sup>43</sup> (see the next paragraph for more details).

The presence of intracellular protein aggregation, due to their polymerization and altered conformation, is another hallmark of PD pathology.  $\alpha$ -synuclein is the most known protein to form aggregates in PD brain patients, contributing to the Lewy bodies formation<sup>44</sup>. The abnormal or misfolded proteins are normally targeted via ubiquitination to the proteasome, where they are degraded. Thus, dysfunction of the Ubiquitin Proteasome System (UPS) could also be responsible for the accumulation of cytosolic damaged proteins, and could be important for the formation of Lewy bodies.

Thus, both mitochondrial damage and protein aggregation need to be taken into account for a complete understanding of PD etiology.

### 2.1.3. SPORADIC FORMS OF PARKINSON'S DISEASE

PD has historically been considered a multifactorial disorder, in which environmental factors played a dominant etiologic role. Eighty five percent of PD cases are sporadic, and the exact cause for the disease onset is unknown<sup>45</sup>. MPTP (1-methyl-4-phenyl-1,2,3,6-tetrahydropyridine) reproduces pathological features of idiopathic Parkinsonism by targeting the nigrostriatal system<sup>46</sup>. MPTP is transported through the blood-brain barrier (BBB) by the plasma membrane dopamine transporter (DAT) and once it crosses the BBB, MPTP is

metabolically activated to the fully oxidized by MAO-B 1-methyl-4-phenylpyridinium species (MPP+) which is then taken up into dopaminergic neurons via DAT<sup>47</sup>. MPP+ induces neurotoxicity by blocking mitochondrial respiratory complex I activity, decreasing ATP production, and increasing ROS generation<sup>48</sup>. MPP+ is structurally similar to Paraquat (PQ), an herbicide, which decreases the dopamine concentration and induces behavioral changes similar to those induced by MPP+ injections<sup>49</sup>. In experimental models, PQ has also been linked to the production of reactive oxygen species (ROS), oxidative stress, and aggregation of  $\alpha$ -synucleins (similarly to Lewy's bodies) in dopaminergic neurons<sup>50</sup>. Another herbicide that exerts preferential cytotoxicity to dopaminergic neurons is complex I inhibitor rotenone. Rotenone is a highly lipophilic pesticide that easily crosses the blood brain barrier (BBB), and for cellular entry, it does not depend on the DAT<sup>47</sup>. Rotenone also blocks proteasome activity and dysfunction in proteasomes has been implicated in the pathogenesis of both genetic and sporadic forms of PD<sup>51</sup>. Interestingly, reduced Complex I activity has been found in tissues from patients with PD and a clear evidence of oxidative stress in postmortem PD brains was also observed<sup>26</sup>. These findings provided evidence that oxidative stress caused by mitochondrial dysfunction, and specifically complex I impairment, might be implicated in the pathophysiology of PD.

#### 2.1.4. FAMILIAL FORMS OF PARKINSON'S DISEASE AND THEIR GENETICS

Although the vast majority of PD cases are sporadic, a small proportion is genetically linked, and shows early manifestation<sup>12,52-54</sup>. These familiar forms, caused by a single mutation in a dominantly or recessively inherited gene, are relatively rare types of PD, representing 5-10% of PD cases<sup>53</sup>. The first gene that was identified to be associated to familiar onset is SNCA encoding for the protein  $\alpha$ -synuclein, a major component of Lewy Bodies. Up to now, six genes (SNCA, LRRK2, Parkin, DJ-1, PINK1, and ATP13A2) have conclusively been shown to cause familial Parkinsonism<sup>11,12,55-58</sup>. Genetic cases of PD are phenotypically identical to sporadic cases, therefore, the development of mutant model organisms for these genes has made a fundamental contribution to the investigation of the molecular mechanisms underlying the pathophysiology of PD and to the development of new therapeutic strategies.

### *Dominant genes*

The discovery of pathogenic missense mutations in the gene *SNCA*, or *PARK1/4*, identified the first PD related gene. *SNCA* encodes for  $\alpha$ -synuclein, a cytosolic protein that is expressed throughout the brain and has potential roles in learning, synaptic plasticity, vesicle dynamics and dopamine synthesis<sup>59</sup>. Only three different missense mutations (A53T, A30P and E46K) have been reported, although also genomic multiplications of the entire genes have been found. These mutations are causative of autosomal-dominant PD<sup>60</sup>.

Alpha-synuclein consists of three domains: an N-terminal region, a central hydrophobic one, and a negatively charged carboxy-terminal region. Due to its hydrophobic central domain, this protein has naturally a high propensity to aggregate that is accentuated in mutants. The mutated proteins tend to form stable  $\beta$ -sheet structures, thus exacerbating the formation of toxic oligomers, protofibrils, and fibrils<sup>61</sup>. Patients with *SNCA* mutations usually have early-onset of PD, before the age of 40<sup>62</sup>.

Mutations in the leucine-rich repeat kinase 2 (*LRRK2*) gene are the most frequent known cause of late-onset autosomal dominant and sporadic PD. The *LRRK2* G2019S mutation leads to the most frequent substitution in Caucasians, which typically accounts for 0.5–2.0% of sporadic PD cases and 5% of familial parkinsonism<sup>63</sup>. *LRRK2*, or *PARK8*, is a large gene that encodes for the cytoplasmic protein LRRK2, which is made of 2,527 amino acids. It consists of a leucine-rich repeat toward the amino terminus of the protein and a kinase domain toward the carboxyl terminus with various conserved domains in between<sup>64</sup>. Among the 50 different missense and nonsense mutations reported in *LRRK2*, at least 16 of them seem to be pathogenic. *LRRK2* is reported to interact with Parkin, suggesting that it should be involved in a pathogenic pathway with other PD-related proteins<sup>65</sup>.

### *Recessive genes*

Recessive forms of parkinsonism are known to be caused by mutations in Parkin (*PARK2*), PINK1 (*PARK6*) and DJ-1 (*PARK7*) genes. These are all relatively rare, loss-of-function mutations that result in an early age onset and slow disease progression.

Parkin mutations are the most common known cause of early onset of PD, accounting for up to 77% of the familial cases with an age of onset <30 years<sup>63</sup>. More than 40 mutations have been identified, but only a weak correlation between clinical manifestation and type of mutation has been pointed out. The role of these mutations in PD is still controversial (see next paragraphs for more details).

Mutations in the phosphatase and tensin homolog (PTEN)-induced putative kinase 1 (PINK1) gene are the second most common cause of autosomal recessive early onset PD. Two thirds of the reported mutations in PINK1 are loss-of-function mutations affecting the kinase domain, suggesting the importance of PINK1's enzymatic activity in the pathogenesis of PD<sup>63</sup> (see next paragraphs for more details).

DJ-1 is the third gene associated with autosomal recessive PD, and it is mutated in about 1%–2% of early onset PD cases<sup>52</sup>. DJ-1 is a mitochondrially enriched, redox-sensitive protein and an atypical peroxiredoxin-like peroxidase that scavenges H<sub>2</sub>O<sub>2</sub><sup>66</sup>. The normal function of DJ-1 and its role in dopamine cell degeneration is unknown, but this protein is linked to oxidative stress response and mitochondrial function. It is a member of the ThiJ/PfpI family of molecular chaperones, which expression is induced upon oxidative stress<sup>66</sup>. In humans, clinically unaffected DJ1 mutation carriers seem to be unaffected in brain neuroimaging studies, indicating that a complete loss of protein function is required for the disease to develop<sup>10</sup>.

Parkin, PINK1 and DJ-1 are linked to mitochondria homeostasis and have a protecting role in case of mitochondrial dysfunction and oxidative stress. Cells derived from patients with mutations in the *parkin* and *PINK1* gene show decreased mitochondrial respiratory Complex I activity<sup>41,67</sup>. Mutations in *PINK1* induce mitochondrial dysfunction, including excess free radical formation. *DJ-1* KO mice accumulate ROS and exhibit fragmented mitochondria<sup>29</sup>. These evidences further highlight the importance of mitochondria physiology in the pathological onset of PD.

In the next paragraphs we provide a detailed description of PD related protein PINK1 and Parkin, and their specific role in mitochondria activity and fitness.

## 2.1.5. PINK1: STRUCTURE AND FUNCTIONS

PINK1 (PTEN Induced Putative Kinase 1) is a serine-threonine kinase codified by *PARK6* gene<sup>12</sup>. Mutations in PINK1 gene are the second most frequent cause of autosomal recessive, young-onset PD, after Parkin mutations. They account for 1–8% of the early onset autosomal recessive PD cases<sup>68</sup>. PINK1 contains an N-terminal mitochondrial targeting sequence (MTS), a transmembrane helix, a serine/threonine kinase domain, and a C-terminal domain of unknown function<sup>69</sup>. Endogenous PINK1 is found at low levels in cells as a result of its high turnover rate. Full-length PINK1 (64 kDa) is ubiquitously expressed and is localized to the outer mitochondrial membrane. PINK1 is constitutively imported into mitochondria, and cleaved<sup>70</sup>. PINK1 processing is linked to mitochondrial function: in healthy mitochondria, the translocase complexes of the outer (OMM) and inner mitochondrial membrane (IMM) import the full-length PINK1. This step is associated with cleavage of the MTS sequence by the mitochondrial processing peptidase (MPP), to give rise to a ~60-kDa form<sup>71,72</sup>. This MPP-cleaved form of PINK1 is further processed by the rhomboid protease of the IMM, PARL (presenilin associated rhomboid-like protease), to generate the 52-kDa form, which is exported to the cytosol and rapidly degraded. When mitochondria are depolarized, PINK1 fails to be imported, and the full-length rapidly accumulates on the mitochondria surface. From this new location, PINK1 selectively recruits the E3 ubiquitin ligase Parkin to promote mitochondrial degradation<sup>71</sup> as described in details in the next paragraphs.

Studies in *Drosophila* demonstrated the fundamental genetic interaction between PINK1 and Parkin, and allowed dissecting the molecular pathway that links PINK1 to Parkin activation, with PINK1 upstream Parkin<sup>4,6</sup>. Further studies proved that Parkin activation by PINK1 is a two-step process consisting of phosphorylation of Parkin at Ser 65, and Ubiquitin<sup>73-76</sup>. Both events are required to release the autoinhibitory state of Parkin, and prime Parkin targets for Parkin dependent ubiquitination.

PINK1 also regulates mitochondrial morphology by promoting Drp1-dependent mitochondrial fragmentation<sup>19,77</sup>. Upon mitochondrial damage, PINK1 inhibits protein kinase A (PKA) mediated-phosphorylation, thus preventing PKA repressive activity on pro mitochondrial fission protein Drp1<sup>78,79</sup>. In this condition, PINK1 promotes mitochondrial fragmentation, which

is a fundamental prerequisite for mitochondrial degradation<sup>22</sup>. In addition, PINK1 regulates mitochondrial trafficking by phospho-priming protein Miro for Parkin-dependent degradation to block mitochondrial movement along the microtubules<sup>80</sup>.

At the physiological level, PINK1 deficiency leads to an altered mitochondrial Ca<sup>2+</sup> buffering capacity and impaired respiration caused by a reduced provision of electron transport chain substrates<sup>81</sup>. PINK1 impairment also results in complex I and complex IV activity loss, decrease ATP production, dysfunctional mitochondrial import and alteration in mtDNA levels<sup>82,83</sup>, leading to altered mitochondria ultrastructure, increased ROS levels and increased susceptibility to apoptotic stimuli<sup>41</sup>.

Many of the mitochondrial functions carried by PINK1 depend on its kinase activity, which has been the focus of several studies. Not surprisingly, most of the PD linked mutations are found in the kinase domain. Interestingly, in PINK1 knock-out mouse embryonic fibroblasts (MEFs) a kinase-dead mutant of PINK1 cannot rescue Parkin mitochondrial recruitment <sup>81</sup>, suggesting that the protective effect of PINK1 operates via Parkin mitochondrial recruitment.

### 2.1.6. PARKIN STRUCTURE AND MECHANISM OF ACTIVATION

The gene encoding the E3 ubiquitin ligase Parkin (*PARK2*) was originally identified as a causative gene for familial early-onset Parkinsonism<sup>11</sup>. Parkin mutations are the most common genetic cause of autosomal recessive PD; mutations in Parkin are identified in about 50% of cases with autosomal recessive early-onset parkinsonism<sup>84</sup>, including single nucleotide changes, deletion and duplications. Ubiquitination is a post-translational modification that typically marks proteins for degradation through the covalent attachment of ubiquitin single molecule (monoubiquitination) or ubiquitin chains (polyubiquitination) to lysine residues or the N-terminal amino group of a substrate protein. The reaction is carried out by the sequential activity of three enzymes, E1 ubiquitin-activating enzymes, E2 ubiquitin-conjugating enzymes and E3 ubiquitin ligases (like Parkin). E1 first uses ATP to activate ubiquitin for conjugation by forming a thioester between its catalytic cysteine and the C-terminal carboxyl group of ubiquitin. The ubiquitin molecule is then passed to the second enzyme of the complex, E2 (ubiquitin-conjugating enzyme), before reaching the final enzyme, E3, the ubiquitin-protein ligase, which binds the target substrate and labels it with the ubiquitin. Following addition of a single ubiquitin

to the target protein, further ubiquitin molecules can be added to the first ubiquitin via lysine (Lys) residue linkage, leading to the formation of a chain of ubiquitins. Because ubiquitin contains several Lys residues, different ubiquitin chains can be formed, some of which (like Lys48 and Lys63) are more common than others<sup>85</sup>. The type of ubiquitin chain that is formed affects the physiological outcome, which can lead to proteasome dependent degradation (typical of Lys48 type-chain) or non-degradative “functional” ubiquitination (Lys63 or Lys11 types-chain are typically signaling functional ubiquitination). Lys48 types-chains were the first identified and are the best-characterized type of ubiquitin chains. At least four ubiquitin molecules are attached to the target protein to be rapidly degraded by the 26S proteasome<sup>86</sup>. In contrast Lys63 types-chains are not associated with proteasomal degradation of the substrate protein<sup>87</sup>. Lys63-linked chains act as signals in intracellular trafficking, DNA repair, and inflammation<sup>88</sup>. Interestingly, E3 ubiquitin ligase Parkin can both mediate degradative as well as functional (non-degradative) ubiquitination, and controls a variety of cellular processes by ubiquitinating several substrates located both in the cytoplasm and on the OMM upon mitochondrial depolarization<sup>4,6,13,89,90</sup>. Not surprisingly, Parkin exists in an autoinhibited state, which structure is well conserved from nematodes to humans. Full-length PARK2 consists of five distinct domains: UBL, RING0, RING1, in-between-RING (IBR) domain, and RING2<sup>19</sup> (Figure 2).

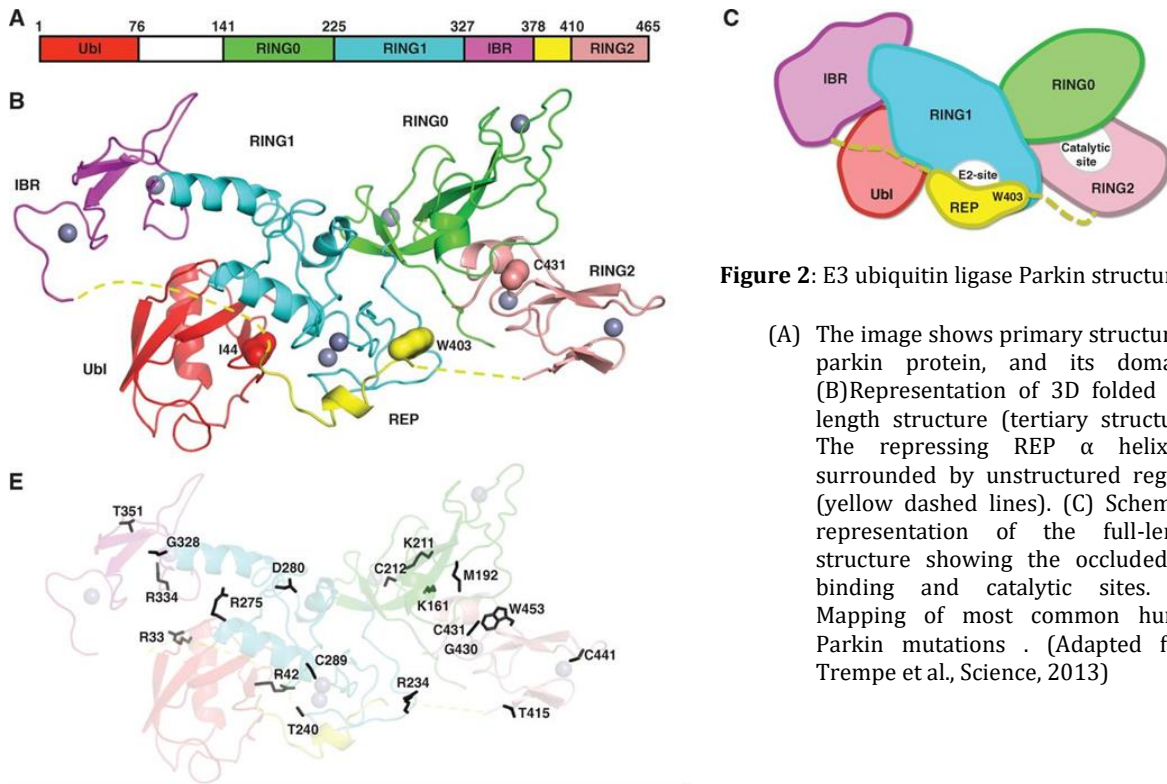


**Figure 2:** E3 ubiquitin ligase Parkin structure.

- (A) The image shows primary structure of parkin protein, and its domains. (B) Representation of 3D folded full-length structure (tertiary structure). The repressing REP  $\alpha$  helix is surrounded by unstructured regions (yellow dashed lines). (C) Schematic representation of the full-length structure showing the occluded E2 binding and catalytic sites. (E) Mapping of most common human Parkin mutations. (Adapted from Trempe et al., Science, 2013)

Parkin forms a rigid core between the RINGs domains stabilized by several key hydrophobic interactions, and it is basically auto-inhibited under normal conditions. The interconnected RINGs domains provide the scaffold for the interaction with the other domains<sup>19</sup>. The N-terminal Ubl domain is bound to RING1 and its dissociation is required to bind its interacting molecular partners (as the ubiquitin-interacting motif of ubiquitin ligases). Recent studies provided a structural understanding of the mechanisms of Parkin autoinhibition, and how this is released upon stimuli. RING0 represents the first structural inhibitory element since it covers the ubiquitin acceptor site Cys431 in RING2, whereas a repressor element of Parkin (REP) binds RING1 and blocks its E2-binding site<sup>19</sup>. REP is a flexible two-turn helix linker between the IBR and RING2. In such conformation, Parkin is inactive and auto-inhibited. In ubiquitin ligases the auto-inhibitory conformation is biologically meaningful since it limits the autoubiquitination and subsequent proteasomal degradation, thus keeping them in an inactive state until their activation is required. Because the active site cysteines of E2 and RING2 domain are separated over a distance of about 50 Å, Parkin has to undergo conformational rearrangements to allow ubiquitin transfer<sup>19</sup>. In a remarkable set of studies<sup>89,91,92</sup> it was found that PINK1 mediated-phosphorylation on Parkin UBL domain Ser65 and on ubiquitin at the same residue allows a conformational change that is instrumental for Parkin translocation and



activation. In details, once phosphoUb binds on RING1 domain, the resulting conformational changes release the UBL domain from the Parkin core, unraveling the auto-inhibited Parkin conformation. PhosphoUb binding also destabilizes the REP and RING2 auto-inhibitory interactions, enables RING1 to bind and discharge E2-Ub conjugates. PhosphoUb-binding site is important for Parkin translocation since phosphoUb-deficient Parkin mutants do not translocate to mitochondrial<sup>93</sup>. Once activated, Parkin ubiquitinates numerous mitochondrial and cytosolic proteins, which in turn recruit other proteins to mitochondria to initiate mitochondrial degradation. Several Parkin OMM substrates have been identified, including pro-mitochondrial fusion proteins MFN1, MFN2 and OMM channel VDAC<sup>4,6,13</sup>. Moreover, the translocase of the OMM (TOM) complex (TOM70, TOM40, and TOM20), the pro-apoptotic factor BAK, MIRO1 and MIRO2 are Parkin targets<sup>94-96</sup>. Accumulating evidence suggests that Parkin also affects cellular physiology through additional, not mitophagy-related processes<sup>97,98</sup>. To ensure sufficient energy production, mitochondria turnover must be strictly regulated, thus mitochondria degradation is coupled with mitochondria biogenesis. Indeed, Parkin is involved also in the regulation of this latter process. Parkin adds ubiquitin chains to target Parkin-interacting substrate (PARIS) for degradation by the proteasome<sup>97</sup>. PARIS is a KRAB and zinc finger protein that accumulates in models of Parkin inactivation and in human PD brains<sup>97</sup>. PARIS is the major transcriptional repressor of mitochondrial biogenesis regulator peroxisome proliferator-activated receptor gamma coactivator 1 $\alpha$  (PGC-1) $\alpha$ . As a result of Parkin-mediated PARIS degradation, mitochondrial biogenesis occurs.

Interestingly, Parkin loss-of-function mutations can impinge of its “degradative” ubiquitinase activity, leading to deleterious accumulation of Parkin substrates, including entire organelles as mitochondria, and neurotoxicity<sup>99</sup>, but also compromise its non-degradative signaling ubiquitination, which can be associated with degeneration of dopaminergic neurons<sup>100</sup>.

Thus, accumulating evidence indicates that PD-associated genes directly or indirectly impinge on mitochondrial integrity, providing a link to pathophysiological alterations observed both in sporadic and familial PD<sup>101</sup>. Mitochondrial dysfunction has indeed been reported in various non-dopaminergic cells and tissue samples from human patients as well as transgenic mouse and fruit fly models of PD<sup>14,17,41,76</sup>. Thus, mitochondria represent a highly promising target for therapeutic intervention.

## 2.2. MITOCHONDRIA

All biological systems require energy for their life and sustainment. Mitochondria are the primary energy convertors of eukaryotic cells. Mitochondria function also extends to the regulation of calcium homeostasis, reactive oxygen species scavenging, cellular differentiation and, cell death, as well as controlling cell cycle and cell growth.

### 2.2.1. MITOCHONDRIA STRUCTURE AND PHYSIOLOGY

Mitochondria are double-wrapped ubiquitous organelles, which are central players within the cell environment. Their structure consists of an inner mitochondrial membrane (IMM) and an outer mitochondrial membrane (OMM), separated by an intermembrane space (IMS). The IMM subsists in two distinct regions, the inner boundary membrane (IBM) and the cristae membrane (CM). The CM forms invaginations of the IBM that protrude into the matrix space. The IMS together with the central electron-dense space, the matrix, are the two soluble components of the mitochondria<sup>102</sup>. The numerous invaginations of the IMM provide a remarkable increase of the surface area of this membrane compared to the OMM, with noteworthy functional importance since the complexes of the respiratory chain are placed within the cristae. The IBM and the CM are connected by tubular structures, termed cristae junctions (CJs)<sup>103</sup>. Ions and most of the metabolites can freely pass the OMM through porins, proteins acting as non-specific pores for small molecules. Due to the presence of porins in the OMM, the molecular content of the IMS is similar to that of the cytoplasm<sup>104</sup>. The IMM is impermeable to most ions and small molecules, thus maintaining the proton gradient between the two soluble compartments of mitochondria. The maintenance of the proton gradient is fundamental for the functioning of the respiratory chain and the subsequent conversion of ATP from ADP+P<sub>i</sub> performed by the complex of ATP synthase, a process known as oxidative phosphorylation. By virtue of their ancestral bacterial origin from a bacterium, mitochondria have their own DNA<sup>105</sup>, mitochondrial DNA (mtDNA). mtDNA is a circular double-stranded molecule consists of a heavy (H) and a light (L) chain,

without any histone coat. mtDNA encodes for 13 proteins of the oxidative phosphorylation system (OXPHOS), and the remaining subunits are encoded by the nuclear DNA.

Beyond ATP production, oxidative phosphorylation can lead to reactive oxygen species (ROS) generation<sup>106</sup>. Overproduction of ROS can damage biomolecules being detrimental for cellular homeostasis, ultimately triggering cell death. This event can be particularly critical for not dividing cells as neurons. Indeed, oxidative stress is tightly correlated with the etiology of neurodegenerative diseases like Parkinson's disease<sup>107,108</sup>.

### *Mitochondria dynamics: when shape meets function*

Mitochondria form a highly interconnected tubular network throughout the cell, and they can regulate their shape and size via two interlinked processes: mitochondrial fusion and fission. Mitochondrial network structure is tightly regulated by the balance between fusion and fission events, thus disequilibrium in these processes causes remarkable morphological changes in the organelle and can affect mitochondria function.

The discovery of a link between human diseases and mutations in fission and fusion proteins highlighted the biological relevance of mitochondrial dynamics<sup>105</sup>.

The main proteins composing the core machinery are large GTPase belonging to the Dynamin family. These mechanoenzymes can oligomerize and undergo conformational changes to drive membrane remodeling, constriction, scission and/or fusion<sup>109</sup>. The major player in mitochondrial fission is dynamin-related protein 1 (Drp1). Drp1 structure is composed of four domains: N-terminal GTP-binding, middle assembly domain, insert B, and C-terminal GTPase effector (GED) domains<sup>110</sup>. Drp1 forms a helical oligomer in a GTP-dependent manner through intramolecular and intermolecular interactions of its domains. Drp1 activity is Ca<sup>2+</sup>-regulated through its phosphorylation and dephosphorylation, by OMM-associated kinase PKA/AKAP1, and phosphatase PP2A/B $\beta$ <sup>278</sup>. In this work, phosphorylation of Drp1 at Ser656 causes mitochondria elongation, while its dephosphorylation induces mitochondrial fragmentation and depolarization<sup>78</sup>. In a different study, Drp1 was found to be dephosphorylated at Ser637 by Ca<sup>2+</sup>-dependent phosphatases Calcineurin (CaN). In this work mitochondrial depolarization associated with sustained cytosolic Ca<sup>2+</sup> rise activates CaN that dephosphorylates Drp1 to promote fragmentation of depolarized mitochondria<sup>21</sup>.

Additional OMM proteins are required for mitochondrial fission, like mitochondrial fission factor (Mff) and mitochondrial fission protein 1 (Fis1). However, it is unclear how these proteins influence the location of the fission points on mitochondria. Nevertheless, both Mff and Fis1 have been found to modulate the number and the size of Drp1 puncta at the OMM, thus modulating the numbers of putative mitochondrial fission points.

The counterpart of mitochondrial fission is the fusion process. Three large GTPases are essential for the fusion of mammalian mitochondria: Optic Atrophy 1 (OPA1), Mitofusin 1 (MFN1) and 2 (MFN2). OPA1 is a large dynamin-like GTPase protein residing on the IMM, responsible for the fusion of the IMM. Besides its function in the regulation of mitochondrial fusion, OPA1 is also involved in the maintenance of the respiratory chain complexes and mitochondrial membrane potential, cristae ultrastructure and control of apoptosis, as well as mtDNA<sup>111-114</sup>. OPA1 activity is regulated by its proteolytic processing at two cleavage sites, S1 and S2. Proteolytic processing of OPA1 results in the loss of the transmembrane domain of long OPA1 form (L-OPA1) and leads to the formation of short OPA1 forms (S-OPA1). L-OPA1 and S-OPA1 assemble into oligomeric complexes regulating cristae structure and in turn cytochrome c release from the intracristal space<sup>115,116</sup>. The two large GTPases homologs Mitofusin 1 (MFN1) and Mitofusin 2 (MFN2) mediate OMM fusion. The GTPase domain is located in the N-terminal, and it is followed by a hydrophobic heptad repeat region (HR1). At the C-terminal region of the protein, there is a second hydrophobic heptad repeat region, HR2<sup>117</sup>. These two hydrophobic regions play important roles in the fusion reaction<sup>118</sup>. Both MFNs are required for mitochondrial fusion<sup>119</sup> and form homo- and hetero-dimers that undergo conformational rearrangements upon GTP hydrolysis to promote OMM fusion. However, MFN1 tethers mitochondrial membranes with higher efficiency than MFN2. Interestingly, MFN2 is also expressed on the ER, and it is enriched in mitochondrial-associated membranes (MAMs) such as endoplasmic reticulum (ER)-contacts sites to promote physical and functional ER-mitochondria interaction<sup>120</sup>.

Mitochondrial shape is intimately related to mitochondria function, and thus it is not surprising how perturbations in mitochondria dynamic has been associated with several human pathologies, including neurodegenerative disorders such as Parkinson's disease (PD).

#### *Mitochondrial Calcium homeostasis: sinks or stores?*

Steady-state Calcium ( $\text{Ca}^{2+}$ ) levels are kept low in the cytoplasm<sup>121</sup>. Mitochondria

participate in the control of  $\text{Ca}^{2+}$  homeostasis, and are capable of transducing  $\text{Ca}^{2+}$  signals, acting as a spatial  $\text{Ca}^{2+}$  buffer. An impaired mitochondrial  $\text{Ca}^{2+}$  uptake can modify the spatiotemporal cytoplasmic  $\text{Ca}^{2+}$  signaling, thus affecting  $\text{Ca}^{2+}$  related processes such as gene transcription, muscular contraction, cell proliferation and cell death<sup>122</sup>. In parallel, slow release of  $\text{Ca}^{2+}$  from mitochondria, particularly in neuronal cells<sup>123</sup>, is also physiologically important and can activate specific  $\text{Ca}^{2+}$ -dependent signaling pathways that in turns might affect mitochondrial activity and turn over in a feed forward loop<sup>124</sup>.

Mitochondrial  $\text{Ca}^{2+}$  uptake predominantly derives from release from IP3 channels located in the ER and plasmatic membranes channels, and it is controlled by voltage-dependent anion channel (VDAC) at the OMM, while the passage through the IMM is regulated by the mitochondrial  $\text{Ca}^{2+}$  uniporter (MCU). MCU is activated by  $\text{Ca}^{2+}$  concentrations higher than 200 nM, which are usually settled within cytosolic  $\text{Ca}^{2+}$  microdomains<sup>125</sup>. These  $\text{Ca}^{2+}$  “hot spot” domains are generated at the MAMs, sites of physical and functional interaction between mitochondria and ER. High  $\text{Ca}^{2+}$  domains that are forming at the MAMs allow the transfer of  $\text{Ca}^{2+}$  across the IMM, through the MCU, which has low affinity for  $\text{Ca}^{2+}$ . The influx of  $\text{Ca}^{2+}$  into the matrix by this route is dependent on the electrochemical potential gradient for  $\text{Ca}^{2+}$ <sup>125,126</sup>, which is maintained through mitochondrial  $\text{Na}^+$ - $\text{Ca}^{2+}$  exchanger (mNCX) and  $\text{Na}^+$ -independent  $\text{Ca}^{2+}$  efflux<sup>125</sup>. This electrochemical gradient is essential for ATP synthesis, therefore  $\text{Ca}^{2+}$  influx from the cytosol controls the rate of mitochondrial energy production<sup>127</sup>. In addition,  $\text{Ca}^{2+}$  concentration regulates the dehydrogenases of the TCA cycle (i.e. pyruvate dehydrogenase, isocitrate dehydrogenase, and  $\alpha$ -ketoglutarate dehydrogenase), and these rate-limiting enzymes are all upregulated by  $\text{Ca}^{2+}$  and  $\text{Ca}^{2+}$ -dependent processes<sup>125</sup>.

Too high  $\text{Ca}^{2+}$  concentration in the matrix, however, leads to Cyclophilin D (CypD) activation to induce the opening of the mitochondrial permeability pore (MPTP), which in turn triggers mitochondrial swelling and OMM rupture, with the consequent release of caspase-activating factors and apoptosis induction<sup>128</sup>. Moreover, cytochrome c residing in the IMS is released in the cytosol where it can bind to the inositol 1,4,5-trisphosphate receptor (IP3R) on the ER surface, thus exacerbating its  $\text{Ca}^{2+}$  leak properties. This event can amplify caspase activation and therefore apoptosis stimulation<sup>128</sup>.

Although mitochondria require  $\text{Ca}^{2+}$  for proper functioning, too high mitochondrial  $\text{Ca}^{2+}$  concentration can be detrimental, and promotes cell death. Therefore mitochondria  $\text{Ca}^{2+}$ -handling

capacity can impinge on cell fate, leading to apoptosis or activating specific  $\text{Ca}^{2+}$  dependent pathways that nevertheless could impinge on mitochondria fitness and turnover. In parallel, the accumulation of  $\text{Ca}^{2+}$  inside organelles, including mitochondria, can determine the generation of cytosolic  $\text{Ca}^{2+}$  microdomains<sup>129</sup>. Enzymes located in their proximity can be  $\text{Ca}^{2+}$ -activated, triggering downstream  $\text{Ca}^{2+}$  mediated-pathways. Given that mitochondria contain very little  $\text{Ca}^{2+}$ , the hypothesis that mitochondria can generate a  $\text{Ca}^{2+}$  signal via mitochondrial  $\text{Ca}^{2+}$  release needs to be further validated and might be physiologically important only in certain cell types, for example neurons<sup>130</sup>. Nevertheless, it is tempting to hypothesize that mitochondria can operate as *bona fide* stores of  $\text{Ca}^{2+}$  that is released upon specific stimulation to trigger specific  $\text{Ca}^{2+}$ -dependent pathways.

## **2.3. CALCINEURIN: CALCIUM-CALMODULIN PHOSPHATASE**

### **2.3.1. CALCINEURIN STRUCTURE AND ROLE IN CELLULAR HOMEOSTASIS**

Calcineurin (CaN) is a cytoplasmic serine-threonine phosphatase, which is activated by sustained elevation in intracellular  $\text{Ca}^{2+}$ <sup>131,132</sup>. The active CaN holoenzyme is composed of a 59-kDa calmodulin-binding catalytic subunit referred to as CnA, a 19-kDa  $\text{Ca}^{2+}$ -binding regulatory subunit referred to as CnB, and the calcium binding protein calmodulin<sup>131,133,134</sup>. CaN owes its name to its significant expression in the nervous system compared to other tissues<sup>134</sup>, it is in fact associated to several neurological disorders<sup>135</sup>.

Biochemical and genetic studies have identified four distinct functional domains of CnA<sup>134</sup>: a catalytic domain, a CaN binding domain, a calmodulin (CaM)-binding domain, and an auto-inhibitory (AI) domain. CnB binds four calcium ions<sup>136</sup>. CaN phosphatase activity is stimulated by  $\text{Ca}^{2+}$  binding to CnB and by  $\text{Ca}^{2+}$ -induced binding of CaM to CnA. Upon CaM binding, the C-terminal autoinhibitory domain is displaced and CaN becomes enzymatically active (Figure 3)<sup>137</sup>.

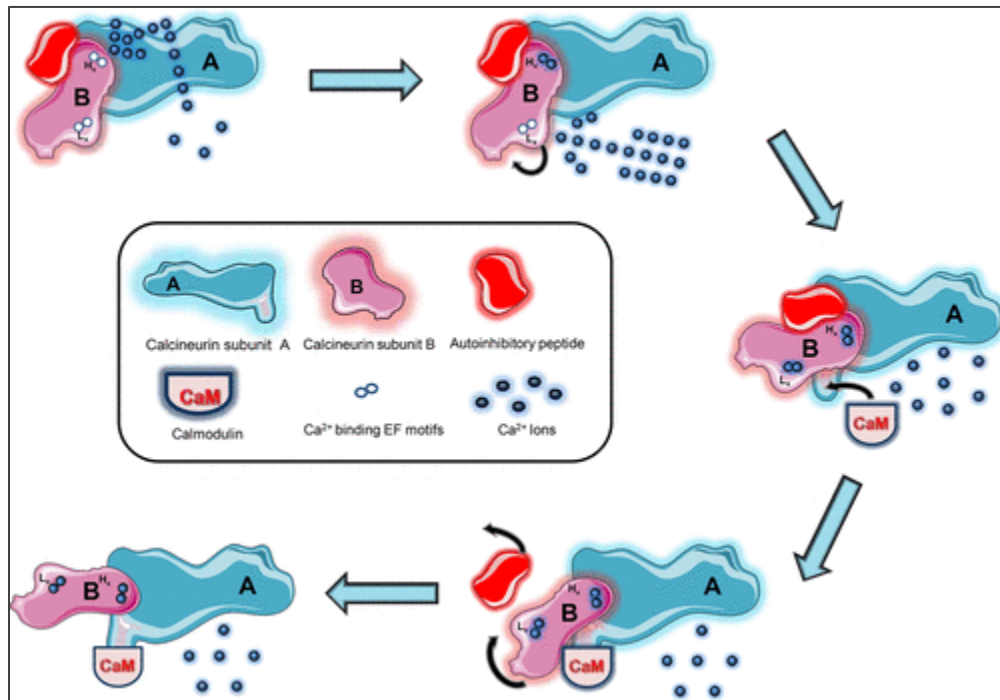


**Figure 3. Mechanism of Calcineurin (CaN) activation.** Calcium ( $\text{Ca}^{2+}$ ) binds to the subunit B of CaN, promoting interaction between subunit B and A and leading to a more stabilized form of the enzyme. A further increase in  $\text{Ca}^{2+}$  levels promotes a conformational change that expose the calmodulin (CaM) binding site. Following CaM bind, a second conformational change is promoted, which release the autoinhibitory peptide leading to fully activated CaN<sup>135</sup>.

In T-cells CaN catalytic activity is inhibited by the immunosuppressive drugs cyclosporine A (CsA) and FK506 through complexes with cyclophilins and FKBP12, respectively<sup>138</sup>. The identification of CaN as a target for CsA and FK506 suggested a critical role for this phosphatase in the regulation of T-cell reactivity and cytokine gene expression. T-cells activation and CaN-mediated cytokines induction has been largely attributed to the family of transcriptional regulators referred to nuclear factor of activated T cells (NF-AT)<sup>138</sup>. CaN interacts with NF-AT transcription factors, resulting their dephosphorylation and subsequent translocation to the nucleus, where they participate in the transcriptional activation of cytokine genes<sup>137,139</sup>. Nevertheless, CaN is not only involved in pro-inflammatory signaling cascade; in reactive astrocytes, CaN activation results in the abrogation of inflammatory cascades by inhibiting NF-AT<sup>140</sup>.

CaN has also been demonstrated to be a key regulator in several pro-apoptotic pathways. In lymphocytes, CaN-activated NF-AT regulates *de novo* protein synthesis of components of death-inducing signaling complex (DISC), such as Fas ligand<sup>141</sup>. Fas ligand binding to its transmembrane receptor leads to DISC formation, and transduction of pro-apoptotic signals<sup>141</sup>.

CaN also plays a crucial role in the mitochondrial programmed cell death pathway. In this context, CaN dephosphorylates pro-apoptotic factor BAD to promote its translocation to mitochondria, and trigger MPTP-dependent caspase 3-apoptosis<sup>142</sup>.

CaN and mitochondria functional interaction is not limited to apoptosis. The evidence that CaN inhibitor, CsA prevents depolarization-induced mitochondria fragmentation, suggested that CaN also controls mitochondria morphology<sup>21</sup>. Following mitochondria depolarization with CCCP, CaN dephosphorylates pro-fission protein Drp1 at Ser637<sup>21</sup>. This event induces Drp1 translocation to depolarized mitochondria, promoting mitochondrial fission.

CaN can also control the nuclear translocation of the lysosomal transcriptional factor TFEB. A recent study demonstrated that a physiological Ca<sup>2+</sup> signal generated via Ca<sup>2+</sup> release through lysosomal channel mucolipin 1 (MCOLN1) triggers CaN activation and binding to TFEB, thus promoting its nuclear translocation<sup>23</sup>. TFEB is a master regulator of lysosomal biogenesis and autophagy. Accordingly CaN plays a leading role in the control of these processes.

### 2.3.2. CALCINEURIN ROLE IN NEURODEGENERATION

CaN is remarkably expressed in the brain, where it represents more than 1% of total proteins<sup>143</sup>. CaN both acts at pre and post synaptic level, regulating Ca<sup>2+</sup> signaling<sup>135</sup>. At the presynaptic level, CaN and cyclin-dependent kinase 5 (CDK5) control vesicular release of neurotransmitters, ensuring the maintenance of proper amount of neurotransmitters reaching the postsynaptic membrane<sup>144</sup>. CDK5 phosphorylates Synapsin 1, a protein coating synaptic vesicles, enhancing its binding to actin filaments<sup>144</sup>, and ultimately affecting the availability of synaptic vesicles for release. By dephosphorylating Synapsin 1, CaN counteracts this effect and it is able to reverse the suppression of exocytosis induced by CDK5<sup>145</sup>.

CaN also participates in clathrin-mediated endocytosis by physically interacting with Dynamin I, a key component of the synaptic endocytic machinery<sup>146,147</sup>. Under resting conditions, CaN and Dynamin 1 are largely unassociated. A rise in intracellular Ca<sup>2+</sup> levels, produced by either neuronal depolarization or extracellular stimuli, induces physical and functional interaction between CaN and Dynamin 1<sup>147</sup>. Subsequently, CaN-Dynamin 1 complex can combine with Amphiphysin 1, the anchor protein of the endocytic complex. CaN mediated



dephosphorylation was proven to allow the endocytic coat complex to remain assembled and functional, to promote clathrin-dependent endocytosis. Accordingly, disruption of the CaN-Dynamin 1 interaction inhibits clathrin-mediated endocytosis<sup>147</sup>. Since the association between CaN and Dynamin 1 is Ca<sup>2+</sup>-dependent, this complex acts as a Ca<sup>2+</sup> sensor.

Postsynaptically, CaN controls Ca<sup>2+</sup> homeostasis by modulating Ca<sup>2+</sup> influx rates. Ca<sup>2+</sup> enters the cell via ligand-gated channels such as the N-methyl-D-aspartate receptors (NMDARs). CaN is localized in proximity of NMDARs where it senses Ca<sup>2+</sup> rise. Following Ca<sup>2+</sup>-dependent activation, CaN dephosphorylates NMDARs, leading to weakening of Ca<sup>2+</sup> flux into the cell by decreasing the duration of the opening of NMDARs<sup>148</sup>.

CaN and NMDARs are also involved in the regulation of synaptic plasticity, a physiological process that modulates the strength of individual synapses, thus affecting memory consolidation<sup>149</sup>. These changes induce bidirectional and long-lasting alterations in synaptic plasticity – defined as long-term potentiation (LTP) and long-term depression (LTD). In both cases, stimulation triggers postsynaptic membrane depolarization, which leads to the activation of synaptic NMDA receptors, and the subsequent elevation of intracellular Ca<sup>2+</sup> concentration<sup>150</sup>. Ca<sup>2+</sup> rise activates CaN which leads to the activation of the protein phosphatase PP1, resulting in facilitating the process leading to LTD induction. Synaptic plasticity is intimately related to memory as result of an intricate and dynamic neuronal network. Not surprisingly, forebrain-specific CaN knock-out mice exhibit severe and selective deficit in working memory<sup>151</sup>.

Finally, CaN functions also extend to neuronal cytoskeleton remodeling. In the developing neurites (the neuronal processes), cytoskeleton rearrangement is a rapid event triggered by extracellular signals that increase intracellular Ca<sup>2+</sup> levels<sup>152</sup>. Sustained Ca<sup>2+</sup> rise activates CaN that is enriched in the growth cone, the apical part of neurites; at this level, CaN directly controls microtubules assembly, through dephosphorylation of tubulin and microtubules associated proteins such as Tau and MAP-2<sup>153,154</sup>. Accordingly, CsA-mediated CaN inhibition blocks neurites elongation<sup>154</sup>. During neurites extension, CaN also dephosphorylates the actin-organizing proteins ADF and cofilin to promote actin polymerization and increase growth cone motility<sup>155</sup>. CaN effect on cofilin seems not to be restricted to the brain and neurite outgrowth, but extended to other cell types as platelets<sup>156</sup> and in tracheal smooth muscle cells<sup>157</sup>.

Thus, CaN is a keystone enzyme in cellular environment. It exerts pleiotropic functions, which span from regulation of mitochondrial dynamics, neuroinflammation and cytoskeleton remodeling. Moreover, CaN play an active role in mTOR-mediated autophagy that will be extensively exposed in the following section.

## **2.4. AUTOPHAGY**

### **2.4.1. MECHANISM OF AUTOPHAGY IN MAMMALIAN**

Autophagy is an intracellular self-degradative process in which cytoplasmic organelles and long-lived proteins are disrupted at the lysosomes and recycled, to maintain cellular homeostasis. The nature of the degraded material defines distinct classes of autophagy into macro-autophagy, micro-autophagy, and chaperone-mediated autophagy<sup>158</sup>. In macro-autophagy (commonly referred to autophagy, as the most prevalent form) the cytoplasmic cargo is sequestered within a double-membraned structure, the autophagosome, which fuses with the lysosomes, forming an autolysosome. Lysosomal acid proteases ensure the proteolytic degradation of the engulfed component. By contrast, in micro-autophagy, the cargo is directly delivered to the lysosome through an invagination of its membrane. Both macro-autophagy and micro-autophagy are required for the clearance of large components, while chaperone-mediated autophagy is involved in the degradation of proteins with KFERQ-like motif. In this type of autophagy, targeted proteins containing the KFERQ sequence are translocated across the lysosomal membrane in a complex with chaperones (such as Hsc-70) that are recognized by the lysosomal membrane protein LAMP-2A (lysosomal-associated membrane protein 2A)<sup>159</sup>.

Autophagy can be mechanistically broken down into the following five steps: initiation of the isolation membrane, elongation, closure of the isolation membrane and autophagosome formation, autophagosome–lysosome fusion, and lysosomal degradation.

Currently, three main autophagic pathways are described in mammalian: Akt/mTOR, Beclin-VSP34 and LC3-ATG proteins signaling pathways. Under nutrients availability conditions, the kinase mTOR (which is conserved from yeast to human) is active to inhibits autophagy and to promote anabolic processes, including biosynthesis of proteins, lipids and organelles<sup>160</sup>. mTOR is composed by two large complexes named mTORC1 and mTORC2. mTORC1, the major negative

autophagy modulator, is upstream-regulated by the phosphatidylinositol 3 kinase (PI3K) and kinase AKT (AKT) pathway<sup>161</sup>. In a nutrient-rich environment, the activation of PI3K leads to the recruitment of AKT and the activation of mTORC1. mTORC1 phosphorylates and inactivates the ubiquitin-like kinase 1 (ULK1), inhibiting autophagy. Conversely, during starvation, mTOR activity is repressed by signals that sense nutrient deprivation and ULK1 inhibitor tag is lost. Activated ULK1 phosphorylates its target proteins to form a complex that is required for autophagosome nucleation<sup>162</sup>. Moreover ULK1 phosphorylates the autophagic scaffold protein AMBRA-1, which promotes Beclin interaction with its target lipid kinase VPS34, thus mediating autophagosome nucleation<sup>163</sup>. The VPS34 complex phosphorylates phosphatidylinositol to produce phosphatidylinositol 3-phosphate (PI3P), inducing the recruitment of autophagy downstream effectors (ATG14L, UVRAG, Bif1) or inhibitors (Bcl-2 and Bcl-xL)<sup>164</sup>.

Lastly, the elongation of the autophagosome involves ubiquitin-like conjugation processes, the Atg12-Atg5-Atg16L complex that oligomerizes and associates to the autophagosomal membrane<sup>165</sup>, and the LC3 complex. LC3 is cleaved by ATG4 to form LC3-I. Upon autophagy induction, LC3-I is conjugated to the membrane lipid phosphatidylethanolamine (PE) and it associates to the membrane of the expanding autophagosome, mediating its closure. The autophagosome fuses with the lysosome, and the content is degraded. Although clearly essential for forming the defining double membranous vesicle of the autophagosome, the origin of the membrane component remains controversial<sup>166</sup> (Figure 4).

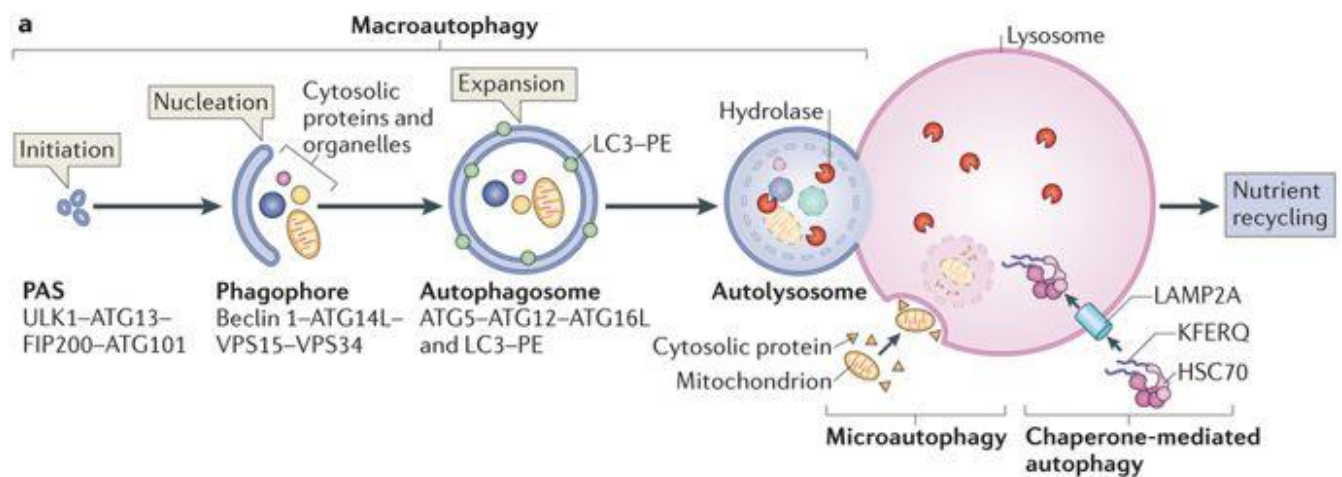


**Figure 4: Overview of mammalian autophagy pathways.** In macroautophagy, the phagophore begins to form following activation of ULK1 (initiation step). Activated ULK1 phosphorylates its target proteins to form a complex that is required for autophagosome nucleation. ULK1 promotes Beclin interaction with its target lipid kinase VPS34, thus mediating autophagosome nucleation. Lastly, the elongation of the autophagosome involves ubiquitin-like conjugation processes, the Atg12-Atg5-Atg16L

complex that oligomerizes and associates to the autophagosomal membrane, and the LC3 complex. Upon autophagy induction, LC3-I is phosphatidylethanolamine (PE) lipidated, and it associates to the membrane of the expanding autophagosome, mediating its closure. The resulting autophagosome fuses with endocytic and lysosomal compartments, ultimately leading to formation of the autolysosome. In microautophagy, substrates are directly engulfed at the boundary of the lysosomal membrane. In chaperone-mediated autophagy, substrates with the pentapeptide motif KFERQ are selectively recognized by the heat shock cognate 70 kDa protein (HSC70) chaperone and translocated to lysosomes in a LAMP2A-dependent manner<sup>167</sup>.

In recent years, emerging studies suggest a correlation between autophagy defects and human diseases. The role of autophagy has most extensively been studied in the context of neurodegenerative diseases, such as some forms of Parkinson's disease and Alzheimer's disease (AD) characterized by the aggregation of misfolded proteins<sup>168,169</sup>. Because autophagy degrades abnormal proteins, the onset and progression of these diseases are likely to be affected by impaired autophagic activity. Indeed, accumulation of autophagosomes is observed in samples from *post mortem* biopsy of brains of affected patients. In addition, studies in cell and mouse models clearly highlighted an impairment in the autophagic process at different levels<sup>170-172</sup>. Interestingly, Atg7-deficient mice, which have impaired autophagy, present obvious neurological defects, including the abnormal limb-clasping reflexes, caused by severe damage to cortical and cerebellar neurons<sup>173</sup>. Importantly, ubiquitin-positive aggregates were detected in neurons. These findings show that autophagy prevents neuronal damage by constitutively eliminating ubiquitin-positive aggregates.

#### 2.4.2. MITOPHAGY: SELECTIVE REMOVAL OF UNWANTED MITOCHONDRIA

Because mitochondria play a central role in cellular metabolism and homeostasis, maintenance of a healthy mitochondria network is crucial in cells. Damaged mitochondria release  $\text{Ca}^{2+}$  and cytochrome c triggering apoptosis<sup>174</sup>, and they can be sources of oxidative stress<sup>175</sup>. At steady-state, mitochondrial mass is regulated by a continuous balance between biogenesis and degradation. Selective autophagic degradation of mitochondria via quality control mechanisms is a crucial event for the maintenance of a healthy mitochondrial network. In this highly regulated process, named mitophagy, mitochondria are sequestered in double-membrane vesicles and delivered to lysosomes for hydrolytic degradation. Mitophagy occurs both at steady-state level, named basal mitophagy, and/or upon mitochondria stress (i.e. stress-induced mitophagy). The

third class of mitophagy takes place during development and is known as programmed mitophagy.

Three major pathways for mitochondria quality control have been described. In the first one, mitochondria unfolded proteins are directly degraded by specific AAA proteases complexes that are resident in the inner mitochondrial membrane and promote mitochondrial protein degradation both at the intermembrane space and in the matrix<sup>176</sup>. The ubiquitin-proteasome system (UPS) has also been shown to mediate degradation of IMM and OMM resident proteins<sup>177</sup>. In addition to proteolytic and proteasomal degradation, vesicles can bud from mitochondrial tubules, to deliver mitochondrial components to the lysosome for degradation. These mitochondrial-derived vesicles (MDVs) may represent a mechanism for selective removal of oxidized mitochondrial proteins while leaving the whole organelle intact<sup>178</sup>. The third pathway involves sequestration of the entire mitochondrion within the autophagosome, followed by fusion with a lysosome (Figure 5).

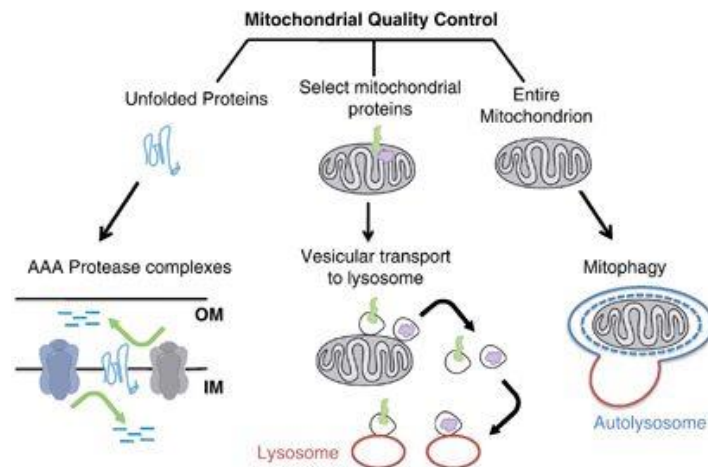


**Figure 5: The three major pathways for mitochondrial quality control.** Unfolded proteins are degraded by specific AAA protease complexes that can function both at the intermembrane space or in the matrix. Mitochondrial proteins can also be degraded by being directly transferred to lysosomes; vesicles budding from mitochondrial tubules sequester selected mitochondrial cargos, and deliver those mitochondrial components to the lysosome for degradation (MDV, mitochondrial derived vesicle pathway). The third pathway, involves sequestration of the entire mitochondrion within the autophagosome, followed by fusion with a lysosome. *From (Ashrafi and Schwarz, 2013).*

Basal mitophagy occurs in most cell types and ensures the recycling of old and damaged organelles<sup>24,179</sup>. *In vivo*, in mouse tissues of high metabolic demand such as muscles, basal mitophagy can be higher than in others like thymus or spleen<sup>24</sup>. Elimination of damaged mitochondria can be divided into two steps: (i) induction of general autophagy, which has been extensively described before and (ii) labeling of damaged mitochondria for selective autophagic recognition. This is mediated by two major pathways: the first one requires the involvement of

the mitophagic receptors as NIP3-like protein X (Nix) and FUN14 domain-containing protein 1 (FUNDC1), and the second one is activated by PINK1-Parkin (Figure 6)<sup>180</sup>.

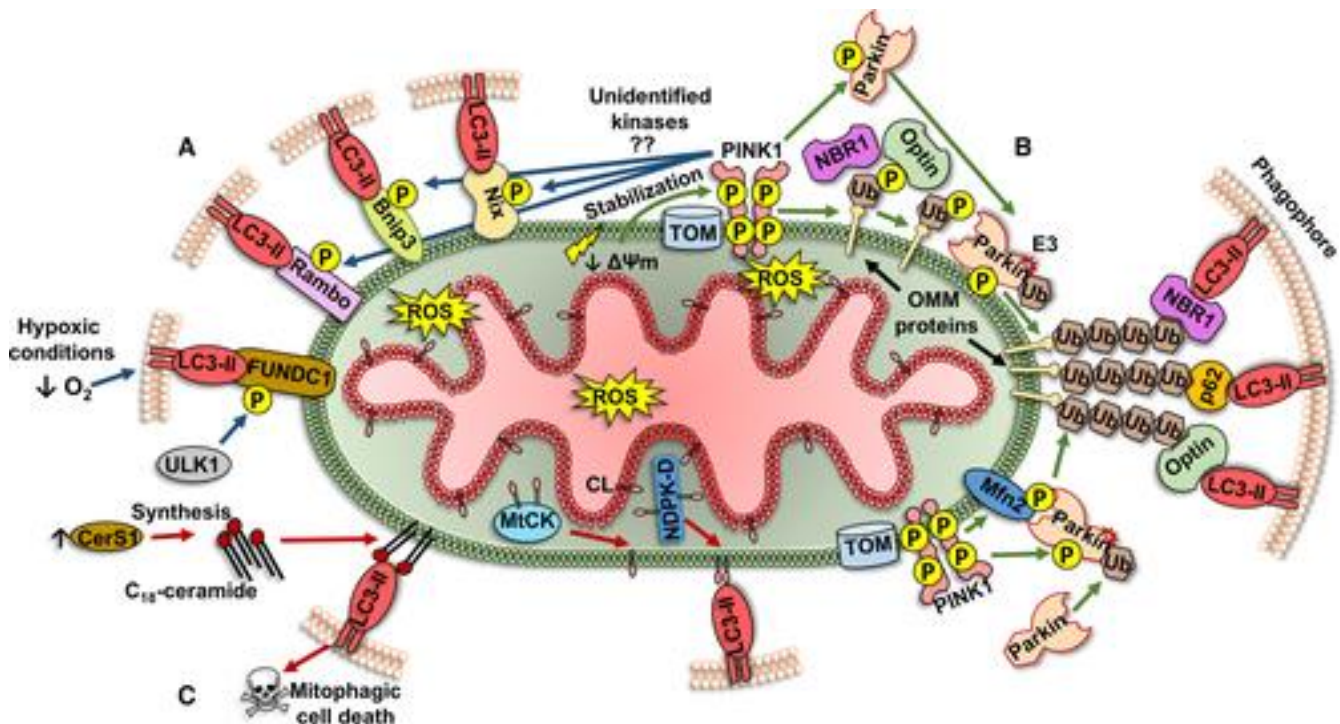


**Figure 6: Mitophagy mechanisms.** Mitophagy selectively targets mitochondria for degradation via two major receptor-mediated mechanisms. (A) OMM receptor-mediated mitophagy. Bnip3, Nix, FUNDC1 directly bind to LC3-II. (B) PINK1/Parkin-mediated mitophagy. Altered mitochondria membrane potential results in PINK1 stabilization on the OMM and subsequent activation. Targets of phosphorylated PINK1 (Ubiquitin/Ub and MFN2) recruit the E3 Ligase Parkin in the OMM. Upon PINK1-dependent activation, Parkin ubiquitinates a subset of OMM proteins that, in turns, attract specific autophagy receptors (p62/SQSTM1, NBR1, optineurin/optin) to mediate mitochondrial engulfment<sup>180</sup>.

Briefly, NIX is localized to the OMM and contains a WXXL-like motif facing the cytosol, which binds LC3, and GABA receptor-associated protein (GABARAP), both localized on the autophagosome membrane. The induction of mitophagy by NIX is thought to be mediated, at least in part, by direct binding to LC3 and GABARAP through its WXXL-like motif<sup>6</sup>. FUNDC1 is an additional OMM mitophagy receptor, which is activated under hypoxic conditions. These receptors contain phosphorylation-regulated LIR (LC3 interacting region) motifs, which directly interact with the LC3-II-labeled phagophore<sup>180</sup>. Notably, upon mitophagy induction, LC3 can also interact with the LIR-containing protein AMBRA1. This event regulates both canonical Parkin-dependent and -independent mitochondrial clearance. Interestingly, targeting AMBRA1 to mitochondria induces mitophagy<sup>181</sup>. A detailed description of the PINK1-Parkin pathway is provided in the next section.

### The PINK1-Parkin pathway

The PINK1-Parkin pathway is perhaps the best characterized ubiquitin-mediated stress-induced mitophagic pathway. As previously described in this thesis, these two genes are mutated in some genetic autosomal recessive forms of PD<sup>11,12</sup>.

In the current model, PINK1, a serine/threonine kinase, is constitutively imported into polarized mitochondria through TOM/TIM complex to the IMM where it is cleaved by several proteases, including the mitochondrial-processing protease (MPP) and the inner membrane presenilin-associated rhomboid-like protease PARL, and ultimately proteolytically degraded<sup>4,71,182</sup>. In depolarized mitochondria, full-length PINK1 accumulates on the surface of mitochondria, and promotes mitochondrial recruitment of E3 ubiquitin ligase Parkin (Figure 7).

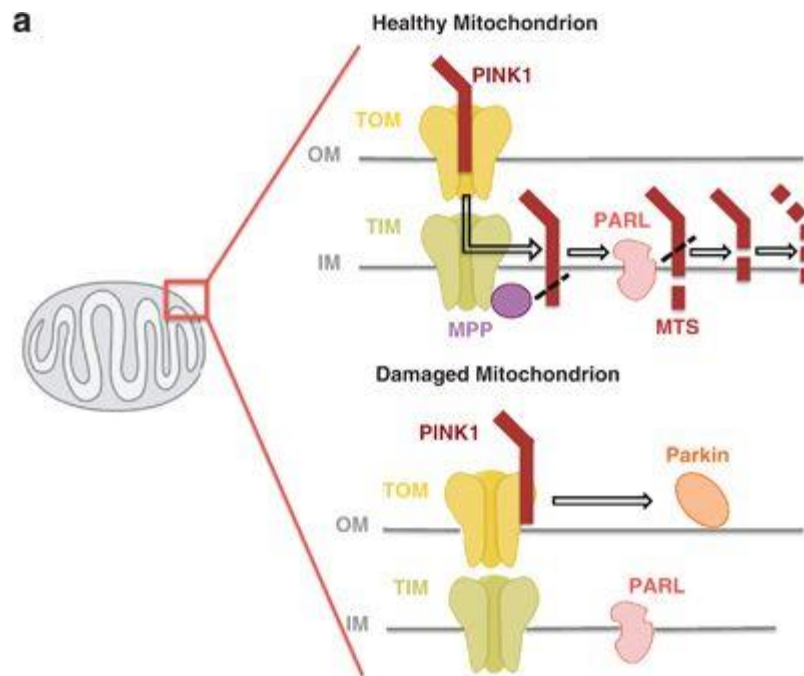


**Figure 7: The PINK1/Parkin pathway.** In polarized mitochondria, PINK1 is imported to the IMM where it is cleaved by mitochondrial protease MPP. PINK1 is also cleaved by the inner membrane presenilin-associated rhomboid-like protease PARL and ultimately proteolytically degraded. Upon mitochondrial damage PINK1 import is prevented. PINK1 accumulates on the OMM, and recruit Parkin to damaged mitochondria. From (Ashrafi and Schwarz, 2013).

In this process, PINK1 phosphorylates Parkin at Ser65, and ubiquitin (Ub) at the same residue<sup>89,183</sup>. PINK1 phosphorylation of Parkin induces a significant conformational change that

is required for Parkin translocation<sup>93</sup>. On depolarized mitochondria, Parkin mediates the poly-ubiquitination of mitochondrial resident proteins, including Mitofusins, VDAC, TOM20 and Fis5,<sup>184-186</sup>. These ubiquitinated proteins serve to recruit essential adapter proteins such as Optineurin, NDP52, p62, HDAC6, or p97, which will tether the phagophore membrane and induce the mitophagic process<sup>3</sup>.

Mitochondrial degradation and mitochondrial dynamic are intimately correlated. Previous studies have demonstrated that mitochondrial fission followed by selective fusion, regulates mitochondrial elimination by autophagy, in a process that depends on mitochondrial membrane potential and the ability of the daughter mitochondrion to fuse<sup>22</sup>. In perfect agreement with this model, it was proposed that Parkin-dependent ubiquitination of Mitofusins prevents mitochondrial fusion of dysfunctional mitochondria by promoting proteasomal degradation of pro-fusion proteins MFN1 and MFN2. This process segregates depolarized mitochondria from the mitochondrial network, impairing their ability to fuse<sup>187</sup>. In addition, PINK1/Parkin directly promotes mitochondrial fission by regulating recruitment and activation of pro-fission protein Drp1. Interestingly, Drp1 is selectively recruited to dysfunctional mitochondria in the proximity of PINK1/Parkin suggesting that mitochondrial division occurs at sites where the PINK1/Parkin-dependent mitochondrial clearance program is initiated<sup>188</sup>. In resting conditions, Drp1 is phospho-inhibited at Ser 637 by AKAP1-PKA (A-kinase anchoring protein complex and protein kinase A, respectively)<sup>21</sup>. Following mitochondria damage, PINK1 becomes active and disrupt the AKAP1-PKA to promote Drp1-dependent fission<sup>77</sup>. Expression of dominant-negative Drp1 to inhibit mitochondrial fission prevents mitophagy, indicating the importance of fission in mitophagy<sup>189</sup>. Studies on yeast homolog of Drp1, Dnm1, confirmed the essential role of fission in the selective removal of damaged mitochondria<sup>190</sup>.

The PINK1/Parkin axis is also implicated in the regulation of mitochondrial trafficking<sup>191</sup>. PINK1 phosphorylates the Miro protein, a mitochondrial outer membrane-localized GTPase that mediates association of mitochondria to the cytoskeleton. PINK1-dependent phosphorylation of Miro primes this protein for Parkin-dependent proteasomal degradation leading to the dissociation of kinesin from mitochondria, ultimately arresting mitochondrial movement along the microtubules<sup>80</sup>. This event isolate damaged mitochondria to facilitate mitophagic clearance<sup>192</sup>.



Thus, in a coordinated set of events, selective mitochondria are deprived of their fusion ability, they are made smaller, and they are isolated from the mitochondrial network.

### 3. AIM

PD can be classified both as a disease of mitochondrial quality control<sup>3</sup> and aberrant protein aggregation, which causes inflammation<sup>193</sup>. In particular, PD onset and progression are associated with decreased mitochondrial function and inflammatory responses deriving from aggregate-activated glial cells. Thus, accumulation of defective mitochondria, and increased inflammation are specific hallmarks of PD. Studies of hereditary forms of PD causally linked to mutations in PINK1 and Parkin have uncovered pathological mechanisms resembling those in sporadic PD patients, and demonstrated quite clearly that deregulation of mitochondrial quality control as a consequence of impaired mitophagy<sup>194-196</sup> and inflammatory response<sup>197</sup> are causative mechanisms leading to neurodegeneration.

This study aims at investigating the potential role of CaN in the molecular pathways that are regulating mitophagy. We specifically focused on CaN for three main reasons. First, CaN plays a role in autophagy, regulating the activation of the lysosomal transcriptional factor TFEB<sup>23</sup>. Second, CaN activity is controlled by Ca<sup>2+</sup>, which homeostasis is regulated by mitochondria<sup>198</sup>. Third, CaN plays a key role in neuroinflammation, a process that is critical and potentially deleterious in not-dividing cells such as neurons<sup>141</sup>.

## 4. RESULTS

# Calcineurin regulates Parkin-translocation to mitochondria and mitophagy

Marchesan Elena<sup>1</sup>, Nardin Alice<sup>2</sup>, von Stockum Sophia<sup>1</sup>, Calciolari Beatrice<sup>1</sup>, Herkenne Stephanie<sup>1</sup>, Schrepfer Emilie<sup>3</sup>, Cendron Laura<sup>1</sup>, Scorrano Luca<sup>1,4</sup> and Ziviani Elena<sup>1</sup>

<sup>1</sup> Department of Biology, University of Padua, Padua, Italy

<sup>2</sup> College of Life Sciences, University of Dundee, Dundee, United Kingdom

<sup>3</sup> Frontiers Media SA, Lausanne, Switzerland

<sup>4</sup> VIMM – Venetian Institute of Molecular Medicine, Padua, Italy

Address correspondence to

Elena Ziviani: [elena.ziviani@unipd.it](mailto:elena.ziviani@unipd.it)

## **Abstract**

The selective removal of dysfunctional mitochondria, named mitophagy, is crucial for the maintenance of cellular homeostasis. This event is initiated by the translocation of the E3 ubiquitin ligase Parkin to intoxicated mitochondria and it requires the kinase PINK1. In a remarkable set of studies it was found that PINK1 operates upstream Parkin in a linear pathway that culminates in the phosphorylation of Parkin, Ubiquitin and Parkin mitochondrial substrates, leading to the ubiquitination of outer mitochondrial membrane proteins. Ubiquitin decorated mitochondria are selectively recruiting autophagy receptors which are required to terminate the organelle via autophagy. In this study we show a previously uncharacterized molecular pathway that correlates the activation of the Ca<sup>2+</sup>-dependent phosphatase Calcineurin (CaN) to PINK1/Parkin-dependent mitophagy. CaN downregulation or genetic inhibition prevents Parkin translocation to intoxicated mitochondria, and impairs stress-induced mitophagy. Moreover, CaN constitutive activation can trigger Parkin translocation under basal conditions also in the absence of PINK1, but requires PINK1 expression to promote mitophagy.

In summary, we identified CaN as a novel key player in the regulation of Parkin translocation and PINK1/Parkin dependent mitophagy.

## Introduction

Mutations in the PARK2 gene, encoding for the E3-ubiquitin ligase Parkin, is the most common cause of Autosomal-Juvenile Recessive-Parkinsonism<sup>11</sup> (AJ-PD), a neurodegenerative disease which hallmarks are almost indistinguishable from sporadic Parkinsonism. Parkin belongs to the RBR (RING-between-RING) type of E3 ubiquitin ligases<sup>199</sup>, also known as RING/HECT hybrids, consisting of an ubiquitin like domain (Ubl), followed by two RING fingers domains (RING0 and RING1), an in between RING finger domain (IBR), a linker domain called Repressor Element of Parkin (REP) and a third RING finger domain called RING2<sup>19</sup>. Under basal conditions, Parkin activity is repressed and the protein maintains a so called “coiled snake” structure with the Ubl domain and the REP fragment occluding the RING1 domain, and the RING0 domain impeding on the catalytic site-containing RING2 domain<sup>19,200-202</sup>.

The gene product has a number of neuroprotective roles and pleiotropic functions and its activation is involved in many different survival pathways<sup>203-205</sup>, including those that are affecting mitochondria function by regulating mitochondria quality control<sup>206-209</sup>. How Parkin controls so many different cellular processes is under intense investigation. However, by being a versatile E3 ubiquitin ligase that both promotes degradative Lys 48-mediated ubiquitination<sup>100</sup> and non classical, proteasomal-independent ubiquitination<sup>210</sup>, Parkin has the potential of controlling a broad spectrum of cellular processes. Not surprisingly, Parkin activity is repressed under basal condition, and its activation is tightly regulated by a number of molecular processes, which are largely mediated by post translational modifications.

Parkin function is closely related to another PD-related gene, PARK6, which encodes for a protein called PINK1<sup>4,187,205</sup>. PINK1 is a Serine/Threonine kinase that is imported into mitochondria, where it gets cleaved by the inner membrane protease PARL and then eliminated by the proteasome<sup>211-213</sup>. On depolarized mitochondria, PINK1 accumulates on the outer mitochondrial membrane, where it promotes Parkin translocation and mitochondrial recruitment<sup>4,186,214,215</sup>. These events lead to ubiquitination and proteasomal degradation of OMM proteins and eventually to selective autophagy of damaged mitochondria<sup>5,13,94,216</sup>.

It has been widely demonstrated that Parkin translocation is PINK1 dependent. Recent works show that PINK1-mediated phosphorylation of Parkin and Ubiquitin at residue Serine 65 (Ser65) is necessary for Parkin translocation to defective mitochondria, and it is fundamental for its E3-

ubiquitin ligase activity<sup>73,92,217</sup>. Moreover, PINK1 phosphorylates a number of Parkin substrates including the pro-fusion protein Mitofusin 2 (Mfn2), which works as Parkin receptor<sup>218</sup>.

All together these evidences suggest a tightly regulated control of the recruitment process that operates at the post-translational level via reversible modifications of proteins in the form of phosphorylation<sup>73,76,219</sup>, ubiquitination<sup>74,220-222</sup>, deubiquitination<sup>223-228</sup>, sumoylation<sup>229,230</sup> and nitrosylation<sup>231,232</sup> and possibly other not yet characterized post-translational events.

Free calcium ( $\text{Ca}^{2+}$ ) concentration is important in the regulation of metabolic processes and for signal transduction. Accordingly, the cytoplasmic pool of  $\text{Ca}^{2+}$  is very limited and is tightly regulated by mitochondria and ER<sup>233-235</sup>.  $\text{Ca}^{2+}$  controls apoptosis and the opening of the permeability transition pore (PTP)<sup>1,2</sup>, a process linked to mitochondrial dysfunctions that increases the permeability of the mitochondrial inner membrane eventually leading to the release of pro-apoptotic factors from mitochondria. Furthermore,  $\text{Ca}^{2+}$  dependent phosphorylation and dephosphorylation of targeted proteins affect their activity by impinging on their subcellular localization, conformation and protein-protein interaction. For example dephosphorylation of transcription factor TFEB by  $\text{Ca}^{2+}$ -dependent phosphatase Calcineurin (CaN) promotes its nuclear translocation and the expression of autophagy and lysosomal genes to promote autophagy and lysosomal biogenesis<sup>23</sup>.

Here, we show that CaN promotes Parkin recruitment to mitochondria and PINK1/Parkin dependent mitophagy. CaN activation is sufficient to promote Parkin translocation and mitophagy under basal condition, and it appears to be an absolute requirement for stress-induced Parkin recruitment and mitophagy. Under this condition, PINK1 is dispensable for Parkin mitochondrial recruitment but not for mitophagy.

# Results

## **Parkin translocation to mitochondria is regulated by Calcineurin**

We transfected mouse embryonic fibroblasts (MEFs), which have undetectable levels of Parkin<sup>236</sup>, with fluorescent mCherry-Parkin and mitochondrial targeted YFP (mitoYFP), and analyzed Parkin subcellular localization by confocal microscopy. Consistent with previous studies<sup>13,237</sup> we observed that mCherry-Parkin was predominantly located in the cytosol in non-intoxicated cells (Figure 1A). Following the treatment with uncoupling agent carbonyl cyanide m-chlorophenylhydrazone (CCCP), a significant proportion of cells ( $75,7\pm 1,9\%$ ) showed mCherry-Parkin accumulated on or near fragmented mitochondria (Figure 1A-B), forming discrete dots called puncta. An automated analysis of the confocal images with Squassh, an ImageJ plugin that calculates the degree of colocalization between two channels<sup>238</sup>, allowed to further consolidate this result. In this analysis, the colocalization coefficient computed by the Squassh plugin ranges from 0 to 1, where 0 indicates no colocalization, and 1 perfect colocalization between mCherry-Parkin and YFP labeled mitochondria. According to this analysis, Squassh index raised from  $0,29\pm 0,03$  to  $0,62\pm 0,06$  following CCCP treatment, indicative of increased Parkin mitochondrial recruitment (Figure 1C). Of note, a small proportion of Parkin puncta did not seem to colocalize with mitochondria (Figure 1A, arrowhead) indicating a potential recruitment of Parkin to other organelles. To test this, we cotransfected mCherry-Parkin expressing MEFs with either lysosomal marker LAMP1GFP (Figure 1D) or the endosomal marker Rab5BGFP (Figure 1E). Colocalization analysis using Squassh demonstrated that in intoxicated cells a small proportion of Parkin puncta colocalized with lysosomes, whether no recruitment to endosomes seems to occur (Figure 1D-E; quantified in Figure 1F).

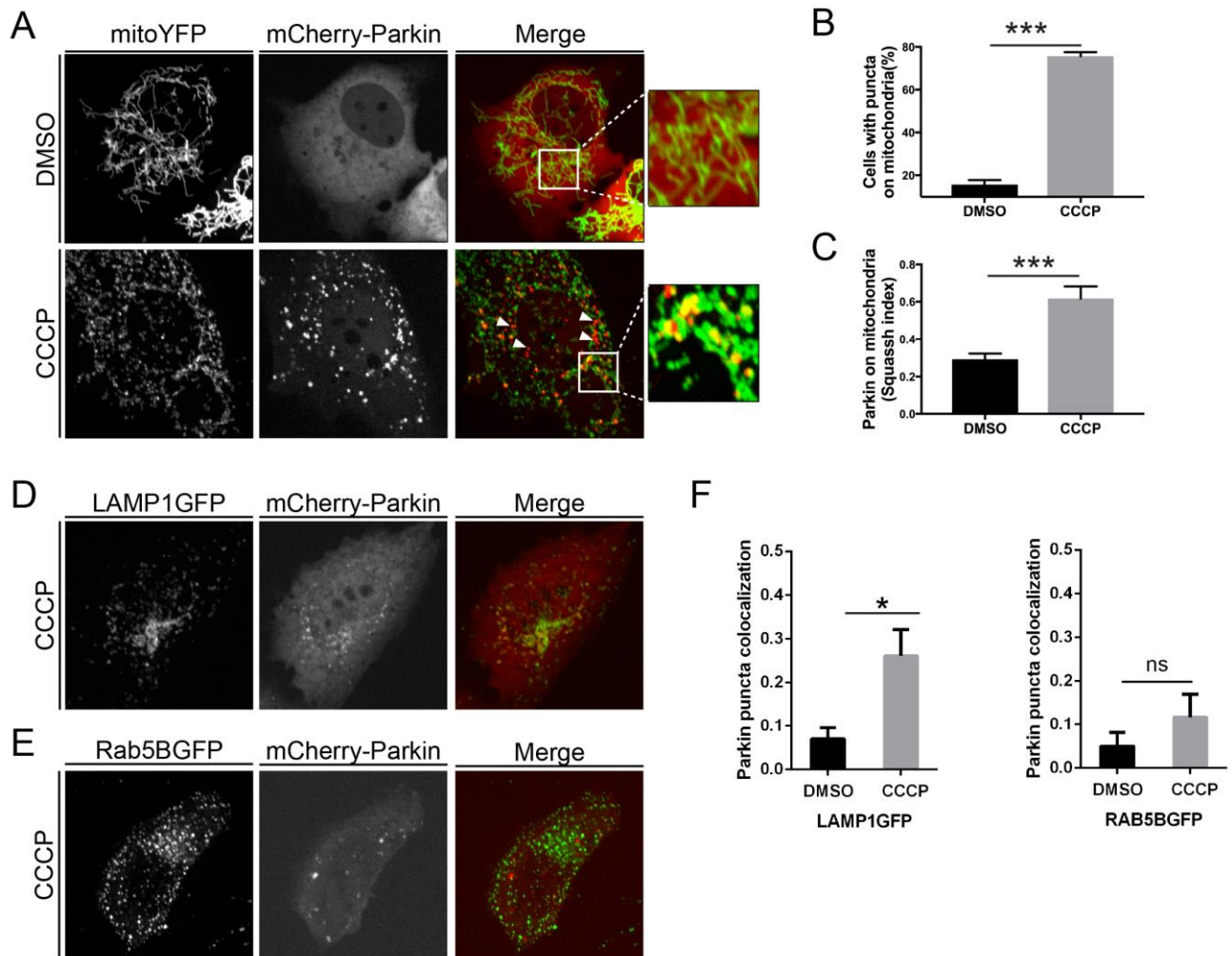


**Figure 1** (A) Representative confocal images of wildtype MEF cells transfected with mCherry-Parkin and mito-YFP for 2 days before being treated with DMSO as control or 10  $\mu$ M CCCP for 3 hours. The panels on the right show enlarged merged views of the boxed areas. (B) Quantification of A. Graph bar shows mean  $\pm$  SEM of percentage of cells with mCherry-Parkin on mitochondria for at least  $\geq 300$  cells. At least 4 independent experiments were performed. (C) Quantification of (A) using Squassh. The graph bars show mean  $\pm$  SEM of Squassh colocalization coefficient for at least  $\geq 50$  images. 0=no colocalization, 1=perfect colocalization. At least 4 independent experiments were performed. (D) Representative confocal images of wildtype MEF cells transfected with mCherry-Parkin and with LAMP1GFP. (E) Representative confocal images of wildtype MEF cells transfected with mCherry-Parkin and with Rab5GFP (F) Quantification of (D-E) using Squassh. The graph bars show mean  $\pm$  SEM of Squassh colocalization coefficient for at least  $\geq 50$  images. 0=no colocalization, 1=perfect colocalization. At least 3 independent experiments were performed.

The addition of the prothophore CCCP, required for triggering Parkin translocation, induces a transient increase of  $\text{Ca}^{2+}$  influx<sup>239</sup>. Previous results produced in our lab showed that  $\text{Ca}^{2+}$  chelation with BAPTA abolished Parkin translocation, suggesting a fundamental role for  $\text{Ca}^{2+}$ -dependent signal in the regulation of Parkin mitochondrial recruitment.  $\text{Ca}^{2+}$  is a highly versatile intracellular signal capable of regulating many different processes, and previous studies had showed that CCCP-generated  $\text{Ca}^{2+}$  rise activates  $\text{Ca}^{2+}$ /calmodulin dependent phosphatase Calcineurin (CaN)<sup>21</sup>. In this study it was found that CaN regulates the translocation of pro



mitochondrial fission protein Drp1 to mitochondria to promote mitochondrial fragmentation<sup>21</sup>. Intriguing, CaN activation also controls nuclear translocation of transcriptional factor TFEB, which in turns regulates transcription of lysosomal and autophagy genes that is required to promote lysosomal biogenesis, and ultimately autophagy<sup>23</sup>. Because mitochondria need to fragment to be engulfed by the autophagosome<sup>5</sup>, and CaN both regulates Drp1 dependent mitochondrial fission and autophagy, we addressed whether CaN is required for Parkin translocation, a fundamental prerequisite for stress-induced mitophagy.

To do so, we took advantage of the already existing CaN dominant negative ( $\Delta\text{CnA}^{\text{H151Q}}$ )<sup>240,241</sup> mutant. CaN is a heterodimer, composed of a catalytic subunit (CnA) that binds calmodulin and a regulatory subunit (CnB) that binds  $\text{Ca}^{2+}$ .  $\text{Ca}^{2+}$ /calmodulin activates CaN upon binding to the calmodulin-binding domain of CnA and inducing the dissociation of the autoinhibitory domain from the catalytic domain<sup>21</sup>.  $\Delta\text{CnA}^{\text{H151Q}}$  dominant negative mutant misses the calmodulin binding domain and the autoinhibitory domain and harbors an inactivating His-151 to Gln point mutation. We cotransfected MEFs with mCherry-Parkin and dominant negative CaN (CnB plus  $\Delta\text{CnA}^{\text{H151Q}}$ ) and looked at Parkin localization. As previously showed, CCCP-induced Parkin mitochondrial recruitment was clearly visible following 3 hrs intoxication (Figure 2A, left panel). This event was completely abolished when in presence of the dominant negative CaN (Figure 2A, right panel; quantified in Figure 2B-C).

CaN downregulating cells (Figure 2G) also exhibited a significant decrease in Parkin recruitment upon CCCP treatment (Figure 2D, quantified in Figure 2E-F).

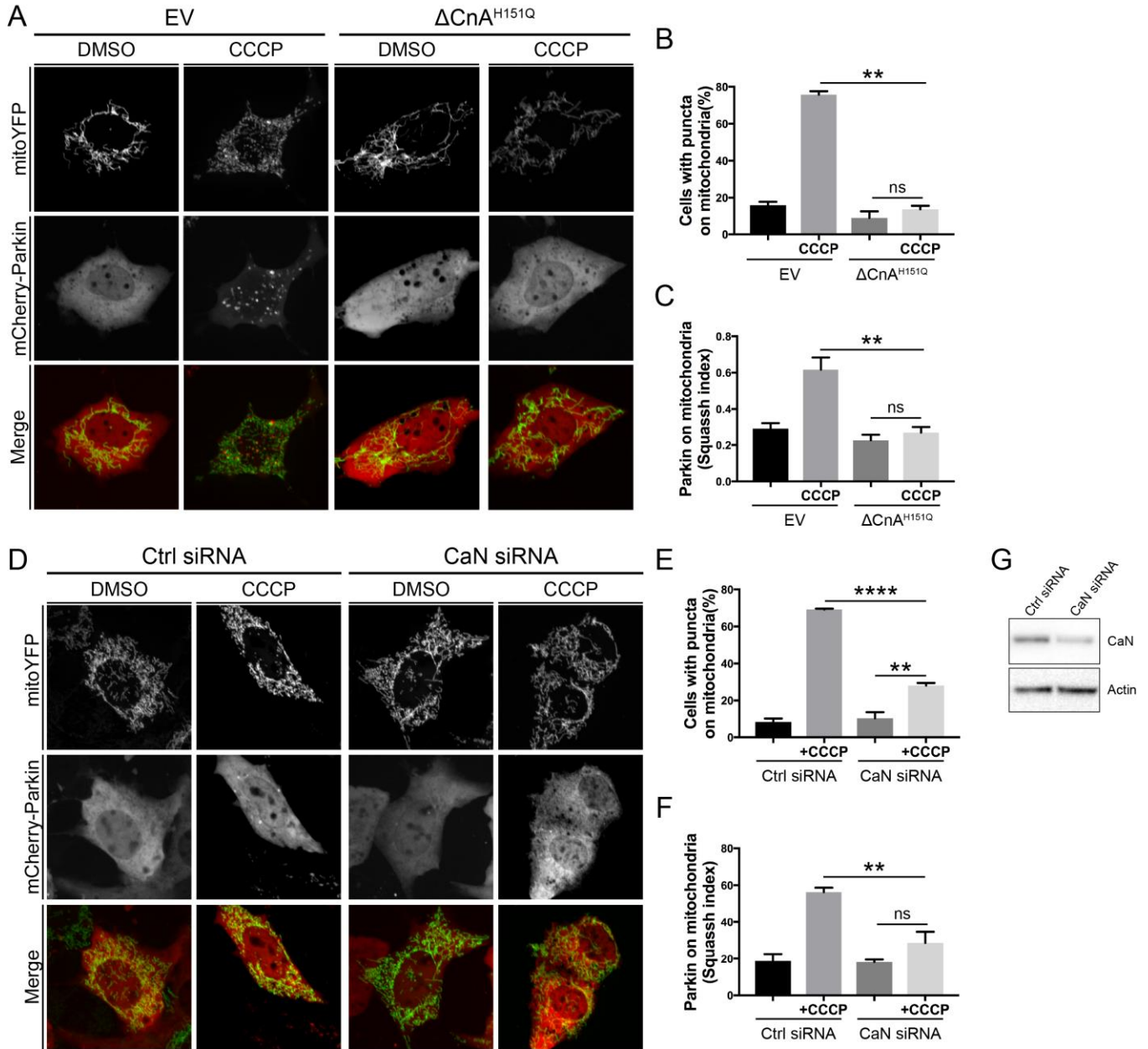


**Figure 2:** (A) Representative confocal images of wildtype MEF cells transfected with mCherry-Parkin, mito-YFP and CaN dominant negative mutant or the empty vector for 2 days before being treated with DMSO as control or 10  $\mu$ M CCCP for 3 hours. (B) Quantification of (A). Graph bar shows mean  $\pm$  SEM of percentage of cells with mCherry-Parkin on mitochondria for at least  $\geq 300$  cells. At least 3 independent experiments were performed. (C) Quantification of (A) using Squassh. The graph bars show mean  $\pm$  SEM of Squassh colocalization coefficient for at least  $\geq 50$  images. 0=no colocalization, 1=perfect colocalization. At least 3 independent experiments were performed. (D) Representative confocal images of wildtype MEF cells transfected with mCherry-Parkin, mito-YFP in which CaN was downregulated and relative control. (E) Quantification of (D). Graph bar shows mean  $\pm$  SEM of percentage of cells with mCherry-Parkin on mitochondria for at least  $\geq 300$  cells. At least 3 independent experiments were performed. (F) Quantification of (D) using Squassh. The graph bar shows mean  $\pm$  SEM of Squassh colocalization coefficient for at least  $\geq 50$  images. 0=no colocalization, 1=perfect colocalization. At least 3 independent experiments were performed. (G) CaN protein level in MEF cells upon CaN siRNA.

## **Parkin translocation is induced by Calcineurin in the absence of PINK1**

Different studies link Parkin translocation to PINK1 activity<sup>185,215,242</sup>. PINK1 directly phosphorylates Parkin and Ubiquitin (Ub) at Serine 65, which is required for Parkin translocation<sup>14,89</sup>. As already reported<sup>4</sup>, we also found that Parkin does not translocate to intoxicated mitochondria in the absence of PINK1 (Figure 3A, left panel). Intriguingly, expression of constitutive active CaN (CnB plus  $\Delta$ CnA) promoted Parkin translocation in PINK1<sup>-/-</sup> cells, even in the absence of CCCP intoxication (Figure 3A, right panel; quantified in Figure 3B-C) a condition that was hold true also in wild-type cells (data not showed).

It was previously demonstrated that PINK1 phosphorylates Parkin and Ubiquitin at residue Serine 65 (Ser65), to promote Parkin translocation and activity<sup>89</sup>. Accordingly, in PINK1<sup>-/-</sup> MEFs transfected with phospho-mimetic Ub (Ub S65E), a large proportion of phospho-mimetic mCherry-Parkin (Parkin S65E) translocated to intoxicated mitochondria (Figure 3D, left panel). In this condition, Parkin translocation was abolished upon expression of CaN dominant negative  $\Delta$ CnA<sup>H151Q</sup> (Figure 3D, right panel; quantified in Figure 3E-F), further supporting the hypothesis that CaN is an absolute requirement for Parkin translocation, independently of PINK1 expression.

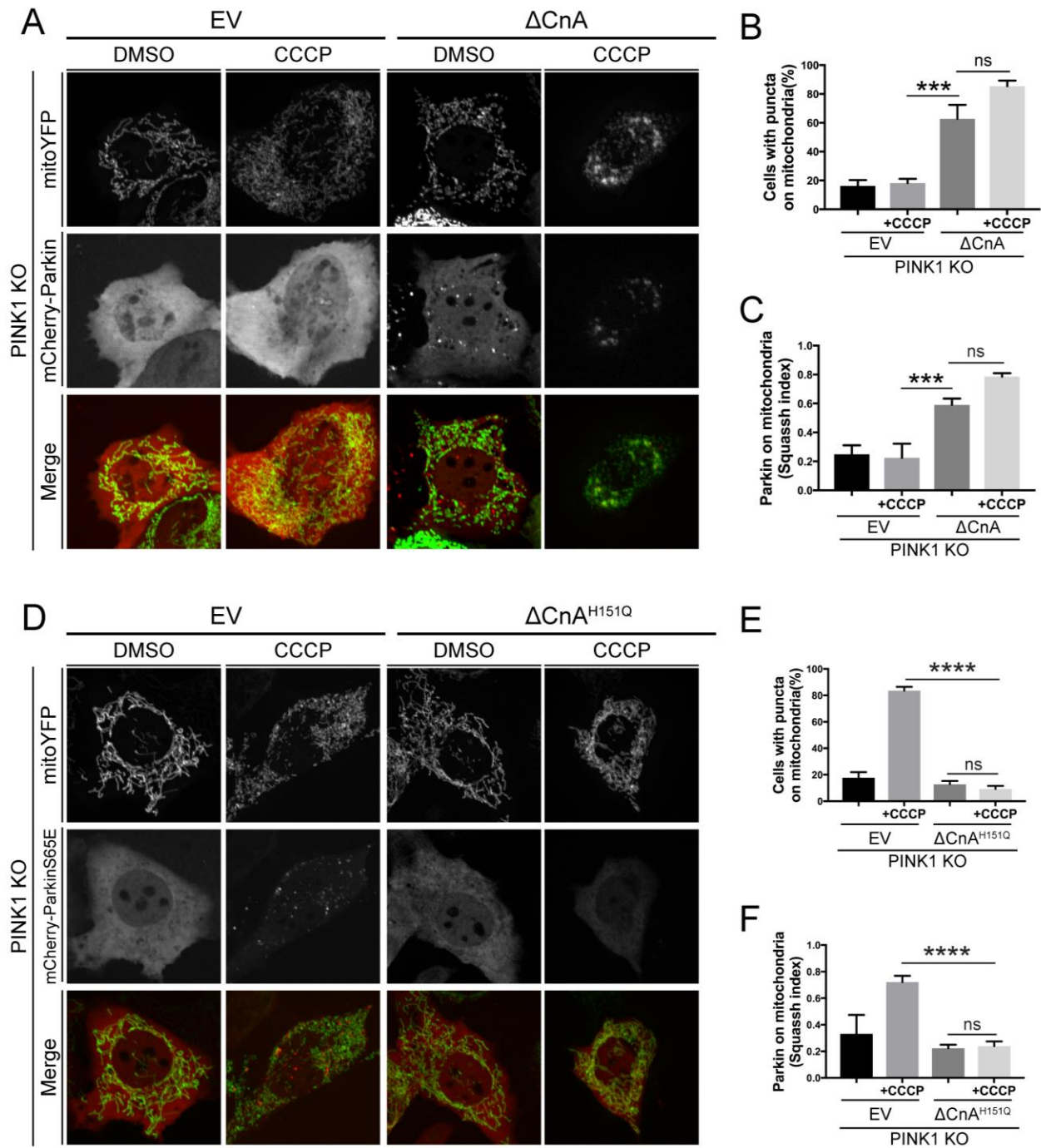


**Figure 3:** (A) Representative confocal images of PINK1 KO MEF cells transfected with mCherry-Parkin, mito-YFP and with empty vector or constitutively active CaN. (B) Quantification of (A) Graph bar shows mean  $\pm$  SEM of percentage of cells with mCherry-Parkin on mitochondria for at least  $\geq 300$  cells. At least 3 independent experiments were performed (C) Quantification of (A) using Squash. The graph bars show mean  $\pm$  SEM of Squash colocalization coefficient for at least  $\geq 50$  images. 0=no colocalization, 1=perfect colocalization. At least 3 independent experiments were performed (D) Representative confocal images of PINK1 KO MEF cells transfected with mCherry-ParkinS65E, UbS65E, mito-YFP and with empty vector or dominant negative CaN (E) Quantification of (D) Graph bar shows mean  $\pm$  SEM of percentage of cells with mCherry-Parkin on mitochondria for at least  $\geq 300$  cells. At least 3 independent experiments were performed (F) Quantification of (D) using Squash. The graph bars show mean  $\pm$  SEM of Squash colocalization coefficient for at least  $\geq 50$  images. 0=no colocalization, 1=perfect colocalization. At least 3 independent experiments were performed

## Calcineurin activation affects Parkin thermal stability

Similarly to other RBR E3 ligases, Parkin translocation and activity are strictly controlled by mechanisms of autoinhibition<sup>200</sup>. Structural studies have provided evidence that phosphorylation of Ubiquitin and Parkin at Serine 65 by PINK1 is an indispensable event regulating Parkin recruitment and activation on dysfunctional mitochondria. We have however showed that the expression of constitutively active CaN promotes Parkin recruitment in PINK1 KO cells i.e. in the absence of PINK1-dependent modifications. It is therefore conceivable that CaN activation can affect the overall closed, autoinhibited conformation of Parkin in the absence of PINK1 to promote Parkin translocation. Because conformational changes are paralleled by changes in protein solubility, which can be assessed by thermal shift<sup>243</sup>, we performed a thermal stability assay for Parkin to test this hypothesis. Intriguing, expression of constitutive active CaN leads to a decrease in Parkin thermal stability (Fig 4A-B), supporting the hypothesis that Parkin undergoes a conformational change in this condition.

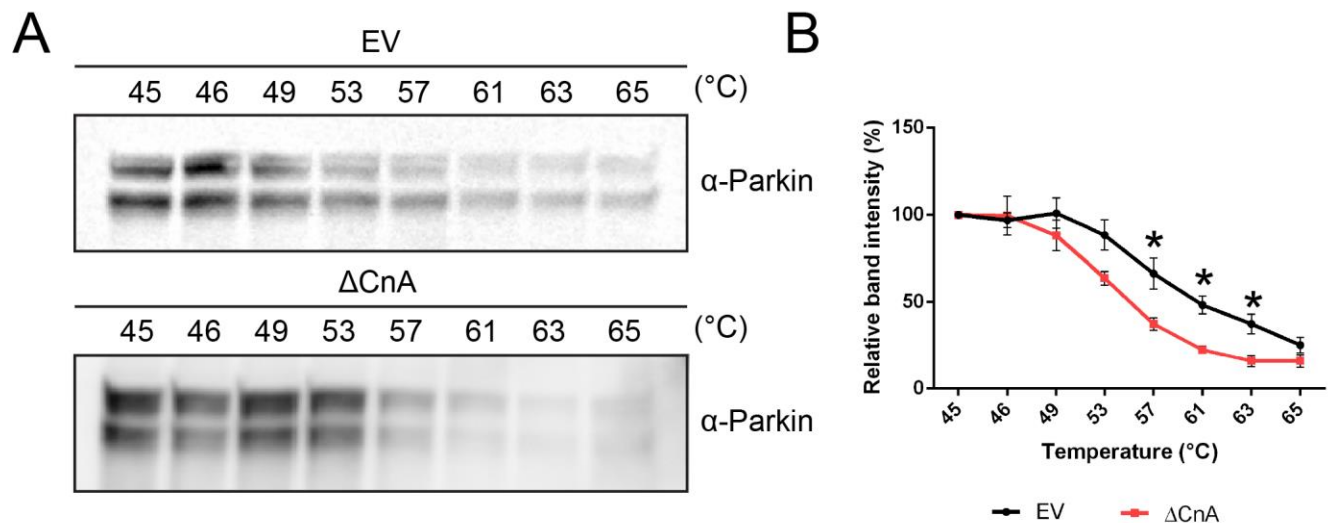


**Figure 4:** (A) Representative western blot of thermal stability of Parkin upon Calcineurin constitutive activation and relative control (B) Densitometric analysis of immunoblot in (A) enables quantification of aggregation temperature for Parkin

## Calcineurin is required for CCCP-induced mitophagy

Our data quite clearly demonstrate that CaN activity is required for Parkin recruitment to mitochondria. We next investigated the potential role of CaN in Parkin-dependent mitophagy. We used four different approaches to evaluate mitophagy *in vitro* in MEFs namely (i) quantification of mitochondrial mass, estimated by western blotting analysis of matrix protein Cyclophilin D (CypD) and inner mitochondrial membrane protein ATP synthase (ATP5A), (ii) confocal analysis of LC3-decorated mitochondria, (iii) FACS and confocal analysis of mitochondria-targeted fluorescent probe mt-Keima<sup>24</sup>, and (iv) electron microscopy (EM).

Because MEFs cells have undetectable levels of Parkin, we generated a Parkin-flag stable cell line by retroviral infection. MEFs stably expressing Parkin-flag were transfected with CaN dominant negative (CnB +  $\Delta$ CnA<sup>H151Q</sup>) or corresponding empty vectors, and mitochondrial mass was assessed following treatment with CCCP. In this condition, mitochondrial proteins (ATP synthase subunit alpha, ATP5A, and the mitochondrial matrix protein Cyclophilin D, CypD) were lost after 36 hrs CCCP treatment, while were retained in cells expressing dominant negative CaN (Figure 5A-B). Cells downregulating CaN also exhibited impaired CCCP-induced mitochondrial degradation (Figure 5C-D). These quantitative immunoblotting data were confirmed by confocal analysis of colocalization of mitochondria with GFP-LC3 labelled autophagosomes (Figure 5E-H). To further confirm impaired mitophagy in CaN inhibited conditions, we infected Parkin expressing MEFs with mt-Keima, which had different excitation spectra at neutral and acidic pH. This pH-dependent fluorescence probe is based on the coral-derived protein Keima, which is targeted to the mitochondrial matrix<sup>24,244</sup>. Keima has a single emission peak at 620 nm with a bimodal excitation spectrum. In the alkaline environment of the cytoplasm, the shorter-wavelength (green) excitation predominates. Within the acidic lysosome, the Keima protein undergoes a gradual shift to the longer-wavelength (red) excitation, with partial overlap in the emission spectra. These properties of mt-Keima allow rapid and faithful determination of “acidic” mitochondria undergoing autolysosome degradation. The mt-Keima assay showed that CCCP-induced mitophagy was impaired in cells downregulating CaN (Figure 5I), in line with the biochemical approaches.

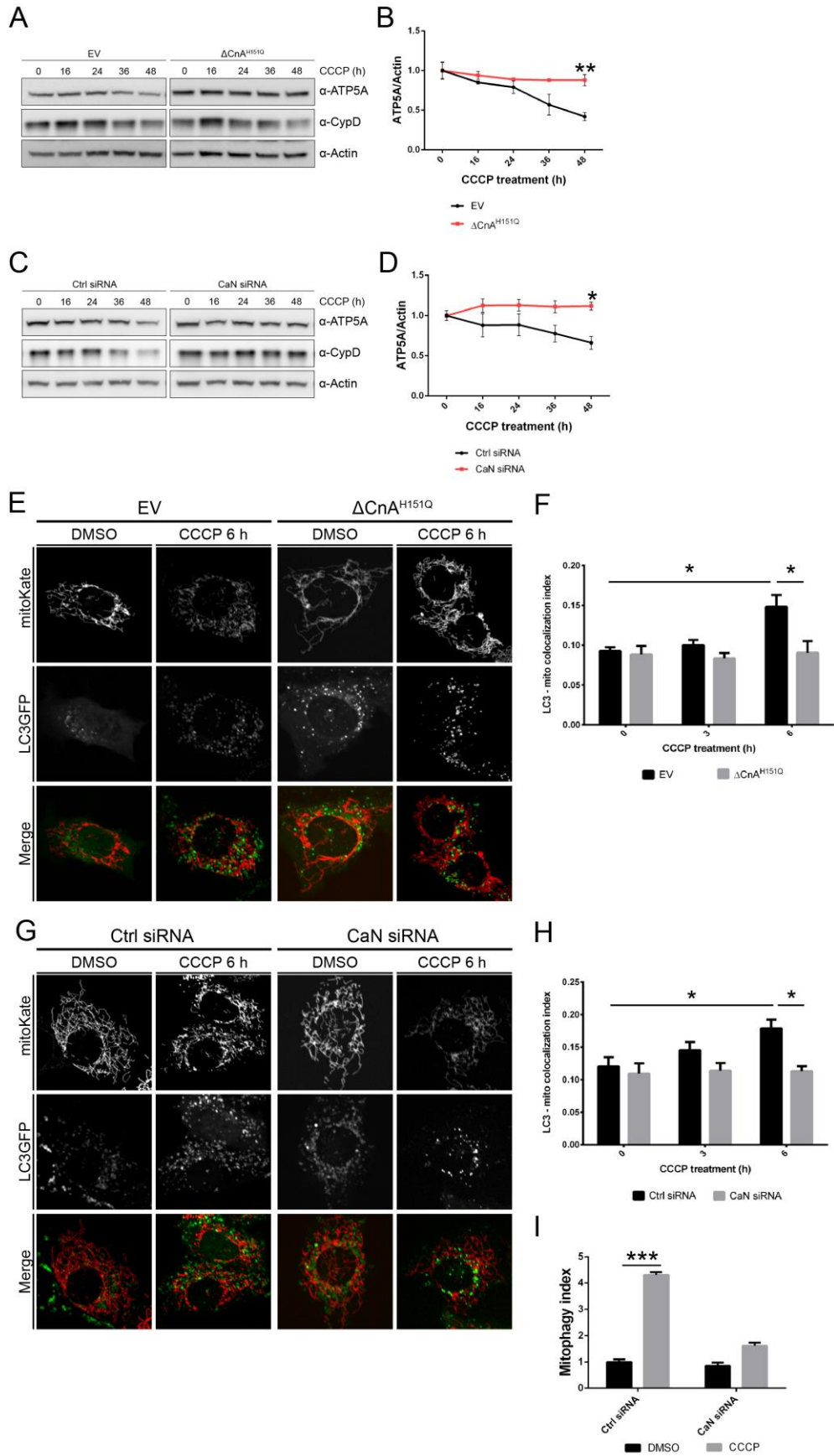


**Figura 5:** (A) Western blot of MEFs cells overexpressing Calcineurin dominant negative mutant and relative control. Cells were treated with 10  $\mu$ M CCCP for the indicated time. (B) Quantification of (A) Graph bars show mean $\pm$ SEM of ATP5A protein level normalized on Actin. (C) Western blot of MEFs cells downregulating Calcineurin and relative control. Cells were treated with 10  $\mu$ M CCCP for the indicated time. (D) Quantification of (C) Graph bars show mean $\pm$ SEM of ATP5A protein level normalized on Actin. (E) Parkin-flag MEFs transfected with LC3GFP and MitoKate with the expression of CaN dominant negative and relative control. (F) Squash analysis of colocalization of (E). (G) Parkin-flag MEFs transfected with LC3GFP and MitoKate with CaN downregulation and relative control. (H) Squash analysis of colocalization of (G). (I) Mt-Keima analysis of Parkin expressing cells in CaN downregulation condition, and control.

### **Calcineurin constitutive active induces an increase in Parkin-basal mitophagy**

We previously demonstrated that the expression of constitutive active CaN leads to Parkin translocation even in absence of CCCP treatment. What about mitophagy? To address this question, we performed mt-Keima assay in Parkin expressing MEFs transiently transfected with constitutively active CaN. In this condition, basal mitophagy (i.e. non-intoxicated cells) resulted significantly increased (Figure 6A-B). As observed for Parkin translocation (Figure 3B-C), CCCP treatment did not exacerbate mitophagy in cells expressing constitutive active CaN. Representative image of mt-Keima acquired at confocal microscope clearly showed increased number of red fluorescence in non-intoxicated cells expressing constitutively active CaN, indicative of enhanced mitophagy in this condition. (Figure 6A). Furthermore, qualitative electron microscopy observation demonstrated an increase in autophagosomes and autolysosomes with mitochondrial like structures inside, in CaN constitutively active expressing MEFs, compared to controls (Figure 6C).



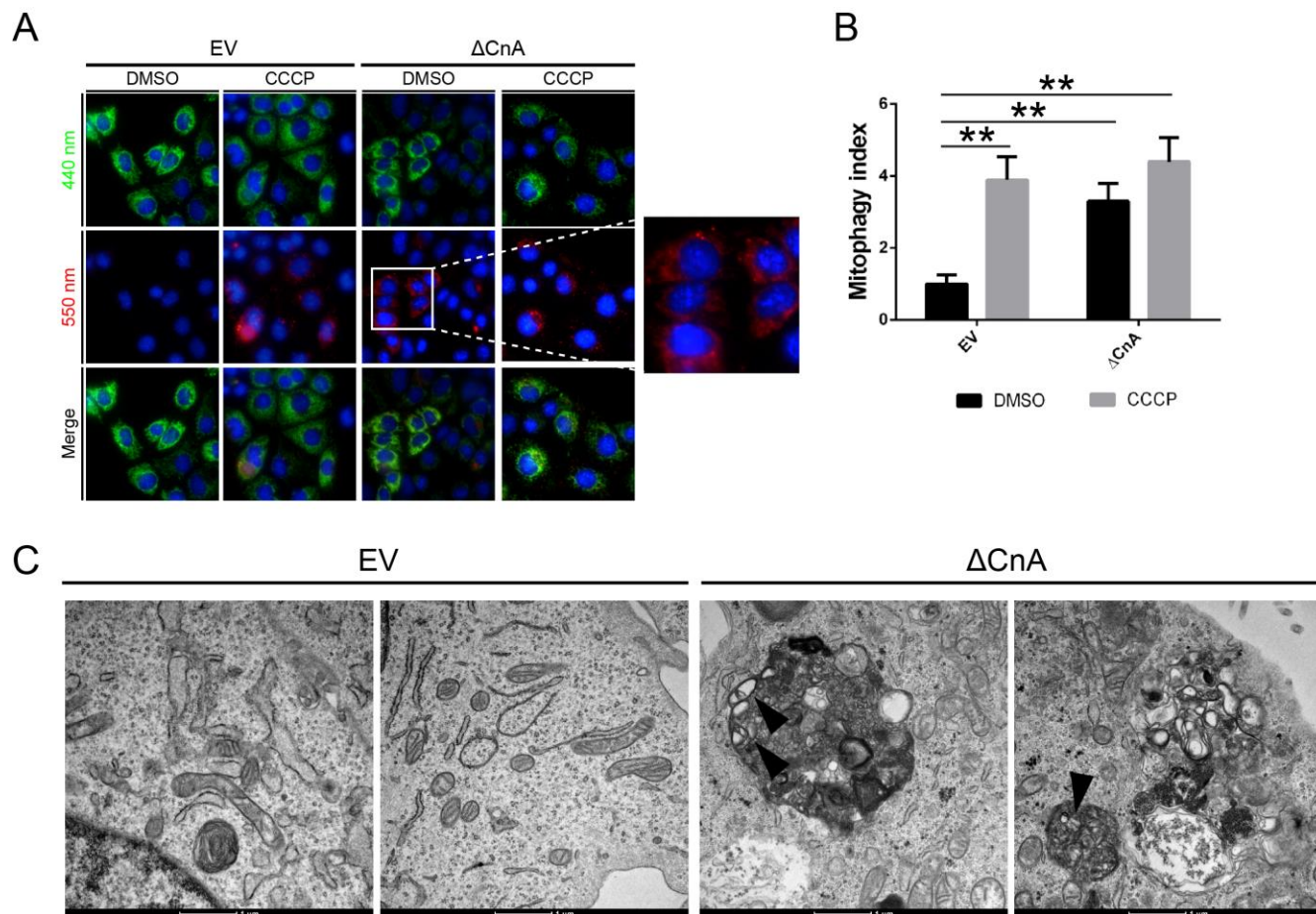


**Figure 6:** (A) Representative image of mt-Keima acquired on confocal microscope Operetta High-Content Imaging system. (B) Mt-Keima mitophagy index in Parkin-flag wildtype MEFs upon CaN constitutively activation and relative control. (C) Representative electron microscope images showing the presence of autophagosomes in Parkin-flag stable line expressing CaN constitutive active ( $\Delta$ CnA).

## Calcineurin requires PINK1 expression to induce mitophagy

While investigating Parkin translocation in PINK1 KO background, we came across the unexpected finding that expression of constitutive active CaN was able to trigger Parkin translocation in the absence of PINK1 (Figure 3A-C). Stress-induced mitophagy was impaired in PINK1 KO background, as expected (Figure 7A-B). Intriguingly, we found that in PINK1 KO cells, expression of constitutive active CaN failed to promote the degradation of mitochondrial proteins ATP5A and CypD (Figure 7C-D). These quantitative immunoblotting data were confirmed by mt-Keima assay (Figure 7E). Thus, CaN activation promotes Parkin recruitment, but requires PINK1 to execute mitophagy.

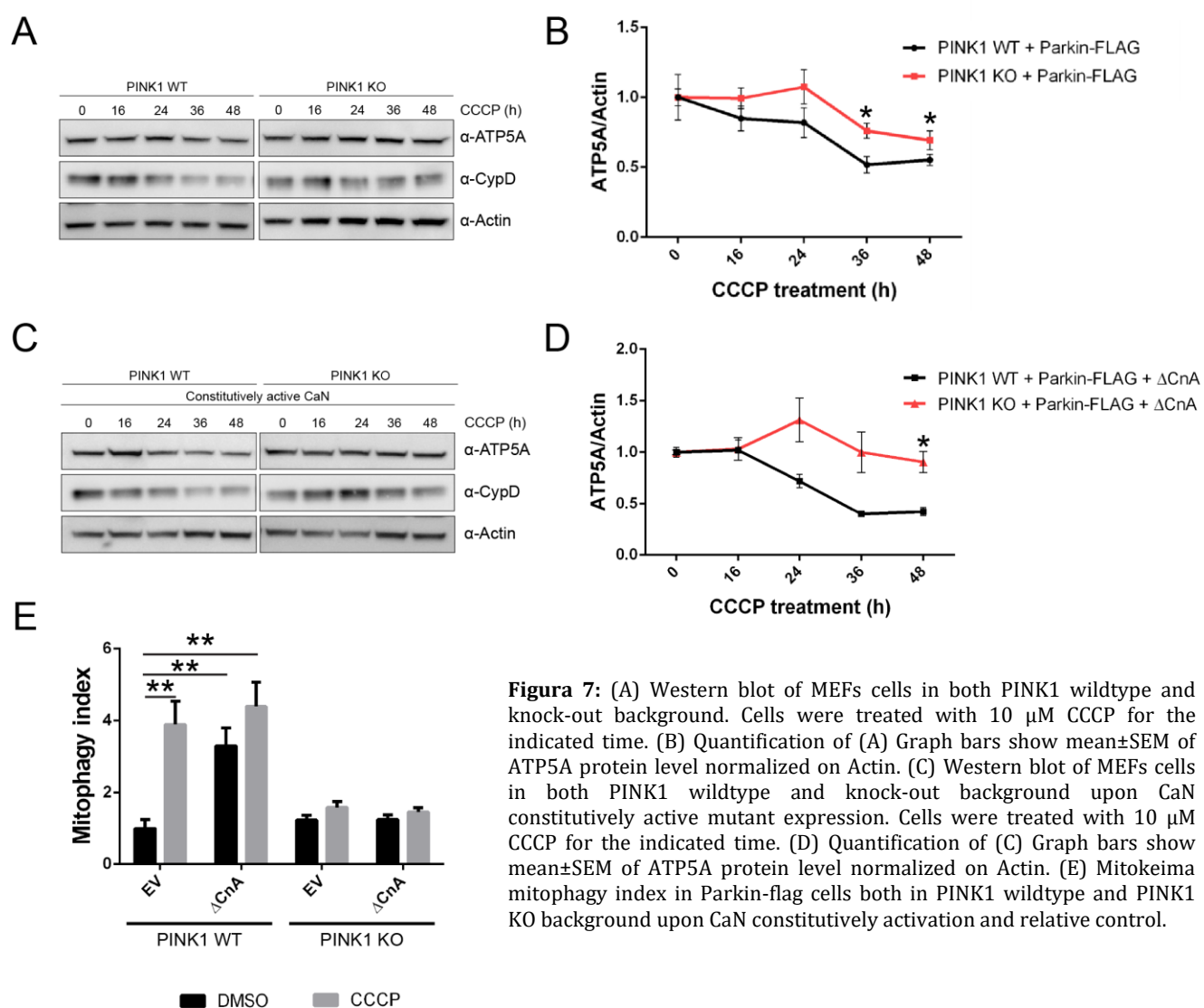


**Figure 7:** (A) Western blot of MEFs cells in both PINK1 wildtype and knock-out background. Cells were treated with 10  $\mu$ M CCCP for the indicated time. (B) Quantification of (A) Graph bars show mean $\pm$ SEM of ATP5A protein level normalized on Actin. (C) Western blot of MEFs cells in both PINK1 wildtype and knock-out background upon CaN constitutively active mutant expression. Cells were treated with 10  $\mu$ M CCCP for the indicated time. (D) Quantification of (C) Graph bars show mean $\pm$ SEM of ATP5A protein level normalized on Actin. (E) Mitokeima mitophagy index in Parkin-flag cells both in PINK1 wildtype and PINK1 KO background upon CaN constitutively activation and relative control.

## DISCUSSION

The molecular events that are leading to neurodegeneration of dopaminergic neurons in PD are not completely understood. In the last decade, research on genes directly linked to familiar forms of the disease, like PINK1, Parkin, DJ-1, LRRK2,  $\alpha$ -synuclein, provided new insights into PD pathogenesis, improving our understanding of the molecular mechanisms underlying the disease. Because sporadic and familiar PD cases are almost indistinguishable at the systemic and cellular level, genetic cases can provide the basis to tackle key events that are leading to neurodegeneration, and potentially identify therapeutic targets. What many neurodegenerative diseases have in common is the accumulation of cytoplasmic inclusions made of misfolded proteins and organelles, like mitochondria. Indeed, dysfunctional, deformed and swollen mitochondria are commonly found in *post mortem* tissue deriving from PD patients, and in cellular models of PD. Thanks to recent studies on the molecular targets of PINK1 and Parkin, two genes which mutations have been linked to the onset of an autosomal recessive juvenile parkinsonism, it became clear that malfunction in the mitochondria quality control might contribute to neurodegeneration by accumulating defective mitochondria. In a set of remarkable discoveries, it was found that mitophagy, a selective kind of autophagy during which defective mitochondria are recognized and degraded, depends on PINK1 and Parkin. PINK1, a Serine/threonine kinase, is stabilized on depolarized mitochondria to recruit the E3 ubiquitin ligase Parkin. Under basal conditions, Parkin exists in an inactive globular form, that resembles a coiled snake and it is repressed by several mechanisms of autoinhibition. Recently, high resolution Parkin crystal structure gave insight into the mechanisms of Parkin autoinhibition, suggesting that Parkin recruitment is a multistep process, which is likely to be regulated by several post-translational modifications, including phosphorylation, ubiquitination, nitrosylation, sumoylation and possibly others not yet characterized modifications. Supporting this hypothesis, it was found that PINK1 phosphorylates Parkin and Ubiquitin on Serine 65<sup>92</sup>, which is an absolute requirement for Parkin translocation and activity<sup>245</sup>. Once on mitochondria, Parkin ubiquitinates a subset of outer mitochondrial membrane (OMM) resident proteins, thereby priming depolarized mitochondria for autophagy-dependent degradation. Ubiquitin decorated mitochondria work as bait for the recruitment of autophagosomes to ubiquitinated protein aggregates, via autophagy adaptors like p62 (SQSTM1)<sup>246</sup>, HDAC6<sup>247</sup>, Optineurin and NDP52<sup>248</sup>.

The autophagic engulfment of dysfunctional mitochondria needs to be paralleled by a tight control of mitochondrial shape. Of note, mitochondria fragment prior to mitophagy, and mitochondrial fusion<sup>5</sup> and mobility<sup>192,249</sup> is inhibited to prevent intoxication of the entire mitochondrial network. As shown in many studies, CCCP treatment is perhaps the most consolidated stimulus to promote Parkin translocation and mitophagy. CCCP is a mitochondrial uncoupler that triggers mitochondrial depolarization by transporting protons inside the mitochondrial matrix. The addition of the protonophore CCCP induces a transient increase of Ca<sup>2+</sup> influx that promotes CaN activation<sup>20</sup>; CaN activation in this context promotes Drp1 translocation to mitochondria to induce mitochondrial fission<sup>21</sup>, which is required in the orchestration of the mitophagy process<sup>22</sup>; CaN can also specifically be activated by lysosomal Ca<sup>2+</sup> release to promote the transcription of autophagy genes via TFEB<sup>23</sup>.

With that in mind, we thought to investigate the potential role of CaN in the regulation of Parkin translocation and Parkin-dependent mitophagy. We found that both chemical and genetic inhibition of CaN resulted in impaired Parkin mitochondrial recruitment upon CCCP intoxication. Intriguingly, constitutive active CaN was able to induce Parkin translocation under basal conditions, even in the absence of PINK1. We corroborated this unexpected finding with data showing a decrease in Parkin thermal stability, indicative of protein conformational change in this condition. At present two hypothesis are under investigation to explain the functional tie between Parkin and CaN: (i) CaN physically interacts with Parkin to release the autoinhibitory state of Parkin, and promote the conformational change that is required for Parkin translocation; (ii) the effect being shown is an indirect effect of CaN function in unrelated pathways that nevertheless impinge on Parkin translocation. One of these pathways could involve the role of CaN in cytoskeleton reorganization<sup>154</sup>.

In line with the translocation studies, we found that CaN inhibition blocked CCCP-induced mitophagy, while its activation enhances mitochondrial degradation, even in the absence of intoxication. It is interesting to note that PINK1 is an absolute requirement for CaN-dependent mitophagy. Although Parkin is efficiently recruited to mitochondria in PINK1 KO cells expressing constitutive active CaN, this is not sufficient to promote mitophagy. A number of hypothesis are under consideration to explain this result: (i) PINK1 is required to prime Parkin targets and Ubiquitin, to promote Parkin activity; (ii) PINK1 is required to recruit Drp1 to mitochondria and promote mitochondrial fission. Thus, in the absence of PINK1 mitochondria do not fragment to

allow mitophagy to occur; (iii) PINK1 is required for the mitochondrial recruitment of the autophagy adaptors that are indispensable for autophagosome docking. .

Further studies are required to deeply elucidate the nature of this functional interaction and, possibly, identify additional CaN targets that might play a role in basal mitophagy.

In conclusion, here we show a fundamental role for the Ca<sup>2+</sup>-Calmodulin dependent protein phosphatase CaN in the regulation of Parkin translocation and mitophagy. This study highlighted an unprecedented role for Ca<sup>2+</sup> and Ca<sup>2+</sup>-dependent phosphatase CaN in the regulation of Parkin translocation, and dissected a novel protective pathway, which can be potentially activated following physiological Ca<sup>2+</sup> rise.

## MATERIALS AND METHODS

**Antibodies.** The following antibodies were used for western blot experiments: Actin (1:5000; Chemicon; MAB1501), ATP5A (1:5000; Abcam; ab14748), Calcineurin (1:1000; BD Bioscience; 556350), Cyclophilin D (1:1000; Abcam; ab110324), Parkin (1:1000, Santa Cruz; SC32282). Secondary antibodies used were sheep anti-mouse or donkey anti-rabbit HRP (GE Healthcare).

**Cells and culture conditions.** MEFs were maintained in DMEM culture media (Life Technologies supplemented with 10% (v/v) fetal bovine serum (Life Technologies), 0,1 mM minimal essential medium nonessential amino acids, 2mM L-glutamine, 50 U ml<sup>-1</sup> penicillin and 50 µg ml<sup>-1</sup> (Life Technologies) and cultured in a 5% CO<sub>2</sub> atmosphere at 37 °C. PINK1 Wildtype and knock-out cells were kindly provided by Prof. Francesco Cecconi lab (Danish Cancer Society, Denmark) and Prof. Juan Pedro Bolaños lab (Universidad de Salamanca, Spain).

**Drug and cellular treatments.** The following drugs were used: CCCP 10 µM (Sigma-Aldrich), Rotenone 2µM (Sigma-Aldrich), Oligomycin 1 mg/ml (Sigma-Aldrich), Antimycin A 2,5 µM (Sigma-Aldrich).

**Electron microscopy.** Samples were fixed with 2.5% glutaraldehyde in 0.1M sodium cacodylate buffer pH 7.4 ON at 4°C. The samples was postfixed with 1% osmium tetroxide plus potassium ferrocyanide 1% in 0.1M sodium cacodylate buffer for 1 hour at 4°. After three water washes, samples were dehydrated in a graded ethanol series and embedded in an epoxy resin (Sigma-Aldrich). Ultrathin sections (60-70nm) were obtained with an Ultratome V (LKB) ultramicrotome, counterstained with uranyl acetate and lead citrate and viewed with a Tecnai G 2 (FEI) transmission electron microscope operating at 100 kV. Images were captured with a Veleta (Olympus Soft Imaging System) digital camera.

**Transient transfection and siRNA knockdown.** Cells were transiently transfected with plasmid DNA using PEI (Polysciences, 24765) according to manufacturer's instructions. GFP-LAMP1 and GFP-Rab5 were purchased from Addgene. ΔCnA plasmid and CnB were a gift from Gian Paolo Fadini (Veneto Institute of Molecular Medicine, Italy). ΔCnA<sup>H151Q</sup> was a gift from Luca Scorrano (Department of Biology, Italy). mCherry Parkin and mitoYFP were already available in the lab.

Cells were silenced with Calcineurin siRNA oligo duplex (OriGene, SR416619) by direct transfection, using Transfectin (BIO-RAD) according to the protocol of the manufacturer. siRNA-transfected cells were collected after 48 h.

**Production of lentiviral particles and infection.** LV-mitoKeima was kindly provided by Toren Finkel (Center for Molecular Medicine, National Heart, Lung, and Blood Institute, NIH, Bethesda, MD, USA). HEK293T cells were seeded onto 100 mm Petri dishes. 24 h after plating, cells were co-transfected using PEI with LV-mitokeima and the packaging plasmids pMDLg/pRRE, pRSV-Rev, pMD2.G. After 8 h, the transfection medium was replaced with fresh culture medium. 2 million MEFs were seeded onto 60 mm Petri dishes. After 48 h, the cells medium was collected and mixed with 6 µg/ml of Polybrene. Receiver MEFs were infected for 36 h, before changing the medium. All procedures for the production and use of lentiviral particles were performed in a biosafety level-2 environment.

**Retroviral infection and generation of Parkin-flag stable cell lines.** To generate Parkin-flag retroviruses, HEK 293T cells were plated at 2 M cells/100-mm-diameter tissue culture dishes and transfected with the pN8E VSGV, Gag-pol packaging vectors and the retroviral vector (empty or containing Parkin-flag) by PEI direct transfection. At 5 h post-transfection, the medium was replaced with fresh DMEM containing 10% FBS, and cells were grown for an additional 24 h, the transfection was repeated. After 24 h, the conditioned medium containing recombinant retroviruses was collected and filtered through 0.45 µm-pore-size filters. Samples of these supernatants were applied immediately to MEFs cells, which had been plated 18 h before infection at a density of 105 cells/60-mm-diameter tissue culture dishes. Polybrene was added to a final concentration of 6 µg/ml, and the supernatants were incubated with the cells for 24 h. After infection, the cells were placed in fresh growth medium and cultured as usual. Selection with 200 µg of Hygromycin B/ml (Sigma-Aldrich) was initiated 24 h after infection. After about 15 days, cells were expanded.

**Mitokeima mitophagy analysis by flow cytometry.** Mitokeima expressing MEFs were analyzed by flow cytometry (BD FACSAria™ sorter) as previously reported<sup>250</sup>. PE-mcherry excitation wavelength 561 nm and emission 610 nm, BV605 excitation wavelength 405 nm and

emission 605 nm were used to detect m-Keima in mitochondria in the cytosol. Excitation ... nm and emission were used to detect mitochondria in lysosomes.

**Thermal shift assay.** Cells were plated onto 100 mm Petri dishes (10 M/dish). After 24 h transfection was performed using PEI with  $\Delta$ CnA and CnB plasmids and the corresponding empty vectors. After 48 h from the transfection, cells were resuspended in PBS and snap-frozen in liquid nitrogen. The solution was aliquot into a PCR strip and incubated at the indicated temperatures for 3 min. The lysates were centrifuged at 16'000 g for 30 min at 4 °C. The soluble fraction was loaded into SDS-PAGE gel.

**Imaging acquisition and processing.** MEFs were plated on 35 mm round glass coverslips and co-transfected with mito-YFP and Parkin-Cherry and the indicated plasmids for 48h before imaging. Images were acquired using an UPlanSApo 60X/1.35 objective (iMIC Adromeda) upon excitation with 561 and 488 lasers. The percentage of Parkin puncta colocalization with mitochondria was measured with an ImageJ colocalization plugin (Squassh).

**Western blotting.** Cells were lysed in 50 mM Tris-HCl pH 7.4, 150 mM NaCl, 1 mM EDTA, 1% NP-40, 0,25% Sodium Deoxycholate, Protease inhibitor cocktail (Sigma) and PhosSTOP (Roche). Lysate were cleared by centrifugation at 20'000 g for 15 min at 4 °C. Proteins were separated on ExpressPlus™ PAGE gels (GenScript) and transferred to PVDF membrane (Millipore). Membranes were incubated with indicated antibodies and imaged with ImageQuant LAS4000. Band densitometry quantification was performed using ImageJ software.

**Statistical analysis.** All values are expressed as Mean  $\pm$  standard error of mean (SEM). Statistical analyses were per-formed using Student's t-test. P-value <0.05 was considered statistically significant.



## REFERENCES

1. Bonora, M., Bravo-San Pedro, J.M., Kroemer, G., Galluzzi, L. & Pinton, P. Novel insights into the mitochondrial permeability transition. *Cell Cycle* **13**, 2666-2670 (2014).
2. De Marchi, E., Bonora, M., Giorgi, C. & Pinton, P. The mitochondrial permeability transition pore is a dispensable element for mitochondrial calcium efflux. *Cell Calcium* **56**, 1-13 (2014).
3. Narendra, D., Walker, J.E. & Youle, R. Mitochondrial quality control mediated by PINK1 and Parkin: links to parkinsonism. *Cold Spring Harb Perspect Biol* **4**(2012).
4. Narendra, D.P., *et al.* PINK1 is selectively stabilized on impaired mitochondria to activate Parkin. *PLoS Biol* **8**, e1000298 (2010).
5. Tanaka, A., *et al.* Proteasome and p97 mediate mitophagy and degradation of mitofusins induced by Parkin. *J Cell Biol* **191**, 1367-1380 (2010).
6. Youle, R.J. & Narendra, D.P. Mechanisms of mitophagy. *Nat Rev Mol Cell Biol* **12**, 9-14 (2011).
7. Arber, C.E., Li, A., Houlden, H. & Wray, S. Review: Insights into molecular mechanisms of disease in neurodegeneration with brain iron accumulation: unifying theories. *Neuropathol Appl Neurobiol* **42**, 220-241 (2016).
8. Ashrafi, G. & Schwarz, T.L. PINK1- and PARK2-mediated local mitophagy in distal neuronal axons. *Autophagy* **11**, 187-189 (2015).
9. Beilina, A. & Cookson, M.R. Genes associated with Parkinson's disease: regulation of autophagy and beyond. *J Neurochem* **139 Suppl 1**, 91-107 (2016).
10. Farrer, M.J. Genetics of Parkinson disease: paradigm shifts and future prospects. *Nat Rev Genet* **7**, 306-318 (2006).
11. Kitada, T., *et al.* Mutations in the parkin gene cause autosomal recessive juvenile parkinsonism. *Nature* **392**, 605-608 (1998).
12. Valente, E.M., *et al.* PINK1 mutations are associated with sporadic early-onset parkinsonism. *Ann Neurol* **56**, 336-341 (2004).
13. Narendra, D., Tanaka, A., Suen, D.F. & Youle, R.J. Parkin is recruited selectively to impaired mitochondria and promotes their autophagy. *J Cell Biol* **183**, 795-803 (2008).
14. Clark, I.E., *et al.* Drosophila pink1 is required for mitochondrial function and interacts genetically with parkin. *Nature* **441**, 1162-1166 (2006).
15. Yang, Y., *et al.* Mitochondrial pathology and muscle and dopaminergic neuron degeneration caused by inactivation of Drosophila Pink1 is rescued by Parkin. *Proc Natl Acad Sci U S A* **103**, 10793-10798 (2006).
16. Park, J., *et al.* Mitochondrial dysfunction in Drosophila PINK1 mutants is complemented by parkin. *Nature* **441**, 1157-1161 (2006).
17. Park, J., Kim, Y. & Chung, J. Mitochondrial dysfunction and Parkinson's disease genes: insights from Drosophila. *Dis Model Mech* **2**, 336-340 (2009).
18. McWilliams, T.G., *et al.* Basal Mitophagy Occurs Independently of PINK1 in Mouse Tissues of High Metabolic Demand. *Cell Metab* **27**, 439-449 e435 (2018).
19. Trempe, J.F., *et al.* Structure of parkin reveals mechanisms for ubiquitin ligase activation. *Science* **340**, 1451-1455 (2013).
20. Snyder, S.H. & Sabatini, D.M. Immunophilins and the nervous system. *Nat Med* **1**, 32-37 (1995).
21. Cereghetti, G.M., *et al.* Dephosphorylation by calcineurin regulates translocation of Drp1 to mitochondria. *Proc Natl Acad Sci U S A* **105**, 15803-15808 (2008).
22. Twig, G. & Shirihai, O.S. The interplay between mitochondrial dynamics and mitophagy. *Antioxid Redox Signal* **14**, 1939-1951 (2011).
23. Medina, D.L., *et al.* Lysosomal calcium signalling regulates autophagy through calcineurin and TFEB. *Nat Cell Biol* **17**, 288-299 (2015).

24. Sun, N., *et al.* A fluorescence-based imaging method to measure in vitro and in vivo mitophagy using mt-Keima. *Nat Protoc* **12**, 1576-1587 (2017).
25. Rizek, P., Kumar, N. & Jog, M.S. An update on the diagnosis and treatment of Parkinson disease. *CMAJ* **188**, 1157-1165 (2016).
26. Hartmann, A. Postmortem studies in Parkinson's disease. *Dialogues Clin Neurosci* **6**, 281-293 (2004).
27. Weber, G. [Cholinesterase content of the brain in cerebral tumors and paralysis agitans]. *Bull Schweiz Akad Med Wiss* **8**, 263-268 (1952).
28. Drozak, J. & Bryla, J. [Dopamine: not just a neurotransmitter]. *Postepy Hig Med Dosw (Online)* **59**, 405-420 (2005).
29. Chan, C.S., *et al.* 'Rejuvenation' protects neurons in mouse models of Parkinson's disease. *Nature* **447**, 1081-1086 (2007).
30. Obeso, J.A., *et al.* Pathophysiology of the basal ganglia in Parkinson's disease. *Trends Neurosci* **23**, S8-19 (2000).
31. Pandya, M., Kubu, C.S. & Giroux, M.L. Parkinson disease: not just a movement disorder. *Cleve Clin J Med* **75**, 856-864 (2008).
32. Nagatsu, T. Tyrosine hydroxylase: human isoforms, structure and regulation in physiology and pathology. *Essays Biochem* **30**, 15-35 (1995).
33. Nagatsua, T. & Sawadab, M. L-dopa therapy for Parkinson's disease: past, present, and future. *Parkinsonism Relat Disord* **15 Suppl 1**, S3-8 (2009).
34. Ogawa, N. Levodopa and dopamine agonists in the treatment of Parkinson's disease: advantages and disadvantages. *Eur Neurol* **34 Suppl 3**, 20-28 (1994).
35. Seeberger, L.C. & Hauser, R.A. Levodopa/carbidopa/entacapone in Parkinson's disease. *Expert Rev Neurother* **9**, 929-940 (2009).
36. Finberg, J.P.M. Inhibitors of MAO-B and COMT: their effects on brain dopamine levels and uses in Parkinson's disease. *J Neural Transm (Vienna)* **126**, 433-448 (2019).
37. Shulman, J.M., De Jager, P.L. & Feany, M.B. Parkinson's disease: genetics and pathogenesis. *Annu Rev Pathol* **6**, 193-222 (2011).
38. Greenamyre, J.T., MacKenzie, G., Peng, T.I. & Stephans, S.E. Mitochondrial dysfunction in Parkinson's disease. *Biochem Soc Symp* **66**, 85-97 (1999).
39. Djarmati, A., *et al.* Detection of Parkin (PARK2) and DJ1 (PARK7) mutations in early-onset Parkinson disease: Parkin mutation frequency depends on ethnic origin of patients. *Hum Mutat* **23**, 525 (2004).
40. Bonifati, V., *et al.* Mutations in the DJ-1 gene associated with autosomal recessive early-onset parkinsonism. *Science* **299**, 256-259 (2003).
41. Morais, V.A., *et al.* Parkinson's disease mutations in PINK1 result in decreased Complex I activity and deficient synaptic function. *EMBO Mol Med* **1**, 99-111 (2009).
42. Parker, W.D., Jr., Parks, J.K. & Swerdlow, R.H. Complex I deficiency in Parkinson's disease frontal cortex. *Brain Res* **1189**, 215-218 (2008).
43. Hauser, D.N. & Hastings, T.G. Mitochondrial dysfunction and oxidative stress in Parkinson's disease and monogenic parkinsonism. *Neurobiol Dis* **51**, 35-42 (2013).
44. Mehra, S., Sahay, S. & Maji, S.K. alpha-Synuclein misfolding and aggregation: Implications in Parkinson's disease pathogenesis. *Biochim Biophys Acta Proteins Proteom* **1867**, 890-908 (2019).
45. Calne, D.B. & Langston, J.W. Aetiology of Parkinson's disease. *Lancet* **2**, 1457-1459 (1983).
46. Di Monte, D.A., Lavasani, M. & Manning-Bog, A.B. Environmental factors in Parkinson's disease. *Neurotoxicology* **23**, 487-502 (2002).
47. Dauer, W. & Przedborski, S. Parkinson's disease: mechanisms and models. *Neuron* **39**, 889-909 (2003).
48. Mizuno, Y., Sone, N. & Saitoh, T. Effects of 1-methyl-4-phenyl-1,2,3,6-tetrahydropyridine and 1-methyl-4-phenylpyridinium ion on activities of the enzymes in the electron transport system in mouse brain. *J Neurochem* **48**, 1787-1793 (1987).

49. Barbeau, A., Dallaire, L., Buu, N.T., Poirier, J. & Rucinska, E. Comparative behavioral, biochemical and pigmentary effects of MPTP, MPP+ and paraquat in *Rana pipiens*. *Life Sci* **37**, 1529-1538 (1985).
50. Kuter, K., *et al.* Toxic influence of subchronic paraquat administration on dopaminergic neurons in rats. *Brain Res* **1155**, 196-207 (2007).
51. Wang, X.F., Li, S., Chou, A.P. & Bronstein, J.M. Inhibitory effects of pesticides on proteasome activity: implication in Parkinson's disease. *Neurobiol Dis* **23**, 198-205 (2006).
52. Abbas, M.M., *et al.* Early Onset Parkinson's disease due to DJ1 mutations: An Indian study. *Parkinsonism Relat Disord* **32**, 20-24 (2016).
53. Bonifati, V. Autosomal recessive parkinsonism. *Parkinsonism Relat Disord* **18 Suppl 1**, S4-6 (2012).
54. Bonifati, V., *et al.* Early-onset parkinsonism associated with PINK1 mutations: frequency, genotypes, and phenotypes. *Neurology* **65**, 87-95 (2005).
55. Polymeropoulos, M.H., *et al.* Mutation in the alpha-synuclein gene identified in families with Parkinson's disease. *Science* **276**, 2045-2047 (1997).
56. Zimprich, A., *et al.* Mutations in LRRK2 cause autosomal-dominant parkinsonism with pleomorphic pathology. *Neuron* **44**, 601-607 (2004).
57. Bonifati, V., *et al.* DJ-1 (PARK7), a novel gene for autosomal recessive, early onset parkinsonism. *Neurol Sci* **24**, 159-160 (2003).
58. Najim al-Din, A.S., Wriekat, A., Mubaidin, A., Dasouki, M. & Hiari, M. Pallido-pyramidal degeneration, supranuclear upgaze paresis and dementia: Kufor-Rakeb syndrome. *Acta Neurol Scand* **89**, 347-352 (1994).
59. Kim, C.Y. & Alcalay, R.N. Genetic Forms of Parkinson's Disease. *Semin Neurol* **37**, 135-146 (2017).
60. Mbefo, M.K., *et al.* Parkinson disease mutant E46K enhances alpha-synuclein phosphorylation in mammalian cell lines, in yeast, and in vivo. *J Biol Chem* **290**, 9412-9427 (2015).
61. Klein, C. & Schlossmacher, M.G. The genetics of Parkinson disease: Implications for neurological care. *Nat Clin Pract Neurol* **2**, 136-146 (2006).
62. Book, A., *et al.* A Meta-Analysis of alpha-Synuclein Multiplication in Familial Parkinsonism. *Front Neurol* **9**, 1021 (2018).
63. Klein, C. & Westenberger, A. Genetics of Parkinson's disease. *Cold Spring Harb Perspect Med* **2**, a008888 (2012).
64. Mills, R.D., Mulhern, T.D., Cheng, H.C. & Culvenor, J.G. Analysis of LRRK2 accessory repeat domains: prediction of repeat length, number and sites of Parkinson's disease mutations. *Biochem Soc Trans* **40**, 1086-1089 (2012).
65. Cookson, M.R. Mechanisms of Mutant LRRK2 Neurodegeneration. *Adv Neurobiol* **14**, 227-239 (2017).
66. Bandyopadhyay, S. & Cookson, M.R. Evolutionary and functional relationships within the DJ1 superfamily. *BMC Evol Biol* **4**, 6 (2004).
67. Muftuoglu, M., *et al.* Mitochondrial complex I and IV activities in leukocytes from patients with parkin mutations. *Mov Disord* **19**, 544-548 (2004).
68. Kilarski, L.L., *et al.* Systematic review and UK-based study of PARK2 (parkin), PINK1, PARK7 (DJ-1) and LRRK2 in early-onset Parkinson's disease. *Mov Disord* **27**, 1522-1529 (2012).
69. Schubert, A.F., *et al.* Structure of PINK1 in complex with its substrate ubiquitin. *Nature* **552**, 51-56 (2017).
70. Deas, E., *et al.* PINK1 cleavage at position A103 by the mitochondrial protease PARL. *Hum Mol Genet* **20**, 867-879 (2011).
71. Greene, A.W., *et al.* Mitochondrial processing peptidase regulates PINK1 processing, import and Parkin recruitment. *EMBO Rep* **13**, 378-385 (2012).
72. Pogson, J.H., Ivatt, R.M. & Whitworth, A.J. Molecular mechanisms of PINK1-related neurodegeneration. *Curr Neurol Neurosci Rep* **11**, 283-290 (2011).
73. Kazlauskaitė, A., *et al.* Parkin is activated by PINK1-dependent phosphorylation of ubiquitin at Ser65. *Biochem J* **460**, 127-139 (2014).

74. Koyano, F. & Matsuda, N. Molecular mechanisms underlying PINK1 and Parkin catalyzed ubiquitylation of substrates on damaged mitochondria. *Biochim Biophys Acta* **1853**, 2791-2796 (2015).
75. Okatsu, K., *et al.* Structural insights into ubiquitin phosphorylation by PINK1. *Sci Rep* **8**, 10382 (2018).
76. Shiba-Fukushima, K., Inoshita, T., Hattori, N. & Imai, Y. PINK1-mediated phosphorylation of Parkin boosts Parkin activity in *Drosophila*. *PLoS Genet* **10**, e1004391 (2014).
77. Pryde, K.R., Smith, H.L., Chau, K.Y. & Schapira, A.H. PINK1 disables the anti-fission machinery to segregate damaged mitochondria for mitophagy. *J Cell Biol* **213**, 163-171 (2016).
78. Dickey, A.S. & Strack, S. PKA/AKAP1 and PP2A/Bbeta2 regulate neuronal morphogenesis via Drp1 phosphorylation and mitochondrial bioenergetics. *J Neurosci* **31**, 15716-15726 (2011).
79. Gomes, L.C., Di Benedetto, G. & Scorrano, L. During autophagy mitochondria elongate, are spared from degradation and sustain cell viability. *Nat Cell Biol* **13**, 589-598 (2011).
80. Wang, X., *et al.* PINK1 and Parkin target Miro for phosphorylation and degradation to arrest mitochondrial motility. *Cell* **147**, 893-906 (2011).
81. Caulfield, T.R., Fiesel, F.C. & Springer, W. Activation of the E3 ubiquitin ligase Parkin. *Biochem Soc Trans* **43**, 269-274 (2015).
82. Liu, W., *et al.* PINK1 defect causes mitochondrial dysfunction, proteasomal deficit and alpha-synuclein aggregation in cell culture models of Parkinson's disease. *PLoS One* **4**, e4597 (2009).
83. Gegg, M.E., Cooper, J.M., Schapira, A.H. & Taanman, J.W. Silencing of PINK1 expression affects mitochondrial DNA and oxidative phosphorylation in dopaminergic cells. *PLoS One* **4**, e4756 (2009).
84. Lucking, C.B., *et al.* Association between early-onset Parkinson's disease and mutations in the parkin gene. *N Engl J Med* **342**, 1560-1567 (2000).
85. Tenno, T., *et al.* Structural basis for distinct roles of Lys63- and Lys48-linked polyubiquitin chains. *Genes Cells* **9**, 865-875 (2004).
86. Hicke, L. Protein regulation by monoubiquitin. *Nat Rev Mol Cell Biol* **2**, 195-201 (2001).
87. Miranda, M. & Sorkin, A. Regulation of receptors and transporters by ubiquitination: new insights into surprisingly similar mechanisms. *Mol Interv* **7**, 157-167 (2007).
88. Grabbe, C. & Dikic, I. Functional roles of ubiquitin-like domain (ULD) and ubiquitin-binding domain (UBD) containing proteins. *Chem Rev* **109**, 1481-1494 (2009).
89. Kane, L.A., *et al.* PINK1 phosphorylates ubiquitin to activate Parkin E3 ubiquitin ligase activity. *J Cell Biol* **205**, 143-153 (2014).
90. Karbowski, M. & Youle, R.J. Regulating mitochondrial outer membrane proteins by ubiquitination and proteasomal degradation. *Curr Opin Cell Biol* **23**, 476-482 (2011).
91. Iguchi, M., *et al.* Parkin-catalyzed ubiquitin-ester transfer is triggered by PINK1-dependent phosphorylation. *J Biol Chem* **288**, 22019-22032 (2013).
92. Kondapalli, C., *et al.* PINK1 is activated by mitochondrial membrane potential depolarization and stimulates Parkin E3 ligase activity by phosphorylating Serine 65. *Open Biol* **2**, 120080 (2012).
93. Wauer, T., Simicek, M., Schubert, A. & Komander, D. Mechanism of phospho-ubiquitin-induced PARKIN activation. *Nature* **524**, 370-374 (2015).
94. Chan, N.C., *et al.* Broad activation of the ubiquitin-proteasome system by Parkin is critical for mitophagy. *Hum Mol Genet* **20**, 1726-1737 (2011).
95. Lopez-Domenech, G., *et al.* Miro proteins coordinate microtubule- and actin-dependent mitochondrial transport and distribution. *EMBO J* **37**, 321-336 (2018).
96. Johnson, B.N., Berger, A.K., Cortese, G.P. & Lavoie, M.J. The ubiquitin E3 ligase parkin regulates the proapoptotic function of Bax. *Proc Natl Acad Sci U S A* **109**, 6283-6288 (2012).
97. Shin, J.H., *et al.* PARIS (ZNF746) repression of PGC-1alpha contributes to neurodegeneration in Parkinson's disease. *Cell* **144**, 689-702 (2011).
98. Castillo-Quan, J.I. Parkin' control: regulation of PGC-1alpha through PARIS in Parkinson's disease. *Dis Model Mech* **4**, 427-429 (2011).

99. Hampe, C., Ardila-Osorio, H., Fournier, M., Brice, A. & Corti, O. Biochemical analysis of Parkinson's disease-causing variants of Parkin, an E3 ubiquitin-protein ligase with monoubiquitylation capacity. *Hum Mol Genet* **15**, 2059-2075 (2006).
100. Imai, Y., Soda, M. & Takahashi, R. Parkin suppresses unfolded protein stress-induced cell death through its E3 ubiquitin-protein ligase activity. *J Biol Chem* **275**, 35661-35664 (2000).
101. Winklhofer, K.F. & Haass, C. Mitochondrial dysfunction in Parkinson's disease. *Biochim Biophys Acta* **1802**, 29-44 (2010).
102. Palade, G.E. An electron microscope study of the mitochondrial structure. *J Histochem Cytochem* **1**, 188-211 (1953).
103. Zick, M., Rabl, R. & Reichert, A.S. Cristae formation-linking ultrastructure and function of mitochondria. *Biochim Biophys Acta* **1793**, 5-19 (2009).
104. Hancock, R.E. Role of porins in outer membrane permeability. *J Bacteriol* **169**, 929-933 (1987).
105. Orth, M. & Schapira, A.H. Mitochondria and degenerative disorders. *Am J Med Genet* **106**, 27-36 (2001).
106. Cadenas, E. & Davies, K.J. Mitochondrial free radical generation, oxidative stress, and aging. *Free Radic Biol Med* **29**, 222-230 (2000).
107. Bosco, D.A., *et al.* Elevated levels of oxidized cholesterol metabolites in Lewy body disease brains accelerate alpha-synuclein fibrilization. *Nat Chem Biol* **2**, 249-253 (2006).
108. Nakabeppu, Y., Tsuchimoto, D., Yamaguchi, H. & Sakumi, K. Oxidative damage in nucleic acids and Parkinson's disease. *J Neurosci Res* **85**, 919-934 (2007).
109. Ferguson, S.M. & De Camilli, P. Dynamin, a membrane-remodelling GTPase. *Nat Rev Mol Cell Biol* **13**, 75-88 (2012).
110. Frohlich, C., *et al.* Structural insights into oligomerization and mitochondrial remodelling of dynamin 1-like protein. *EMBO J* **32**, 1280-1292 (2013).
111. Griparic, L., van der Wel, N.N., Orozco, I.J., Peters, P.J. & van der Bliek, A.M. Loss of the intermembrane space protein Mgm1/OPA1 induces swelling and localized constrictions along the lengths of mitochondria. *J Biol Chem* **279**, 18792-18798 (2004).
112. Cogliati, S., *et al.* Mitochondrial cristae shape determines respiratory chain supercomplexes assembly and respiratory efficiency. *Cell* **155**, 160-171 (2013).
113. Olichon, A., *et al.* Loss of OPA1 perturbs the mitochondrial inner membrane structure and integrity, leading to cytochrome c release and apoptosis. *J Biol Chem* **278**, 7743-7746 (2003).
114. Kim, J.Y., *et al.* Mitochondrial DNA content is decreased in autosomal dominant optic atrophy. *Neurology* **64**, 966-972 (2005).
115. Frezza, C., *et al.* OPA1 controls apoptotic cristae remodeling independently from mitochondrial fusion. *Cell* **126**, 177-189 (2006).
116. Ehses, S., *et al.* Regulation of OPA1 processing and mitochondrial fusion by m-AAA protease isoenzymes and OMA1. *J Cell Biol* **187**, 1023-1036 (2009).
117. Rojo, M., Legros, F., Chateau, D. & Lombes, A. Membrane topology and mitochondrial targeting of mitofusins, ubiquitous mammalian homologs of the transmembrane GTPase Fzo. *J Cell Sci* **115**, 1663-1674 (2002).
118. Griffin, E.E. & Chan, D.C. Domain interactions within Fzo1 oligomers are essential for mitochondrial fusion. *J Biol Chem* **281**, 16599-16606 (2006).
119. Ishihara, N., Eura, Y. & Mihara, K. Mitofusin 1 and 2 play distinct roles in mitochondrial fusion reactions via GTPase activity. *J Cell Sci* **117**, 6535-6546 (2004).
120. Pon, L.A. Mitochondrial fission: rings around the organelle. *Curr Biol* **23**, R279-281 (2013).
121. Rizzuto, R., *et al.* Mitochondria as biosensors of calcium microdomains. *Cell Calcium* **26**, 193-199 (1999).
122. Berridge, M.J., Lipp, P. & Bootman, M.D. The versatility and universality of calcium signalling. *Nat Rev Mol Cell Biol* **1**, 11-21 (2000).
123. Crompton, M., Moser, R., Ludi, H. & Carafoli, E. The interrelations between the transport of sodium and calcium in mitochondria of various mammalian tissues. *Eur J Biochem* **82**, 25-31 (1978).

124. Clapham, D.E. Calcium signaling. *Cell* **131**, 1047-1058 (2007).
125. Hoppe, U.C. Mitochondrial calcium channels. *FEBS Lett* **584**, 1975-1981 (2010).
126. Rapizzi, E., *et al.* Recombinant expression of the voltage-dependent anion channel enhances the transfer of Ca<sup>2+</sup> microdomains to mitochondria. *J Cell Biol* **159**, 613-624 (2002).
127. Griffiths, E.J. & Rutter, G.A. Mitochondrial calcium as a key regulator of mitochondrial ATP production in mammalian cells. *Biochim Biophys Acta* **1787**, 1324-1333 (2009).
128. Pinton, P., Giorgi, C., Siviero, R., Zecchini, E. & Rizzuto, R. Calcium and apoptosis: ER-mitochondria Ca<sup>2+</sup> transfer in the control of apoptosis. *Oncogene* **27**, 6407-6418 (2008).
129. Rizzuto, R. & Pozzan, T. Microdomains of intracellular Ca<sup>2+</sup>: molecular determinants and functional consequences. *Physiol Rev* **86**, 369-408 (2006).
130. Kohlhaas, M. & Maack, C. Calcium release microdomains and mitochondria. *Cardiovasc Res* **98**, 259-268 (2013).
131. Crabtree, G.R. Generic signals and specific outcomes: signaling through Ca<sup>2+</sup>, calcineurin, and NF-AT. *Cell* **96**, 611-614 (1999).
132. Klee, C.B., Ren, H. & Wang, X. Regulation of the calmodulin-stimulated protein phosphatase, calcineurin. *J Biol Chem* **273**, 13367-13370 (1998).
133. Kissinger, C.R., *et al.* Crystal structures of human calcineurin and the human FKBP12-FK506-calcineurin complex. *Nature* **378**, 641-644 (1995).
134. Klee, C.B., Crouch, T.H. & Krinks, M.H. Calcineurin: a calcium- and calmodulin-binding protein of the nervous system. *Proc Natl Acad Sci U S A* **76**, 6270-6273 (1979).
135. Saraf, J., *et al.* A Friend or Foe: Calcineurin across the Gamut of Neurological Disorders. *ACS Cent Sci* **4**, 805-819 (2018).
136. Ke, H. & Huai, Q. Structures of calcineurin and its complexes with immunophilins-immunosuppressants. *Biochem Biophys Res Commun* **311**, 1095-1102 (2003).
137. Molkentin, J.D. Calcineurin and beyond: cardiac hypertrophic signaling. *Circ Res* **87**, 731-738 (2000).
138. Breuder, T., Hemenway, C.S., Movva, N.R., Cardenas, M.E. & Heitman, J. Calcineurin is essential in cyclosporin A- and FK506-sensitive yeast strains. *Proc Natl Acad Sci U S A* **91**, 5372-5376 (1994).
139. Shibasaki, F., Price, E.R., Milan, D. & McKeon, F. Role of kinases and the phosphatase calcineurin in the nuclear shuttling of transcription factor NF-AT4. *Nature* **382**, 370-373 (1996).
140. Fernandez, A.M., Fernandez, S., Carrero, P., Garcia-Garcia, M. & Torres-Aleman, I. Calcineurin in reactive astrocytes plays a key role in the interplay between proinflammatory and anti-inflammatory signals. *J Neurosci* **27**, 8745-8756 (2007).
141. Asai, A., *et al.* High level calcineurin activity predisposes neuronal cells to apoptosis. *J Biol Chem* **274**, 34450-34458 (1999).
142. Wang, H.G., *et al.* Ca<sup>2+</sup>-induced apoptosis through calcineurin dephosphorylation of BAD. *Science* **284**, 339-343 (1999).
143. Sola, C., Tusell, J.M. & Serratos, J. Comparative study of the pattern of expression of calmodulin messenger RNAs in the mouse brain. *Neuroscience* **75**, 245-256 (1996).
144. Verstegen, A.M., *et al.* Phosphorylation of synapsin I by cyclin-dependent kinase-5 sets the ratio between the resting and recycling pools of synaptic vesicles at hippocampal synapses. *J Neurosci* **34**, 7266-7280 (2014).
145. Kim, S.H. & Ryan, T.A. Balance of calcineurin Aalpha and CDK5 activities sets release probability at nerve terminals. *J Neurosci* **33**, 8937-8950 (2013).
146. Cottrell, J.R., *et al.* Calcineurin Agamma is a Functional Phosphatase That Modulates Synaptic Vesicle Endocytosis. *J Biol Chem* **291**, 1948-1956 (2016).
147. Lai, M.M., *et al.* The calcineurin-dynamamin 1 complex as a calcium sensor for synaptic vesicle endocytosis. *J Biol Chem* **274**, 25963-25966 (1999).
148. Krupp, J.J., Vissel, B., Thomas, C.G., Heinemann, S.F. & Westbrook, G.L. Calcineurin acts via the C-terminus of NR2A to modulate desensitization of NMDA receptors. *Neuropharmacology* **42**, 593-602 (2002).

149. Hunt, D.L. & Castillo, P.E. Synaptic plasticity of NMDA receptors: mechanisms and functional implications. *Curr Opin Neurobiol* **22**, 496-508 (2012).
150. Cooke, S.F. & Bliss, T.V. Plasticity in the human central nervous system. *Brain* **129**, 1659-1673 (2006).
151. Zeng, H., *et al.* Forebrain-specific calcineurin knockout selectively impairs bidirectional synaptic plasticity and working/episodic-like memory. *Cell* **107**, 617-629 (2001).
152. Letourneau, P.C. The cytoskeleton in nerve growth cone motility and axonal pathfinding. *Perspect Dev Neurobiol* **4**, 111-123 (1996).
153. Goto, S., *et al.* Dephosphorylation of microtubule-associated protein 2, tau factor, and tubulin by calcineurin. *J Neurochem* **45**, 276-283 (1985).
154. Ferreira, A., Kincaid, R. & Kosik, K.S. Calcineurin is associated with the cytoskeleton of cultured neurons and has a role in the acquisition of polarity. *Mol Biol Cell* **4**, 1225-1238 (1993).
155. Meberg, P.J., Ono, S., Minamide, L.S., Takahashi, M. & Bamburg, J.R. Actin depolymerizing factor and cofilin phosphorylation dynamics: response to signals that regulate neurite extension. *Cell Motil Cytoskeleton* **39**, 172-190 (1998).
156. Pandey, D., Goyal, P., Dwivedi, S. & Siess, W. Unraveling a novel Rac1-mediated signaling pathway that regulates cofilin dephosphorylation and secretion in thrombin-stimulated platelets. *Blood* **114**, 415-424 (2009).
157. Zhao, R., Du, L., Huang, Y., Wu, Y. & Gunst, S.J. Actin depolymerization factor/cofilin activation regulates actin polymerization and tension development in canine tracheal smooth muscle. *J Biol Chem* **283**, 36522-36531 (2008).
158. Ghosh, R. & Pattison, J.S. Macroautophagy and Chaperone-Mediated Autophagy in Heart Failure: The Known and the Unknown. *Oxid Med Cell Longev* **2018**, 8602041 (2018).
159. Saftig, P., Beertsen, W. & Eskelinen, E.L. LAMP-2: a control step for phagosome and autophagosome maturation. *Autophagy* **4**, 510-512 (2008).
160. Sabatini, D.M. mTOR and cancer: insights into a complex relationship. *Nat Rev Cancer* **6**, 729-734 (2006).
161. Gingras, A.C., Kennedy, S.G., O'Leary, M.A., Sonenberg, N. & Hay, N. 4E-BP1, a repressor of mRNA translation, is phosphorylated and inactivated by the Akt(PKB) signaling pathway. *Genes Dev* **12**, 502-513 (1998).
162. Jung, C.H., *et al.* ULK-Atg13-FIP200 complexes mediate mTOR signaling to the autophagy machinery. *Mol Biol Cell* **20**, 1992-2003 (2009).
163. Russell, R.C., *et al.* ULK1 induces autophagy by phosphorylating Beclin-1 and activating VPS34 lipid kinase. *Nat Cell Biol* **15**, 741-750 (2013).
164. Volinia, S., *et al.* A human phosphatidylinositol 3-kinase complex related to the yeast Vps34p-Vps15p protein sorting system. *EMBO J* **14**, 3339-3348 (1995).
165. Mizushima, N., *et al.* Mouse Apg16L, a novel WD-repeat protein, targets to the autophagic isolation membrane with the Apg12-Apg5 conjugate. *J Cell Sci* **116**, 1679-1688 (2003).
166. Tooze, S.A. & Yoshimori, T. The origin of the autophagosomal membrane. *Nat Cell Biol* **12**, 831-835 (2010).
167. Kaur, J. & Debnath, J. Autophagy at the crossroads of catabolism and anabolism. *Nat Rev Mol Cell Biol* **16**, 461-472 (2015).
168. Rubinsztein, D.C., *et al.* Autophagy and its possible roles in nervous system diseases, damage and repair. *Autophagy* **1**, 11-22 (2005).
169. Nixon, R.A. Autophagy in neurodegenerative disease: friend, foe or turncoat? *Trends Neurosci* **29**, 528-535 (2006).
170. Levine, B. & Kroemer, G. Autophagy in the pathogenesis of disease. *Cell* **132**, 27-42 (2008).
171. Yue, Z., *et al.* A novel protein complex linking the delta 2 glutamate receptor and autophagy: implications for neurodegeneration in lurcher mice. *Neuron* **35**, 921-933 (2002).
172. Martinez-Vicente, M. Autophagy in neurodegenerative diseases: From pathogenic dysfunction to therapeutic modulation. *Semin Cell Dev Biol* **40**, 115-126 (2015).

173. Komatsu, M., *et al.* Loss of autophagy in the central nervous system causes neurodegeneration in mice. *Nature* **441**, 880-884 (2006).
174. Parsons, M.J. & Green, D.R. Mitochondria in cell death. *Essays Biochem* **47**, 99-114 (2010).
175. Lenaz, G. Role of mitochondria in oxidative stress and ageing. *Biochim Biophys Acta* **1366**, 53-67 (1998).
176. Gerdes, F., Tatsuta, T. & Langer, T. Mitochondrial AAA proteases--towards a molecular understanding of membrane-bound proteolytic machines. *Biochim Biophys Acta* **1823**, 49-55 (2012).
177. Lavie, J., *et al.* Ubiquitin-Dependent Degradation of Mitochondrial Proteins Regulates Energy Metabolism. *Cell Rep* **23**, 2852-2863 (2018).
178. Sugiura, A., McLelland, G.L., Fon, E.A. & McBride, H.M. A new pathway for mitochondrial quality control: mitochondrial-derived vesicles. *EMBO J* **33**, 2142-2156 (2014).
179. McWilliams, T.G., *et al.* mito-QC illuminates mitophagy and mitochondrial architecture in vivo. *J Cell Biol* **214**, 333-345 (2016).
180. Ploumi, C., Daskalaki, I. & Tavernarakis, N. Mitochondrial biogenesis and clearance: a balancing act. *FEBS J* **284**, 183-195 (2017).
181. Strappazzon, F., *et al.* AMBRA1 is able to induce mitophagy via LC3 binding, regardless of PARKIN and p62/SQSTM1. *Cell Death Differ* **22**, 517 (2015).
182. Meissner, C., Lorenz, H., Weihofen, A., Selkoe, D.J. & Lemberg, M.K. The mitochondrial intramembrane protease PARL cleaves human Pink1 to regulate Pink1 trafficking. *J Neurochem* **117**, 856-867 (2011).
183. Koyano, F., *et al.* Ubiquitin is phosphorylated by PINK1 to activate parkin. *Nature* **510**, 162-166 (2014).
184. Glauser, L., Sonnay, S., Stafa, K. & Moore, D.J. Parkin promotes the ubiquitination and degradation of the mitochondrial fusion factor mitofusin 1. *J Neurochem* **118**, 636-645 (2011).
185. Ziviani, E., Tao, R.N. & Whitworth, A.J. Drosophila parkin requires PINK1 for mitochondrial translocation and ubiquitinates mitofusin. *Proc Natl Acad Sci U S A* **107**, 5018-5023 (2010).
186. Geisler, S., *et al.* PINK1/Parkin-mediated mitophagy is dependent on VDAC1 and p62/SQSTM1. *Nat Cell Biol* **12**, 119-131 (2010).
187. Ashrafi, G. & Schwarz, T.L. The pathways of mitophagy for quality control and clearance of mitochondria. *Cell Death Differ* **20**, 31-42 (2013).
188. Buhlman, L., *et al.* Functional interplay between Parkin and Drp1 in mitochondrial fission and clearance. *Biochim Biophys Acta* **1843**, 2012-2026 (2014).
189. Burman, J.L., *et al.* Mitochondrial fission facilitates the selective mitophagy of protein aggregates. *J Cell Biol* **216**, 3231-3247 (2017).
190. Kanki, T., *et al.* A genomic screen for yeast mutants defective in selective mitochondria autophagy. *Mol Biol Cell* **20**, 4730-4738 (2009).
191. Weihofen, A., Thomas, K.J., Ostaszewski, B.L., Cookson, M.R. & Selkoe, D.J. Pink1 forms a multiprotein complex with Miro and Milton, linking Pink1 function to mitochondrial trafficking. *Biochemistry* **48**, 2045-2052 (2009).
192. Safiulina, D., *et al.* Miro proteins prime mitochondria for Parkin translocation and mitophagy. *EMBO J* **38**(2019).
193. Braak, H., *et al.* Staging of brain pathology related to sporadic Parkinson's disease. *Neurobiol Aging* **24**, 197-211 (2003).
194. Corti, O. & Brice, A. Mitochondrial quality control turns out to be the principal suspect in parkin and PINK1-related autosomal recessive Parkinson's disease. *Curr Opin Neurobiol* **23**, 100-108 (2013).
195. Suliman, H.B. & Piantadosi, C.A. Mitochondrial Quality Control as a Therapeutic Target. *Pharmacol Rev* **68**, 20-48 (2016).
196. Whitworth, A.J. & Pallanck, L.J. PINK1/Parkin mitophagy and neurodegeneration-what do we really know in vivo? *Curr Opin Genet Dev* **44**, 47-53 (2017).



197. Sliter, D.A., *et al.* Parkin and PINK1 mitigate STING-induced inflammation. *Nature* **561**, 258-262 (2018).
198. Cali, T., Ottolini, D. & Brini, M. Calcium signaling in Parkinson's disease. *Cell Tissue Res* **357**, 439-454 (2014).
199. Tanaka, K., Suzuki, T. & Chiba, T. The ligation systems for ubiquitin and ubiquitin-like proteins. *Mol Cells* **8**, 503-512 (1998).
200. Seirafi, M., Kozlov, G. & Gehring, K. Parkin structure and function. *FEBS J* **282**, 2076-2088 (2015).
201. Dove, K.K. & Klevit, R.E. Structural Biology: Parkin's Serpentine Shape Revealed in the Year of the Snake. *Curr Biol* **23**, R691-693 (2013).
202. Wauer, T. & Komander, D. Structure of the human Parkin ligase domain in an autoinhibited state. *EMBO J* **32**, 2099-2112 (2013).
203. Dorn, G.W., 2nd. Central Parkin: The evolving role of Parkin in the heart. *Biochim Biophys Acta* **1857**, 1307-1312 (2016).
204. Zhang, C.W., Hang, L., Yao, T.P. & Lim, K.L. Parkin Regulation and Neurodegenerative Disorders. *Front Aging Neurosci* **7**, 248 (2015).
205. Winklhofer, K.F. Parkin and mitochondrial quality control: toward assembling the puzzle. *Trends Cell Biol* **24**, 332-341 (2014).
206. Yang, H., Zhou, H.Y., Li, B. & Chen, S.D. Neuroprotection of Parkin against apoptosis is independent of inclusion body formation. *Neuroreport* **16**, 1117-1121 (2005).
207. Yasuda, T., *et al.* Parkin-mediated protection of dopaminergic neurons in a chronic MPTP-minipump mouse model of Parkinson disease. *J Neuropathol Exp Neurol* **70**, 686-697 (2011).
208. Trempe, J.F. & Fon, E.A. Structure and Function of Parkin, PINK1, and DJ-1, the Three Musketeers of Neuroprotection. *Front Neurol* **4**, 38 (2013).
209. Hang, L., Thundiyil, J. & Lim, K.L. Mitochondrial dysfunction and Parkinson disease: a Parkin-AMPK alliance in neuroprotection. *Ann N Y Acad Sci* **1350**, 37-47 (2015).
210. Lim, K.L., *et al.* Parkin mediates nonclassical, proteasomal-independent ubiquitination of synphilin-1: implications for Lewy body formation. *J Neurosci* **25**, 2002-2009 (2005).
211. Lin, W. & Kang, U.J. Characterization of PINK1 processing, stability, and subcellular localization. *J Neurochem* **106**, 464-474 (2008).
212. Jin, S.M., *et al.* Mitochondrial membrane potential regulates PINK1 import and proteolytic destabilization by PARL. *J Cell Biol* **191**, 933-942 (2010).
213. Yamano, K. & Youle, R.J. PINK1 is degraded through the N-end rule pathway. *Autophagy* **9**, 1758-1769 (2013).
214. Vives-Bauza, C., *et al.* PINK1-dependent recruitment of Parkin to mitochondria in mitophagy. *Proc Natl Acad Sci U S A* **107**, 378-383 (2010).
215. Matsuda, N., *et al.* PINK1 stabilized by mitochondrial depolarization recruits Parkin to damaged mitochondria and activates latent Parkin for mitophagy. *J Cell Biol* **189**, 211-221 (2010).
216. Yoshii, S.R., Kishi, C., Ishihara, N. & Mizushima, N. Parkin mediates proteasome-dependent protein degradation and rupture of the outer mitochondrial membrane. *J Biol Chem* **286**, 19630-19640 (2011).
217. Caulfield, T.R., *et al.* Phosphorylation by PINK1 releases the UBL domain and initializes the conformational opening of the E3 ubiquitin ligase Parkin. *PLoS Comput Biol* **10**, e1003935 (2014).
218. Chen, Y. & Dorn, G.W., 2nd. PINK1-phosphorylated mitofusin 2 is a Parkin receptor for culling damaged mitochondria. *Science* **340**, 471-475 (2013).
219. Okatsu, K., *et al.* Phosphorylated ubiquitin chain is the genuine Parkin receptor. *J Cell Biol* **209**, 111-128 (2015).
220. Ziviani, E. & Whitworth, A.J. How could Parkin-mediated ubiquitination of mitofusin promote mitophagy? *Autophagy* **6**, 660-662 (2010).
221. Sarraf, S.A., *et al.* Landscape of the PARKIN-dependent ubiquitylome in response to mitochondrial depolarization. *Nature* **496**, 372-376 (2013).
222. Escobar-Henriques, M. Mitofusins: ubiquitylation promotes fusion. *Cell Res* **24**, 387-388 (2014).

223. Durcan, T.M. & Fon, E.A. USP8 and PARK2/parkin-mediated mitophagy. *Autophagy* **11**, 428-429 (2015).
224. Nardin, A., Schrepfer, E. & Ziviani, E. Counteracting PINK/Parkin Deficiency in the Activation of Mitophagy: A Potential Therapeutic Intervention for Parkinson's Disease. *Curr Neuropharmacol* **14**, 250-259 (2016).
225. Dikic, I. & Bremm, A. DUBs counteract parkin for efficient mitophagy. *EMBO J* **33**, 2442-2443 (2014).
226. Bingol, B., *et al.* The mitochondrial deubiquitinase USP30 opposes parkin-mediated mitophagy. *Nature* **510**, 370-375 (2014).
227. Cornelissen, T., *et al.* The deubiquitinase USP15 antagonizes Parkin-mediated mitochondrial ubiquitination and mitophagy. *Hum Mol Genet* **23**, 5227-5242 (2014).
228. Durcan, T.M., *et al.* USP8 regulates mitophagy by removing K6-linked ubiquitin conjugates from parkin. *EMBO J* **33**, 2473-2491 (2014).
229. Um, J.W. & Chung, K.C. Functional modulation of parkin through physical interaction with SUMO-1. *J Neurosci Res* **84**, 1543-1554 (2006).
230. Eckermann, K. SUMO and Parkinson's disease. *Neuromolecular Med* **15**, 737-759 (2013).
231. Yao, D., *et al.* Nitrosative stress linked to sporadic Parkinson's disease: S-nitrosylation of parkin regulates its E3 ubiquitin ligase activity. *Proc Natl Acad Sci U S A* **101**, 10810-10814 (2004).
232. Chung, K.K., *et al.* S-nitrosylation of parkin regulates ubiquitination and compromises parkin's protective function. *Science* **304**, 1328-1331 (2004).
233. van Vliet, A.R., Verfaillie, T. & Agostinis, P. New functions of mitochondria associated membranes in cellular signaling. *Biochim Biophys Acta* **1843**, 2253-2262 (2014).
234. Kaufman, R.J. & Malhotra, J.D. Calcium trafficking integrates endoplasmic reticulum function with mitochondrial bioenergetics. *Biochim Biophys Acta* **1843**, 2233-2239 (2014).
235. Krebs, J., Agellon, L.B. & Michalak, M. Ca(2+) homeostasis and endoplasmic reticulum (ER) stress: An integrated view of calcium signaling. *Biochem Biophys Res Commun* **460**, 114-121 (2015).
236. Lee, J.Y., Nagano, Y., Taylor, J.P., Lim, K.L. & Yao, T.P. Disease-causing mutations in parkin impair mitochondrial ubiquitination, aggregation, and HDAC6-dependent mitophagy. *J Cell Biol* **189**, 671-679 (2010).
237. Shimura, H., *et al.* Immunohistochemical and subcellular localization of Parkin protein: absence of protein in autosomal recessive juvenile parkinsonism patients. *Ann Neurol* **45**, 668-672 (1999).
238. Rizk, A., *et al.* Segmentation and quantification of subcellular structures in fluorescence microscopy images using Squash. *Nat Protoc* **9**, 586-596 (2014).
239. Pereira, M.B., *et al.* Carbonyl cyanide m-chlorophenylhydrazone induced calcium signaling and activation of plasma membrane H(+)-ATPase in the yeast *Saccharomyces cerevisiae*. *FEMS Yeast Res* **8**, 622-630 (2008).
240. Zou, Y., *et al.* Calcineurin plays a critical role in the development of pressure overload-induced cardiac hypertrophy. *Circulation* **104**, 97-101 (2001).
241. Zou, Y., *et al.* Isoproterenol activates extracellular signal-regulated protein kinases in cardiomyocytes through calcineurin. *Circulation* **104**, 102-108 (2001).
242. Okatsu, K., Kimura, M., Oka, T., Tanaka, K. & Matsuda, N. Unconventional PINK1 localization to the outer membrane of depolarized mitochondria drives Parkin recruitment. *J Cell Sci* **128**, 964-978 (2015).
243. Ishii, T., *et al.* CETSA quantitatively verifies in vivo target engagement of novel RIPK1 inhibitors in various biospecimens. *Sci Rep* **7**, 13000 (2017).
244. Katayama, H., Kogure, T., Mizushima, N., Yoshimori, T. & Miyawaki, A. A sensitive and quantitative technique for detecting autophagic events based on lysosomal delivery. *Chem Biol* **18**, 1042-1052 (2011).
245. Shiba-Fukushima, K., *et al.* PINK1-mediated phosphorylation of the Parkin ubiquitin-like domain primes mitochondrial translocation of Parkin and regulates mitophagy. *Sci Rep* **2**, 1002 (2012).

246. Bjorkoy, G., *et al.* p62/SQSTM1 forms protein aggregates degraded by autophagy and has a protective effect on huntingtin-induced cell death. *J Cell Biol* **171**, 603-614 (2005).
247. Lee, J.Y., *et al.* HDAC6 controls autophagosome maturation essential for ubiquitin-selective quality-control autophagy. *EMBO J* **29**, 969-980 (2010).
248. von Muhlinen, N., Thurston, T., Ryzhakov, G., Bloor, S. & Randow, F. NDP52, a novel autophagy receptor for ubiquitin-decorated cytosolic bacteria. *Autophagy* **6**, 288-289 (2010).
249. Shlevkov, E., Kramer, T., Schapansky, J., LaVoie, M.J. & Schwarz, T.L. Miro phosphorylation sites regulate Parkin recruitment and mitochondrial motility. *Proc Natl Acad Sci U S A* **113**, E6097-E6106 (2016).
250. Um, J.H., Kim, Y.Y., Finkel, T. & Yun, J. Sensitive Measurement of Mitophagy by Flow Cytometry Using the pH-dependent Fluorescent Reporter mt-Keima. *J Vis Exp* (2018).

## 5. ABBREVIATIONS

AD: Alzheimer's disease

ADP: Adenosine Diphosphate

AIF: Apoptosis Inducing Factor

Ala: Alanine

Apaf1: Apoptotic Protease Activating Factor 1

ATP: Adenosine Triphosphate

ATP5A: ATP synthase subunit alpha

BBB: blood-brain barrier

Ca<sup>2+</sup>: Calcium

CaN: Calcineurin

CCCP: m-chlorophenyl hydrazone

CnA: Calcineurin catalytic subunit

CnB: Calcineurin regulatory subunit

COMT: Catechol-O-methyl-transferase

C-terminal: carboxyl-terminal

CypD: Cyclophilin D

cyt c: cytochrome c

DA: Dopamine

DAT: dopamine transporter

DDCI: peripheral DOPA decarboxylase inhibitor  
DMEM: Dulbecco's modified Eagle medium  
DNA: Deoxyribonucleic acid  
DOPAC: 3,4-Dihydroxyphenyl acetic acid  
Drp1: Dynamin-related protein 1  
EM: Electron microscopy  
ER: endoplasmic reticulum  
FBS: fetal bovine serum  
Fis1: Fission 1  
FK506: Tacrolimus  
g: times gravity  
GED: GTPase effector domain  
GFP: Green Fluorescent Protein  
GTP: guanosine triphosphate  
GTPase: GTP-binding proteins  
HEK293: Human Embryonic Kidney 293 cells  
His: Histidine  
HtrA2: High Temperature Requirement protein A2  
IBR: in-between-RING  
IMM: inner mitochondrial membrane  
IMS: intermembrane space  
IP3: inositol 1,4,5-thriphosphate  
kDa: kiloDalton  
LB: Lewy bodies  
LRRK2: leucine rich repeat kinase 2 gene  
MAO-B: Monoamine Oxidase B  
MAO-B: Monoamine Oxidase B  
Mb: Megabase  
MEFs: mouse embryonic fibroblasts  
MFN1/2: Mitofusin 1/2  
min: minute

mm: millimeters  
MOMP: mitochondrial outer membrane permeabilization  
MOPS: compound 3-(N-morpholino)propanesulfonic acid  
MPP: Mitochondria Processing Peptidase  
MPP+: 1-methyl-4-phenylpyridinium species  
MPTP: 1-methyl-4-phenyl-1,2,3,6-tetrahydropyridine  
mtDNA: mitochondrial DNA  
MTS: mitochondria targeting sequence  
Na+: Sodium  
NADH: reduced Nicotinamide Adenine Dinucleotide  
ng: nanograms  
nm: nanometer  
N-terminal: amino-terminal  
OMM: outer mitochondrial membrane  
OPA1: Optic Atrophy 1  
OXPHOS: oxidative phosphorylation system  
PARL: Presenilins-Associated Rhomboid-Like protein  
PBS: Phosphate buffered saline  
PCR: Polymerase chain reaction  
PD: Parkinson's disease  
PINK1: PTEN induced kinase 1  
PKG: murine phosphoglycerate kinase  
PQ: Paraquat  
PTEN: Phosphatase and Tensin homolog  
RBR: RING1-IBR-RING2  
ROS: Reactive Oxygen Species  
rpm: revolutions per minute  
s: second  
SDS-PAGE: sodium dodecyl sulfate polyacrylamide gel electrophoresis  
Ser: Serine  
Smac: Second Mitochondria-derived Activator of Caspases

SN: substantia nigra

SNpc: substantia nigra pars compacta

Thr: Threonine

TM: transmembrane

Ub: ubiquitin

UBL: ubiquitin-like domain

UPD: unique Parkin domain

UPS: Ubiquitin Proteasome System

VDAC: Voltage-Dependent Anion Channel

$\Delta$ CnA: Calcineurin constitutive active mutant

$\Delta$ CnAH151Q: Calcineurin dominant negative mutant


$\mu$ l: microliters

$\mu$ M: microMolar

## **6. ANNEX**



# USP14 inhibition corrects an *in vivo* model of impaired mitophagy

Joy Chakraborty<sup>1</sup>, Sophia von Stockum<sup>2</sup>, Elena Marchesan<sup>2</sup>, Federico Caicci<sup>1</sup>, Vanni Ferrari<sup>1</sup>, Aleksandar Rakovic<sup>3</sup>, Christine Klein<sup>3</sup>, Angelo Antonini<sup>4</sup>, Luigi Bubacco<sup>1</sup> & Elena Ziviani<sup>1,2,\*</sup> 

## Abstract

Mitochondrial autophagy or mitophagy is a key process that allows selective sequestration and degradation of dysfunctional mitochondria to prevent excessive reactive oxygen species, and activation of cell death. Recent studies revealed that ubiquitin–proteasome complex activity and mitochondrial membrane rupture are key steps preceding mitophagy, in combination with the ubiquitination of specific outer mitochondrial membrane (OMM) proteins. The deubiquitinating enzyme ubiquitin-specific peptidase 14 (USP14) has been shown to modulate both proteasome activity and autophagy. Here, we report that genetic and pharmacological inhibition of USP14 promotes mitophagy, which occurs in the absence of the well-characterised mediators of mitophagy, PINK1 and Parkin. Critical to USP14-induced mitophagy is the exposure of the LC3 receptor Prohibitin 2 by mitochondrial fragmentation and mitochondrial membrane rupture. Genetic or pharmacological inhibition of USP14 *in vivo* corrected mitochondrial dysfunction and locomotion behaviour of PINK1/Parkin mutant *Drosophila* model of Parkinson's disease, an age-related progressive neurodegenerative disorder that is correlated with diminished mitochondrial quality control. Our study identifies a novel therapeutic target that ameliorates mitochondrial dysfunction and *in vivo* PD-related symptoms.

**Keywords** mitochondrial membrane rupture; mitophagy; proteasome; USP14

**Subject Categories** Neuroscience; Pharmacology & Drug Discovery

**DOI** 10.15252/emmm.201809014 | Received 19 February 2018 | Revised 22

August 2018 | Accepted 24 August 2018 | Published online 24 September 2018

**EMBO Mol Med (2018) 10: e9014**

## Introduction

Mitochondria generate ATP through oxidative phosphorylation at the inner mitochondrial membrane. However, they can quickly switch from transforming energy to sustain cell viability, to producing reactive oxygen species (ROS) and releasing proteins that activate cell death pathways. In order to prevent the build-up of ROS

and accumulation of aberrant proteins and organelles, cells eliminate dysfunctional mitochondria via autophagy, a process known as mitophagy that requires both autophagy machinery and the ubiquitin–proteasome complex. Key pivotal elements in the orchestration of mitophagy are proteasome localisation to depolarised mitochondria, the degradation of outer mitochondrial membrane (OMM)-ubiquitinated proteins, and the disruption of the mitochondrial membrane (Tanaka *et al*, 2010; Chan *et al*, 2011; Yoshii *et al*, 2011). It was not clear, however, how mitochondrial membrane rupture can facilitate mitophagy until recently, when Wei *et al* (2017) demonstrated that OMM rupture leads to the exposure of Prohibitin 2, which functions as a receptor for LC3 to form mitophagic vesicles (Wei *et al*, 2017).

These findings raise the possibility that fine-tuning UPS activity in combination with enhancing autophagy may in turn regulate mitochondrial quality control.

The ubiquitin–proteasome system (UPS) is affected in many neurodegenerative disorders and thus a key target for therapeutic intervention. One possible avenue of intervention is proteasome-associated deubiquitinating enzymes (DUBs) which regulate proteasome activity. Among the three DUBs associated with mammalian proteasome, USP14 is an attractive target because it was demonstrated to negatively influence UPS activity by increasing protein dwelling time on the proteasome (Hanna *et al*, 2006; Peth *et al*, 2009; Lee *et al*, 2010; Kim & Goldberg, 2017) and is specifically inhibited by a small molecule IU1 (Lee *et al*, 2010) that increases proteasome activity. Interestingly, suppressing USP14 activity, either by knocking USP14 down or by IU1, leads to Beclin1-dependent autophagy (Xu *et al*, 2016). Because of the unique capability of USP14 to enhance both proteasome complex activity and autophagy, we hypothesised that USP14 inhibition may offer additional advantages over other DUBs in promoting mitochondrial clearance. Also, the availability of the specific inhibitor IU1 makes it an ideal candidate for potential therapy development (Lee *et al*, 2010).

To monitor the therapeutic potential of USP14 inhibition in a mitophagy-deficient background *in vivo*, we selected animal models of Parkinson's disease (PD), which are associated with mutations in the protein kinase PINK1 and E3 ubiquitin ligase Parkin, both key regulators of mitophagy (Kitada *et al*, 1998;

1 Department of Biology, University of Padova, Padova, Italy

2 Fondazione Ospedale San Camillo IRCCS, Venezia, Italia

3 Institute of Neurogenetics, University of Lübeck, Lübeck, Germany

4 Department of Neuroscience, University of Padova, Padova, Italy

\*Corresponding author. Tel: +39 49 827 6237; E-mail elena.ziviani@unipd.it

Shimura *et al*, 2000; Valente *et al*, 2004; Silvestri *et al*, 2005; Narendra *et al*, 2008, 2010; Ziviani *et al*, 2010). Upon mitochondrial depolarisation, PINK1 anchors onto the mitochondrial membrane and recruits Parkin to ubiquitinate specific OMM proteins, which signals the elimination of dysfunctional mitochondria via autophagy (Shimura *et al*, 2000; Silvestri *et al*, 2005; Narendra *et al*, 2008, 2010; Ziviani *et al*, 2010; Chen & Dorn, 2013; Harper *et al*, 2018). Though there are other suggested pathways that may lead to the same outcome, the absence of one of them and the level of compensation may impact the efficiency of mitophagy (Baumann, 2018; Pickles *et al*, 2018). Apart from the few genes known to cause familial PD, most cases are sporadic and without any known common genetic trait. However, mitochondrial dysfunction is a key feature in both sporadic and familial PD (Parker *et al*, 1989; Schapira *et al*, 1990; Mizuno *et al*, 1998), indicating that mitochondrial quality control may hold immense therapeutic implications in this disorder.

Here, we report that pharmacological or genetic inhibition of USP14 leads to increased mitochondrial clearance. Mitochondrial fragmentation and mitochondrial membrane rupture to expose the LC3 autophagy receptor Prohibitin 2 are key elements for USP14-induced mitophagy. *In vivo*, USP14 inhibition corrected mitochondrial dysfunction and locomotion impairment in the established PINK1 and Parkin mutant *Drosophila* model of neurodegeneration, highlighting the potential of USP14 inhibitors as therapeutics for PD symptoms.

## Results

### USP14 inhibition/knockdown induces mitophagy

To standardise a dose of USP14 inhibitor IU1, we incubated SH-SY5Y cells with different concentrations (1–500  $\mu\text{M}$ ) for 24 h and assessed cell viability by MTT assay. We found that doses > 200  $\mu\text{M}$  reduce cell viability, whereas doses up to 100  $\mu\text{M}$  have no effect on cell viability (Appendix Fig S1A). To reconfirm the MTT assay results, we stained the cells with propidium iodide and Hoechst (Appendix Fig S1B). We found that 100  $\mu\text{M}$  does not cause cell death. The number of apoptotic cells in the 200  $\mu\text{M}$  dose was highly variable, but 500  $\mu\text{M}$  IU1 caused severe cell death. To further confirm that IU1 does not affect neuronal survivability at similar doses *in vivo*, *Drosophila* expressing neuronal GFP (UAS CD8-GFP, elavC155-Gal4) were treated with different concentrations of IU1 (1–100  $\mu\text{M}$ , 3 days, mixed with food; Appendix Fig S1C). The treatment did not cause any adverse effects on the gross morphology of wing motor neurons of *Drosophila*. To ensure IU1 is effective in human and mouse cells (the two main cell types used for the study) and increases proteasome activity, we used a substrate that is dependent on ubiquitin and UPS. We transfected cells with Ub-R-GFP, a proteasomal substrate that is maintained at low levels in normal conditions (Dantuma *et al*, 2000), and then treated the cells with 100  $\mu\text{M}$  IU1 for 24 h. We found a clear decrease in the Ub-R-GFP protein levels after IU1 treatment. This effect was reversed by co-incubation with the UPS inhibitor MG132 (Appendix Fig S2A). Before assessing mitophagy with this concentration of IU1, we wanted to confirm that USP14 inhibition can increase autophagy in SH-SY5Y cells, as

previously suggested (Xu *et al*, 2016). In accordance with the study by Xu *et al* (2016), we found an increase in LC3-II protein levels after 24 h of IU1 (100  $\mu\text{M}$ ) treatment (Fig 1A) or USP14 siRNA treatment (Appendix Fig S3A). We also found an increase in the LC3-II levels after IU1 treatment when cells were co-incubated with chloroquine or  $\text{NH}_4\text{Cl}$  (Appendix Fig S2B). Furthermore, electron microscopy analysis of SH-SY5Y cells revealed a high number of autophagic vesicles after 24 h of IU1 (100  $\mu\text{M}$ ) treatment (Fig 1B–D). An increased number of autophagosomes and autolysosomes was also detected when USP14 was knocked down by siRNA (Appendix Fig S3B and C), thus confirming the specificity of IU1. To characterise the autophagic vacuoles further, we counted the number of initial (AVi) and degradative/mature autophagic vacuoles (Klionsky *et al*, 2016). We found a clear increase in the number of total and degradative autophagic vacuoles (Appendix Fig S2C).

In order to evaluate mitochondrial content in SH-SY5Y cells, we next measured total mitochondrial volume as well as the levels of the mitochondrial inner membrane- and matrix-resident proteins, ATP5a and HSP60, respectively. Potential enhancement of mitophagy should be reflected by a decrease in these two parameters. We monitored the levels of ATP5a and HSP60 by immunoblot and found that USP14 inhibition by IU1 (Fig 1E) or its knockdown (Appendix Fig S3D) resulted in a significant decrease when compared to the respective control group. Analysis of mitochondrial shape (elongated/fragmented) and mitochondrial volume of SH-SY5Y cells expressing mito-YFP revealed increased mitochondrial fragmentation and decreased mitochondrial volume when USP14 was inhibited (Fig 1F–I) or knocked down (Appendix Fig S3E–G). Next, we transfected cells with mito-YFP and immunostained them for LC3. IU1-treated cells showed increased LC3 puncta formation as well as increased overlap with mitochondria-like structures (Fig 1J–L). USP14 knockdown also showed similar results when the mitochondrial marker ATP5a and the LC3 protein were immunostained, and co-localisation was measured (Appendix Fig S3H–K). An increased number of autophagic vesicles with a mitochondria-like structure were confirmed by electron microscopy analysis in both IU1- and USP14 siRNA-treated groups (Appendix Fig S4A and B, respectively). Next, we verified the hypothesis that IU1-mediated mitochondrial loss requires the autophagic machinery. Because  $\text{NH}_4\text{Cl}$  treatment along with IU1 showed an increase in LC3-II levels (Appendix Fig S2B), which was also depicted earlier by Xu *et al* (2016), we co-incubated cells with IU1 and  $\text{NH}_4\text{Cl}$  (Appendix Fig S5A) and probed them for HSP60/ATP5a. We could not find any significant decrease in these mitochondrial markers after IU1 treatment when  $\text{NH}_4\text{Cl}$  was co-administered (Appendix Fig S5A). To further support our hypothesis by using a genetic approach, we incubated ATG7 WT/KO MEF cells with IU1. While a decrease in both ATP5a and HSP60 protein levels was evident in ATG7 WT cells, there was no significant decrease in the ATG7 KO cells (Appendix Fig S5B). To further confirm enhanced mitophagy in USP14-inhibited cells, we transfected SH-SY5Y cells with mito-Keima, which has different excitation spectra at neutral (405/615 nm) and acidic pH (561/615 nm). IU1-treated cells showed a clear shift in spectra (Fig 1M) with a significant increase in the average signal intensity at 561 nm (i.e. acidic pH) (Fig 1N). Together, these results support that USP14 pharmacological or genetic inhibition induces mitophagy.



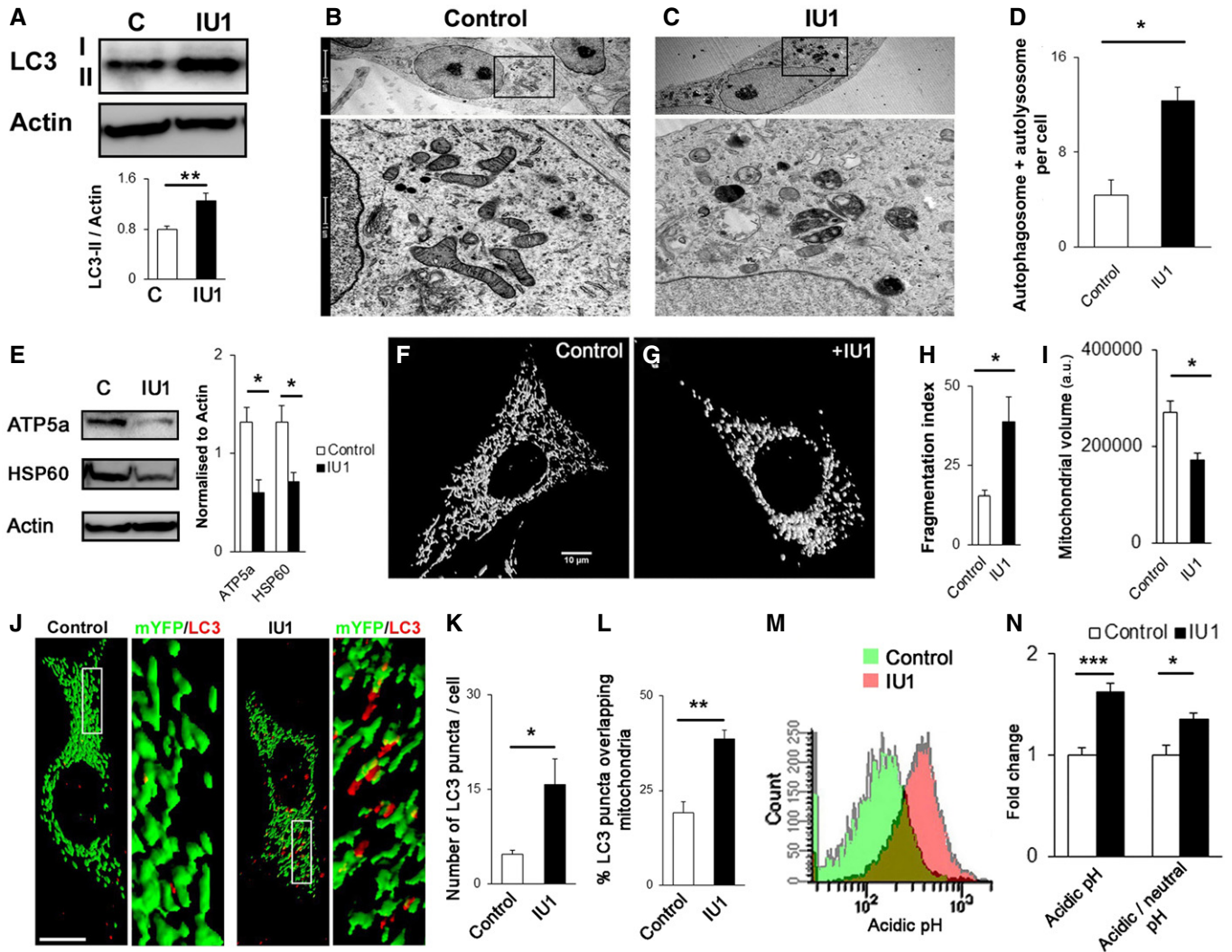


**Figure 1. Treatment with the USP14 inhibitor IU1 induces mitophagy in SH-SY5Y cells.**

A Western blot analysis of LC3 in SH-SY5Y cells after IU1 treatment (100  $\mu$ M, 24 h). Graphs represent the mean  $\pm$  SEM.  $N = 8$ .  
 B–D Electron microscopy images were taken to quantify the number of autophagosomes and autolysosomes present in control (DMSO) or IU1-treated cells. At least 55 cells were analysed from three different experiments. Graphs represent the mean  $\pm$  SEM.  
 E Western blot analysis of mitochondrial marker proteins ATP5a and HSP60, normalised by actin after 24 h of DMSO (C) or IU1 (100  $\mu$ M) treatment.  $N = 3$ . Graphs represent the mean  $\pm$  SEM.  
 F–I Confocal images of cells transfected with mito-YFP and treated with DMSO (F, control) or IU1 (G) for 24 h. Fragmentation index (H) and total mitochondrial volume/cell were measured and are represented in (I) as mean  $\pm$  SEM. At least 35 cells were analysed from three different experimental conditions. Scale bar: 10  $\mu$ m.  
 J–L Mito-YFP-transfected cells were treated with IU1 (100  $\mu$ M, 24 h), fixed and immunolabelled for LC3. The number of LC3 dots/cell (K) and LC3 dots overlapping mitochondria (L) was counted and represented as mean  $\pm$  SEM. At least 35 cells from three independent experiments were analysed. Scale bar: 10  $\mu$ m.  
 M, N Cells were transfected with mito-Keima and treated with DMSO or IU1 for 24 h and subjected to FACS analysis, counting 10,000 cells per experiment. (M) represents the shift of the signal intensity in IU1-treated cells when excited at 560 nm (false colour). (N) represents the average intensity of the mito-Keima protein when excited at 560 nm and the ratio between 560:405 nm. Graphs represent the mean  $\pm$  SEM from three different sets of experiments.

Data information: Student's *t*-test. \* $P \leq 0.05$ , \*\* $P \leq 0.01$ , \*\*\* $P \leq 0.001$ .  
 Source data are available online for this figure.

### USP14-mediated mitophagy is DRP1 and Mfn2 dependent

Because mitochondrial shape and size can affect mitophagy (fragmented ones are preferred over the elongated ones) (Twig *et al*, 2008; Gomes *et al*, 2011), we next evaluated the levels of the mitochondria-shaping proteins DRP1, Fis1, Mfn1, Mfn2 and OPA1

in USP14-inhibited cells. SH-SY5Y cells treated with IU1 (1–100  $\mu$ M) for 24 h showed a dose-dependent decrease in the level of TOM20, reflecting the decrease in mitochondrial content (Fig 2A and B). The levels of the mitochondrial pro-fission protein DRP1 were increased after 24 h, whereas the levels of Fis1 and the mitochondrial fusion proteins Mfn1 and Mfn2 were reduced in a

dose-dependent manner (Fig 2A and B). There was only a trend towards a decrease in the level of the mitochondrial pro-fusion protein OPA1 after IU1 treatment (Fig 2A and B). USP14 knockdown by siRNA also showed similar results after 24 h, except for OPA1, which was also significantly decreased (Appendix Fig S6A and B). A further follow-up after 72 h of USP14 knockdown showed decreased levels of all the dynamics-related proteins, except for Fis1, which could be due to further reduction of mitochondrial content (Appendix Fig S6C and D). These results indicated a shift towards mitochondrial fission at 24 h, consistent with mitochondrial fragmentation prior to mitophagy. To confirm that this shift is essential for USP14-mediated mitophagy, we incubated MEF cells genetically ablated for DRP1/Mfn1/Mfn2 or WT MEF cells with 100  $\mu$ M IU1 for 48 h and measured mitochondrial volume by confocal imaging as well as the levels of the mitochondrial inner membrane- and matrix-resident proteins, ATP5a and HSP60, by Western blot. IU1-mediated mitochondrial volume loss was abolished in DRP1 and Mfn2 KO cells, while the effect persisted in the WT and Mfn1 KO cells (Fig 2C and D). Measurement of HSP60 and ATP5a protein levels by Western blot also confirmed DRP1 and Mfn2 dependency for mitochondrial clearance by IU1 (Fig 2E and F). Transfection of wild-type MEF cells with DRP1-K38A (a dominant negative form of DRP1) also abolished the effect of IU1, which was reflected on the HSP60 and ATP5a protein levels (Fig 2E and F). Thus, USP14-mediated mitophagy requires DRP1 and Mfn2.

#### USP14-induced mitochondrial clearance is PINK1/Parkin independent

We next evaluated whether USP14-mediated mitophagy is dependent on the canonical PINK1/Parkin mitophagy pathway. To assess PINK1 dependency, we used PINK1 KO MEF cells, and to evaluate Parkin dependency, we used HeLa cells and Parkin mutant human fibroblasts derived from skin biopsies of human patients with compound heterozygous (R275W and exon 3 deletion) *parkin* mutations (see Materials and Methods for clinical details). Wild-type MEF cells and HeLa cells, which express low and undetectable amounts of Parkin, respectively, and PINK1 KO MEF cells were treated with 100  $\mu$ M IU1 for 48 h and analysed by electron microscopy. Increased autophagosome and/or autolysosome formation was detected in all three cell types (Fig 3A–D), as well as decreases in HSP60 and ATP5a protein levels (Fig 3E). Human control fibroblast and *Parkin* mutant patient fibroblast cells also exhibited decreased levels of HSP60 and ATP5a proteins after IU1 treatment (Fig 3E), further supporting the notion that USP14-induced mitochondrial clearance is PINK1/Parkin independent.

#### USP14 inhibition and knockdown lead to mitochondrial membrane rupture

Given that translocation of the proteasome to mitochondria is required for mitophagy (Tanaka *et al*, 2010; Chan *et al*, 2011; Yoshii *et al*, 2011), we next monitored localisation of proteasome complex (20S subunit  $\alpha$ + $\beta$ ) after IU1 treatment in SH-SY5Y cells. Co-localisation studies by confocal microscopy revealed an increased association of the 20S proteasome complex subunit with mitochondria after 12-h IU1 treatment, which started to decrease at

24 h (Fig 4A and B). Increased association of the 20S proteasome complex subunit with mitochondria was also observed following 24 h of USP14 siRNA treatment (Appendix Fig S7A and B). To further investigate the subcellular localisation of the proteasome, we performed electron microscopy following immunogold labelling of the 20S proteasome complex subunit at 12 and 24 h of IU1 treatment (Fig 4C) or 24 h of USP14 siRNA treatment (Appendix Fig S7C). These results confirmed the confocal microscopy co-localisation studies. During mitophagy, mitochondrial inner membrane proteins, including Prohibitin 2 (PHB2), are exposed and act as receptors for LC3 to form mitophagic vesicles (Wei *et al*, 2017). To evaluate this possibility, we performed proximity ligation assay for PHB2 and LC3 after 24 h of IU1 treatment (100  $\mu$ M) in SH-SY5Y cells. IU1-treated cells exhibited an increased number of dots per cell, representative of increased PHB2–LC3 interaction (Fig 4D and E). Of note, IU1-induced mitochondrial volume loss (Appendix Fig S8A and B) and the decrease in HSP60 and ATP5a levels (Appendix Fig S8C–E) were inhibited in PHB2<sup>F/F</sup> cells upon expression of Cre recombinase, indicating that IU1-mediated mitochondrial clearance is PHB2 dependent.

Given the increased association between mitochondrial inner membrane protein PHB2 and the autophagy machinery, we hypothesised that USP14 inhibition might result in altered mitochondrial membrane integrity. Indeed, close monitoring by electron microscopy showed that inhibition of USP14 leads to an increased number of mitochondria with ruptured mitochondrial membranes in SH-SY5Y cells (Fig 5A). Of note, mitochondria isolated from IU1-treated cells showed increased susceptibility to trypsin-dependent digestion of HSP60 and ATP5a (Fig 5B), further supporting the hypothesis that USP14-inhibited cells present altered mitochondrial membrane integrity. To exclude the possibility that the mitochondrial isolation procedure can interfere with mitochondrial membrane integrity, we treated digitonin-permeabilised cells with trypsin and measured mitochondrial marker protein levels. The results were comparable to those obtained from trypsin-digested isolated mitochondria (Appendix Fig S9). Inhibition of USP14 resulted in an increased number of mitochondria with ruptured mitochondrial membranes in WT MEF, PINK1 KO MEF and HeLa cells also (Fig 5C, E and G). Accordingly, digestion of isolated mitochondria from these cells resulted in increased susceptibility to trypsin-dependent degradation of HSP60 and ATP5a (Fig 5D, F and H), corroborating the hypothesis that the effect of USP14 upon mitochondrial clearance is PINK1/Parkin independent. These results were confirmed in digitonin-permeabilised cells as well (Appendix Fig S9).

We next monitored the effect of USP14 knockdown on mitochondrial membrane integrity *ex vivo*. Mitochondrial ultrastructure was evaluated by electron microscopy in thoracic muscle from control (actin-Gal4) and USP14-knocked-down *Drosophila* (UAS USP14: actin-Gal4). A marginal increase in the number of ruptured mitochondria was observed in the latter (Fig 5I). Mitochondria from 3- to 4-day-old control and USP14-knockdown (KD) flies were isolated from the whole body and subjected to trypsin digestion assay. As previously observed *in vitro*, mitochondria from USP14-knockdown (KD) flies resulted in increased susceptibility to trypsin-dependent degradation of HSP60 and ATP5a (Fig 5J). In conclusion, USP14 inhibition and knockdown lead to mitochondrial membrane rupture *in vitro* and *ex vivo*.

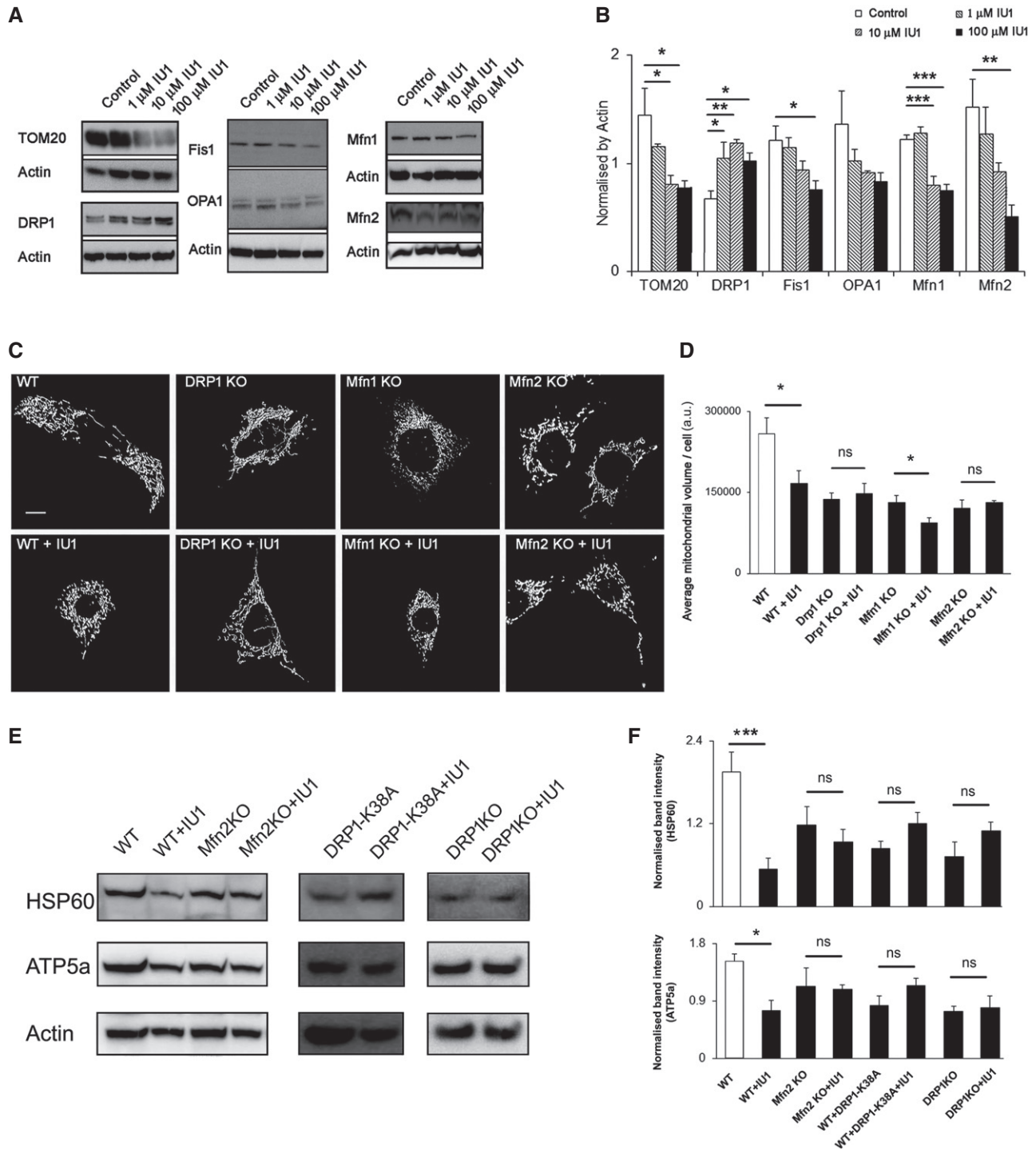


**Figure 2. IU1-facilitated mitochondrial clearance is DRP1 and Mfn2 dependent.**

A, B Western blot analysis of the indicated proteins in cell lysates from SH-SY5Y cells, treated with different concentrations of IU1 (1–100  $\mu$ M) for 24 h. Bar graphs represent the mean  $\pm$  SEM. Blots are representative of three independent experiments. ANOVA followed by Dunnett's test.

C, D Representative images of MEF cells knocked out for the indicated mitochondrial dynamics proteins and transfected with mito-YFP (C) with/without IU1 treatment (100  $\mu$ M, 48 h). Scale bar: 10  $\mu$ m. (D) Mitochondrial volume/cell was measured as described and is represented as mean  $\pm$  SEM. At least 35 cells were evaluated. Student's *t*-test.

E, F Western blot analysis of HSP60 and ATP5a as mitochondrial markers in the indicated knockout MEF cells (with/without the indicated DRP1 variant) after 48 h of IU1 treatment. Bar graphs represent the mean  $\pm$  SEM; *n* = at least 3. Student's *t*-test.

Data information: \**P*  $\leq$  0.05, \*\**P*  $\leq$  0.01, \*\*\**P*  $\leq$  0.001.

Source data are available online for this figure.

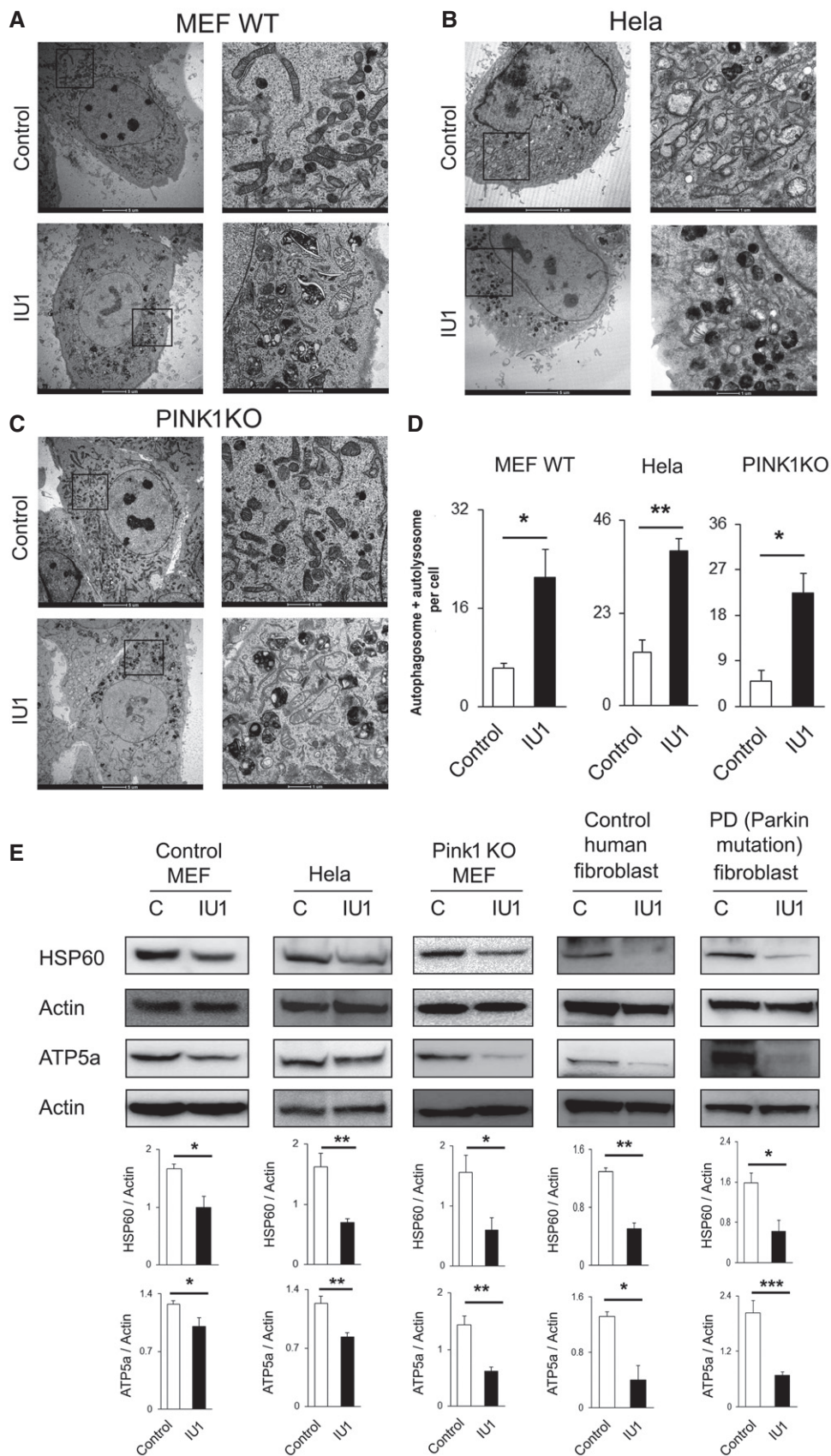


Figure 3.

**Figure 3. IU1 treatment-mediated mitophagy is Parkin/PINK1 independent.**

A–D Wild-type MEF (A), HeLa (B) and PINK1 KO MEF (C) cells were treated with IU1 (48 h, 100  $\mu$ M), and electron microscopy images were evaluated for autophagic vesicle formation. (D) Bar graphs represent the mean  $\pm$  SEM of the number of autophagosomes and autolysosomes per cell from three different sets of experiments; at least 40 cells were analysed from each group. Student's *t*-test.

E Western blot analysis of HSP60 protein with or without IU1 treatment in the indicated cell type. Bar graphs represent the mean  $\pm$  SEM. *N* = at least three independent experiments. Student's *t*-test.

Data information: \**P*  $\leq$  0.05, \*\**P*  $\leq$  0.01, \*\*\**P*  $\leq$  0.001.

Source data are available online for this figure.

**USP14 inhibition/knockdown rescues PINK1- and Parkin-deficient flies by correcting mitochondrial dysfunction *in vivo***

To assess the therapeutic aspects of our findings and evaluate the effect of USP14 inhibition, we turned to two well-established *Drosophila* models of impaired mitophagy, i.e. PINK1 and Parkin mutant flies. Before generating the USP14 KD PINK1 or Parkin mutant fly lines, we compared life span of control (actin-Gal4) and USP14 KD flies. We found no significant difference in life expectancy of USP14 KD flies (Appendix Fig S10A). Respiration of isolated mitochondria from 3- to 6-day-old USP14 KD flies also showed no differences when compared with control flies (Appendix Fig S10B and C). Accordingly, mitochondria from thoracic muscles of USP14 KD flies showed no gross differences in distribution or morphology, except for the previously reported increased number of ruptured mitochondria in the USP14 KD group (Appendix Fig S10D).

Life span analysis revealed a reduced life expectancy in the PINK1 mutant (KO) flies (PINK1B9) as previously reported (Poddighe *et al*, 2013) (Fig 6A). Interestingly, USP14 down-regulation ameliorated the shorter longevity of the PINK1 KO mutant flies (Fig 6A). USP14 knockdown also improved climbing ability (3 days old; Fig 6B), mitochondrial respiration (3–5 days old; Fig 6C) and dopamine levels in PINK1 mutant (KO) flies (15 days old; Fig 6D). Mitochondria in the thoracic muscle of PINK1 mutant flies were found to be less electron dense with complete disruption of the mitochondrial cristae when compared to the control group (Fig 6E), a phenotype that was partially corrected by USP14 knockdown (Fig 6E). In order to examine the effect of USP14 inhibition in flies, we first confirmed that IU1 treatment could induce fragmentation and decrease mitochondrial volume in S2R+ fly cells. We incubated S2R+ cells with IU1 (100  $\mu$ M), which induced mitochondrial fragmentation and a decrease in mitochondrial volume after 24 h (Appendix Fig S11A–C). As USP14 inhibition in fly cells

recapitulated the effects observed in mammalian cells, we mixed different concentrations of IU1 (1–100  $\mu$ M) in the fly food to pharmacologically inhibit USP14 *in vivo*. Although none of the doses alone affected climbing ability (Appendix Fig S12A), increasing inhibitor concentrations decreased fly food uptake (Appendix Fig S12B). In the 1  $\mu$ M IU1-treated group, food consumption by the flies was normal (Appendix Fig S12B). Assessing chymotrypsin-like activity of the proteasome complex indicated that this dose was sufficient to elevate proteasome activity *ex vivo* in flies (Appendix Fig S12C). Of note, 1  $\mu$ M IU1 partially corrected the climbing ability of the PINK1 mutant (KO) flies (Appendix Fig S12D) and improved the number of electron-dense mitochondrial population in thoracic flight muscles (Appendix Fig S12E). Again, IU1 treatment (1  $\mu$ M) alone had no effect on life span (Appendix Fig S13A) or thoracic muscle mitochondrial morphology (Appendix Fig S13B).

As previously reported for PINK1 mutant (KO) flies, Parkin mutant (KO) flies also exhibited a reduced life span in comparison with the control flies (Saini *et al*, 2011). USP14 knockdown improved the life expectancy of Parkin mutant flies (Fig 7A). Both genetic knockdown and pharmacological inhibition resulted in improved climbing activity (Fig 7B, Appendix Fig S14B) and partially corrected mitochondrial respiration (Fig 7C). Parkin mutant flies do not show significant dopamine depletion, which is previously reported by the other studies (Greene *et al*, 2003; Bingol *et al*, 2014). In Parkin mutant flies, mitochondria were not as severely affected as in PINK1 mutant flies, but the number of less electron-dense mitochondria with ruptured cristae was higher than in the wild type (Fig 7D and Appendix Fig S14B). USP14 knockdown (Fig 7D) or IU1 treatment (Appendix Fig S14B) improved the thoracic flight muscle mitochondrial ultrastructure of the Parkin mutant flies as depicted in the bar graphs. We next tested induced pluripotent stem (iPS) cell lines derived from PD patients with

**Figure 4. IU1 treatment mediates the translocation of the 20S proteasome subunit to mitochondria.**

A, B SH-SY5Y cells were immunostained for ATP5a (green) and 20S proteasome core (red) after IU1 treatment (6–24 h). Scale bar: 10  $\mu$ m. Colour mapping of the co-localisation of HSP60 and 20S proteasome from the selected regions was generated by ImageJ and is represented in the bottom panel. The intensity of the co-localisation is represented in the colour map scale at the bottom of the panel. (B) 20S proteasome subunit and mitochondrial co-localisation was quantified by measuring Mander's coefficient. Bar graphs represent the mean fold change (mean  $\pm$  SEM) from three different experiments. At least 30 cells were evaluated for the calculations. ANOVA followed by Dunnett's test.

C Electron microscopy images showing subcellular localisation of immunogold-labelled 20S subunit of proteasome complex after 12 or 24 h of IU1 treatment. Experiments were repeated twice in two biological replicates with similar results. The contrast in the magnified region is enhanced from the original image to highlight the immunogold-labelled signals.

D, E Protein proximity ligation assay for Prohibitin 2 (PHB2) and LC3 after 24-h IU1 treatment. Images showing signal are merged with bright-field images to count the signal dots (cyan false colour) as depicted in the figure. In the inset, only fluorescence signal is shown, without merging with the bright field from the selected regions. Scale bar: 10  $\mu$ m. (E) Bar graph represents the mean  $\pm$  SEM of the number of signal dots per cell from three different experiments. Student's *t*-test.

Data information: \**P*  $\leq$  0.05, \*\**P*  $\leq$  0.01, \*\*\**P*  $\leq$  0.001.

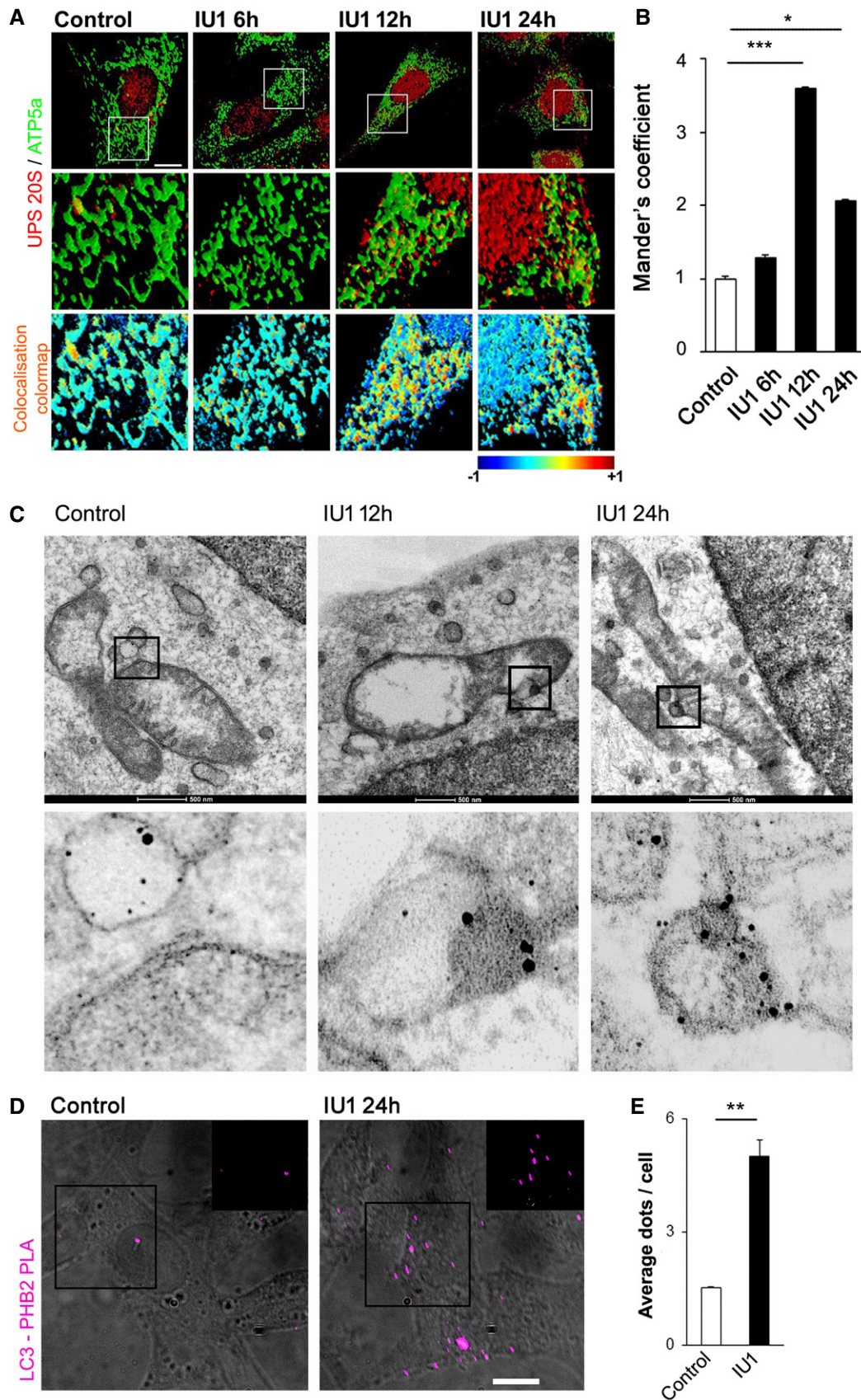
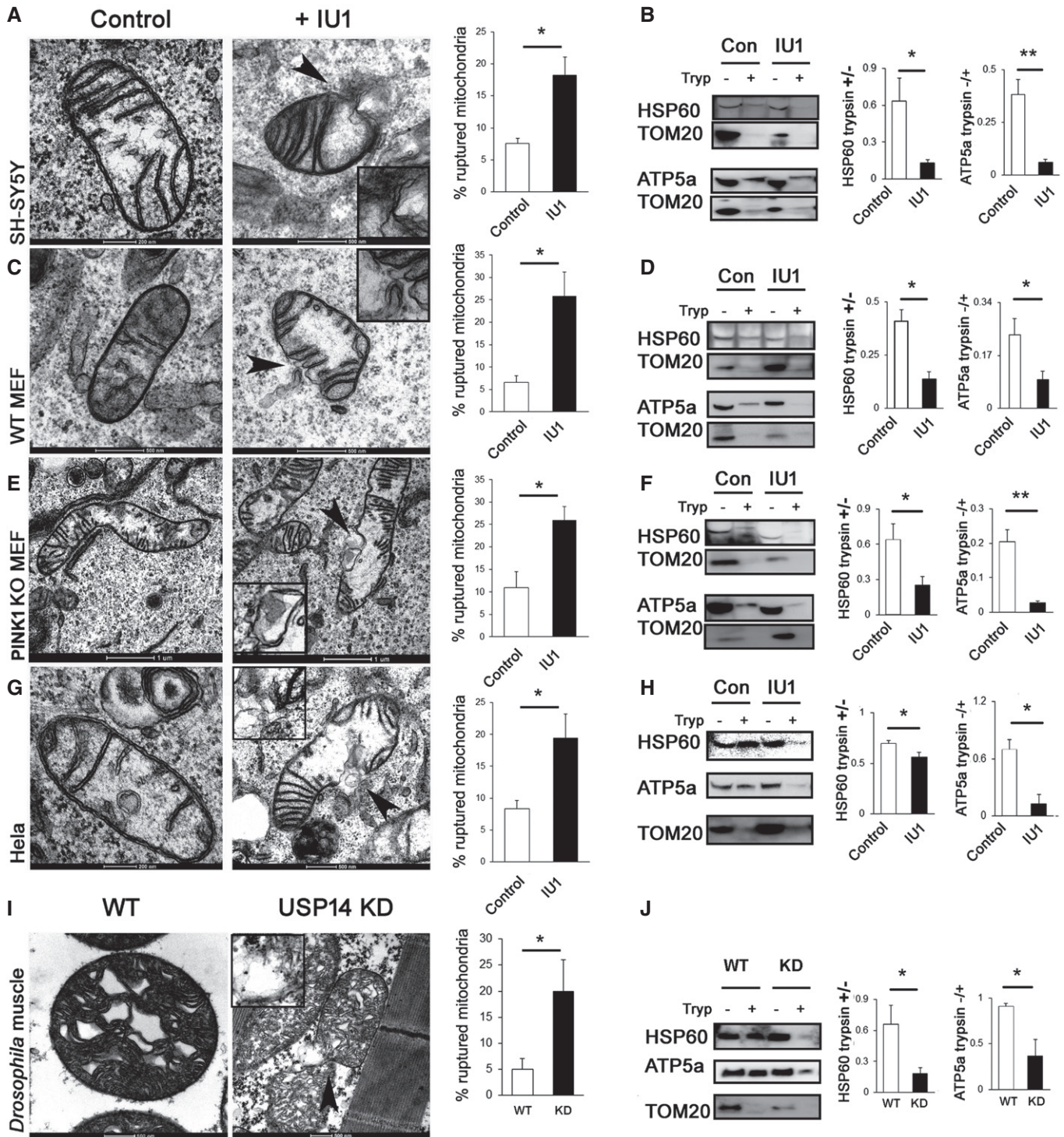


Figure 4.



**Figure 5. USP14 inhibition or knockdown ruptured mitochondrial membrane integrity.**

A–J | (A, C, E, G, I) Electron microscopy images of mitochondria from SH-SY5Y, MEF WT, MEF PINK1 KO HeLa and *Drosophila* thoracic muscle, as indicated in the figure, with/without USP14 inhibition/knockdown. Arrowheads in the IU1-treated groups indicate the mitochondrial rupture point. Bar graphs represent the mean ( $\pm$  SEM) of the percentage of ruptured mitochondria from at least three different experiments. For cells, a total of 150–300 mitochondria for the control group and 150–190 mitochondria from the IU1-treated groups were counted. For flies, more than 200 mitochondria from each group were counted from five different experiments. (B, D, F, H, J) Representative immunoblots of isolated mitochondria from the indicated groups treated with/without trypsin and probed for HSP60, ATP5a and TOM20. Bar graphs represent the mean  $\pm$  SEM of the ratio of densitometric levels of the indicated proteins (with/without trypsin) from at least three independent experiments. Student's *t*-test; \* $P \leq 0.05$ , \*\* $P \leq 0.01$ .

Source data are available online for this figure.

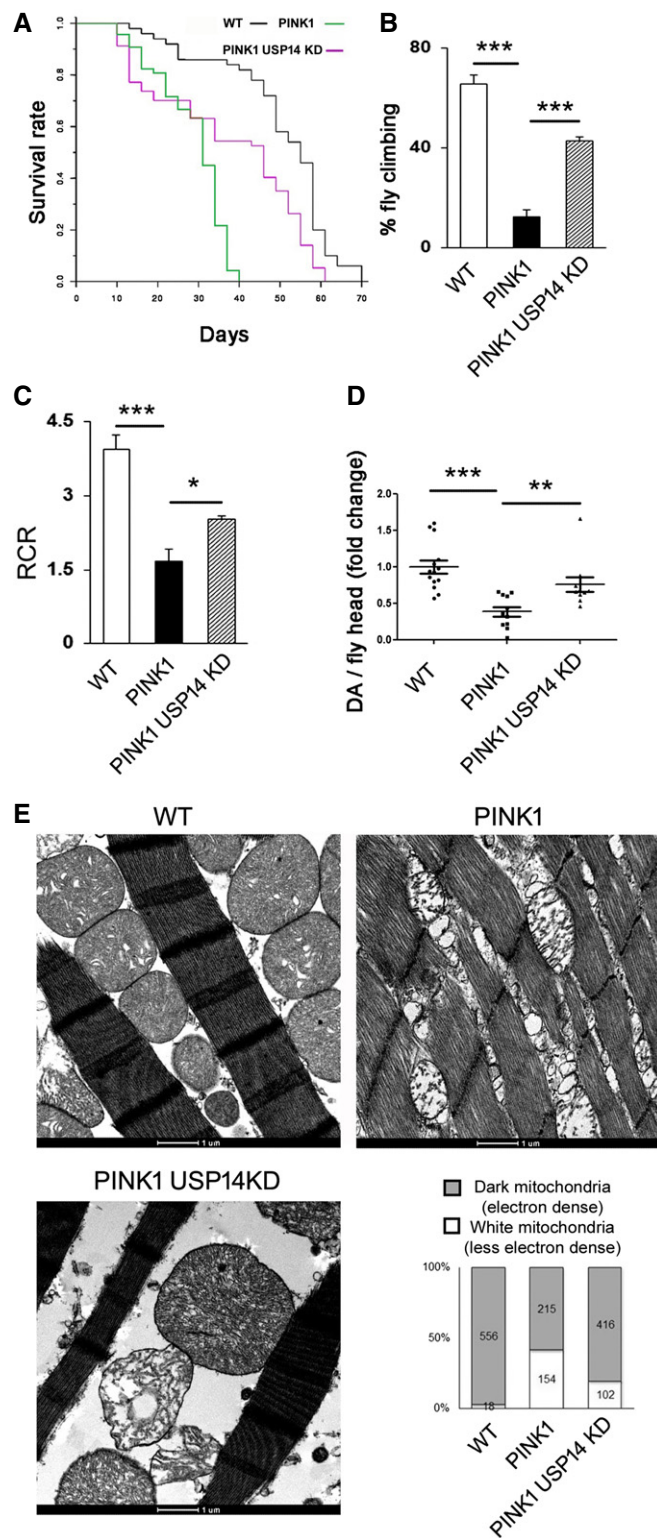


**Figure 6. USP14 knockdown corrects life span, locomotor impairment, mitochondrial respiratory defects and muscle degeneration of PINK1-deficient flies.**

- A** Life span analysis of flies of the indicated genetic background. At least 50 flies were monitored from each group. Log-rank test (Mantel–Cox test, Mantel–Haenszel test,  $P < 0.0001$ ).
- B** Bar graph represents the mean  $\pm$  SEM of the climbing performance of flies of the indicated genotypes.  $n = 4-7$ . ANOVA followed by Newman–Keuls test.
- C** Quantitative analysis of respiratory fitness of isolated mitochondria extracted from flies of the indicated genotypes. Graph shows respiratory control rate (RCR) calculated as described in Materials and Methods and represents the mean  $\pm$  SEM.  $N = 4-5$ , ANOVA followed by Newman–Keuls test.
- D** Dopamine content in the fly heads (15 days old) was measured by HPLC, and the individual fold change values are represented in the scatter plot. Graph represents the mean  $\pm$  SEM.  $N = 14, 11$  and 11 fly heads for control, PINK1 and PINK1+USP14 KD flies, respectively. ANOVA followed by Newman–Keuls test.
- E** Enlarged representative TEM images of flight muscle mitochondria of the indicated genotypes. The experiment was repeated three times in replicate. Bar graph represents quantification of electron-dense mitochondria (represented as grey bar) and depolarised mitochondria with ruptured cristae (represented as white bars) from the indicated genotypes.
- Data information: \* $P \leq 0.05$ , \*\* $P \leq 0.01$ , \*\*\* $P \leq 0.001$ .

(Appendix Fig S15). Since this result was not in accordance with what was previously reported, we could not test the potential protective effect of USP14 inhibition in this cell model.

## Discussion

Currently, the efficient clearance of dysfunctional mitochondria is modelled to be dependent on three key steps: (i) mitochondrial-shaping and outer membrane protein post-translational modifications (Gomes *et al*, 2011; Kageyama *et al*, 2014); (ii) UPS-mediated mitochondrial membrane rupture (Tanaka *et al*, 2010; Yoshii *et al*, 2011); and (iii) engulfment of mitochondria by autophagic vesicles (Wei *et al*, 2017). Although the precise sequence of events is not clear, it is unequivocally accepted that both UPS and autophagic machinery are required for the completion of mitophagy. Therefore, enhancement of proteasome activity and increased autophagy together might lead to maximal mitophagy. Based on this rationale, recently deubiquitinating enzymes (DUBs) emerged as an alternative to antagonise Parkin/PINK1 dependency for mitophagy (Bingol *et al*, 2014; Durcan *et al*, 2014). In this regard, USP14 stands in a unique juncture because of its non-selectiveness to the type of ubiquitination (Xu *et al*, 2015) that can influence both autophagy and proteasome activity, other than its well-known direct inhibitory effect on UPS.

In this study, we found that USP14 modulation can affect mitophagy by inducing autophagy and by enhancing proteasome-mediated mitochondrial rupture. Among the other factors, we found that USP14-mediated mitophagy is dependent on mitochondrial dynamics DRP1 and Mfn2 and occurs independently of PINK1 and Parkin. Most importantly, we report for the first time that USP14 knockdown or its pharmacological inhibition with specific inhibitor IU1 offers beneficial effects upon PINK1 or Parkin loss dependent phenotype *in vivo*.

PINK1 mutations (i.e. c.1366C>T; p.Q456X nonsense mutations; L2124) to assess the potential effect of USP14 inhibition. We tested the overall ATP content in iPSC cells derived from PINK1 patients as previously reported (Morais *et al*, 2014). However, we did not find a significant decrease in the overall ATP content in cells derived from PINK1 patients as compared to age-matched control fibroblasts



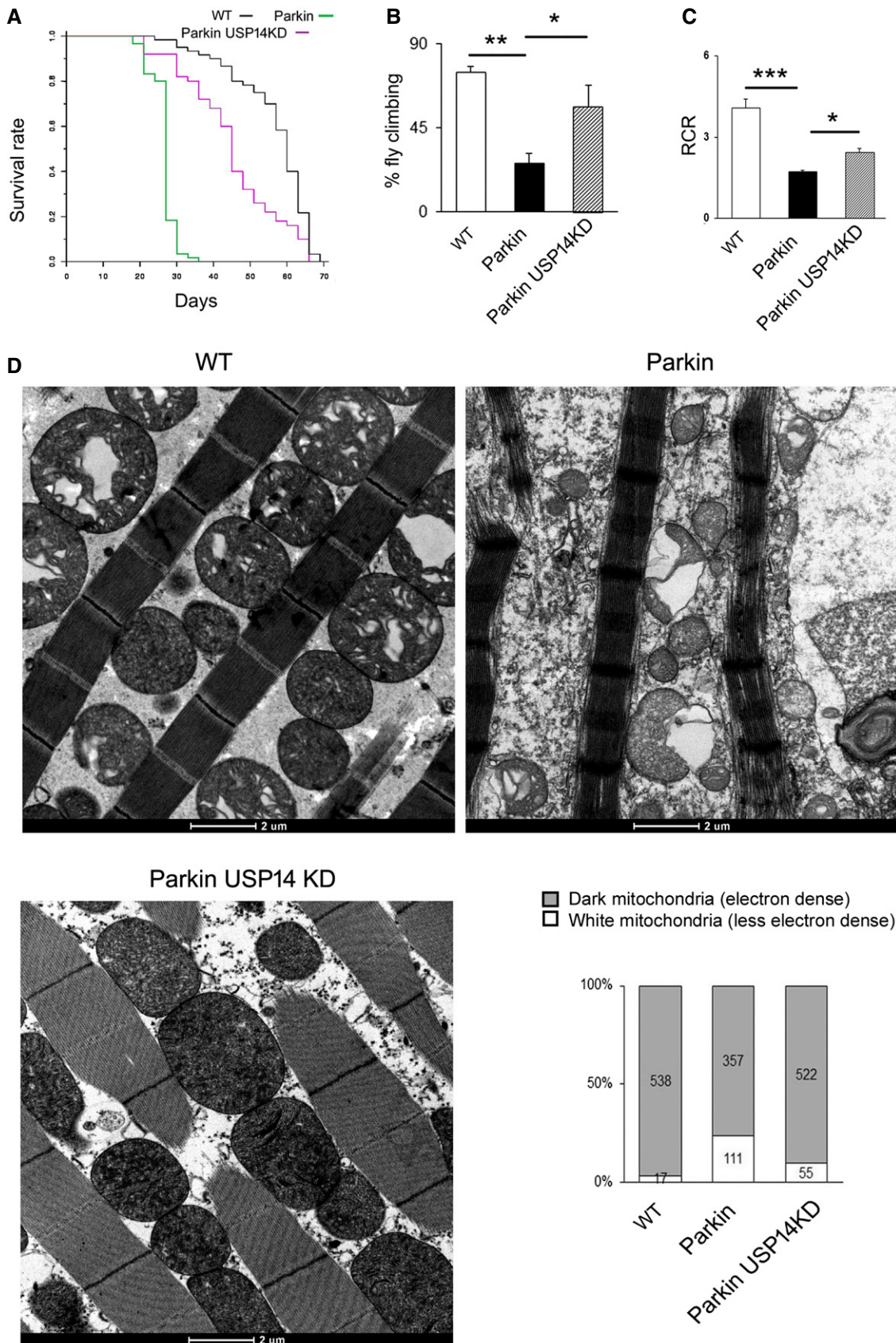


Figure 7.

**Figure 7. USP14 knockdown corrects life span, locomotor impairment, mitochondrial respiratory defects and muscle degeneration of Parkin-deficient flies.**

- A Life span analysis of flies of the indicated genetic background. At least 50 flies were analysed for each group. Log-rank test (Mantel–Cox test, Mantel–Haenszel test,  $P < 0.0001$ ).
- B Bar graph represents the mean  $\pm$  SEM of the climbing performance of flies of the indicated genotypes. One-way ANOVA followed by Newman–Keuls test,  $n = 3$ .
- C Quantitative analysis of respiratory fitness of isolated mitochondria extracted from flies of the indicated genotypes. Graph shows (mean  $\pm$  SEM,  $n = 3$  independent experiments) respiratory control rate (RCR) calculated as described. One-way ANOVA followed by Newman–Keuls test.
- D Enlarged representative TEM images of flight muscle mitochondria of the indicated genotypes. The experiment was repeated three times in replicate. Bar graph represents quantification of electron-dense mitochondria (represented as grey bar) and mitochondria with ruptured cristae (represented as white bars) from the indicated genotypes.
- Data information: \* $P \leq 0.05$ , \*\* $P \leq 0.01$ , \*\*\* $P \leq 0.001$ .

USP14 can negatively regulate proteasome activity by increasing the docking time of the protein onto proteasome (Hanna *et al*, 2006; Lee *et al*, 2016; Kuo & Goldberg, 2017); however, the mechanism by which it does so remains unclear. USP14 is reported to affect the 20S gate opening as well as affect its activity allosterically (Peth *et al*, 2009; Kim & Goldberg, 2017). IU1, a specific inhibitor of USP14, binds to active or proteasome-associated USP14 without showing any effect on other DUBs. This inhibitor was identified as an enhancer of proteasome activity from a molecular screening of small-molecule library (Lee *et al*, 2010). In addition to its well-documented activity as an enhancer of the proteasome, USP14 inhibition by IU1 has also been shown to lead to increased autophagy by stabilising K63 ubiquitination of Beclin1 (Xu *et al*, 2016). However, previous studies did not investigate the potential effect of IU1 or USP14 knockdown on mitophagy.

In accordance with earlier studies, we found increased degradation of proteasomal substrates and increased proteasome activity in IU1-treated cells and upon USP14 knockdown. In addition, we found that genetic and pharmacological inhibition of USP14 increases autophagosome/autolysosome formation and enhance mitochondrial clearance in a human dopaminergic cell line. Mito-Keima and LC3–mitochondria co-localisation experiments along with electron microscopic studies also support that USP14 inhibition enhances mitophagy.

USP14 inhibition activates the proteasome and promotes autophagy, but how does that impact mitophagy? Proteasome can influence mitophagy by different ways. Proteasome-mediated Miro degradation, which disrupts its complex with mitochondria, halts the movement of the organelle. This is essential for mitophagy (Wang *et al*, 2011; Hsieh *et al*, 2016). Also, effective mitophagy requires the translocation of the proteasome complex on mitochondria to rupture the mitochondrial membrane (Tanaka *et al*, 2010; Yoshii *et al*, 2011; Wei *et al*, 2017). In the current study, immunofluorescence and immunogold labelling assays confirmed the close physical interaction between the proteasome and mitochondria after USP14 inhibition or knockdown. Thus, one of the key downstream events in the activation of mitophagy (i.e. recruitment of proteasome complex onto mitochondria) is sustained upon USP14 inhibition. Furthermore, by employing two different approaches (i.e. electron microscopy analyses and trypsin digestion assays), we demonstrated a clear correlation between proteasome translocation to mitochondria and mitochondrial membrane rupture upon USP14 inhibition, both prerequisites for mitophagy.

Among the other factors, we found that USP14-mediated mitophagy requires the mitochondria-shaping proteins DRP1 and Mfn2. The dependency on DRP1 is due to the fact that mitochondria fragment before clearance (Gomes *et al*, 2011). On the other

hand, Mfn2 overexpression has detrimental effects on mitochondrial quality control *in vivo* (Yun *et al*, 2014) and Mfn2 is indispensable for efficient mitophagy (Hailey *et al*, 2010; Hamasaki *et al*, 2013), operating as a molecular receptor for the recruitment of Parkin (Chen & Dorn, 2013). Mfn2 is also a key modulator of ER–mitochondria interaction at the mitochondria–endoplasmic reticulum (ER) membrane contacts (MERCs), which are sites of close juxtaposition between the two organelles that are required for DRP1-mediated mitochondrial fission (de Brito & Scorrano, 2008; Friedman *et al*, 2011; Naon *et al*, 2016; which itself is a prerequisite for mitophagy), LC3 recruitment (Yang & Yang, 2013) and autophagosome formation (Hailey *et al*, 2010; Hamasaki *et al*, 2013). In the light of this, it is conceivable that USP14 inhibition depends on Mfn2 for mitophagy.

Next, we addressed whether USP14 inhibition-mediated mitophagy is dependent on the PD proteins Parkin and PINK1, which are required for stress-induced mitophagy (Narendra *et al*, 2008, 2010; Ziviani *et al*, 2010). Much has been unveiled about the functioning of the two proteins using *Drosophila* as the fast and reliable genetic model (Clark *et al*, 2006; Park *et al*, 2006; Yang *et al*, 2006; Poole *et al*, 2008). The canonical pathway illustrates that upon translocation to mitochondria, PINK1 becomes membrane potential-dependently inactivated, by MPP-AFG3L2-PARL proteins (Narendra *et al*, 2008). In depolarised mitochondria, PINK1 recruits Parkin in a process that requires phosphorylation of Parkin (Murialdo *et al*, 1986; Merkwirth *et al*, 2008; Merkwirth & Langer, 2009), ubiquitin (Lee *et al*, 2016) and Mfn2 (Chen & Dorn, 2013). Parkin recruitment and activation results in the ubiquitination of a number of OMM-resident proteins, including Mfn1 and Mfn2, TOM20, VDAC and Fis1, which is a prerequisite for the orchestration of the mitophagic process (Chen & Dorn, 2013). However, we did not evaluate the synergistic effect of IU1 upon stress-induced PINK1/Parkin-dependent mitophagy in the current study, and it remains open for further investigations. Here, we show that USP14 affects mitophagy independently of PINK1 or Parkin and that USP14 knockdown offers beneficial effects *in vivo* by correcting PINK1- or Parkin-loss-mediated decreased life span, locomotor deficit and mitochondrial dysfunction. In addition, and perhaps more importantly, our study showed that pharmacological inhibition of USP14 by IU1 is also protective *in vivo*, paving the way for a potential therapeutic potential for this drug. Our study showed no toxicity by IU1, in terms of life span and motor neuron survivability of *Drosophila*. Other studies also showed no toxicity of IU1 on neuronal population (Boselli *et al*, 2017; Min *et al*, 2017). However, while chronic intranasal administration is an option, the blood–brain barrier permeability of the drug is yet to be studied. The study by Lee

*et al* (2010) has already shown that IU1 crosses cell membrane quite readily, advocating the possibility that it may also cross the blood–brain barrier; however, the metabolism of the drug needs further characterisation in higher mammals.

This study is the first effort to fully characterise the *in vivo* biology of a proteasome-associated deubiquitinating enzyme in the context of mitophagy. A similar effort has also been made earlier by Bingol *et al* (2014) where a mitochondrial DUB showed antagonising effect with PINK1/Parkin. These data reveal a new mechanism for mitochondrial quality control mediated by USP14 supporting the notion of a physiological cross-talk between mitophagy and the UPS *in vivo*. In conclusion, our study demonstrates for the first time how regulating UPS activity, autophagy and mitochondrial clearance may offer a therapeutic strategy to reduce the levels of aberrant proteins and organelles in cells and in the whole organism *in vivo*.

## Materials and Methods

### Antibodies and reagents

The following primary antibodies were used: anti-LC3, anti-ATP5a, anti-OPA1, anti-Mfn1, anti-Mfn2 and anti-proteasome 20S ( $\alpha$ + $\beta$ ) were from Abcam; anti-HSP60, anti-TOM20 and anti-PHB2 were from Santa Cruz Biotechnology; anti-DRP1 and anti-USP14 were from Cell Signaling; anti-GFP was from Thermo Fisher Scientific; and anti-Fis1 was from Enzo Life Sciences. HRP-conjugated anti-mouse or anti-rabbit secondary antibodies were from Thermo Fisher Scientific, and Alexa Fluor 488/555-conjugated anti-mouse or anti-rabbit secondary antibodies were from Life Technology. IU1 was purchased from Sigma-Aldrich. Other sources of the reagents are indicated below when mentioned.

### Plasmids

Mito-Keima was acquired from MBL International. Ub-R-GFP was obtained from Addgene. Mito-YFP, DRP1 variant and Cre in adenoviral or retroviral backbone were procured from Dr. Luca Scorrano's laboratory (Cereghetti *et al*, 2008; Costa *et al*, 2010).

### Cell culture, transfection, treatment and viability assays

Human midbrain dopaminergic cell line SH-SY5Y, mouse embryonic fibroblast (MEF) cells, HeLa cells and human control or Parkin mutant (exon 3 deletion plus Arg275 to Tryp) fibroblast cells were maintained in Dulbecco's modified Eagle's medium (DMEM; Thermo Fisher), supplemented with 10% heat-inactivated foetal bovine serum (Thermo Fisher). PHB2<sup>F/F</sup> cells were a kind gift from Dr. Thomas Langer. ATG7 KO cells were procured from Dr. Luca Scorrano's laboratory. Cells were maintained in a humidified incubator at 5% CO<sub>2</sub> level. *Drosophila* S2R+ cells were cultured in Schneider's medium (Invitrogen) supplemented with 10% heat-inactivated foetal calf serum (Sigma) and were maintained at 25°C.

Human fibroblasts from skin biopsy were obtained from B.A., a 55-year-old man who was diagnosed with PD at the age of 28 and presented an excellent response to a combination of levodopa and

dopamine agonists until 2008. He then started complaining about motor fluctuations and involuntary movements and more recently developed pathological gambling, excessive impulsivity, aggressiveness and substance abuse (mainly cocaine). Cognitive testing in 2016 showed abnormalities in frontal executive and attention domains. His MRI revealed modest cortical and subcortical atrophy. Cells were grown in Dulbecco's modified Eagle's medium (DMEM) (Gibco) with the addition of 1% penicillin/streptomycin, 1% non-essential amino acid solution, L-glutamine and 10% FBS at 37°C with 5% CO<sub>2</sub> atmosphere.

Cells were transfected with mito-YFP/mito-Keima/DRP1K38A-YFP/Ub-GFP plasmids using TransFectin™ (Bio-Rad) and expressed for at least 24 h, and then split into different treatment groups to achieve a homogeneously transfected cell population among the vehicle/IU1 treatment groups. For USP14 (Cell Signaling) siRNA transfection, we used Oligofectamine™ reagent (Invitrogen) using 100 nM siRNA for each treatment. We used the same amount of scrambled siRNA as the control. USP14 knockdown was done for 24–72 h. For Cre transfection in PHB2<sup>F/F</sup> cells, we used either adenoviral (for immunoblot) or retroviral transfection (for imaging) using standard protocol, exposing the cells at least for 24 h before starting the treatment.

For MTT assay, the cells were plated on 96-well plates, and after the treatment period, 100  $\mu$ l MTT solution (10 mg in 10 ml DMEM) was added. The cells were incubated for 2 h and then lysed using DMSO. The reading was taken at 550 nm.

For Hoechst and propidium iodide staining, we followed the standard protocol and concentrations (Hoechst: 1  $\mu$ g/ml; and propidium iodide: 1.5  $\mu$ M). Automated imaging and analysis was done using the Operetta imaging system (PerkinElmer).

### Chymotrypsin-like activity assay of proteasome complex

After treatment, 25  $\mu$ g whole-fly tissue lysate in proteasome assay buffer (Tris 10 mM, pH 7.4, EDTA 1 mM, ATP 5 mM, DTT 5 mM and glycerol 20%, v/v) was taken onto proteasome activity buffer (Tris 50 mM, pH 7.4, EDTA 0.5 mM) and incubated with 50  $\mu$ M substrate for chymotrypsin-like activity (N-Suc-Leu-Leu-Val-Tyr-7-amido-4-methylcoumarin) for 1 h at 37°C. The reading was taken at 380 nm excitation and 460 nm emission. MG132 was used to monitor the specificity, only protein lysate (no substrate) was kept in activity buffer to monitor autofluorescence, and only substrate (no protein sample) was used to monitor spontaneous breakdown of the substrate.

### Mitochondrial morphology analysis

For mitochondrial volume measurements, SH-SY5Y/MEF cells were transfected with mito-YFP plasmid and the next day plated on coverslips for the appropriate treatment. For S2R+ cells, mitochondria were stained with MitoTracker Green (Life Technologies). Z-stack images (with 0.2  $\mu$ m increments) of mitochondria from the cells were taken using a confocal microscope (Andromeda iMIC spinning disc live cell microscope, TILL Photonics, 60 $\times$  objective). We used the ImageJ plugin Volumej for the 3D-rendered representative images of mitochondria. The ImageJ plugin MitoLoc (Vowinckel *et al*, 2015) was used to determine the volume and fragmentation index. For fragmentation index

calculation, we considered sum of fragment volume which individually constituted  $\leq 20\%$  of the total volume of mitochondria in a SH-SY5Y cell, whereas for S2R+ cells, we considered 25%.

### Trypsin digestion assay in isolated mitochondria or permeabilised cells

Mitochondria were extracted from cells/flyes by differential centrifugation. Each sample was homogenised using a Dounce glass–glass potter in mannitol–sucrose buffer (225 mM mannitol, 75 mM sucrose, 5 mM HEPES, 0.1 mM EGTA, pH 7.4) supplemented with 2% BSA. The samples were first centrifuged at  $1,500 \times g$  at  $4^\circ\text{C}$  for 6 min, and the supernatant was then centrifuged again for 6 min at  $6,000 \times g$ . The pellet was washed with mannitol–sucrose buffer and centrifuged again at  $6,000 \times g$  for 6 min. The pellet was then re-suspended in a small volume of mannitol–sucrose buffer. Around 100  $\mu\text{g}$  of mitochondria was treated with 200  $\mu\text{g}/\text{ml}$  trypsin (TPCK treated; Worthington Biochemical) for 15–20 min (depending on the cell type) at  $4^\circ\text{C}$  in trypsin digestion buffer (10 mM sucrose, 0.1 mM EGTA/Tris and 10 mM Tris/HCl, pH 7.4); then, the samples were mixed with LDS sample buffer (Life Technologies) +  $\beta$ -mercaptoethanol (Sigma). The samples were run for immunoblotting as described.

For the intact cells, first, the cells were digitonin-treated (0.015%, 2 min), washed twice in PBS, re-suspended in trypsin digestion buffer and divided into two parts. One part was treated with trypsin (200  $\mu\text{g}/\text{ml}$ ) for 15–20 min (depending on the cell type) at  $4^\circ\text{C}$ . Digestion was stopped by adding LDS sample buffer (Life Technologies) +  $\beta$ -mercaptoethanol (Sigma). Quantification of the corresponding protein intensity is represented in the bar graphs as ratio of - after trypsin : without trypsin digestion of the corresponding proteins. Protein levels of the OMM protein TOM20 were monitored as positive control for trypsin digestion efficiency.

### Mitochondrial respiration

The rate of mitochondrial  $\text{O}_2$  consumption was monitored using an Oxytherm System (Hansatech) with magnetic stirring and temperature control, maintained at  $25^\circ\text{C}$ . Isolated *Drosophila* mitochondria were re-suspended in respiration buffer (120 mM KCl, 5 mM Pi-Tris, 3 mM HEPES, 1 mM EGTA, 1 mM  $\text{MgCl}_2$ , pH 7.2) in the Oxytherm System.  $\text{O}_2$  consumption was analysed according to the slope of the graph, after adding malate–pyruvate (10 mM) and ADP (200  $\mu\text{M}$ ). Respiratory control ratios state III versus state IV (200 mM ADP-stimulated respiration over 1  $\mu\text{g}/\text{ml}$  oligomycin-administered respiration) were also determined from the registered graphs.

### Immunoblotting

In brief, the cells were collected in RIPA buffer (SH-SY5Y or MEF cells) supplemented with 10 mM NEM, 10 mM MG132 (Sigma) and protease inhibitor cocktail (Roche). The lysate was incubated on ice for 30 min before being centrifuged at  $10,000 \times g$  for 15 min at  $4^\circ\text{C}$ . 25–40  $\mu\text{g}$  protein was run on SDS gels and transferred to PVDF membranes. The following commercial antibodies were used: anti-LC3 (1:1,000; Abcam), anti-PHB2 (1:1,000; Santa Cruz Biotechnology), anti-HSP60 (1:1,000; Santa Cruz

Biotechnology), anti-ATP5a (1:3,000; Abcam), anti-actin (1:10,000; Chemicon), anti-GFP (1:1,000; Invitrogen), anti-TOM20 (1:5,000; Santa Cruz Biotechnology), anti-Mfn1 (1:1,000; Abcam), anti-Mfn2 (1:1,000; Abcam), anti-USP14 (1:2,000; Cell Signaling), anti-OPA1 (1:2,000; Abcam), anti-DRP1 (1:1,000; Cell Signaling) and anti-Fis1 (1:500; Enzo Life Sciences). For detection, secondary antibodies conjugated to HRP (Chemicon) were used (1:3,000), and immunoreactivity was visualised with ECL chemiluminescence (Amersham).

### Immunostaining and proximity ligation assay

For immunofluorescence analysis, the cells were plated on coverslips and grown for 24 h. After the treatment for the scheduled time period, the cells were washed with 0.1 M PBS (pH 7.2), fixed with 4% paraformaldehyde for 30 min, permeabilised with 0.1% Triton X-100 (Sigma) for 5 min, blocked with 4% BSA (Sigma) for 30 min and finally incubated overnight with the primary antibody prepared in PBS containing 2% BSA and 0.05% Triton X-100. The next day, after washing with PBS, the cells were incubated with a fluorescently tagged secondary antibody for 1 h. After washing with PBS, the cells were taken onto slides and mounted with anti-fade mounting media (Invitrogen). Z-stack images (with 0.2 or 0.4  $\mu\text{M}$  increment) were taken using a confocal microscope (Andromeda iMIC spinning disc live cell microscope, TILL Photonics, 60 $\times$  objective). The following primary antibodies were used for the study: LC3 (rabbit polyclonal, Abcam, 1:200), HSP60 (rabbit polyclonal, Santa Cruz Biotechnology, 1:200), ATP5a (mouse monoclonal, Abcam, 1:500) and proteasome 20S  $\alpha+\beta$  (rabbit polyclonal, Abcam, 1:100). Secondary antibodies tagged with Alexa Fluor 488 or 555 (Invitrogen, 1:500) were used for the corresponding primary antibody.

For proximity ligation assay, we used a kit from Sigma-Aldrich and followed the manufacturer's instructions. We fixed the subconfluent cells grown on coverslips with 4% PFA and incubated with Prohibitin 2 (Santa Cruz Biotechnology, 1:100) and LC3 antibody (Abcam, 1:200).

### Electron microscopy

Cells cultured in 24-well plates or thoraces from adult male flies were fixed in 2% paraformaldehyde and 2.5% glutaraldehyde for 1 h/overnight. After rinsing in 0.1 M cacodylate buffer with 1% tannic acid, the samples were post-fixed in 1:1 2%  $\text{OsO}_4$  and 0.2 M cacodylate buffer for 1 h. The samples were rinsed, dehydrated in ethanol and embedded in Epon. Ultrathin sections were examined using a transmission electron microscope. Data are represented as the number of dark and white mitochondria for electron-dense or depolarised mitochondria, respectively.

For characterising autophagic vacuoles, we followed the standard guidelines (Klionsky et al, 2016).

For immunogold labelling, cells fixed with 4% PFA were permeabilised with saponin and incubated overnight with proteasome 20S antibody (Abcam, 1:100). Nanogold-labelled secondary antibody (1:100) was incubated for 2 h, fixed with 1% glutaraldehyde and enhanced for 5–10 min by Gold enhancer (Nanoprobes).

## Drosophila stocks, treatment and climbing assay

*Drosophila* stocks were maintained under standard conditions at 25°C on agar, cornmeal and yeast food. Park25 mutants have been described before (Greene *et al*, 2003). PINK1B9 mutants were provided by Dr. J. Chung (KAIST, South Korea). Actin-Gal4 strains were obtained from the Bloomington *Drosophila* Stock Center (Bloomington). UAS-USP14 KD lines were obtained from VDRC Stock Center.

The USP14 inhibitor IU1 (Sigma) was administered to flies in the food. IU1 (or DMSO) was diluted in water to the desired concentration and used to reconstitute dry Formula 4–24 Instant *Drosophila* Medium (Carolina Biological Supply). Three-day-old mutant or control flies in groups of ten were fed on the supplemented food for 72 h, and subsequently, climbing assay was performed.

For the climbing assay, after scheduled time point, groups of 9–10 flies were collected and placed into empty transparent tubes (12 × 5 cm). Tubes were placed under a light source, and flies were gently tapped to the bottom of the tube. The number of flies that successfully climbed above the 6-cm mark after 10 s was counted. Fifteen consecutive trials were performed for each experiment, and the average was taken.

Food intake was measured by adding food colouring (Patent Blue E131) in the fly food supplemented with vehicle or IU1. Flies kept for 3 days in the food were weighed (10/group) and homogenised in 10 volumes of PBS. The homogenate was centrifuged, and food colouring in the supernatant was measured by monitoring the absorption at 615 nm.

## Life span analysis

*Drosophila* from the mentioned genotypes were collected during 12 h after hatching and grouped into 20 flies per food vial. At least 50 flies were used for the analysis. The flies were transferred to fresh food (and fresh drug for the inhibitor treatment) every 3 days, and the number of dead flies was counted simultaneously.

## Dopamine measurement

Fifteen-day-old male *Drosophila* heads were dissected out and collected separately in 20 µl of ice-cold 0.2 N perchloric acid. Then, the tissue was homogenised by sonication for 15 s and kept on ice for another 20 min and centrifuged at 12,000 × g for 10 min, and 5 µl of the supernatant was injected into a HPLC system equipped with a Rheodyne injector and a guard cell, set to +350 mV (E1 = +150 mV, E2 = –350 mV, s: 2 nA). A C<sub>18</sub> ion-pair, reverse-phase analytical column (4.6 × 250 mm; 5 µm particle size; Agilent Technologies, USA) was used for the separation with a flow rate of 0.8 ml/min. The mobile phase contained 75 mM sodium phosphate monobasic monohydrate, 6% acetonitrile, 1.7 mM 1-octane sulfonic acid and 25 µM EDTA (pH 3 ± 0.01). Dopamine values were determined by comparing with the standard peak value.

## Human fibroblasts and iPSC cells derived from PINK1 PD-causing mutation

The PINK1-derived induced pluripotent stem (iPS) cells were obtained according to the previously described protocol (Twig *et al*,

## The paper explained

### Problem

Cells need to clear damaged mitochondria through autophagy (mitophagy) for cell survival. Not surprisingly, perturbation of mitophagy has been correlated with age-related neurodegenerative disorders. Mitophagy is a multi-step process requiring both activation of autophagy and the proteasome. However, how to orchestrate both in order to stimulate mitophagy for therapeutic applications has not been fully addressed.

### Results

Our results show that USP14 inhibition activates both the proteasome and autophagy and results in mitochondrial clearance. Mitochondrial fragmentation and mitochondrial membrane rupture to expose Prohibitin 2 were found to be essential to exhibit USP14 effect. *In vivo*, genetic or pharmacological inhibition of USP14 corrected mitochondrial dysfunction and locomotion performance of the PINK1 and Parkin mutant *Drosophila* model of Parkinson's disease (PD), an age-related progressive neurodegenerative disorder whose aetiology has been directly correlated with deficient mitochondrial quality control.

### Impact

Our study identified a novel therapeutic target antagonising mitochondrial dysfunction and *in vivo* PD-related symptoms and may lead to a novel strategy design for neurodegenerative disorders.

2008), where previously published patient (L2124) and age-matched control (HFF NT and L2131) lines were analysed.

## ATP determination

ATP levels measured in lysates from cell lines were determined as described in Harper *et al* (2018) using a luminescent solution (ATP Determination Kit; Invitrogen) according to the supplier's protocol. Luminescence values was measured on an EnVision Multilabel Reader (PerkinElmer), and luminescent ATP (nmol) was determined using a standard curve and normalised to total protein content (mg) measured by BCA assay (Pierce).

## Statistics

Representative graphs presented in the figures are mean ± standard error of the mean or as mentioned in the figure legends. Two-tailed Student's *t*-test or one-way ANOVA was employed to determine the level of significance of comparisons between two groups or more than two groups, respectively, unless mentioned in the text. Dunnett's *post hoc* test was done to compare the experimental groups with the control group. The Newman–Keuls test was used for multiple comparisons where only three groups were involved, and Tukey's multiple comparison test was employed for comparisons where more than three groups were involved, as mentioned in the figure legends.  $P \leq 0.05$  was considered as significant difference. For survival study, we used log-rank test (Mantel–Cox test, Mantel–Haenszel test). Please refer to Table EV1 for exact *n* and *P*-values.

The sample size was chosen to ensure 80% power to detect an effect size of 0.75 on the basis of 5% type I error rate. No samples or animals were excluded from the analysis. Animals as well as samples were randomly chosen for treatment.

## Human subjects

The study protocol was approved by the ethics committee of Fondazione Ospedale San Camillo IRCCS, Venice, Italy. Informed consent was obtained from all subjects, and the experiments conformed to the WMA Declaration of Helsinki and the Department of Health and Human Services Belmont Report.

**Expanded View** for this article is available online.

## Acknowledgements

This work was supported by grants from the Italian Ministry of Health “Ricerca Finalizzata” [GR-2011-02351151], Rita Levi Montalcini “Brain Gain” programme and Michael J. Fox RRIA 2014 [Grant ID 9795] to E.Z. We also thank PISCOPIA-Marie Curie fellowship for the support provided to Dr. Chakraborty. We would like to acknowledge Francesco Boldrin from the EM Facility for his help and technical support. We are also deeply grateful to Professor Luca Scorrano and Dr. Lena Pernas for critical reading of the manuscript.

## Author contributions

JC designed and performed the experimental work and data analysis and contributed to manuscript writing. SvS designed, performed and analysed *in vivo* fly experiments. EM performed Hoechst/propidium iodide viability assay and some of the Western blots. FC performed electron microscopy acquisition and provided technical support. VF performed the HPLC experiment. AR generated PINK1-derived iPS cells and performed ATP content analysis. AA provided human primary fibroblasts from *parkin* patient. CK and LB read the manuscript and intellectually contributed to the work. EZ designed the experiments and wrote the manuscript.

## Conflict of interest

The authors declare that they have no conflict of interest.

## References

- Baumann K (2018) Mitochondria: the needless PINK1. *Nat Rev Mol Cell Biol* 19: 76
- Bingol B, Tea JS, Phu L, Reichelt M, Bakalarski CE, Song Q, Foreman O, Kirkpatrick DS, Sheng M (2014) The mitochondrial deubiquitinase USP30 opposes parkin-mediated mitophagy. *Nature* 510: 370–375
- Boselli M, Lee BH, Robert J, Prado MA, Min SW, Cheng C, Silva MC, Seong C, Elsasser S, Hatle KM *et al* (2017) An inhibitor of the proteasomal deubiquitinating enzyme USP14 induces tau elimination in cultured neurons. *J Biol Chem* 292: 19209–19225
- de Brito OM, Scorrano L (2008) Mitofusin 2 tethers endoplasmic reticulum to mitochondria. *Nature* 456: 605–610
- Cereghetti GM, Stangherlin A, Martins de Brito O, Chang CR, Blackstone C, Bernardi P, Scorrano L (2008) Dephosphorylation by calcineurin regulates translocation of Drp1 to mitochondria. *Proc Natl Acad Sci USA* 105: 15803–15808
- Chan NC, Salazar AM, Pham AH, Sweredoski MJ, Kolawa NJ, Graham RL, Hess S, Chan DC (2011) Broad activation of the ubiquitin-proteasome system by Parkin is critical for mitophagy. *Hum Mol Genet* 20: 1726–1737
- Chen Y, Dorn GW II (2013) PINK1-phosphorylated mitofusin 2 is a Parkin receptor for culling damaged mitochondria. *Science* 340: 471–475
- Clark IE, Dodson MW, Jiang C, Cao JH, Huh JR, Seol JH, Yoo SJ, Hay BA, Guo M (2006) *Drosophila* pink1 is required for mitochondrial function and interacts genetically with parkin. *Nature* 441: 1162–1166
- Costa V, Giacomello M, Hudec R, Lopreiato R, Ermak G, Lim D, Malorni W, Davies KJ, Carafoli E, Scorrano L (2010) Mitochondrial fission and cristae disruption increase the response of cell models of Huntington’s disease to apoptotic stimuli. *EMBO Mol Med* 2: 490–503
- Dantuma NP, Lindsten K, Glas R, Jellne M, Masucci MG (2000) Short-lived green fluorescent proteins for quantifying ubiquitin/proteasome-dependent proteolysis in living cells. *Nat Biotechnol* 18: 538–543
- Durcan TM, Tang MY, Perusse JR, Dashti EA, Aguilera MA, McLelland GL, Gros P, Shaler TA, Faubert D, Coulombe B *et al* (2014) USP8 regulates mitophagy by removing K6-linked ubiquitin conjugates from parkin. *EMBO J* 33: 2473–2491
- Friedman JR, Lackner LL, West M, DiBenedetto JR, Nunnari J, Voeltz GK (2011) ER tubules mark sites of mitochondrial division. *Science* 334: 358–362
- Gomes LC, Di Benedetto G, Scorrano L (2011) During autophagy mitochondria elongate, are spared from degradation and sustain cell viability. *Nat Cell Biol* 13: 589–598
- Greene JC, Whitworth AJ, Kuo I, Andrews LA, Feany MB, Pallanck LJ (2003) Mitochondrial pathology and apoptotic muscle degeneration in *Drosophila* parkin mutants. *Proc Natl Acad Sci USA* 100: 4078–4083
- Hailey DW, Rambold AS, Satpute-Krishnan P, Mitra K, Sougrat R, Kim PK, Lippincott-Schwartz J (2010) Mitochondria supply membranes for autophagosome biogenesis during starvation. *Cell* 141: 656–667
- Hamasaki M, Furuta N, Matsuda A, Nezu A, Yamamoto A, Fujita N, Oomori H, Noda T, Haraguchi T, Hiraoka Y *et al* (2013) Autophagosomes form at ER-mitochondria contact sites. *Nature* 495: 389–393
- Hanna J, Hathaway NA, Tone Y, Crosas B, Elsasser S, Kirkpatrick DS, Leggett DS, Gygi SP, King RW, Finley D (2006) Deubiquitinating enzyme Ubp6 functions noncatalytically to delay proteasomal degradation. *Cell* 127: 99–111
- Harper JW, Ordureau A, Heo JM (2018) Building and decoding ubiquitin chains for mitophagy. *Nat Rev Mol Cell Biol* 19: 93–108
- Hsieh CH, Shaltouki A, Gonzalez AE, Bettencourt da Cruz A, Burbulla LF, St Lawrence E, Schule B, Krainc D, Palmer TD, Wang X (2016) Functional impairment in Miro degradation and mitophagy is a shared feature in familial and sporadic Parkinson’s disease. *Cell Stem Cell* 19: 709–724
- Kageyama Y, Hoshijima M, Seo K, Bedja D, Sysa-Shah P, Andrabi SA, Chen W, Hoke A, Dawson VL, Dawson TM *et al* (2014) Parkin-independent mitophagy requires Drp1 and maintains the integrity of mammalian heart and brain. *EMBO J* 33: 2798–2813
- Kim HT, Goldberg AL (2017) The deubiquitinating enzyme Usp14 allosterically inhibits multiple proteasomal activities and ubiquitin-independent proteolysis. *J Biol Chem* 292: 9830–9839
- Kitada T, Asakawa S, Hattori N, Matsumine H, Yamamura Y, Minoshima S, Yokochi M, Mizuno Y, Shimizu N (1998) Mutations in the parkin gene cause autosomal recessive juvenile parkinsonism. *Nature* 392: 605–608
- Klionsky DJ, Abdelmohsen K, Abe A, Abedin MJ, Abeliovich H, Acevedo Arozena A, Adachi H, Adams CM, Adams PD, Adeli K *et al* (2016) Guidelines for the use and interpretation of assays for monitoring autophagy (3rd edition). *Autophagy* 12: 1–222
- Kuo CL, Goldberg AL (2017) Ubiquitinated proteins promote the association of proteasomes with the deubiquitinating enzyme Usp14 and the ubiquitin ligase Ube3c. *Proc Natl Acad Sci USA* 114: E3404–E3413
- Lee BH, Lee MJ, Park S, Oh DC, Elsasser S, Chen PC, Gartner C, Dimova N, Hanna J, Gygi SP *et al* (2010) Enhancement of proteasome activity by a small-molecule inhibitor of USP14. *Nature* 467: 179–184






- Lee BH, Lu Y, Prado MA, Shi Y, Tian G, Sun S, Elsasser S, Gygi SP, King RW, Finley D (2016) USP14 deubiquitinates proteasome-bound substrates that are ubiquitinated at multiple sites. *Nature* 532: 398–401
- Merkwirth C, Dargazanli S, Tatsuta T, Geimer S, Lower B, Wunderlich FT, von Kleist-Retzow JC, Waisman A, Westermann B, Langer T (2008) Prohibitins control cell proliferation and apoptosis by regulating OPA1-dependent cristae morphogenesis in mitochondria. *Genes Dev* 22: 476–488
- Merkwirth C, Langer T (2009) Prohibitin function within mitochondria: essential roles for cell proliferation and cristae morphogenesis. *Biochim Biophys Acta* 1793: 27–32
- Min JW, Lu L, Freeling JL, Martin DS, Wang H (2017) USP14 inhibitor attenuates cerebral ischemia/reperfusion-induced neuronal injury in mice. *J Neurochem* 140: 826–833
- Mizuno Y, Yoshino H, Ikebe S, Hattori N, Kobayashi T, Shimoda-Matsubayashi S, Matsumine H, Kondo T (1998) Mitochondrial dysfunction in Parkinson's disease. *Ann Neurol* 44: S99–S109
- Morais VA, Haddad D, Craessaerts K, De Bock PJ, Swerts J, Vilain S, Aerts L, Overbergh L, Grunewald A, Seibler P et al (2014) PINK1 loss-of-function mutations affect mitochondrial complex I activity via Ndufa10 ubiquinone uncoupling. *Science* 344: 203–207
- Murialdo G, De Maria A, Bonura ML, Polleri A, Menardo G, Falchero M, Perata A, Marengo G (1986) Changes of testosterone-binding protein and free testosterone in patients with acute viral hepatitis. *Presse Med* 15: 78
- Naon D, Zaninello M, Giacomello M, Varanita T, Grespi F, Lakshminarayanan S, Serafini A, Semenzato M, Herkenne S, Hernandez-Alvarez MI et al (2016) Critical reappraisal confirms that Mitofusin 2 is an endoplasmic reticulum-mitochondria tether. *Proc Natl Acad Sci USA* 113: 11249–11254
- Narendra D, Tanaka A, Suen DF, Youle RJ (2008) Parkin is recruited selectively to impaired mitochondria and promotes their autophagy. *J Cell Biol* 183: 795–803
- Narendra DP, Jin SM, Tanaka A, Suen DF, Gautier CA, Shen J, Cookson MR, Youle RJ (2010) PINK1 is selectively stabilized on impaired mitochondria to activate Parkin. *PLoS Biol* 8: e1000298
- Park J, Lee SB, Lee S, Kim Y, Song S, Kim S, Bae E, Kim J, Shong M, Kim JM et al (2006) Mitochondrial dysfunction in *Drosophila* PINK1 mutants is complemented by parkin. *Nature* 441: 1157–1161
- Parker WD Jr, Boyson SJ, Parks JK (1989) Abnormalities of the electron transport chain in idiopathic Parkinson's disease. *Ann Neurol* 26: 719–723
- Peth A, Besche HC, Goldberg AL (2009) Ubiquitinated proteins activate the proteasome by binding to Usp14/Ubp6, which causes 20S gate opening. *Mol Cell* 36: 794–804
- Pickles S, Vigie P, Youle RJ (2018) Mitophagy and quality control mechanisms in mitochondrial maintenance. *Curr Biol* 28: R170–R185
- Poddighe S, Bhat KM, Setzu MD, Solla P, Angioy AM, Marotta R, Ruffilli R, Marrosu F, Liscia A (2013) Impaired sense of smell in a *Drosophila* Parkinson's model. *PLoS ONE* 8: e73156
- Poole AC, Thomas RE, Andrews LA, McBride HM, Whitworth AJ, Pallanck LJ (2008) The PINK1/Parkin pathway regulates mitochondrial morphology. *Proc Natl Acad Sci USA* 105: 1638–1643
- Saini N, Georgiev O, Schaffner W (2011) The parkin mutant phenotype in the fly is largely rescued by metal-responsive transcription factor (MTF-1). *Mol Cell Biol* 31: 2151–2161
- Schapira AH, Cooper JM, Dexter D, Clark JB, Jenner P, Marsden CD (1990) Mitochondrial complex I deficiency in Parkinson's disease. *J Neurochem* 54: 823–827
- Shimura H, Hattori N, Kubo S, Mizuno Y, Asakawa S, Minoshima S, Shimizu N, Iwai K, Chiba T, Tanaka K et al (2000) Familial Parkinson disease gene product, parkin, is a ubiquitin-protein ligase. *Nat Genet* 25: 302–305
- Silvestri L, Caputo V, Bellacchio E, Atorino L, Dallapiccola B, Valente EM, Casari G (2005) Mitochondrial import and enzymatic activity of PINK1 mutants associated to recessive parkinsonism. *Hum Mol Genet* 14: 3477–3492
- Tanaka A, Cleland MM, Xu S, Narendra DP, Suen DF, Karbowski M, Youle RJ (2010) Proteasome and p97 mediate mitophagy and degradation of mitofusins induced by Parkin. *J Cell Biol* 191: 1367–1380
- Twig G, Elorza A, Molina AJ, Mohamed H, Wikstrom JD, Walzer G, Stiles L, Haigh SE, Katz S, Las G et al (2008) Fission and selective fusion govern mitochondrial segregation and elimination by autophagy. *EMBO J* 27: 433–446
- Valente EM, Abou-Sleiman PM, Caputo V, Muqit MM, Harvey K, Gispert S, Ali Z, Del Turco D, Bentivoglio AR, Healy DG et al (2004) Hereditary early-onset Parkinson's disease caused by mutations in PINK1. *Science* 304: 1158–1160
- Vowinckel J, Hartl J, Butler R, Ralser M (2015) MitoLoc: a method for the simultaneous quantification of mitochondrial network morphology and membrane potential in single cells. *Mitochondrion* 24: 77–86
- Wang X, Winter D, Ashrafi G, Schlehe J, Wong YL, Selkoe D, Rice S, Steen J, LaVoie MJ, Schwarz TL (2011) PINK1 and Parkin target Miro for phosphorylation and degradation to arrest mitochondrial motility. *Cell* 147: 893–906
- Wei Y, Chiang WC, Sumpter R Jr, Mishra P, Levine B (2017) Prohibitin 2 is an inner mitochondrial membrane mitophagy receptor. *Cell* 168: 224–238 e210
- Xu D, Shan B, Lee BH, Zhu K, Zhang T, Sun H, Liu M, Shi L, Liang W, Qian L et al (2015) Phosphorylation and activation of ubiquitin-specific protease-14 by Akt regulates the ubiquitin-proteasome system. *Elife* 4: e10510
- Xu D, Shan B, Sun H, Xiao J, Zhu K, Xie X, Li X, Liang W, Lu X, Qian L et al (2016) USP14 regulates autophagy by suppressing K63 ubiquitination of Beclin 1. *Genes Dev* 30: 1718–1730
- Yang Y, Gehrke S, Imai Y, Huang Z, Ouyang Y, Wang JW, Yang L, Beal MF, Vogel H, Lu B (2006) Mitochondrial pathology and muscle and dopaminergic neuron degeneration caused by inactivation of *Drosophila* Pink1 is rescued by Parkin. *Proc Natl Acad Sci USA* 103: 10793–10798
- Yang JY, Yang WY (2013) Bit-by-bit autophagic removal of parkin-labelled mitochondria. *Nat Commun* 4: 2428
- Yoshii SR, Kishi C, Ishihara N, Mizushima N (2011) Parkin mediates proteasome-dependent protein degradation and rupture of the outer mitochondrial membrane. *J Biol Chem* 286: 19630–19640
- Yun J, Puri R, Yang H, Lizzio MA, Wu C, Sheng ZH, Guo M (2014) MUL1 acts in parallel to the PINK1/parkin pathway in regulating mitofusin and compensates for loss of PINK1/parkin. *Elife* 3: e01958
- Ziviani E, Tao RN, Whitworth AJ (2010) *Drosophila* parkin requires PINK1 for mitochondrial translocation and ubiquitinates mitofusin. *Proc Natl Acad Sci USA* 107: 5018–5023



**License:** This is an open access article under the terms of the Creative Commons Attribution 4.0 License, which permits use, distribution and reproduction in any medium, provided the original work is properly cited.



# Inhibition of the deubiquitinase USP8 corrects a *Drosophila* PINK1 model of mitochondria dysfunction

Sophia von Stockum<sup>1</sup>, Alvaro Sanchez-Martinez<sup>2</sup> , Samantha Corrà<sup>3,4</sup>, Joy Chakraborty<sup>3</sup>, Elena Marchesan<sup>1</sup>, Lisa Locatello<sup>3</sup> , Caterina Da Rè<sup>3,4</sup>, Paola Cusumano<sup>3,4</sup>, Federico Caicci<sup>3</sup>, Vanni Ferrari<sup>3</sup>, Rodolfo Costa<sup>3,4</sup> , Luigi Bubacco<sup>3</sup>, Maria Berica Rasotto<sup>3</sup>, Ildiko Szabo<sup>3</sup>, Alexander J Whitworth<sup>2</sup> , Luca Scorrano<sup>3,5</sup>, Elena Ziviani<sup>1,3</sup> 

**Aberrant mitochondrial dynamics disrupts mitochondrial function and contributes to disease conditions. A targeted RNA interference screen for deubiquitinating enzymes (DUBs) affecting protein levels of multifunctional mitochondrial fusion protein Mitofusin (MFN) identified USP8 prominently influencing MFN levels. Genetic and pharmacological inhibition of USP8 normalized the elevated MFN protein levels observed in PINK1 and Parkin-deficient models. This correlated with improved mitochondrial function, locomotor performance and life span, and prevented dopaminergic neurons loss in *Drosophila* PINK1 KO flies. We identified a novel target antagonizing pathologically elevated MFN levels, mitochondrial dysfunction, and dopaminergic neuron loss of a *Drosophila* model of mitochondrial dysfunction.**

DOI [10.26508/lsa.201900392](https://doi.org/10.26508/lsa.201900392) | Received 1 April 2019 | Revised 4 April 2019 | Accepted 5 April 2019 | Published online 15 April 2019

## Introduction

Mitochondria dysfunction plays critical role in neurodegenerative conditions affecting the elderly, such as Parkinson's disease (PD) (Moore et al, 2005; Bueler, 2009; Vives-Bauza et al, 2010a; Ryan et al, 2015). Mitochondria function directly correlates with mitochondria dynamics and balanced remodeling of the mitochondrial network through fission and fusion events to control mitochondria shape and ultrastructure. Intuitively, fusion maintains the mitochondrial network and allows intermixing of matrix contents, such as mtDNA and metabolites; fission is needed to populate new cells with new mitochondria (Twig et al, 2008b; Gomes & Scorrano, 2008; Malena et al, 2009) and plays a substantial role in the mitochondria quality control. A key aspect of mitochondrial quality control is a well-characterized process called mitophagy that segregates and selectively eliminates damaged mitochondria via autophagy (Twig et al, 2008a; Twig & Shirihai, 2011). During stress-induced mitophagy, the

cytoplasmic protein Parkin, mutated in familial PD and encoding an E3 ubiquitin ligase (Shimura et al, 2000), translocates in a PINK1-dependent manner to dysfunctional mitochondria (Narendra et al, 2008; Vives-Bauza et al, 2010b; Ziviani et al, 2010). In this process, kinase PINK1, also mutated in familial PD (Silvestri et al, 2005), phosphorylates Parkin (Sha et al, 2010), its targets (Wang et al, 2011; Chen & Dorn, 2013), and ubiquitin itself (Koyano et al, 2014) promoting Parkin translocation (Narendra et al, 2010; Ziviani et al, 2010) and Parkin activity (Lazarou et al, 2013; Koyano et al, 2014; Zhang et al, 2014). On depolarized mitochondria, Parkin ubiquitinates the mitochondrial pro-fusion protein Mitofusin (MFN) (Gegg et al, 2010; Poole et al, 2010; Tanaka et al, 2010; Ziviani et al, 2010; Sarraf et al, 2013) leading to p97/VCP-mediated retrotranslocation and proteasomal degradation (Tanaka et al, 2010). In addition, Parkin ubiquitinates the mitochondrial protein translocase TOM20, mitochondrial VDAC/Porin and Fis1 (Sarraf et al, 2013), and it also promotes the degradation of Miro (Wang et al, 2011), a protein that couples mitochondria to microtubules. Selected mitochondria are, therefore, deprived of their pro-fusion protein MFN, isolating them from the mitochondrial network, before degradation via autophagy. This mechanism is consistent with observations showing that mitochondria cluster around the perinuclear area (Vives-Bauza et al, 2010b) and fragment before mitophagy (Twig et al, 2008a; Poole et al, 2008). Genetic studies in *Drosophila* showed that down-regulation of MFN or promotion of mitochondrial fission by expressing pro-fission protein DRP1 rescues Parkin KO phenotypes, and those of kinase PINK1 (Deng et al, 2008; Poole et al, 2008), which acts upstream of Parkin (Clark et al, 2006; Park et al, 2006; Yang et al, 2006). This genetic interaction can be in part explained biochemically by the fact that Parkin ubiquitinates MFN to control its steady-state levels (Gegg et al, 2010; Tanaka et al, 2010; Ziviani et al, 2010; Rakovic et al, 2011) that are elevated in Parkin and PINK1 KO models (Ziviani et al, 2010). Thus, interventions that restore MFN levels can ameliorate Parkin and PINK1 phenotypes, presumably by impinging on the numerous

<sup>1</sup>Fondazione Ospedale San Camillo, IRCCS, Venezia, Italy <sup>2</sup>MRC Mitochondrial Biology Unit, Cambridge Biomedical Campus, Cambridge, UK <sup>3</sup>Department of Biology, University of Padova, Padova, Italy <sup>4</sup>Neurogenetics and Behavior of *Drosophila* Lab, Department of Biology, University of Padova, Padova, Italy <sup>5</sup>Dulbecco-Telethon Institute, Venetian Institute of Molecular Medicine, Padova, Italy

Correspondence: [elena.ziviani@unipd.it](mailto:elena.ziviani@unipd.it)



MFN functions that in the fruit fly include both promotion of fusion and ER–mitochondria crosstalk (Debattisti et al, 2014).

To identify other mechanisms regulating MFN levels, we performed an RNA interference screen for deubiquitinating enzymes (DUBs) that affect steady-state levels of MFN. DUBs participate in important reversible signaling pathways (Salmena & Pandolfi, 2007) and are attractive druggable candidates (Hussain et al, 2009; Colland, 2010). We identified USP8, an evolutionary conserved DUB whose down-regulation correlates with decreased MFN levels. USP8 has previously been linked to PINK1/Parkin-dependent mitophagy in cell culture and under intoxicating conditions (Durcan et al, 2014), but no in vivo studies have been reported. Here, we demonstrate that in vivo under basal conditions, genetic and pharmacological inhibition of USP8 ameliorates *Drosophila* phenotypes deriving from loss of function of PINK1 and Parkin.

## Results

### A targeted siRNA screening identifies DUBs affecting MFN protein levels

Steady-state levels of MFN protein in *Drosophila* PINK1 or Parkin KO background are increased (Ziviani et al, 2010), and interventions that decrease MFN levels can ameliorate *Drosophila* PINK1 and Parkin phenotypes (Celardo et al, 2016; Deng et al, 2008; Poole et al, 2008). Given the importance of MFN in inter-organellar communication (Cosson et al, 2012; de Brito & Scorrano, 2008; Filadi et al, 2015) and mitophagy (Chen & Dorn, 2013), we set out to identify regulators of its steady-state levels. We designed an unbiased loss-of-function screen using dsRNA to inhibit the expression of 35 known or predicted fly DUBs. Fly DUBs were identified by domain similarity and based on the list of 79 human DUBs (Dupont et al, 2009) (Table 1). We transiently expressed flag-tagged MFN in S2R+ cells to mimic pathologically elevated MFN and down-regulated each of the 35 DUBs. To assess the effect of DUB silencing on steady-state MFN levels, we performed Western blotting analysis on cell lysates and quantified the levels of unmodified MFN normalized for the loading control and expressed it as fold change (Fig 1A). Flag-tagged MFN exhibited mitochondrial subcellular localization, and its expression in S2R+ cells resulted in an elongated mitochondrial network (Fig S1A). We identified two DUBs whose down-regulation resulted in decreased MFN levels (CG5798/USP8 and CG5384/USP14) and two DUBs, whose down-regulation resulted in increased MFN levels (CG5505/USP36, CG2904/Echinus) (Fig 1B). Down-regulation of Parkin or PINK1 increased MFN levels, as previously described (Tanaka et al, 2010; Ziviani et al, 2010). Of the two DUBs causing decreased MFN levels, USP8 was the highest scoring hit that decreased MFN levels (Fig 1B). USP8 interacts with many substrates such as the epidermal growth factor receptor, an essential regulator of proliferation and differentiation, and regulates endosomal trafficking by ubiquitin-mediated sorting of the endocytosed cargoes (Mizuno et al, 2005; Row et al, 2006; Williams & Urbe, 2007). Moreover, USP8 knockdown protects from  $\alpha$ -synuclein-induced locomotor deficits and cell loss in an  $\alpha$ -synuclein fly model of PD (Alexopoulou et al, 2016). It was also shown that USP8 regulates induced mitophagy by

controlling Parkin recruitment to depolarized mitochondria after CCCP treatment (Durcan et al, 2014). More recently, it has been found that it can regulate basal autophagy in the absence of CCCP, although its role has not been thoroughly characterized in this process and it is controversial (Jacomin et al, 2015). USP8 is also highly expressed in the brain and up-regulated in neurodegenerative conditions (Paardi et al, 2014), which makes it of neurological interest.

### USP8 down-regulation correlates with decreased MFN protein levels

We next validated if USP8 down-regulation correlated with changes in MFN protein levels. Upon efficient USP8 down-regulation in fly cells, as assessed by qPCR (Fig S1B), steady-state levels of endogenous (Figs 1C and S1C) or exogenously expressed tagged MFN were decreased (Fig 1D) and mitochondria appeared accordingly fragmented (Fig S1D). The effect was specific for USP8 because re-expression of USP8 in USP8 RNAi cells restored MFN levels (Fig 1D). In contrast, in cells overexpressing USP8, levels of exogenously expressed (Fig 1D) and endogenous MFN were increased (Fig 1E) and mitochondria were elongated and clumped, accumulating in the perinuclear area (Fig S1E).

We next assessed the impact of USP8 down-regulation on MFN levels in vivo. To this aim, we drove efficient whole body USP8 knockdown (KD) by using the Actin5C driver (Act-GAL4>USP8-RNAi), achieving significant USP8 down-regulation at 29°C (Fig S1F). Attempts to increase USP8 down-regulation efficiency by using the stronger GAL4 driver *daughterless* (*da*) caused larvae lethality, suggesting that USP8 expression levels in vivo are tightly regulated. Act-GAL4>USP8-RNAi on the other hand was viable with no apparent locomotor defects. As previously observed in vitro, levels of MFN were reduced in vivo in USP8 down-regulating flies (Fig 1F). We also found decreased MFN levels in protein extracts coming from flies carrying heterozygous USP8 gene deletion (USP8<sup>-/+</sup>) (Mukai et al, 2010), further supporting that the effect is specific for USP8 (Fig 1G).

### USP8 down-regulation ameliorates the phenotype of PINK1 KO flies

We addressed whether USP8 knockdown in PINK1 KO flies prevented the multiple phenotypes recapitulating key features of locomotor and cellular defects manifested in the flies as degeneration of dopaminergic (DA) neurons and reduced climbing ability. We also assessed the flight muscle, mitochondria ultrastructure, male fertility, and life span, all degenerated or affected in PINK1 KO flies (Clark et al, 2006; Park et al, 2006; Yang et al, 2006). Immunostaining for the specific DA neuronal marker tyrosine hydroxylase (TH) allowed the inspection of the DA neuronal network composed of well-characterized DA neuron clusters (PPM1, PPM2, PPM3, PPL1, PPL2, and VUM) in brains (Fig 2A). PINK1 KO showed the expected reduction in TH staining and exhibited a small but significant decrease in the number of DA neurons in the PPL1 DA neuronal cluster (Fig 2B and C) (Park et al, 2006; Wang et al, 2006; Yang et al, 2006). Accordingly, dopamine levels measured from PINK1 KO heads were significantly lower compared with control flies (Fig 2D). USP8 down-regulation completely prevented the loss of

**Table 1. Complete list of the 75 human known or predicted DUBs and their fly homologue, when known or predicted, based on sequence similarity. Where available, Entrez/PubMed gene ID and fly gene name is provided.**

Gene name	Gene ID	Fly homologue	Fly gene name
UCHL1	7345	CG4265	
UCHL3	7347	CG4265	
BAP1	8314	CG8445	CALYPSO
UCHL5/UCH37	51377	CG3431	
DUB3	377630	CG5505	USP36/SCRAWNY
USP1	7398	CG15817	USP1
USP2	9099	CG14619	
USP3	9960	CG5798	UBPY/USP8
USP4	7375	CG8334	
USP5	8078	CG12082	
USP6	9098	CG8334	
USP7/HAUSP	7874	CG1490	USP7
USP8/USPY	9101	CG5798	UBPY/USP8
USP9X/FAM	8239	CG1945	FAT FACETS
USP10	9100	CG32479	
USP11	8237	CG8334	
USP12	219333	CG7023	USP12-46
USP13	8975	CG12082	USP5
USP14	9097	CG5384	
USP15	9958	CG12082	
USP16	10600	CG4165	USP16-45
USP18	11274	CG5486	USP64E/USP47
USP19	10869	CG8334	
USP20	10868	CG8494	
USP21	27005	CG14619	
USP22	23326	N/A	
USP24	23358	CG1945	FAT FACETS
USP25	29761	CG5794	PUF/USP34
USP26	83844	CG5798	USP8/USPY
USP27X	389856	CG4166	NOT
USP28	57646	CG5794	PUF/USP34
USP29	57663	CG5798	USP8/USPY
USP30	84749	CG3016	
USP31	57478	CG30421	USP15-31
USP32	84669	CG8334	
USP33	23032	CG8494	USP20-33
USP34	9736	CG5794	PUF/USP34
USP35	57558	CG8830	DUBAI
USP36	57602	CG5505	
USP37	57695	CG5798	USP8/USPY
USP38	84640	CG8830	DUBAI

(Continued on following page)

**Table 1. Continued**

Gene name	Gene ID	Fly homologue	Fly gene name
USP39	10713	CG7288	
USP40	55230	CG5486	USP64E/USP47
USP41	373856	CG5486	USP64E/USP47
USP42	84132	CG5505	USP36/SCRAWNY
USP43	124739	CG30421	USP15-31
USP44	84101	CG5798	USP8/USPY
USP45	85015	CG4165	USP16-45
USP46	64854	CG7023	USP12-46
USP47	55031	CG5486	USP64E/USP47
USP48	84196	CG1490	USP7
USP49	25862	CG5798	USP8/USPY
USP50	373509	CG5798	USP8/USPY
USP51	158880	CG4166	NOT
USP52	9924	CG8232	PAN2
USP53	54532	CG2904	ECHINUS
USP54	159195	CG2904	ECHINUS
OTUB1	55611	CG4968	
CYLD	1540	CG5603	
TNFAIP3/A20	7128	CG9448	TRABID
OTUD1	220213	CG6091	
YOD1	55432	CG4603	
OTUD3	23252	CG6091	
OTUD4	54726	CG12743	OTU
OTUD6A	139562	CG7857	
OTUD6B	51633	CG7857	
OTUD7A	161725	CG9448	TRABID
OTUD7B	56957	CG9448	TRABID
TRABID	54764	CG9448	TRABID
ATXN3	4287	CG13379	
ATX3L	N.A.	CG13379	
JOSD1	9929	CG3781	
JOSD2	126119	CG3781	
AMSH/STAMBIP	10617	CG2224	
AMSH-LP	57559	CG2224	

PINK1 KO DA neurons (Fig 2B and C), restoring dopamine to wild-type levels (Fig 2D). Moreover, USP8 down-regulation ameliorated the shorter longevity (Fig 2E), corrected thoracic muscle fiber disorganization with enlarged electron transparent mitochondria and irregular myofibril arrays (Park et al, 2006) (Fig 2F) typical of the PINK1 KO flies (Park et al, 2006). More importantly, ultrastructural transmission electron microscopy (TEM) analysis showed that the mitochondrial cristae, fragmented and sparsely packed in PINK1 mutants, were recovered with highly increased electron-dense staining intensity (Fig 2G). USP8 knockdown also ameliorated the PINK1 climbing defect (Fig 2H).

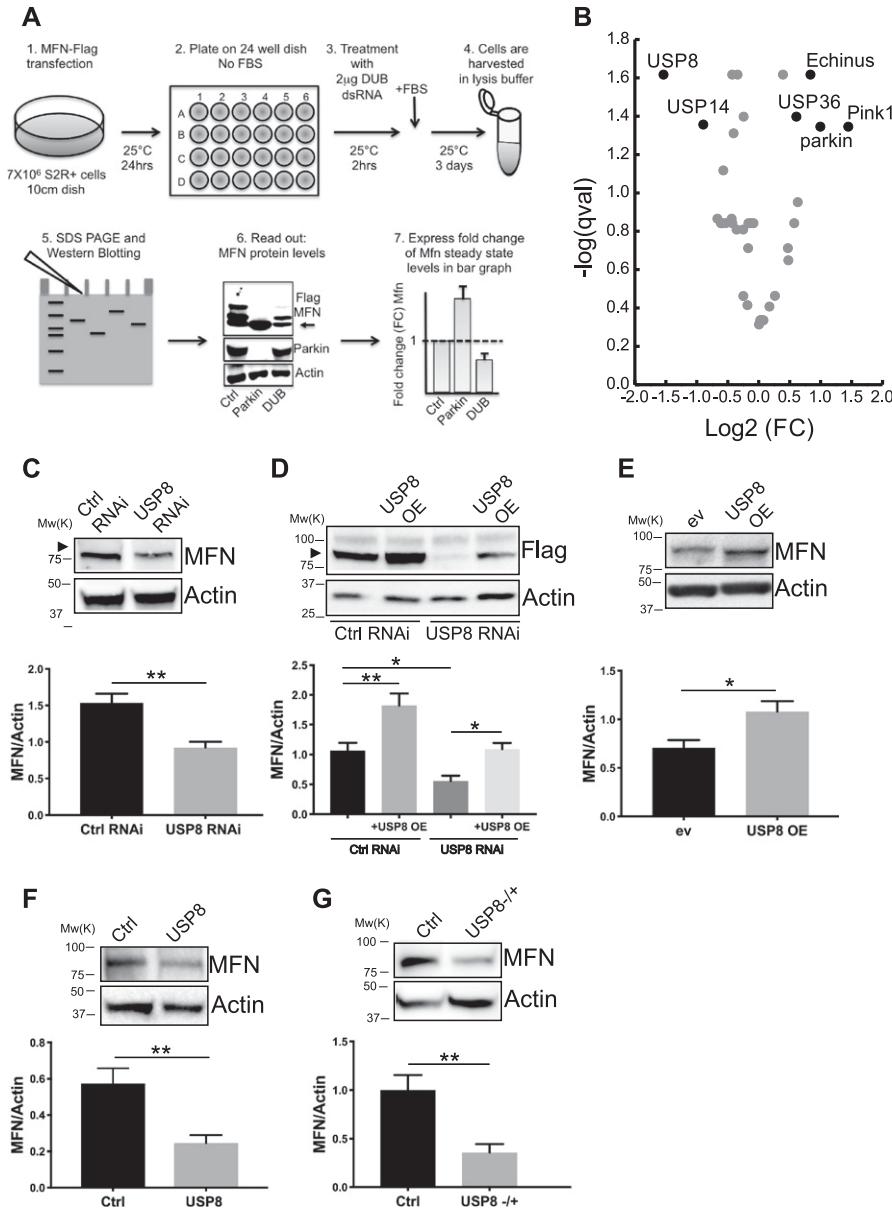


**Figure 1. A targeted siRNA screening identified DUB USP8 whose down-regulation correlates with decreased MFN levels.**

**(A)** siRNA screen to identify DUBs affecting pathologically elevated MFN protein levels. Protein extracts from *Drosophila* S2R+ cells expressing equal amounts of Flag-MFN and treated with 2  $\mu$ g dsRNA probe were separated by SDS-PAGE and immunoblotted using an anti-Flag antibody. Densitometric analysis of MFN signal normalized to loading control and expressed as fold change (FC) versus control dsRNA was used as read out to identify DUBs whose down-regulation affects MFN protein levels. **(B)** Volcano plot constructed by plotting the negative log of the FDR corrected *P* value (*qval*) on the y-axis against the log of the FC calculated in (A). Those points that are found toward the top of the plot far to either the left- or right-hand side represent values with large FC and high statistical significance. A threshold of  $P < 0.05$  and  $0.75 < FC < 1.3$  led to the identification of four DUBs whose down-regulation resulted in either decreased MFN levels (USP8 FC =  $0.345 \pm 0.04$ , *qval* = 0.024; USP14 FC =  $0.537 \pm 0.06$ , *qval* = 0.044) or increased MFN levels (Echinus FC =  $1.784 \pm 0.13$ , *qval* = 0.024; USP36 FC =  $1.524 \pm 0.12$ , *qval* = 0.040). Down-regulation of PINK1 or Parkin led to increased MFN levels (FC =  $2.724 \pm 0.44$ , *qval* = 0.045; and FC =  $1.994 \pm 0.28$ , *qval* = 0.045, respectively). **(C)** S2R+ cells were transfected with the indicated siRNA (Ctrl and USP8) and lysed after 3 d. Equal amounts of protein (30  $\mu$ g) were separated by SDS-PAGE and immunoblotted using the indicated antibodies. Representative of *n* = 6. Graph bar shows mean  $\pm$  SEM of ratio between densitometric levels of MFN and those of Actin from at least eight independent experiments. Means are significantly different according to *t* test;  $P = 0.0025$  (\*\*), *n* = 6. **(D)** S2R+ cells were transfected with the indicated plasmid (MFN-Flag, USP8) and siRNA (Ctrl and USP8) and lysed after 3 d. Equal amounts of protein (30  $\mu$ g) were separated by SDS-PAGE and immunoblotted using the indicated antibodies. Representative of *n* = 5. Graph bar shows mean  $\pm$  SEM of ratio between densitometric levels of Flag (MFN) and those of Actin relatively to control from at least four independent experiments. One-way ANOVA;  $P < 0.0001$  (\*\*\*\*), followed by Tukey's multiple comparison test. *n* = 5. **(E)** S2R+ cells were transfected with the indicated plasmids (empty vector, ev or USP8) and lysed after 3 d. Equal amounts of protein (30  $\mu$ g) were separated by SDS-PAGE and immunoblotted using the indicated antibodies. Representative of *n* = 4. Graph bar shows mean  $\pm$  SEM of ratio between densitometric levels of MFN and those of Actin relatively to control from at least four independent experiments. Means are significantly

different according to the *t* test;  $P = 0.0313$  (\*), *n* = 4. **(F)** Equal amounts of protein (70  $\mu$ g), isolated from wild-type (Ctrl) flies or those down-regulating USP8 (USP8) separated by SDS-PAGE and immunoblotted using the indicated antibodies. Representative of *n* = 8. Graph bar shows mean  $\pm$  SEM of ratio between densitometric levels of MFN and those of Actin relatively to control from at least three independent experiments. Means are significantly different according to the *t* test;  $P = 0.0044$  (\*\*), *n* = 8. The flies were raised at 29 $^{\circ}$ C to allow efficient down-regulation of USP8. **(G)** Equal amounts of protein (70  $\mu$ g), isolated from wild-type (Ctrl) flies and those carrying heterozygous deletion of USP8 (USP8<sup>-/+</sup>) separated by SDS-PAGE and immunoblotted using the indicated antibodies. Representative of *n* = 5. Graph bar shows mean  $\pm$  SEM of ratio between densitometric levels of MFN and those of Actin relatively to control from at least four independent experiments. Means are significantly different according to the *t* test;  $P = 0.0069$  (\*\*), *n* = 5. Source data are available for this figure.

To independently validate the previous results, we analyzed a bona fide genetic mutant for USP8. Heterozygous USP8 gene deletion (USP8<sup>-/+</sup>) in PINK1 KO background also completely prevented the loss of DA neurons (Fig 3A and B), restored dopamine levels to wild-type (Fig 3C), corrected thoracic muscle fiber disorganization (Fig 3D) and mitochondrial structure (Fig 3E), ameliorated the shorter longevity (Fig 3F), and completely corrected the locomotor defects (Fig 3G). Thus, these observations support the specificity of

the previous results and confirm that loss of USP8 ameliorates PINK1 KO phenotypes.

### USP8 down-regulation rescues mitochondria defects of PINK1 KO flies

To verify if USP8 down-regulation also correlates to the amelioration of mitochondrial function, impaired in PINK1 KO/KD models

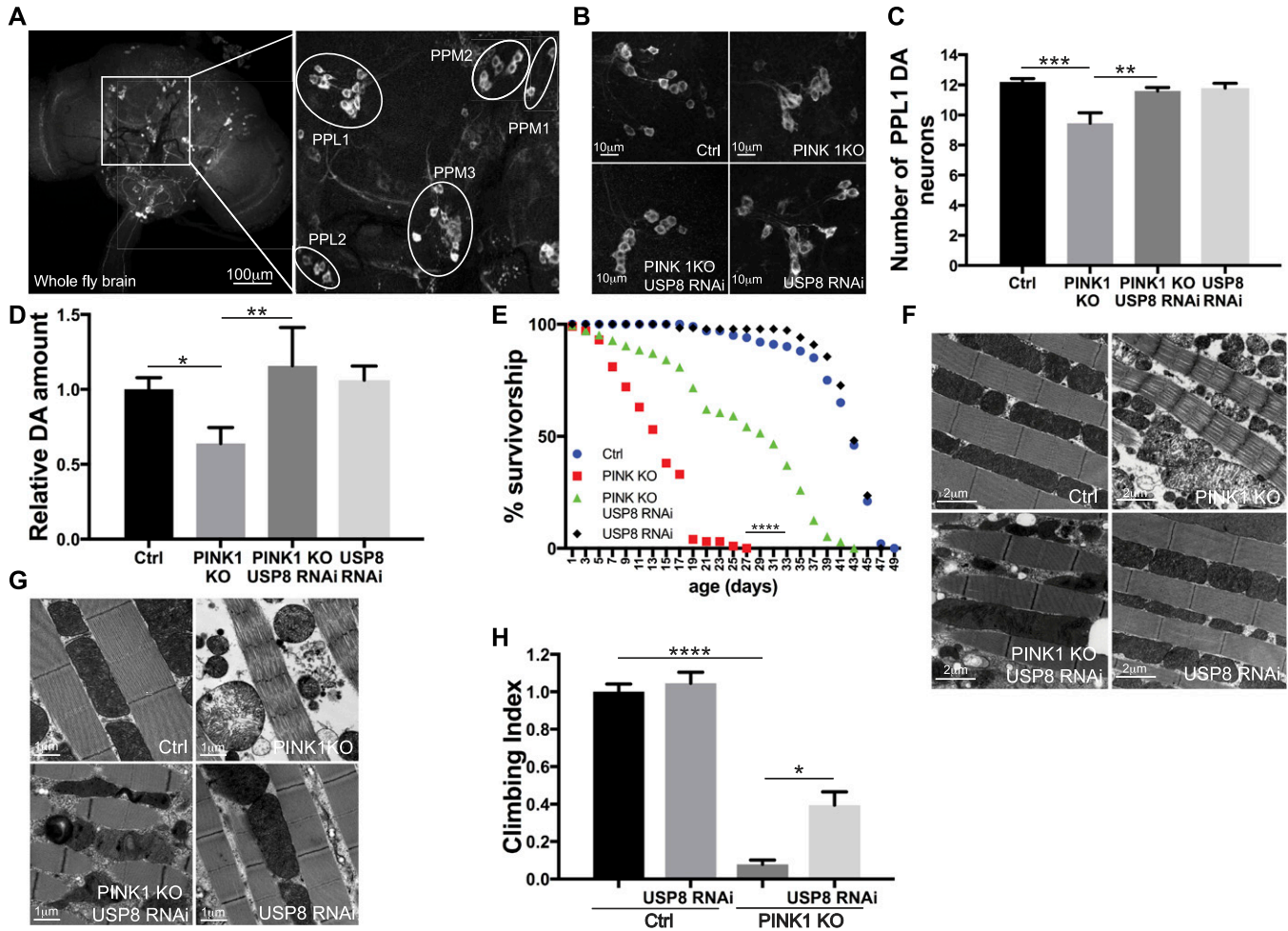


**Figure 2. USP8 down-regulation corrects DA neuron loss, life span, muscle degeneration, and locomotor impairment of PINK1-deficient flies.** (A) Confocal images (projection, Z stack) of whole-mount adult brain (left panel) showing DA neuron clusters marked with an anti-TH antibody. Immunostaining for the specific DA neuronal marker TH allows the inspection of the DA neuronal network composed by well-characterized DA neuron clusters (PPM1, PPM2, PPM3, PPL1, PPL2, and VUM) in brains (right panel). (B) Whole brains of 15-d-old male flies of the indicated genotypes were immunostained with anti-TH antibody. Panel shows confocal images of PPL1 cluster DA neurons of the indicated genotypes. Representative of  $n = 15$ . (C) Bar graph shows the number of DA neurons in the PPL1 cluster of the brains of the indicated genotypes. One-way ANOVA,  $P < 0.0001$  (\*\*\*\*) followed by Tukey's multiple comparison test;  $n = 15$ . (D) Relative dopamine amount from 15-d-old adult heads of the indicated genotype normalized to control flies. One-way ANOVA,  $P = 0.0073$  (\*\*) followed by Tukey's multiple comparison test.  $n = 4$ . (E) Life span analysis of adult males of the indicated genotypes. Male flies of the indicated genotypes were collected during 12 h after hatching and transferred to fresh food every 2 d and dead flies were counted in the same interval. At least 100 flies per genotype were used for the analysis. Log-rank, Mantel-Cox test (Ctrl versus PINK1 KO  $P < 0.0001$ ; Ctrl versus PINK1 KO USP8 RNAi  $P < 0.0001$ ; Ctrl versus USP8 RNAi  $P > 0.05$ ; PINK1 KO versus PINK1 KO USP8 RNAi  $P < 0.0001$ ; PINK1 KO versus USP8 RNAi  $P < 0.0001$ ; and PINK1 KO USP8 RNAi versus USP8 RNAi  $P < 0.0001$   $P < 0.0001$ ). (F) Ultrastructural analysis of the indirect flight muscles from fly thoraces of the indicated genotypes. Images show TEM images of thorax muscles from flies of the indicated genotypes. Representative of  $n = 3$ . (G) Enlarged TEM images of flight muscle mitochondria of the indicated genotypes. Representative of  $n = 3$ . (H) Graph bar shows mean  $\pm$  SEM of the climbing performance of flies of the indicated genotype from at least three independent experiments. One-way ANOVA,  $P < 0.0001$  (\*\*\*\*); Tukey's multiple comparison test;  $n = 3$ .

(Clark et al, 2006; Gandhi et al, 2009; Morais et al, 2014; Park et al, 2006), we measured mitochondrial respiration in digitonin-permeabilized cells, where mitochondria are directly accessible to substrates. In line with what has been previously reported (Gandhi et al, 2009; Morais et al, 2009), we found that ADP-stimulated glutamate-supported respiration (state 3) was significantly reduced in cells lacking PINK1 (Fig S2A). State 3/basal (state 4) respiration ratio, also known as respiratory control ratio (RCR), was reduced (Fig S2B). USP8 down-regulation did not perturb mitochondrial respiration per se; however, it corrected the respiratory defects of the PINK1-deficient cells (Fig S2A and B). In cells

lacking PINK1, mitochondrial dysfunction is mirrored also by changes in mitochondrial membrane potential ( $\Delta\psi_m$ ) (Gandhi et al, 2009; Morais et al, 2009; Mortiboys et al, 2008). When we measured latent mitochondrial dysfunction using a well-established assay based on the response of  $\Delta\psi_m$  to the ATPase inhibitor oligomycin, as expected (Gandhi et al, 2009; Morais et al, 2009), we noticed that PINK1-deficient mitochondria sustain their  $\Delta\psi_m$  by hydrolyzing cytosolic ATP and therefore depolarize after oligomycin treatment (Fig S2C–E). Although down-regulation of USP8 had no effect on  $\Delta\psi_m$ , in PINK1-deficient cells, it fully prevented the oligomycin-induced depolarization, further confirming its beneficial effects on

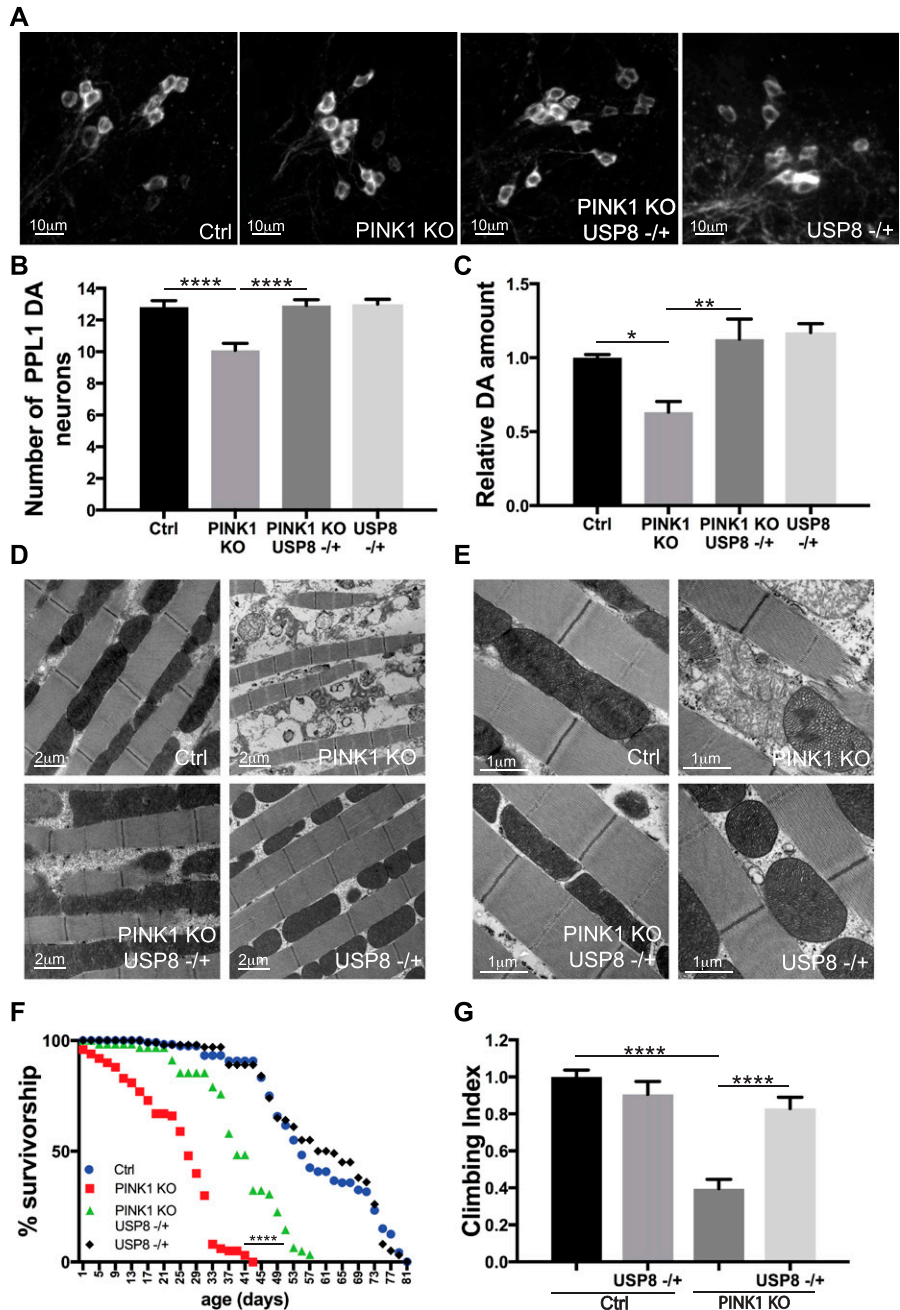


**Figure 3. Heterozygous USP8 gene deletion corrects DA neuron loss, life span, muscle degeneration, and locomotor impairment of PINK1-deficient flies.** (A) Whole brains of 15-d-old male flies of the indicated genotypes were immunostained with anti-TH antibody. Panel shows confocal images of DA neuron of the PPL1 cluster of the indicated genotypes. Representative of  $n = 11$ . (B) Bar graph shows the number of DA neurons in the PPL1 cluster of the brains of the indicated genotypes. One-way ANOVA,  $P < 0.0001$  (\*\*\*\*); Tukey's multiple comparison test;  $n = 11$ . (C) Relative dopamine amount from 15-d-old adult heads of the indicated genotype normalized to control flies. One-way ANOVA,  $P = 0.0002$  (\*\*\*); Tukey's multiple comparison test;  $n = 5$ . (D) TEM images of thorax muscles from flies of the indicated genotypes. Representative of  $n = 3$ . (E) Enlarged TEM image of flight muscle mitochondria of the indicated genotypes. Representative of  $n = 3$ . (F) Life span analysis of adult males of the indicated genotypes. Male flies of the indicated genotypes were collected during 12 h after hatching and transferred to fresh food every 2 d and dead flies were counted in the same interval. At least 100 flies per genotype were used for the analysis. Log-rank, Mantel-Cox test (Ctrl versus PINK1 KO  $P < 0.0001$ ; Ctrl versus PINK1 KO USP8 -/+  $P < 0.0001$ ; Ctrl versus USP8 -/+  $P > 0.05$ ; PINK1 KO versus PINK1 KO USP8 -/+  $P < 0.0001$ ; PINK1 KO versus USP8 -/+  $P < 0.0001$ ; and PINK1 KO USP8 -/+ versus USP8 -/+  $P < 0.0001$   $P < 0.0001$ ). (G) Graph bar shows mean  $\pm$  SEM of the climbing performance of flies of the indicated genotype from at least three independent experiments. One-way ANOVA,  $P < 0.0001$  (\*\*\*\*); Tukey's multiple comparison test;  $n = 3$ .

mitochondrial function (Fig S2C–E). Because USP8 participates in a multiplicity of pathways (Alexopoulou et al, 2016; Durcan & Fon, 2015; Mizuno et al, 2005; Row et al, 2006), the beneficial effects on mitochondrial function measured in situ might be indirect. We, therefore, compared the function of mitochondria purified from PINK1-mutant (KO) flies with that recorded in mitochondria isolated from PINK1 KO flies where we down-regulated USP8 (Fig 4A and B) or from double heterozygous USP8-deficient (USP8<sup>-/+</sup>), PINK1 KO flies (Fig 4C and D). As expected, glutamate-supported ADP-stimulated respiration was reduced, resulting in lower RCR in isolated PINK1 KO mitochondria (Gandhi et al, 2009; Morais et al, 2009) (Fig 4A–D). On

the other hand, USP8 RNAi (Fig 4A and B) or heterozygous USP8 gene deletion (Fig 4C and D) in PINK1 KO flies normalized ADP-stimulated respiration and RCR.

Blue Native PAGE (BN-PAGE) of mitochondrial extracts lent further biochemical support to the measured functional amelioration. Extracts from PINK1-deficient flies displayed reduced levels of respiratory complex I, which was corrected by heterozygous deletion of USP8 (Fig 4E and F). PINK1 mutants show reduced enzymatic activity of complex I (Morais et al, 2014; Pogson et al, 2014). Both USP8 fly lines (USP8<sup>-/+</sup> and USP8 RNAi) restored complex I activity of PINK1 mutants (Fig 4G and H).

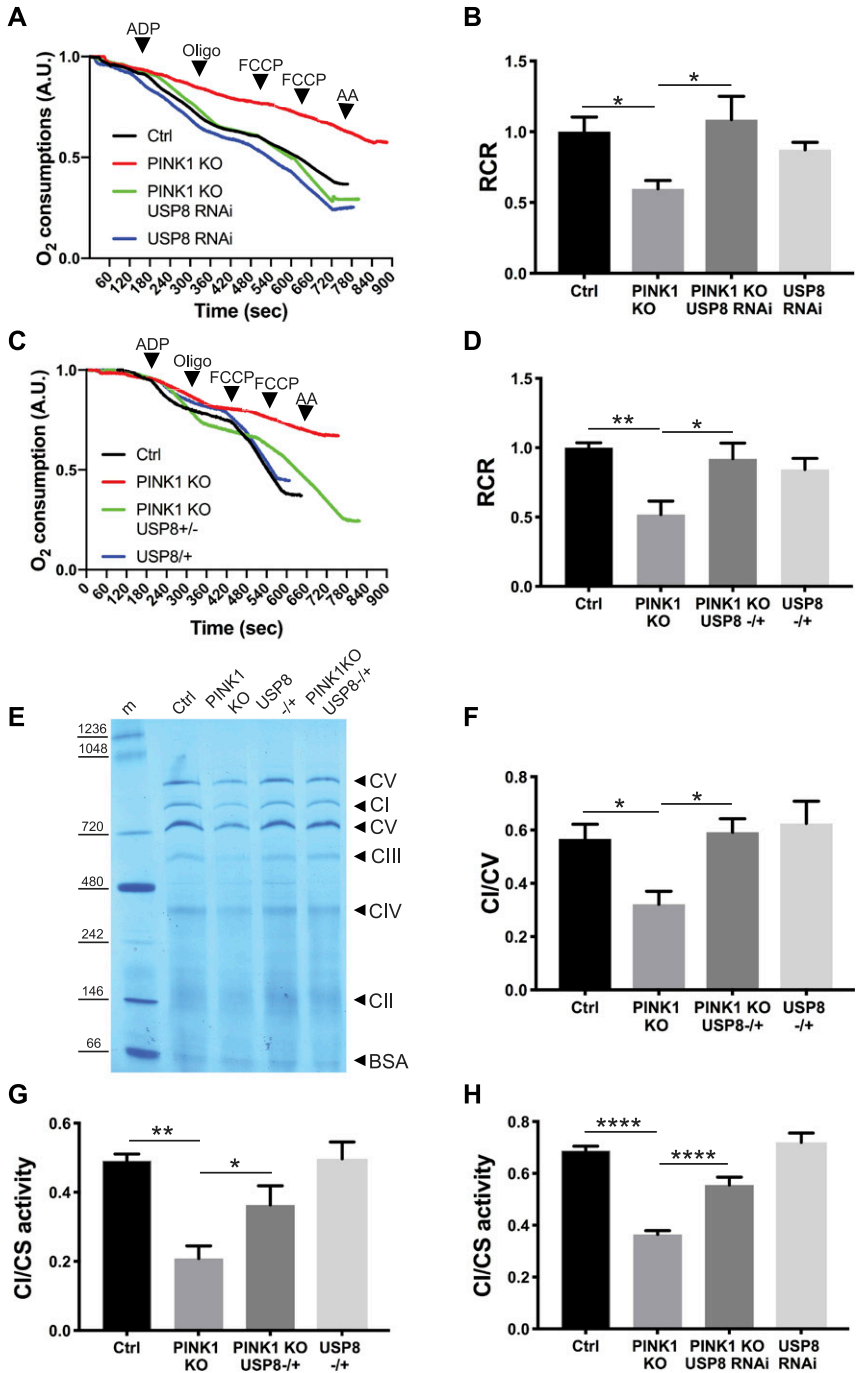


**Figure 4. USP8 down-regulation rescues PINK1-deficient mitochondria respiratory defects ex vivo.**  
**(A)** Representative traces of oxygen consumption of intact isolated mitochondria extracted from flies of the indicated genotype and subjected to 10 mM/5 mM pyruvate/malate 200  $\mu$ M ADP, 2  $\mu$ g/ml oligomycin, and 200 nM FCCP, 2  $\mu$ M antimycinA, respectively. Representative of n = 5. **(B)** Quantitative analysis of respiratory fitness of isolated mitochondria extracted from flies of the indicated genotype treated as in (A). Graph shows mean  $\pm$  SEM (n = 5 independent experiments) of RCR relative to ctrl. One-way ANOVA,  $P = 0.0074$  (\*\*); Tukey's multiple comparison test; n = 5. **(C)** Representative traces of oxygen consumption of intact isolated mitochondria extracted from flies of the indicated genotype and subjected to 10 mM/5 mM pyruvate/malate 200  $\mu$ M ADP, 2  $\mu$ g/ml oligomycin, and 200 nM FCCP, 2  $\mu$ M antimycinA, respectively. Representative of n = 5. **(D)** Quantitative analysis of respiratory fitness of isolated mitochondria extracted from flies of the indicated genotype treated as in (C). Graph shows mean  $\pm$  SEM (n = 5 independent experiments) of RCR relative to ctrl. One-way ANOVA,  $P = 0.0064$  (\*\*); Tukey's multiple comparison test; n = 5. **(E)** Blue Native PAGE of mitochondrial extracts from flies of the indicated genotypes. Respiratory complexes were separated in a non-denaturing polyacrylamide gel. Representative of n = 3. **(F)** Densitometric analysis of (E). Graph bar shows mean  $\pm$  SEM of ratio between densitometric levels of complex I (C1) and those of complex V (CV). One-way ANOVA,  $P = 0.0282$  (\*\*); Tukey's multiple comparison test; n = 3. **(G)** Graph shows mean  $\pm$  SEM (n = 4 independent experiments) of complex I activity relatively to citrate synthase (CS) activity in isolated 2.5  $\mu$ M alamethicin-treated mitochondria extracted from flies of the indicated genotype. One-way ANOVA,  $P = 0.0012$  (\*\*); Tukey's multiple comparison test; n = 4. **(H)** Graph shows mean  $\pm$  SEM (n = 7 independent experiments) of complex I activity relatively to CS activity in isolated 2.5  $\mu$ M alamethicin-treated mitochondria extracted from flies of the indicated genotype. One-way ANOVA,  $P < 0.0001$  (\*\*\*\*); Tukey's multiple comparison test; n = 7.

PINK1-null mutant males are sterile, as a consequence of spermatogenesis defects deriving from mitochondrial dysfunction (Clark et al, 2006; Deng et al, 2008; Greene et al, 2003; Park et al, 2006). Of note, heterozygous USP8 gene deletion favours the restoring of sperm production of the PINK1 KO, rescuing male sterility (Fig S3). The seminal vesicles of Ctrl and USP8<sup>-/+</sup> males were well developed, swollen, and brownish in color (Fig S3A and B), whereas those of PINK1 KO were reduced in volume and more transparent (Fig S3C). Puncturing the vesicles of Ctrl and USP8<sup>-/+</sup> males released

a large amount of sperm (Fig S3E and F), whereas sperm was almost absent in PINK1 KO vesicles (Fig S3G). Rescued males (PINK1 KO, USP8<sup>-/+</sup>) showed an intermediate pattern, with swollen, opaque vesicles (Fig S3D) releasing some sperm groups (Fig S3H). The fluorescence staining revealed a difference among the four male groups also in the accessory glands' wall, whose cells appeared alive (green) in ctrl and USP8<sup>-/+</sup> males (Fig S3I and J) and dead (red) in PINK1 KO (Fig S3K). In rescued males (PINK1 KO, USP8<sup>-/+</sup>), part of the accessory glands' cells was alive (Fig S3L). The result of

fluorescence staining proves that the effect is not limited to sperm production, but it is also extended to the functionality of the accessory glands, that play a crucial role on both male fertilization success and female fertility (Simmons & Fitzpatrick, 2012).

Taken together, these analyses show that the mitochondrial-defective phenotype of PINK1 KO flies can be recovered by decreasing USP8 expression, including complex I levels and activity.

**Pharmacological inhibition of USP8 corrects PINK1-deficient flies**

The genetic experiments showed that USP8 inhibition ameliorates all the phenotypes that we tested that are associated to *Drosophila* PINK1 KO. We, therefore, decided to test in vivo the effect of DUBs-IN-2 (ChemScene LLC), a potent and membrane-permeant USP8 drug inhibitor. DUBs-IN-2 is highly selective for USP8 with a half maximal inhibitory concentration (IC<sub>50</sub>) of 0.28 μM (Colombo et al, 2010) and small or no effect on USP7 (IC<sub>50</sub> > 100 μM for USP7). The compound has been described as an inhibitor of human USP8, which shares about ~45% sequence homology to the fly ortholog. DUBs-IN-2 was mixed in the fly food

with the food-coloring patent blue V (E131) to monitor drug ingestion (Fig S4A). Increasing inhibitor concentrations did not affect the food uptake of flies as measured by E131 absorbance in fly lysates (Fig S4B) and did not affect locomotor behavior in a control background (Fig S4C). Remarkably, DUBs-IN-2 administered to adult PINK1-deficient flies significantly suppressed the locomotor deficits (Fig 5A). Dose-response curve indicated the best rescue of PINK1 KO climbing performance upon 10 μM DUBs-IN-2 administration (Fig S4C). DUBs-IN-2 administration to PINK1 KO flies also prevented loss of DA neurons (Fig 5B and C), restored dopamine levels (Fig 5D), and it modestly ameliorated longevity (Fig 5E).

**USP8 down-regulation corrects pathologically elevated MFN levels of PINK1 and Parkin KO flies**

PINK1 loss-of-function results in increased MFN protein levels (Tanaka et al, 2010; Ziviani et al, 2010), altered mitochondrial morphology (Mortiboys et al, 2008; Narendra et al, 2008; Tanaka et al, 2010; Ziviani et al, 2010), impaired mitophagy (Gegg et al, 2010;

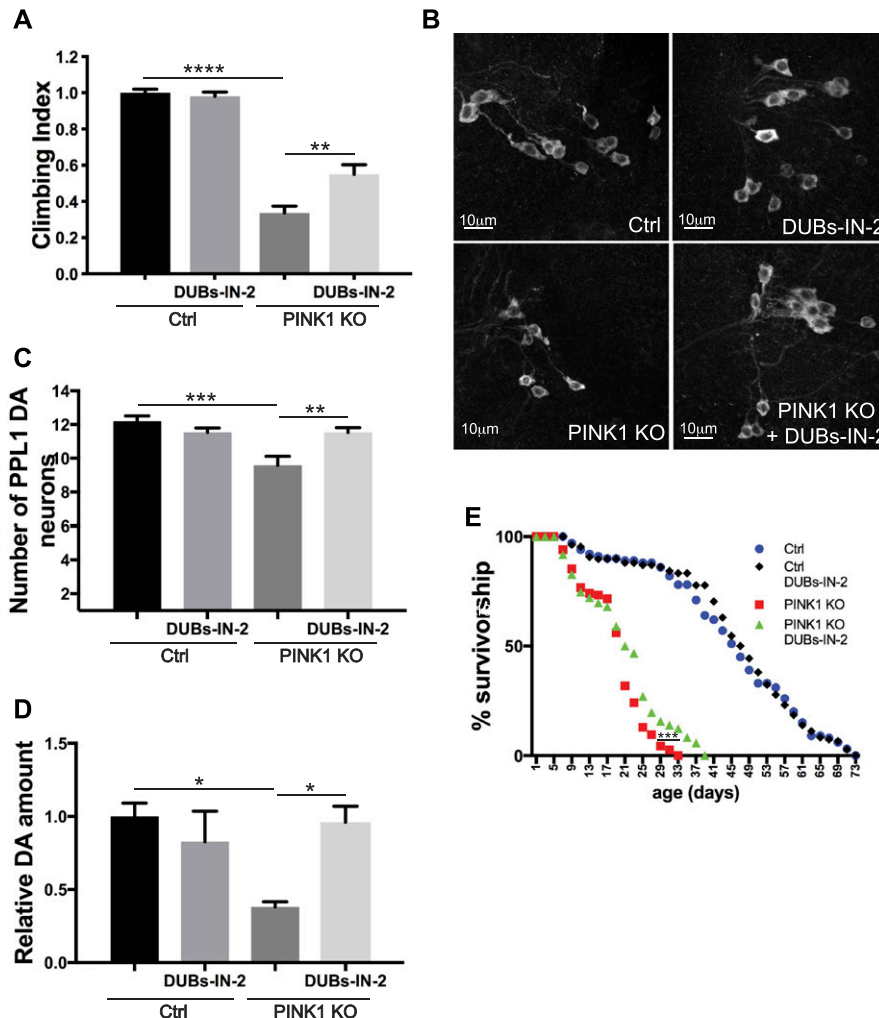


**Figure 5. Pharmacological USP8 inhibition corrects DA neuron loss, life span, muscle degeneration, and locomotor impairment of PINK1-deficient flies.**

(A) Graph bar shows mean ± SEM of the climbing performance of 3-d-old flies of the indicated genotype or treated with DUBs-IN-2 or DMSO for 48 h from at least four independent experiments. Two-way ANOVA  $P < 0.0001$  (\*\*\*\*); Tukey's multiple comparison test;  $n = 8$ . (B) Whole brains of 15-d-old male flies of the indicated genotypes or treated with DUBs-IN-2 for 15 d were immunostained with anti-TH antibody. Panel shows (projection, Z stack) confocal images of PPL1 cluster DA neurons of the indicated genotypes. Representative of  $n = 9$ . (C) Bar graph shows the number of PPL1 cluster DA neurons in brains of the indicated genotypes treated with DUBs-IN-2 or DMSO for 15 d. Two-way ANOVA,  $P = 0.0004$  (\*\*\*); Tukey's multiple comparison test;  $n = 15$ . (D) Relative dopamine amount from 15 d old adult heads of the indicated genotype treated with DUBs-IN-2 or DMSO for 15 d normalized to control flies. Two-way ANOVA  $P = 0.0217$  (\*); Tukey's multiple comparison test;  $n = 3$ . (E) Life span analysis of male flies of the indicated genotypes treated with DUBs-IN-2 or DMSO. At least 100 flies were used for the analysis. Log-rank, Mantel-Cox test (Ctrl versus PINK1 KO  $P < 0.0001$ ; Ctrl versus PINK1 KO+DUBs-IN-2,  $P < 0.0001$ ; Ctrl versus Ctrl+DUBs-IN-2  $P > 0.05$ ; PINK1 KO versus PINK1 KO+DUBs-IN-2  $P < 0.001$ ; PINK1 KO versus Ctrl+DUBs-IN-2  $P < 0.0001$ ; and PINK1 KO+DUBs-IN-2 versus Ctrl+DUBs-IN-2  $P < 0.0001$ ).

Narendra et al, 2008; Ziviani et al, 2010), and oxidative phosphorylation (Morais et al, 2009, 2014), with mitochondrial Ca<sup>2+</sup> overload and increased reactive oxygen species production (Gandhi et al, 2009). Similar phenotypes are caused by altered MFN, which prompted us to investigate whether USP8 down-regulation corrected pathologically elevated MFN levels of PINK1 KO flies. Indeed, USP8 down-regulation in vivo completely normalized increased MFN levels of PINK1 KO (Fig 6A). Pharmacological inhibition of USP8 also led to reduced PINK1 KO MFN protein levels in flies, indicating that the inhibitor phenocopied genetic inhibition of USP8 (Fig 6B). Like PINK1, Parkin KO/KD also results in increased MFN protein levels (Gegg et al, 2010; Tanaka et al, 2010; Ziviani et al, 2010). We, therefore, assessed the effect of USP8 KD in a Parkin loss-of-function model of pathologically elevated MFN levels. USP8 KD corrected elevated MFN levels of Parkin KO flies (Fig 6C). It also recovered the disorganized muscle fibers with irregular arrangement of myofibrils and the swollen mitochondria of Parkin flies

(Fig 6D), and normalized the number of DA neurons that are decreased in Parkin KO background (Fig 6E). Interestingly, USP8 KD or inhibition did not correct climbing defects in Parkin KO flies (Fig 6F), nor in PINK1:Parkin double KO (Fig 6G).

## Discussion

Interventions that decrease MFN levels in PINK1 or Parkin KO flies can ameliorate the multiple phenotypes that are associated with the KO backgrounds (Deng et al, 2008; Poole et al, 2008; Liu et al, 2011; Vilain et al, 2012; Celardo et al, 2016). We, therefore, conducted an RNAi-based screening to identify DUBs that regulate MFN protein levels. We found USP8, a DUB previously identified in the regulation of endosomal trafficking (Mizuno et al, 2005; Row et al, 2006), CCCP-induced mitophagy (Durcan et al, 2014) and basal autophagy (Jacomin et al, 2015), and which down-regulation is protective from

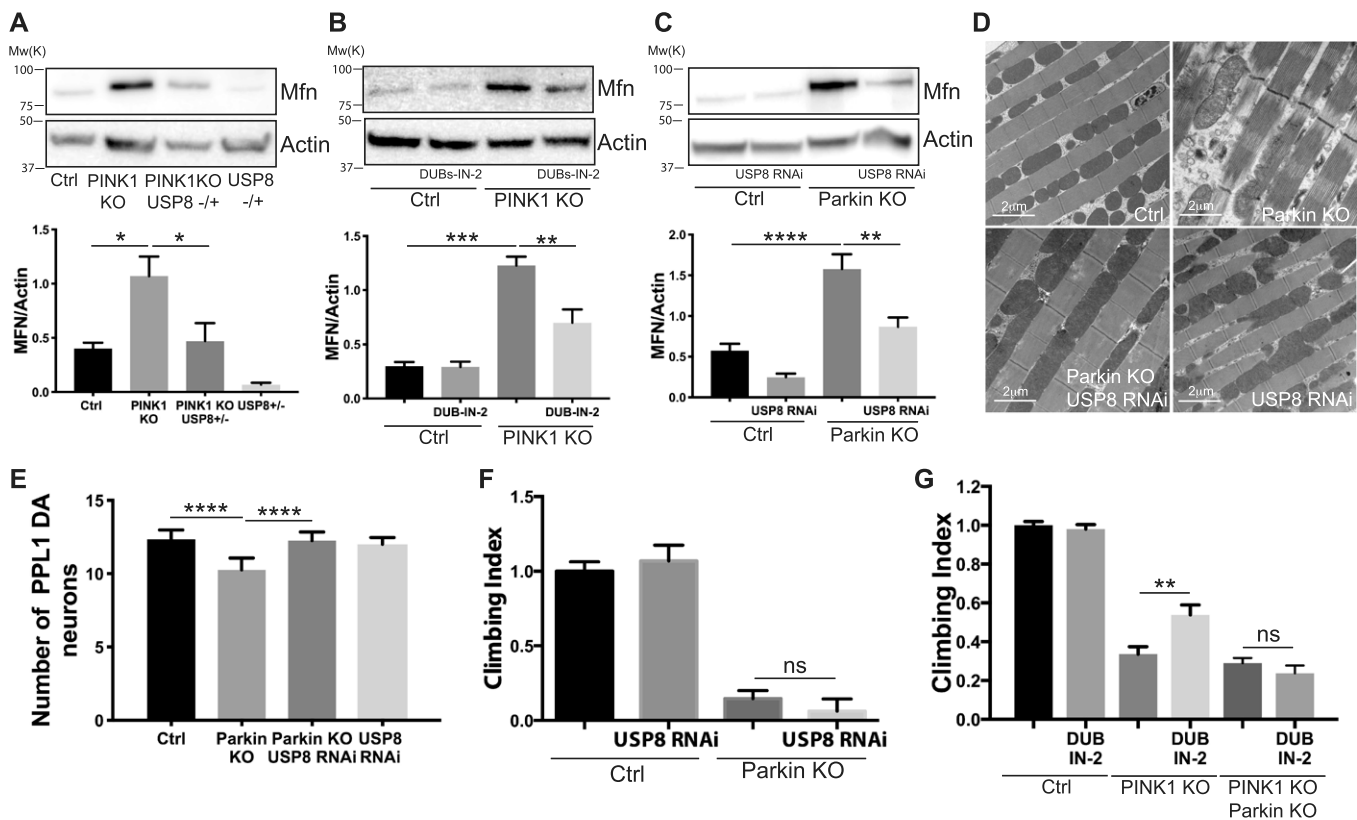


**Figure 6. USP8 down-regulation corrects pathologically elevated MFN levels of PINK1 and Parkin KO flies.**

(A) Equal amounts of protein (70  $\mu$ g), isolated from flies of the indicated phenotype were separated by SDS-PAGE and immunoblotted using the indicated antibodies. Representative of n = 6. Graph bar shows mean  $\pm$  SEM of ratio between densitometric levels of MFN and those of Actin from at least six independent experiments. One-way ANOVA,  $P = 0.0003$  (\*\*\*); Tukey's multiple comparison test; n = 6. (B) Equal amounts of protein (70  $\mu$ g), isolated from flies treated with DUBs-IN-2 or DMSO for 48 h were separated by SDS-PAGE and immunoblotted using the indicated antibodies. Representative of n = 3. Graph bar shows mean  $\pm$  SEM of ratio between densitometric levels of MFN and those of Actin from at least three independent experiments. Two-way ANOVA,  $P < 0.00001$  (\*\*\*\*); Tukey's multiple comparison test; n = 3. (C) Equal amounts of protein (70  $\mu$ g), isolated from flies of the indicated phenotype were separated by SDS-PAGE and immunoblotted using the indicated antibodies. Representative of n = 9. Graph bar shows mean  $\pm$  SEM of ratio between densitometric levels of MFN and those of Actin from at least nine independent experiments. One-way ANOVA,  $P < 0.0001$  (\*\*\*\*); Tukey's multiple comparison test; n = 9. (D) TEM images of thorax muscles from flies of the indicated genotypes. Thoraces were dissected from 3-d-old adult flies and fixed in 2% paraformaldehyde and 2.5% glutaraldehyde. The samples were rinsed, dehydrated, and embedded using Epon. Ultrathin sections were examined using TEM. Representative of n = 3. (E) Bar graph shows the number of DA neurons in the PPL1 cluster of the brains of the indicated genotypes. One-way ANOVA,  $P < 0.0001$  (\*\*\*\*); Tukey's multiple comparison test; n = 10. (F) Graph bar shows mean  $\pm$  SEM of the climbing performance of flies of the indicated genotype from at least nine independent experiments. One-way ANOVA,  $P < 0.0001$  (\*\*\*\*); n = 3. (G) Graph bar shows mean  $\pm$  SEM of the climbing performance of flies of the indicated genotype from at least three independent experiments. Two-way ANOVA,  $P < 0.0001$  (\*\*\*\*); Tukey's multiple comparison test; n = 7.



$\alpha$ -synuclein-induced locomotor deficits in flies (Alexopoulou et al, 2016). Our data show that inhibition of USP8 *in vitro* and *in vivo* correlated with decreased mitochondrial fusion protein MFN, one of the bona fide Parkin targets (Gegg et al, 2010; Poole et al, 2010; Tanaka et al, 2010; Ziviani et al, 2010; Sarraf et al, 2013) (Fig 1), ameliorated PINK1 KO phenotypes *in vivo* (Figs 2, 3, and 5) and PINK1 KO mitochondrial dysfunction (Fig 4), and corrected MFN protein levels, increased in PINK1 KO models (Fig 6). Interestingly, USP8 KD also corrected MFN protein levels of Parkin KO flies, indicating that the effect on the levels of MFN is Parkin independent. USP8 KD also prevented Parkin KO DA neurons loss and normalized mitochondrial morphological defects, although it did not ameliorate Parkin climbing performance (Fig 6).

It has been shown that the knockdown of MFN is able to rescue the mitochondrial defects and the overall phenotypes of *Drosophila* PINK1 KO flies (Deng et al, 2008; Poole et al, 2008). More recently, it was shown that MFN knockdown can suppress loss of DA neurons of the PPL1 cluster and thorax deformation resulting from crushed thoracic muscle of the PINK1 KO flies, but not the mitochondrial defects (Celardo et al, 2016). We found that normalizing MFN levels of PINK1 KO flies by driving efficient whole body MFN KD (Debattisti et al, 2014) ameliorated the disorganized muscle fibers and mitochondria ultrastructure of PINK1 KO flies, but dopamine content and climbing performance were only modestly recovered, even if MFN levels of PINK1 KO flies were completely corrected (Fig S5). This result indicates that MFN normalization deriving from USP8 KD likely contributes to the amelioration of the PINK1 phenotype but does not explain the full recovery of the multiple phenotypes that are associated with PINK1 loss. Indeed, our *in vivo* analysis indicates that USP8 KD has a broader protective effect than MFN KD and unlike MFN KD (Celardo et al, 2016; Vilain et al, 2012), it correlates with full correction of mitochondrial respiratory defects, complex I content and activity, and mitochondrial membrane potential of PINK1 KO flies (Figs 4 and S2). Previous examination of the PINK1-mutant phenotype demonstrated that although decreasing mitochondrial fusion rescues morphological mitochondrial defects of PINK1 flies, manipulation of mitochondrial fusion (or fission) does not rescue other PINK1-related phenotypes such as the reduced activity of complex I, loss of mitochondrial membrane potential, ATP content, and defective neurotransmitter release (Vilain et al, 2012; Vos et al, 2012). In light of this, we hypothesize that the protective effect of USP8 inhibition comes from a combination of signaling pathways, which directly or indirectly impinges on MFN levels and mitochondrial function. In mammals, it is established that USP8 is involved in endosomal trafficking (Clague et al, 2013), although its activity can have opposing effects. For instance, deubiquitination by USP8 was reported to slow the degradation of substrates (Mizuno et al, 2005; Mukai et al, 2010), but also to facilitate endosomal trafficking and lysosomal degradation (Row et al, 2007; Ali et al, 2013). shRNA against USP8 in SH-SY5Y neuroblastoma cells promotes  $\alpha$ -synuclein degradation by the lysosome, which exerts a protective effect *in vivo* in an  $\alpha$ -synuclein fly model of PD (Alexopoulou et al, 2016). It was also reported that USP8 is required for lysosomal biogenesis and productive autophagy in *Drosophila* larval fat body but inhibits basal autophagy *in vitro* in HeLa cells (Jacomin et al, 2015). Finally, deubiquitination of Parkin by USP8 is required for Parkin recruitment to CCCP-intoxicated

mitochondria and to promote stress-induced mitophagy *in vitro* (Durcan et al, 2014). Thus, USP8 down-regulation in this context inhibits Parkin recruitment to mitochondria, causing a delay in mitochondria clearance by mitophagy. In light of these seemingly opposing phenotypic outcomes, it is clear that USP8 has pleiotropic effects that depends on the specific genetic repertoire of the cell/tissue, varies in response to physiological versus pathological conditions, or might simply operate differently in cell lines versus the whole organism. Our model is consistent with a role of USP8 in controlling mitochondrial function via Parkin-independent regulation of pathologically elevated MFN protein levels. Yet, it does not exclude MFN-unrelated pathways that nevertheless impinge on mitochondrial function via Parkin, like the mitochondrial-derived vesicle pathway regulating mitochondria quality control (McLelland et al, 2014), or the endosomal-lysosomal pathway that can also play a role in selective degradation of dysfunctional mitochondria (Hammerling et al, 2017a, 2017b). Interestingly, it was shown in the latter that the autophagic activity is increased when the endosomal activity is impaired, sustaining the hypothesis that there is crosstalk between the various degradation pathways to ensure effective clearance. It is tempting to hypothesize an enhancement of autophagy deriving from USP8 KD to complement for impaired endosomal-mediated quality control. For these reasons, future studies need to be conducted *in vivo* to validate this hypothesis and clearly dissect coordination and timing of activation of these pathways in different tissues under physiological and pathological conditions.

Because of their involvement in the regulation of important signaling pathways, DUBs are emerging as extremely attractive druggable candidates (Sugiura et al, 2013). In recent years, many DUBs emerged as therapeutic targets to compensate for impaired mitophagy in PD (Bingol et al, 2014; Cornelissen et al, 2014; Wang et al, 2015; Chakraborty et al, 2018). Mitophagy is triggered by ubiquitin modification of mitochondrial proteins, which is in principle subject to suppression by deubiquitination. It is, therefore, reasonable that inhibition of specific DUBs should induce mitophagy and that it does so by deubiquitination mitochondrial proteins. Clinical trials for specific inhibitors of the ubiquitin-proteasome system have already been approved in cancer therapy for the treatment of multiple myeloma (Colland, 2010). Moreover, high-throughput screening of small chemical libraries identified non-selective DUB inhibitors as potent inducers of apoptosis in various cancer cells (Liu et al, 2003; Brancolini, 2008; Engels et al, 2009; Hussain et al, 2009; Py et al, 2013). Similarly, specific DUB inhibitors (or activators) can affect cellular response to stimuli that induce cell death. In this respect, the identification of a specific DUB that normalizes mitochondrial function might be instrumental to develop specific isopeptidase inhibitors that can modulate the fundamental biological process of mitochondria physiology and fitness, supporting the potential of USP8 inhibitors as therapeutics.

## Online methods

### Cell culture and transfection

*Drosophila* S2R+ cells were cultured in Schneider's medium (Invitrogen) supplemented with 10% heat-inactivated fetal calf serum (Sigma-Aldrich). The cells were maintained at 25°C and

passed routinely before they reached confluence, to maintain a logarithmic growth. The cells were transfected using TransFectin lipid reagent (Bio-Rad) or Effectene (QIAGEN) following the manufacturer's instructions. In brief, 0.6 million cells were plated in six-well plate and transfected with 2  $\mu\text{g}$  DNA/5  $\mu\text{l}$  TransFectin or 1  $\mu\text{g}$  DNA/10  $\mu\text{l}$  Effectene + 8  $\mu\text{l}$  Enhancer, 1 d after plating. The cells were collected 24–48 h after transfection. 500  $\mu\text{M}$  copper sulfate solution was added to the cells to induce plasmid expression when required.

### Plasmids

MitoDsRed was subcloned from pDsRed2-Mito vector (Clontech) into pAct-PPA expression plasmid. C-terminal Flag tag MFN was obtained by amplification from cDNA clone (RE04414) and subcloned into pAct-PPA expression plasmid. CG5798/USP8 was amplified from cDNA clone and subcloned into pMt copper-inducible vector (Invitrogen).

### Gene silencing

*Drosophila* dsRNA probes were prepared using MEGA script kit (Ambion) following the manufacturer's instructions. The following primers have been used to prepare the RNAi probes: PINK1 CAATGTGACTTCTCCAGCGA and TCGTAGCGTTTCATCAGCAG; Parkin CTGTTGCAATTTGGAGGGA and CTTTGGCACGGACTCTTCT; and MFN GGAACCTCTTTATTCTCTAT and GGTTTGCTTGGCCCAACAT. CG5798/USP8 dsRNA probe was acquired from the Sheffield RNAi Screening Facility. 1.2 millions cells were plated on a six-well plate and treated with 7  $\mu\text{g}$  RNAi probe in serum-free medium. 2 h after the probe treatment, complete medium was added to the wells, and the cells were cultured for 2 d before being transfected with indicated fly expression plasmids as previously described.

### Immunoblotting

Western blotting was performed using standard techniques. In brief, the cells were collected in lysis buffer (50 mM Tris-HCl, pH 8, 150 mM NaCl, 1 mM MgCl<sub>2</sub>, 2 mM EGTA, 1% Triton X, 10% glycerol, 10 mM NEM, 10  $\mu\text{M}$  MG132 and protease inhibitor cocktail by Roche) and incubated on ice for 30 min before being centrifuged at maximum speed at 4°C. Ten to twelve flies were homogenized using a mortar and pestle in protein extraction buffer (200–300  $\mu\text{l}$ , 150 mM NaCl, 5 mM EDTA, pH 8.0, 50 mM Tris, pH 8.0, 1% NP-40, 0.1% SDS 0.1, supplemented with 10  $\mu\text{M}$  MG132, 10 mM NEM, and protease inhibitor cocktail). The following commercial antibodies were used: anti-Flag (1:1,000; Cell Signaling Technology), anti-Actin (1:10,000; Chemicon) has been described before. Anti-*Drosophila* Mitofusin (1:2000) was raised in rabbit against an N-terminal peptide, DTVDKSGPGSPLSRF. For detection, secondary antibodies conjugated with HRP (Chemicon) were used (1:3,000), and immunoreactivity was visualized with ECL chemiluminescence (Amersham).

### Live imaging

Cells were grown on imaging dishes (Chamber Slide Lab-Tek II 8; Thermo Fisher Scientific) or coverslips. After appropriate treatment, when indicated, the cells were treated with the selective mitochondrial dye Mitotracker (50 nM; Molecular Probe) for 10 min, washed three times with PBS, and imaged live in growing medium

under ambient conditions on an Andromeda iMIC spinning disk live cell microscope with confocal resolution (TILL Photonics, 60X objective). For confocal z-axis stacks, 40 images separated by 0.2  $\mu\text{m}$  along the z-axis were acquired.

For measurements of mitochondrial membrane potential, the cells were loaded with 25 nM tetramethylrhodamine methyl ester (TMRM) for 30 min at room temperature, and the dye was present during the experiment together with the multidrug resistance inhibitor cyclosporine H (1  $\mu\text{M}$ ). The cells were then observed using an Olympus IX81 inverted microscope equipped with a cell imaging system. Sequential images of TMRM fluorescence were acquired every 60 s with a 40 $\times$  objective (Olympus). Where indicated, oligomycin (2.5  $\mu\text{g}/\text{ml}$ ; Sigma-Aldrich) or the uncoupler carbonyl cyanide p-trifluoromethoxyphenylhydrazone (CCCP, 10  $\mu\text{M}$ ; Sigma-Aldrich) was added. TMRM fluorescence analysis over the mitochondrial regions of interest was performed using ImageJ. A reduction in TMRM fluorescence represents mitochondrial membrane depolarization. In the graph bars, we indicated TMRM fluorescence after 30-min oligomycin administration in the cells of the indicated genotypes. The cells were always loaded in the presence of the multidrug resistance inhibitor cyclosporine H.

### Mitochondria morphology analysis

Quantification of mitochondria length was performed by using ImageJ software. To measure mitochondrial length, we created maximum-intensity projections of z-series with 0.2- $\mu\text{m}$  increments. Quantification was then performed by using “Squassh” (Segmentation and QUantification of Subcellular SHapes), a plugin compatible with the image processing software ImageJ or Fiji, freely available from <http://mosaic.mpi-cbg.de/?q=downloads/imagej>. Squassh is a segmentation method that enables both colocalization and shape analyses of subcellular structures in fluorescence microscopy images (Rizk et al, 2014). For our analysis, segmentation was performed with the minimum intensity threshold set to 0.15 and the regularization weight to 0.015.

The mitochondria morphology score was assigned as in Pogson et al (2014). Briefly, a morpho score is assigned to each imaged cell according to the morphology of its mitochondrial network. Numbers represent the designated “morphology score”: 0 = cell with a full complement of mitochondria; 1 = cell with a full complement of mitochondria and some clumped mitochondria; 2 = cell with a reduced mitochondrial network and some clumped mitochondria; 3 = cell with a clumped mitochondrial network; and 4 = cell with a complete clumped mitochondrial network.

### Total RNA extraction and qRT-PCR

Total RNA was extracted from *Drosophila* S2R+ cells using TRI Reagent (Sigma-Aldrich) according to the manufacturer's instructions. The RNA pellet was dissolved in 5–10  $\mu\text{l}$  RNAase-free water. Total RNA was extracted from approximately 10 flies using Trizol (Life Technologies) and further purified by precipitation with LiCl 8M. RNA samples were checked for integrity by capillary electrophoresis (RNA 6000Nano LabChip; Agilent Technologies). For each sample, 1  $\mu\text{g}$  of RNA was used for first-strand cDNA synthesis, using 10  $\mu\text{M}$  deoxynucleotides, 10  $\mu\text{M}$  oligo-dT, and SuperScript II (Life Technologies). qRT-PCRs were performed in triplicate in a 7500 Real-Time PCR System (Life Technologies) using SYBR Green

chemistry (Promega). The  $2^{-\Delta\Delta Ct}$  (RQ, relative quantification) method implemented in the 7500 Real-Time PCR System software was used to calculate the relative expression ratio (ref.). The *USP8* oligonucleotides primer used were *USP8\_F* (CACCCATTCAAATTGTCGAG) and *USP8\_R* (TCGATGGTCTCAATGTCGTT). *Rp49* was used as endogenous control and the oligonucleotides used were *Rp49 F* (ATCGGTTACGATCGAACAA) and *R* (GACAATCTCCTTGCGCTTCT).

### **Drosophila stocks and procedures**

*Drosophila* were raised under standard conditions at 25°C unless differently stated on agar, cornmeal, yeast food. *park*<sup>25</sup> mutants and UAS-Parkin have been described before (Greene et al, 2003). *PINK1*<sup>B9</sup> mutants (Park et al, 2006) were provided by Dr. J Chung (KAIST). *w<sup>1118</sup>* and *Act-GAL4* strains were obtained from the Bloomington *Drosophila* Stock Center. UAS-*USP8* RNAi and UAS-Marf RNAi lines were obtained from the VDRC Stock Center. *Usp8*<sup>-/+</sup> and UAS-*Usp8* (*uspy*) lines were kindly provided by S Goto (Mukai et al, 2010).

### **Climbing assays**

Climbing assays were performed as previously described (Greene et al, 2003). For the climbing assay upon drug treatment, groups of 10 flies were collected and placed into an empty vial (12 × 5 cm) with a line drawn at 6 cm from the bottom of the tube. The flies were gently tapped to the bottom of the tube, and the number of flies that successfully climbed above the 6-cm mark after 10 s was noted. Fifteen separate and consecutive trials were performed for each experiment, and the results were averaged. At least 40 flies were tested for each genotype or condition. Data collection and analysis were performed blind to the conditions of the experiments unless otherwise indicated.

### **Isolation of mitochondria**

Mitochondria were extracted from whole flies by differential centrifugation. Each sample was homogenized using a Dounce glass-glass potter and a loose-fitting pestle in a mannitol-sucrose buffer (225 mM mannitol, 75 mM sucrose, 5 mM Hepes, and 0.1 mM EGTA, pH 7.4) supplemented with 2% BSA. The samples were then centrifuged at 1,500 *g* at 4°C for 6 min. The pellet was discarded by filtering the sample through a fine mesh, and the supernatant was centrifuged at 7,000 *g* at 4°C for 6 min. The resulting pellet was resuspended in mannitol-sucrose buffer without BSA before being centrifuged at 7,000 *g* under the same conditions as above and resuspended in a small volume of mannitol-sucrose buffer. Protein concentration was measured using the biuret test.

### **Mitochondrial respiration**

Rates of mitochondrial respiration were measured using the Oxytherm System (Hansatech) with magnetic stirring and thermostatic control maintained at 25°C. Isolated *Drosophila* mitochondria (1 mg/ml) were incubated in 120 mM KCl, 5 mM P<sub>i</sub>-Tris, 3 mM Hepes, 1 mM EGTA, and 1 mM MgCl<sub>2</sub>, pH 7.2, and additions were made as indicated in the figure legends. O<sub>2</sub> consumption was calculated according to the slope of the registered graph and plotted as ng atoms: O<sub>2</sub> × min<sup>-1</sup> × mg<sup>-1</sup>. RCR (ADP-stimulated respiration over basal respiration) was calculated.

### **Immunostaining of whole-mounted brains**

Brains of 15-d-old male control or mutant flies were dissected in ice-cold PBS and fixed in 4% PFA at room temperature for 20 min. Samples were washed six times for 10 min with PBS + 0.3% Triton X-100, permeabilized with PBS + 1% Triton X-100 for 10 min, and blocked with PBS + 0.3% Triton X-100 containing 1% BSA overnight at 4°C. For immunostaining of DA neurons, rabbit anti-TH antibody (Millipore) diluted 1:100 in PBS + 0.3% Triton X-100 containing 0.3% BSA was added and incubated over three nights at 4°C. Brains were washed and blocked again as described above, despite the blocking this time being carried out at RT for 1 h. The immunoreaction was revealed with Cy3-conjugated anti-rabbit IgG (Jackson ImmunoResearch) at a working dilution of 1:500 in PBS + 0.3% Triton X-100 containing 0.3% BSA overnight at 4°C. After another six washing steps, whole brains were mounted with Vectashield (Vector Laboratories). Z-stack images were obtained by a Zeiss LSM700 confocal microscope.

### **Drug treatment**

The specific *USP8* inhibitor DUBs-IN-2 (ChemScene LLC) was administered to flies in the food. DUBs-IN-2 (or DMSO) was diluted in water to the desired concentration and used to reconstitute dry Formula 4-24 Instant *Drosophila* Medium (Carolina Biological Supply). 1-d-old male mutant or control flies in groups of 10 were fed on the supplemented food for 48 h and subsequently climbing assay was performed. In the case of DA neuron staining and measurement of dopamine levels, mutant and control flies were aged for 15 d on the supplemented food that was exchanged every 2 d adding fresh drug or vehicle. The use of non-harmful food coloring demonstrated food uptake and excluded the possibility that smell or taste of the drug prevented the latter. Toxic concentrations were excluded beforehand by performing dose-dependent viability curves on control flies.

### **Drosophila head dopamine amount measurement (HPLC)**

*Drosophila* heads of 15-d-old male flies were dissected out and collected separately in 10 μl of ice-cold 0.2 N perchloric acid. The tissue was homogenized by sonication for 15 s and kept on ice for 20 min, then centrifuged at 12,000 *g* for 10 min, and the supernatant was collected. The samples were further diluted and 5 μl was injected into a HPLC system equipped with a rheodyne injector and a guard cell, set to +350 mV (*E*<sub>1</sub> = +150 mV, *E*<sub>2</sub> = -350 mV, *s*: 2 nA). A C<sub>18</sub> ion-pair, reverse phase analytical column (4.6 × 250 mm; 5 μm particle size; Agilent Technologies) was used for the separation of biogenic amines with a flow rate of 0.8 ml/min. Composition of the mobile phase was 75 mM sodium phosphate monobasic monohydrate, 6% acetonitrile, 1.7 mM 1-octane sulfonic acid, and 25 μM EDTA (pH 3 ± 0.01). Dopamine values were determined by comparing with the standard peak value.

### **Electron microscopy**

Thoraces were prepared from 3-d-old adult flies and fixed overnight in 2% paraformaldehyde and 2.5% glutaraldehyde. After rinsing in 0.1 M cacodylate buffer with 1% tannic acid, the samples were postfixed in 1:1.2% OsO<sub>4</sub> and 0.2 M cacodylate buffer for 1 h. The samples were rinsed, dehydrated in an ethanol series, and

embedded using Epon. Ultrathin sections were examined using a transmission electron microscope.

### Life span analysis

Male flies of the indicated genotypes were collected during 12 h after hatching and grouped into 20 flies per food vial. At least 100 flies were used for the analysis (exact numbers are indicated in the figure legends). The flies were transferred to fresh food (and fresh drug for the inhibitor treatment) every 2 d, and dead flies were counted in the same interval.

### Measurement of food uptake

Dry Formula 4-24 Instant *Drosophila* Medium (Carolina Biological Supply) was reconstituted with a mix of water and food-coloring patent blue V (E131) (1:1) previously supplemented with DMSO or the desired DUBs-IN-2 concentration. Three groups of 10 male 1–3-d-old *w1118* flies were kept in the food vials for 48 h. Afterward, the flies were weighed and homogenized in 20 volumes of PBS with an electric potter. The homogenate was centrifuged for 10 min at 15,000 g and absorbance of the supernatant was measured at 640 nm.

### BN PAGE

Pellets of mitochondria isolated from adult male flies of the indicated genotypes were suspended at  $10 \text{ mg} \times \text{ml}^{-1}$  in  $1 \times$  native PAGE sample buffer (Invitrogen) supplemented with protease inhibitor mixture (Sigma-Aldrich), solubilized with 2% (wt/vol) digitonin and immediately centrifuged at 100,000 g for 25 min at 4°C. The supernatants were supplemented with native PAGE 5% G-250 sample additive (Invitrogen) and quickly loaded onto a blue native polyacrylamide 3–12% gradient gel (Invitrogen). After electrophoresis, the gels were fixed in 50% methanol + 10% acetic acid for 20 min at RT, stained in 0,025% Coomassie + 10% acetic acid overnight at RT and destained with 10% acetic acid.

### Sperm content and reproductive apparatus viability assay

The anatomy of male reproductive apparatus was analyzed on 10 males per group. To this aim, the reproductive apparatus was removed, placed on a slide with few drops of *Drosophila* Ringer's solution (182 mM KCl, 46 mM NaCl, 3 mM  $\text{CaCl}_2 \cdot 2\text{H}_2\text{O}$ , and 10 mM Tris-HCl, pH 7.2) and freshly examined under a light microscope. To verify the presence of sperm inside the seminal vesicles, these were then removed from the whole apparatus and gently punctured with a needle to let the sperm pouring out. Five more intact apparatuses per group were stained with a dead/alive cell viability kit (Molecular Probes) that allows differentiation between live green cells, permeable to green SYBR 14 nucleic acid stain, and red dead cells, permeable to propidium iodide nucleic acid stain, which penetrates through compromised membranes.

### Statistical analysis

Where multiple groups were compared, statistical significance was calculated by one-way or two-way ANOVA with a post hoc Tukey or Dunnett correction. All statistical significance was calculated at  $P = 0.05$ , using GraphPad Prism 8. For all the analysis, the samples were

collected and processed simultaneously and, therefore, no randomization was appropriate (GraphPad Prism. \*\*\*\* $P < 0.0001$ , \*\*\* $P < 0.001$ , \*\* $P < 0.01$ , and \* $P < 0.05$ ). Please refer to the enclosed document for detailed statistical tests.

## Supplementary Information

Supplementary Information is available at <https://doi.org/10.26508/lsa.201900392>.

## Acknowledgements

This work was supported by grants from the Italian Ministry of Health “Ricerca Finalizzata” (GR-2011-02351151), Rita Levi Montalcini “Brain Gain” program, and Michael J Fox RRIA 2014 (Grant ID 9795) to E Ziviani and by ERC FP7-282280, FP7 CIG PCIG13-GA-2013-618697, and Italian Ministry of Research FIRB RBAP11Z3YA\_005 to L Scorrano. AJ Whitworth is funded by MRC Core funding (MC\_UU\_00015/6). We would like to acknowledge Francesco Boldrin from the EM facility for the help and technical support. We thank the Sheffield RNAi Screening Facility, Biomedical Sciences, University of Sheffield, for providing the RNAi library and reagents used in this study supported by the Wellcome Trust (grant reference number 084757)”

### Author Contributions

S von Stockum: data curation, formal analysis, validation, investigation, methodology, and writing—review and editing.  
A Sanchez-martinez: data curation, formal analysis, validation, investigation, and methodology.  
S Corrà: data curation, formal analysis, methodology, and writing—review and editing.  
J Chakraborty: formal analysis and methodology.  
E Marchesan: data curation and methodology.  
L Locatello: conceptualization, formal analysis, and methodology.  
C Da Rè: conceptualization, data curation, formal analysis, and methodology.  
P Cusumano: conceptualization and methodology.  
F Caicci: data curation and methodology.  
V Ferrari: methodology.  
R Costa: supervision and writing—review and editing.  
L Bubacco: conceptualization, data curation, formal analysis, and writing—review and editing.  
MB Rasotto: conceptualization, data curation, formal analysis, supervision, and methodology.  
I Szabo: conceptualization, supervision, and writing—review and editing.  
AJ Whitworth: conceptualization, data curation, formal analysis, supervision, funding acquisition, methodology, and writing—review and editing.  
L Scorrano: conceptualization, data curation, formal analysis, funding acquisition, methodology, and writing—review and editing.  
E Ziviani: conceptualization, data curation, formal analysis, supervision, funding acquisition, methodology, writing—original draft, and project administration.

## Conflict of Interest Statement

The authors declare that they have no conflict of interest.

## References

- Alexopoulos Z, Lang J, Perrett RM, Elschami M, Hurry ME, Kim HT, Mazaraki D, Szabo A, Kessler BM, Goldberg AL, et al (2016) Deubiquitinase Usp8 regulates alpha-synuclein clearance and modifies its toxicity in Lewy body disease. *Proc Natl Acad Sci U S A* 113: E4688–E4697. doi:10.1073/pnas.1523597113
- Ali N, Zhang L, Taylor S, Mironov A, Urbe S, Woodman P (2013) Recruitment of UBPY and ESCRT exchange drive HD-PTP-dependent sorting of EGFR to the MVB. *Curr Biol* 23: 453–461. doi:10.1016/j.cub.2013.02.033
- Bingol B, Tea JS, Phu L, Reichelt M, Bakalarski CE, Song Q, Foreman O, Kirkpatrick DS, Sheng M (2014) The mitochondrial deubiquitinase USP30 opposes parkin-mediated mitophagy. *Nature* 510: 370–375. doi:10.1038/nature13418
- Brancolini C (2008) Inhibitors of the Ubiquitin-Proteasome System and the cell death machinery: How many pathways are activated? *Curr Mol Pharmacol* 1: 24–37. doi:10.2174/1874-470210801010024
- Bueler H (2009) Impaired mitochondrial dynamics and function in the pathogenesis of Parkinson's disease. *Exp Neurol* 218: 235–246. doi:10.1016/j.expneurol.2009.03.006
- Celardo I, Costa AC, Lehmann S, Jones C, Wood N, Mencacci NE, Mallucci GR, Loh SH, Martins LM (2016) Mitofusin-mediated ER stress triggers neurodegeneration in pink1/parkin models of Parkinson's disease. *Cell Death Dis* 7: e2271. doi:10.1038/cddis.2016.173
- Chakraborty J, von Stockum S, Marchesan E, Caicci F, Ferrari V, Rakovic A, Klein C, Antonini A, Bubacco L, Ziviani E (2018) USP14 inhibition corrects an in vivo model of impaired mitophagy. *EMBO Mol Med* 10: e9014. doi:10.15252/emmm.201809014
- Chen Y, Dorn GW, 2nd (2013) PINK1-phosphorylated mitofusin 2 is a Parkin receptor for culling damaged mitochondria. *Science* 340: 471–475. doi:10.1126/science.1231031
- Clague MJ, Barsukov I, Coulson JM, Liu H, Rigden DJ, Urbe S (2013) Deubiquitylases from genes to organism. *Physiol Rev* 93: 1289–1315. doi:10.1152/physrev.00002.2013
- Clark IE, Dodson MW, Jiang C, Cao JH, Huh JR, Seol JH, Yoo SJ, Hay BA, Guo M (2006) Drosophila pink1 is required for mitochondrial function and interacts genetically with parkin. *Nature* 441: 1162–1166. doi:10.1038/nature04779
- Colland F (2010) The therapeutic potential of deubiquitinating enzyme inhibitors. *Biochem Soc Trans* 38: 137–143. doi:10.1042/bst0380137
- Colombo M, Vallese S, Peretto I, Jacq X, Rain JC, Colland F, Guedat P (2010) Synthesis and biological evaluation of 9-oxo-9H-indeno[1,2-b]pyrazine-2,3-dicarbonitrile analogues as potential inhibitors of deubiquitinating enzymes. *ChemMedChem* 5: 552–558. doi:10.1002/cmdc.200900409
- Cornelissen T, Haddad D, Wauters F, Van Humbeeck C, Mandemakers W, Koentjoro B, Sue C, Gevaert K, De Strooper B, Verstreken P, et al (2014) The deubiquitinase USP15 antagonizes Parkin-mediated mitochondrial ubiquitination and mitophagy. *Hum Mol Genet* 23: 5227–5242. doi:10.1093/hmg/ddu244
- Cosson P, Marchetti A, Ravazzola M, Orzi L (2012) Mitofusin-2 independent juxtaposition of endoplasmic reticulum and mitochondria: An ultrastructural study. *PLoS One* 7: e46293. doi:10.1371/journal.pone.0046293
- de Brito OM, Scorrano L (2008) Mitofusin 2 tethers endoplasmic reticulum to mitochondria. *Nature* 456: 605–610. doi:10.1038/nature07534
- Debattisti V, Pendin D, Ziviani E, Daga A, Scorrano L (2014) Reduction of endoplasmic reticulum stress attenuates the defects caused by Drosophila mitofusin depletion. *J Cell Biol* 204: 303–312. doi:10.1083/jcb.201306121
- Deng H, Dodson MW, Huang H, Guo M (2008) The Parkinson's disease genes pink1 and parkin promote mitochondrial fission and/or inhibit fusion in Drosophila. *Proc Natl Acad Sci U S A* 105: 14503–14508. doi:10.1073/pnas.0803998105
- Dupont S, Mamidi A, Cordenonsi M, Montagner M, Zacchigna L, Adorno M, Martello G, Stinchfield MJ, Soligo S, Morsut L, et al (2009) FAM/USP9x, a deubiquitinating enzyme essential for TGFbeta signaling, controls Smad4 monoubiquitination. *Cell* 136: 123–135. doi:10.1016/j.cell.2008.10.051
- Durcan TM, Fon EA (2015) USP8 and PARK2/parkin-mediated mitophagy. *Autophagy*: 11: 428–429. doi:10.1080/15548627.2015.1009794
- Durcan TM, Tang MY, Perusse JR, Dashti EA, Aguilera MA, McLelland GL, Gros P, Shaler TA, Faubert D, Coulombe B, et al (2014) USP8 regulates mitophagy by removing K6-linked ubiquitin conjugates from parkin. *EMBO J* 33: 2473–2491. doi:10.15252/emj.201489729
- Engels IH, Daguia C, Huynh T, Urbina H, Buddenkotte J, Schumacher A, Caldwell JS, Brinker A (2009) A time-resolved fluorescence resonance energy transfer-based assay for DEN1 peptidase activity. *Anal Biochem* 390: 85–87. doi:10.1016/j.ab.2009.03.035
- Filadi R, Greotti E, Turacchio G, Luini A, Pozzan T, Pizzo P (2015) Mitofusin 2 ablation increases endoplasmic reticulum-mitochondria coupling. *Proc Natl Acad Sci U S A* 112: E2174–E2181. doi:10.1073/pnas.1504880112
- Gandhi S, Wood-Kaczmar A, Yao Z, Plun-Favreau H, Deas E, Klupsch K, Downward J, Latchman DS, Tabrizi SJ, Wood NW, et al (2009) PINK1-associated Parkinson's disease is caused by neuronal vulnerability to associated-induced cell death. *Mol Cell* 33: 627–638. doi:10.1016/j.molcel.2009.02.013
- Gegg ME, Cooper JM, Chau KY, Rojo M, Schapira AH, Taanman JW (2010) Mitofusin 1 and mitofusin 2 are ubiquitinated in a PINK1/parkin-dependent manner upon induction of mitophagy. *Hum Mol Genet* 19: 4861–4870. doi:10.1093/hmg/ddq419
- Gomes LC, Scorrano L (2008) High levels of Fis1, a pro-fission mitochondrial protein, trigger autophagy. *Biochim Biophys Acta* 1777: 860–866. doi:10.1016/j.bbabi.2008.05.442
- Greene JC, Whitworth AJ, Kuo I, Andrews LA, Feany MB, Pallanck LJ (2003) Mitochondrial pathology and apoptotic muscle degeneration in Drosophila parkin mutants. *Proc Natl Acad Sci U S A* 100: 4078–4083. doi:10.1073/pnas.0737556100
- Hammerling BC, Najor RH, Cortez MQ, Shires SE, Leon LJ, Gonzalez ER, Boassa D, Phan S, Thor A, Jimenez RE, et al (2017a) A Rab5 endosomal pathway mediates Parkin-dependent mitochondrial clearance. *Nat Commun* 8: 14050. doi:10.1038/ncomms14050
- Hammerling BC, Shires SE, Leon LJ, Cortez MQ, Gustafsson AB (2017b) Isolation of Rab5-positive endosomes reveals a new mitochondrial degradation pathway utilized by BNIP3 and Parkin. *Small GTPases*: 1–8. doi:10.1080/21541248.2017.1342749
- Hussain S, Zhang Y, Galardy PJ (2009) DUBs and cancer: The role of deubiquitinating enzymes as oncogenes, non-oncogenes and tumor suppressors. *Cell cycle* 8: 1688–1697. doi:10.4161/cc.8.11.8739
- Jacomini AC, Bescond A, Soleilhac E, Gallet B, Schoehn G, Fauvarque MO, Taillebourg E (2015) The deubiquitinating enzyme UBPY is required for lysosomal biogenesis and productive autophagy in Drosophila. *PLoS One* 10: e0143078. doi:10.1371/journal.pone.0143078
- Koyano F, Okatsu K, Kosako H, Tamura Y, Go E, Kimura M, Kimura Y, Tsuchiya H, Yoshihara H, Hirokawa T, et al (2014) Ubiquitin is phosphorylated by PINK1 to activate parkin. *Nature* 510: 162–166. doi:10.1038/nature13392
- Lazarou M, Narendra DP, Jin SM, Tekle E, Banerjee S, Youle RJ (2013) PINK1 drives Parkin self-association and HECT-like E3 activity upstream of



- Twig G, Hyde B, Shirihai OS (2008b) Mitochondrial fusion, fission and autophagy as a quality control axis: The bioenergetic view. *Biochim Biophys Acta* 1777: 1092–1097. doi:[10.1016/j.bbabi.2008.05.001](https://doi.org/10.1016/j.bbabi.2008.05.001)
- Twig G, Shirihai OS (2011) The interplay between mitochondrial dynamics and mitophagy. *Antioxid Redox Signal* 14: 1939–1951. doi:[10.1089/ars.2010.3779](https://doi.org/10.1089/ars.2010.3779)
- Vilain S, Esposito G, Haddad D, Schaap O, Dobrev MP, Vos M, Van Meensel S, Morais VA, De Strooper B, Verstreken P (2012) The yeast complex I equivalent NADH dehydrogenase rescues pink1 mutants. *PLoS Genet* 8: e1002456. doi:[10.1371/journal.pgen.1002456](https://doi.org/10.1371/journal.pgen.1002456)
- Vives-Bauza C, Tocilescu M, Devries RL, Alessi DM, Jackson-Lewis V, Przedborski S (2010a) Control of mitochondrial integrity in Parkinson's disease. *Prog Brain Res* 183: 99–113. doi:[10.1016/s0079-6123\(10\)83006-7](https://doi.org/10.1016/s0079-6123(10)83006-7)
- Vives-Bauza C, Zhou C, Huang Y, Cui M, de Vries RL, Kim J, May J, Tocilescu MA, Liu W, Ko HS, et al (2010b) PINK1-dependent recruitment of Parkin to mitochondria in mitophagy. *Proc Natl Acad Sci U S A* 107: 378–383. doi:[10.1073/pnas.0911187107](https://doi.org/10.1073/pnas.0911187107)
- Vos M, Esposito G, Edirisinghe JN, Vilain S, Haddad DM, Slabbaert JR, Van Meensel S, Schaap O, De Strooper B, Meganathan R, et al (2012) Vitamin K2 is a mitochondrial electron carrier that rescues pink1 deficiency. *Science* 336: 1306–1310. doi:[10.1126/science.1218632](https://doi.org/10.1126/science.1218632)
- Wang D, Qian L, Xiong H, Liu J, Neckameyer WS, Oldham S, Xia K, Wang J, Bodmer R, Zhang Z (2006) Antioxidants protect PINK1-dependent dopaminergic neurons in Drosophila. *Proc Natl Acad Sci U S A* 103: 13520–13525. doi:[10.1073/pnas.0604661103](https://doi.org/10.1073/pnas.0604661103)
- Wang X, Winter D, Ashrafi G, Schlehe J, Wong YL, Selkoe D, Rice S, Steen J, LaVoie MJ, Schwarz TL (2011) PINK1 and Parkin target Miro for phosphorylation and degradation to arrest mitochondrial motility. *Cell* 147: 893–906. doi:[10.1016/j.cell.2011.10.018](https://doi.org/10.1016/j.cell.2011.10.018)
- Wang Y, Serricchio M, Jauregui M, Shanbhag R, Stoltz T, Di Paolo CT, Kim PK, McQuibban GA (2015) Deubiquitinating enzymes regulate PARK2-mediated mitophagy. *Autophagy* 11: 595–606. doi:[10.1080/15548627.2015.1034408](https://doi.org/10.1080/15548627.2015.1034408)
- Williams RL, Urbe S (2007) The emerging shape of the ESCRT machinery. *Nat Rev Mol Cell Biol* 8: 355–368. doi:[10.1038/nrm2162](https://doi.org/10.1038/nrm2162)
- Yang Y, Gehrke S, Imai Y, Huang Z, Ouyang Y, Wang JW, Yang L, Beal MF, Vogel H, Lu B (2006) Mitochondrial pathology and muscle and dopaminergic neuron degeneration caused by inactivation of Drosophila Pink1 is rescued by Parkin. *Proc Natl Acad Sci U S A* 103: 10793–10798. doi:[10.1073/pnas.0602493103](https://doi.org/10.1073/pnas.0602493103)
- Zhang C, Lee S, Peng Y, Bunker E, Giaime E, Shen J, Zhou Z, Liu X (2014) PINK1 triggers autocatalytic activation of Parkin to specify cell fate decisions. *Curr Biol* 24: 1854–1865. doi:[10.1016/j.cub.2014.07.014](https://doi.org/10.1016/j.cub.2014.07.014)
- Ziviani E, Tao RN, Whitworth AJ (2010) Drosophila parkin requires PINK1 for mitochondrial translocation and ubiquitinates mitofusin. *Proc Natl Acad Sci U S A* 107: 5018–5023. doi:[10.1073/pnas.0913485107](https://doi.org/10.1073/pnas.0913485107)



**License:** This article is available under a Creative Commons License (Attribution 4.0 International, as described at <https://creativecommons.org/licenses/by/4.0/>).



## Regulation of ER-mitochondria contacts by Parkin via Mfn2

Valentina Basso<sup>a,b</sup>, Elena Marchesan<sup>b</sup>, Caterina Peggion<sup>c</sup>, Joy Chakraborty<sup>a,b</sup>,  
Sophia von Stockum<sup>b</sup>, Marta Giacomello<sup>a</sup>, Denis Ottolini<sup>a</sup>, Valentina Debattisti<sup>d</sup>, Federico Caicci<sup>a</sup>,  
Elisabetta Tasca<sup>b</sup>, Valentina Pegoraro<sup>b</sup>, Corrado Angelini<sup>b</sup>, Angelo Antonini<sup>e</sup>, Alessandro Bertoli<sup>c</sup>,  
Marisa Brini<sup>a</sup>, Elena Ziviani<sup>a,b,\*</sup>

<sup>a</sup> Department of Biology, University of Padova, Padova, Italy

<sup>b</sup> Fondazione Ospedale San Camillo, IRCCS, Lido di Venezia, Venezia, Italy

<sup>c</sup> Department of Biomedical Science (DSB), University of Padova, Padova, Italy

<sup>d</sup> MitoCare Center for Mitochondrial Imaging Research and Diagnostics, Department of Pathology, Anatomy and Cell Biology, Thomas Jefferson University, Philadelphia, PA, USA

<sup>e</sup> Department of Neuroscience, University of Padova, Padova, Italy

### ARTICLE INFO

#### Keywords:

Mitochondria  
Parkinson's disease  
ER-mitochondria tethering  
Mitofusin  
Parkin  
PINK1  
Ubiquitination  
ER-mitochondria synthetic tether  
*Drosophila* model of PD

### ABSTRACT

Parkin, an E3 ubiquitin ligase and a Parkinson's disease (PD) related gene, translocates to impaired mitochondria and drives their elimination via autophagy, a process known as mitophagy. Mitochondrial pro-fusion protein Mitofusins (Mfn1 and Mfn2) were found to be a target for Parkin mediated ubiquitination. Mfns are trans-membrane GTPase embedded in the outer membrane of mitochondria, which are required on adjacent mitochondria to mediate fusion. In mammals, Mfn2 also forms complexes that are capable of tethering mitochondria to endoplasmic reticulum (ER), a structural feature essential for mitochondrial energy metabolism, calcium (Ca<sup>2+</sup>) transfer between the organelles and Ca<sup>2+</sup> dependent cell death. Despite its fundamental physiological role, the molecular mechanisms that control ER-mitochondria cross talk are obscure. Ubiquitination has recently emerged as a powerful tool to modulate protein function, via regulation of protein subcellular localization and protein ability to interact with other proteins. Ubiquitination is also a reversible mechanism, which can be actively controlled by opposing ubiquitination-deubiquitination events. In this work we found that in Parkin deficient cells and *parkin* mutant human fibroblasts, the tether between ER and mitochondria is decreased. We identified the site of Parkin dependent ubiquitination and showed that the non-ubiquitinatable Mfn2 mutant fails to restore ER-mitochondria physical and functional interaction. Finally, we took advantage of an established *in vivo* model of PD to demonstrate that manipulation of ER-mitochondria tethering by expressing an ER-mitochondria synthetic linker is sufficient to rescue the locomotor deficit associated to an *in vivo Drosophila* model of PD.

### 1. Introduction

Parkinson's disease (PD) is the second most common neurodegenerative disease, for which there is no cure. Although the exact cause of most cases is unknown, both environmental and genetic factors are implicated in the onset of the disease. In the last few years, a number of genes have been identified, which cause inherited PD and account for ~10% of PD cases [1]. Some of these genes encode for proteins that are either expressed in the mitochondria or targeted to the mitochondria upon stressful condition. Indeed, mitochondrial dysfunction is strongly implicated in the aetiology of the disease and impaired mitochondria are found in animal and cell models of PD [2].

Mitochondria form a tubular, reticulated network which shape is controlled by opposing fusion and fission events [3]. The Mitofusins 1 and 2 (Mfn1 and Mfn2) are conserved dynamin-like GTPases, composed of a large cytosolic GTPase domain, an HR1 domain, a double trans-membrane domain embedded in the outer mitochondrial membrane (OMM) and a second HR2 domain (HR2) [4]. Mfn1 mediate mitochondrial fusion of OMM in coordination with OPA1, which mediates the fusion of IMM [5,6]. While Mfn1 seems primarily involved in organellar docking and fusion, Mfn2 is enriched at contact sites between ER and mitochondria called MERC (mitochondria-ER contact sites) where it regulates organelles tethering [7–10]. MERCs are sites of dynamic physical and functional interaction that regulate phospholipid

\* Corresponding author at: Department of Biology, University of Padova, Padova, Italy.

E-mail address: [elena.ziviani@unipd.it](mailto:elena.ziviani@unipd.it) (E. Ziviani).

<https://doi.org/10.1016/j.phrs.2018.09.006>

Received 2 March 2018; Received in revised form 4 July 2018; Accepted 6 September 2018

Available online 13 September 2018

1043-6618/© 2018 The Author. Published by Elsevier Ltd. This is an open access article under the CC BY-NC-ND license (<http://creativecommons.org/licenses/by-nc-nd/4.0/>).



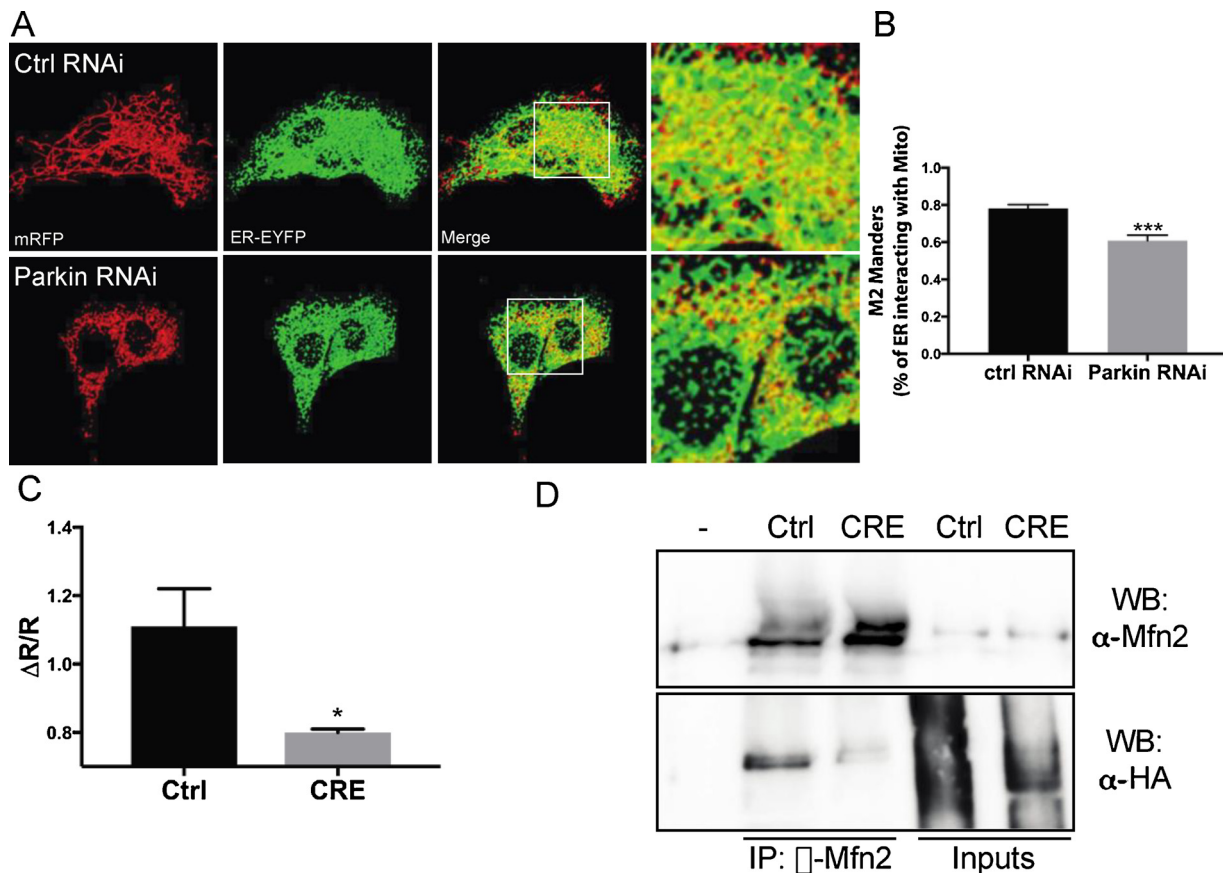


**Fig. 1.** Parkin regulates ER-mitochondria contacts.

(A) MEFs were transfected with either Parkin siRNA or Scamle siRNA (Ctrl RNAi). Mitochondria and ER were probed using organelles targeted fluorescence probes (mRFP and ER-YFP respectively). The overlap between red and green fluorescence (yellow spots) represents area of organelle tethering. Panels on the right show enlarged views of the boxed areas. B) Graph bar indicates mean  $\pm$  SEM of percentage of ER co-localizing with mitochondria (degree of tethering) by using Mander's coefficient of co-localization upon volume-rendered 3D reconstruction of z-axis stacks of confocal images (n = 8, 12–15 cells per experiment). Unpaired Two-tailed *t*-test P value = 0.0005 (C) Parkin<sup>Flox/Flox</sup> MEFs were transfected with pcDNA 3.1 (Ctrl) or pcDNA 3.1-Cre (CRE) and in combination with the FEMP probe. FRET ratio ( $\Delta R/R$ ) was calculated as described in materials and methods. Graph bar indicates mean  $\pm$  SEM. n = 4; Unpaired Two-tailed *t*-test P value = 0.0485. (D) Parkin<sup>Flox/Flox</sup> MEF cells were transfected with pcDNA 3.1-CRE or empty vector, Mfn2 (Myc-Mfn2) and HA-Ub and subjected to immunoprecipitation (IP) of Mfn2 using  $\alpha$ -Mfn2 antibody (Abcam). WB analysis was performed with antibodies  $\alpha$ -Mfn2 (Abnova) or  $\alpha$ -HA (cell signaling) on the pulled down samples. (-) identify samples incubated without antibody (negative control). Inputs represent 10% of the protein lysates and IP eluate 100% of the protein lysates (For interpretation of the references to colour in this figure legend, the reader is referred to the web version of this article.).

exchange and synthesis, Ca<sup>2+</sup> homeostasis, autophagosome formation and mitochondria fission [11–,1–13]. Recently it became clear that ER-mitochondria contacts are altered under pathological conditions. In particular, a number of proteins which mutations are linked to the onset of familiar cases of PD, such as Alpha-synuclein, PINK1, Parkin and DJ1, have been localised at the MERCs, and are able to modulate ER-mitochondria cross talk *in vitro* [13–,14,15,16,17].

Parkin, an E3-ubiquitin ligase mutated in familiar PD is selectively recruited to dysfunctional mitochondria and promotes their elimination via autophagy, a process known as mitophagy [18]. PINK1, a protein kinase, also a PD related gene, is required for Parkin recruitment and stress induced mitophagy [19]. In 2008 Poole et al. showed a strong genetic interaction between PINK1/Parkin pathway and mitochondrial fission and fusion machinery. By using the fruitfly *Drosophila*, they found that PINK1 or Parkin mutant (knock out) phenotypes, including locomotor defects, loss of dopaminergic neurons and degeneration of the muscle of the thorax, is suppressed by inhibiting mitochondrial fusion or by promoting mitochondrial fission [20]. This genetic interaction was explained by the subsequent discovery that Parkin physically interacts with and ubiquitinates Marf (dMfn), fly homologue of mammalian Mitofusins, to control its steady state levels [19]. This work was followed by others that showed that in several model systems, including HeLa cells [21] and human neuroblastoma cells SH-SY5Y [22],

Parkin selectively ubiquitinates mammalian Mfn1 and Mfn2. Accordingly, lack of Parkin (or PINK1 which operates upstream Parkin in the same pathway) [23–26] results in increased amount of the steady state levels of dMfn and a reduction of dMfn ubiquitination forms [19].

In this work we show that a post-translational modification (PTM), e.g. a Parkin dependent ubiquitination, plays an indispensable role in the formation of ER-mitochondria contacts sites via Mfn2. Moreover, we demonstrate that *in vivo* manipulation of ER-mitochondria tethering by expressing an ER-mitochondria synthetic linker is sufficient to rescue the locomotor deficits associated to an *in vivo Drosophila* model of PD.

## 2. Results

### 2.1. Parkin regulates ER-mitochondria contacts

In S2R+ *Drosophila* cells overexpression of Flag tagged dMfn allows the identification of four bands by western blotting (WB). As previously shown, the smaller molecular weight band (~90KDa) corresponds to unmodified dMfn whereas the upper bands (~100KDa, 130KDa and 140KDa) correspond to monoubiquitinated and multiubiquitinated forms of dMfn, respectively [19]. A similar pattern of ubiquitination was also previously described for Mfn2 in HeLa cells [21], human neuroblastoma cells SH-SY5Y [22] and for the yeast Mfn homologue,

fuzzy onions (Fzo1) [27]. This pattern of ubiquitination is PINK1/Parkin dependent. Accordingly, in the absence of PINK1 or Parkin, steady state levels of dmfn are increased and the pattern of ubiquitination is abolished [19]. Considering that dmfn in the fruit fly includes both promotion of fusion and ER-mitochondria crosstalk [28] and the role of Mfn2 in ER-mitochondria tethering [7–10,29], we investigated the degree of tethering between ER and mitochondria upon Parkin downregulation, i.e. in a condition where dmfn ubiquitination is impaired. Volume rendered 3D reconstruction of z-axis stacks of confocal images of fluorescent-tagged mitochondria and ER has been previously used to measure contact sites between the two organelles [12]. We transfected S2R + fly cells with expression vectors encoding mitochondrial and endoplasmic reticulum fluorescent marker (mDsRed and ER-GFP respectively) and upon treatment with Ctrl or Parkin dsRNA to specifically knock down Parkin. We then measured the degree of tethering by using Mander's coefficient of co-localization upon volume-rendered 3D reconstruction of z-axis stacks of confocal images. In such 3D reconstruction, the overlap between red and green fluorescence (yellow spots) represents area of organelle tethering. We found a clear decrease in ER-mitochondria interaction in Parkin downregulating cells (Supplementary Fig. 1A–B). To consolidate these data, we performed electron microscopy (EM) analysis on control and *parkin* downregulating cells and measured the average distance between mitochondria and the juxtaposing ER. We found a significant increase in ER-mitochondria distance (i.e. MERCs width) in *parkin* deficient S2R + cells (Supplementary Fig. 1C–D) and an overall decrease in the average number of ER-mitochondria contacts per mitochondria (Supplementary Fig. 1E) compared to control cells. To validate our findings, we performed the same measurement in a different cell type. MEFs cells, treated with scramble (Ctrl) or Parkin siRNA, were transfected with mitochondrial and endoplasmic reticulum fluorescent marker (mRFP and ER-YFP respectively). We observed a clear reduction in ER-mitochondria contacts in Parkin downregulating cells (Fig. 1A–B), as previously showed [14]. To consolidate these data, we also measured ER-mitochondria proximity by using a modified FRET-based indicator of ER-mitochondria proximity named FEMP [29]. This sensor is targeted to the mitochondrial outer membrane (OMM) (targeting sequence mAKAP1 connected to YFP fluorescent protein) and ER (targeting sequence Sac1 connected to CFP fluorescent protein) and contains a self-leaving Tav2A peptide, which undergoes autocleavage releasing YFP and CFP. This sensor is designed to guarantee almost equimolar expression of YFP on the mitochondrial outer membrane (OMM) and of the Cyan fluorescent protein (CFP) on the ER surface. FRET intensity is inversely proportional to the distance between the two fluorophores, thus allowing a quantitative measurement of organelles proximity. In the FEMP probe, OMM and ER targeting sequence are coupled with the two components of the FKBP-FRP heterodimerization system that allows covalent linkage between ER and mitochondria upon rapamycin administration. ER-mitochondria juxtaposition can therefore be correlated to FRET intensity and rapamycin treatment allows heterodimerization between adjacent FKBP and FRB domains to maximize energy transfer. We analyzed FRET ratio changes in MEFs coming from conditional Parkin KO mice in which Parkin expression can be deleted upon expression of Cre recombinase by recombining loxP sites *ad hoc* inserted in exon 7 (Parkin<sup>Flx/Flx</sup> mice) [30,31]. Transfection of MEFs with pcDNA 3.1-Cre leads to an obvious decrease in Parkin mRNA as compared to pcDNA 3.1 transfected cells (Supplementary Fig. 1F). We transfected Parkin<sup>Flx/Flx</sup> MEFs with pcDNA 3.1 (CTRL) or pcDNA 3.1-Cre (CRE) and in combination with the FEMP probe. We measured a decrease in the FEMP FRET ratio in Parkin downregulating cells further sustaining the knowledge that ER-mitochondria tethering is reduced in Parkin downregulating conditions (Fig. 1C). We thought to extend these data and investigate the pattern of Mfn2 ubiquitination in these conditions. To do that, we transfected Parkin<sup>Flx/Flx</sup> MEFs with empty vector, pcDNA 3.1 (CTRL), or pcDNA 3.1-Cre (CRE) and in combination with Myc-tagged form of Mfn2 (MFN2) and hemagglutinin (HA)-tagged

ubiquitin (HA-Ub). Western blotting analysis of Mfn2 by using anti Mfn2 antibody revealed a single band of the predicted size of Mfn2 (~86 KDa) in the total lysate. Western blotting analysis of the total lysate with antibody against HA revealed the expected smear of ubiquitinated forms, which was partially decreased upon Parkin deletion. To assess whether Mfn2 is ubiquitin modified, we performed coimmunoprecipitation analysis against HA-Ub. Immunoprecipitates of Mfn2 were prepared by using anti Mfn2 antibody and WB analysis was performed with antibody against HA on the pulled down samples. Following enrichment by immunoprecipitation, we observed a clear reduction of Mfn2-Ub (Fig. 1D). Thus, also in a mammalian cell type, impaired Mfn2 ubiquitination correlates to defective ER-mitochondria tethering.

These results sustain the hypothesis that aberrant ER-mitochondria interaction occurs in the absence of *parkin*, a condition that leads to impaired Mfn2 ubiquitination.

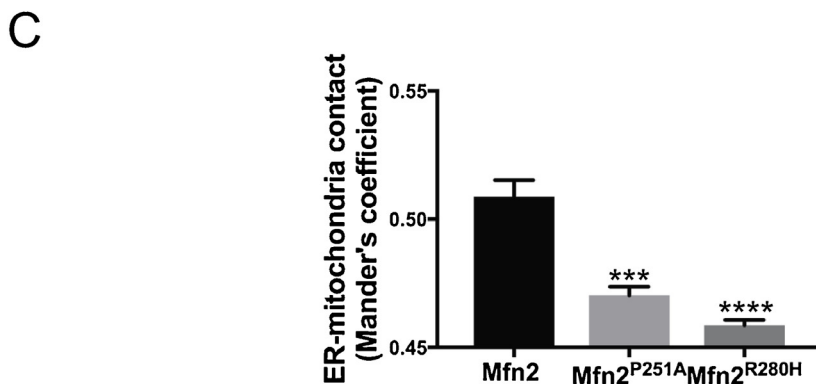
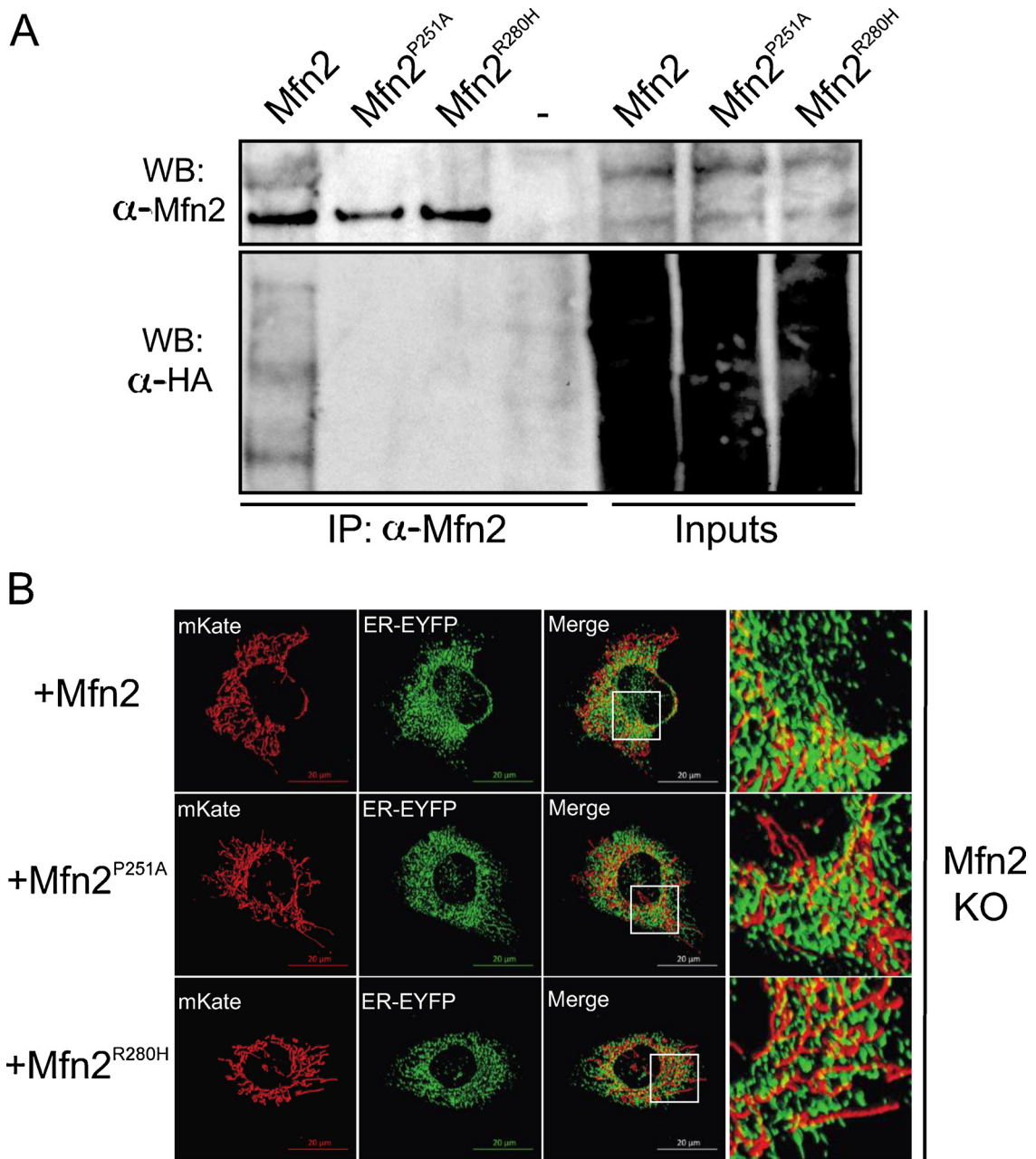
## 2.2. CMT type 2A disease-associated MFN mutants are not ubiquitinated and are incompetent in promoting ER-mitochondria interaction

Ablation of *Mfn2* in mice is embryonically lethal and *Mfn2* mutations in humans are associated with the onset of Charcot-Marie-Tooth neuropathy type 2A (CMT2A), an hereditary axonal peripheral neuropathy with patients developing early and severe motor disabilities that in the most severe cases constrict them to wheelchair [32,33]. The most frequent mutation in Mfn2 found in CMT2A patients, R94Q, cannot restore ER-mitochondria contacts in *Mfn2* KO MEFs [8]. We looked at the pattern of ubiquitination in S2R + *Drosophila* cells upon expression of Flag-tagged form of MFN<sup>R94Q</sup> mutant and two additional CMT type 2A disease-associated MFN mutations (P251A and R280H, respectively) and we found a complete loss of the ubiquitinated MFN forms in S2R + *Drosophila* cells (Supplementary Fig. 2). To examine whether this was also the case in mammalian cells, we looked at the pattern of Mfn2 ubiquitination in *Mfn2* KO MEFs transiently reconstituted with either wild type Mfn2 or mutants Mfn2<sup>P251A</sup> and Mfn2<sup>R280H</sup>. Western blotting analysis of Mfn2 by using anti Mfn2 antibody revealed a single band of the predicted size of Mfn2 (~86 KDa) (Fig. 2A). Immunoprecipitates of wt Mfn2, Mfn2<sup>P251A</sup> and Mfn2<sup>R280H</sup> were prepared by using anti Mfn2 antibody and WB analysis was performed with antibody against Ubiquitin on the pulled down samples to identify ubiquitinated forms of Mfn2. We observed a clear reduction of Mfn2-Ub in all CMT type 2A disease-associated Mfn2 mutants (Fig. 2A). Remarkably, we observed a reduction in ER-mitochondria contacts in *Mfn2* KO MEFs reconstituted with Mfn2<sup>P251A</sup> or Mfn2<sup>R280H</sup> as compared to wt Mfn2 (Fig. 2B–C).

These results further sustain the intriguing hypothesis that ubiquitination of Mfn2, rather than its steady state levels, is an essential prerequisite for ER-mitochondria tethering.

## 2.3. Ubiquitination of Lysine 416 in the HR1 Mfn2 domain control physical and functional ER-mitochondria interaction

Our results indirectly suggest that lack of MFN ubiquitination correlates to impaired ER-mitochondria interaction. With that in mind, we conducted a bioinformatics study to identify the potential Mfn2 site that could be ubiquitinated by Parkin. Mfn1 and Mfn2 are anchored at the outer mitochondrial membrane and have N- and C-terminal domains that protrude into the cytosol. At the N-terminus, there is a GTP binding domain, followed by a hydrophobic heptad repeat region (HR1) and a transmembrane domain (TM), which allows anchorage to the outer membrane. At the C-terminal, there is a second hydrophobic heptad repeat (HR2) [4]. This protein structure is highly conserved between different species [4], although an interesting work recently challenged this model, providing functional evidences that mammalian Mfns are single-spanning outer membrane proteins with an N<sub>out</sub>-C<sub>in</sub> orientation [34]. Nevertheless, a number of publications reported an almost identical pattern of ubiquitination for yeast homologue *fuzzy onion* (*fzo1*)



(caption on next page)

**Fig. 2.** CMT type 2A disease-associated MFN mutants are not ubiquitinated and are incompetent in promoting ER-mitochondria interaction.

(A) *Mfn2* KO MEFs were transfected with the indicated plasmids and in combination with HA-Ub. After 24 h, cells were lysed and subjected to immunoprecipitation (IP) by  $\alpha$ -Mfn2 antibody (Abcam). Western blotting analysis was performed by using  $\alpha$ -HA antibody and  $\alpha$ -Mfn2 (Abnova) on the pulled down samples. Inputs represent 10% of the protein lysates and IP eluate 100% of the protein lysates. (B) *Mfn2* KO MEFs were transfected the indicated plasmids. Mitochondria and ER were probed using organelles targeted fluorescence probes (mitoKate and ER-YFP respectively). Yellow spots represent area of organelle tethering. Panels on the right show enlarged views of the boxed areas. The scale bar is 20  $\mu$ m. (C) Graph bar indicates mean  $\pm$  SEM of percentage of ER co-localizing with mitochondria (degree of tethering) by using Mander's coefficient of co-localization upon volume-rendered 3D reconstruction of z-axis stacks of confocal images of cells transfected as indicated. (n = 4, 15 cells per experiment). One way ANOVA, p value < 0.0001. Dunnett's multiple comparison test (*Mfn2* vs *Mfn2*<sup>R251A</sup> p value = 0.0003; *Mfn2* vs *Mfn2*<sup>R280H</sup> p value = 0.0001) (For interpretation of the references to colour in this figure legend, the reader is referred to the web version of this article.)

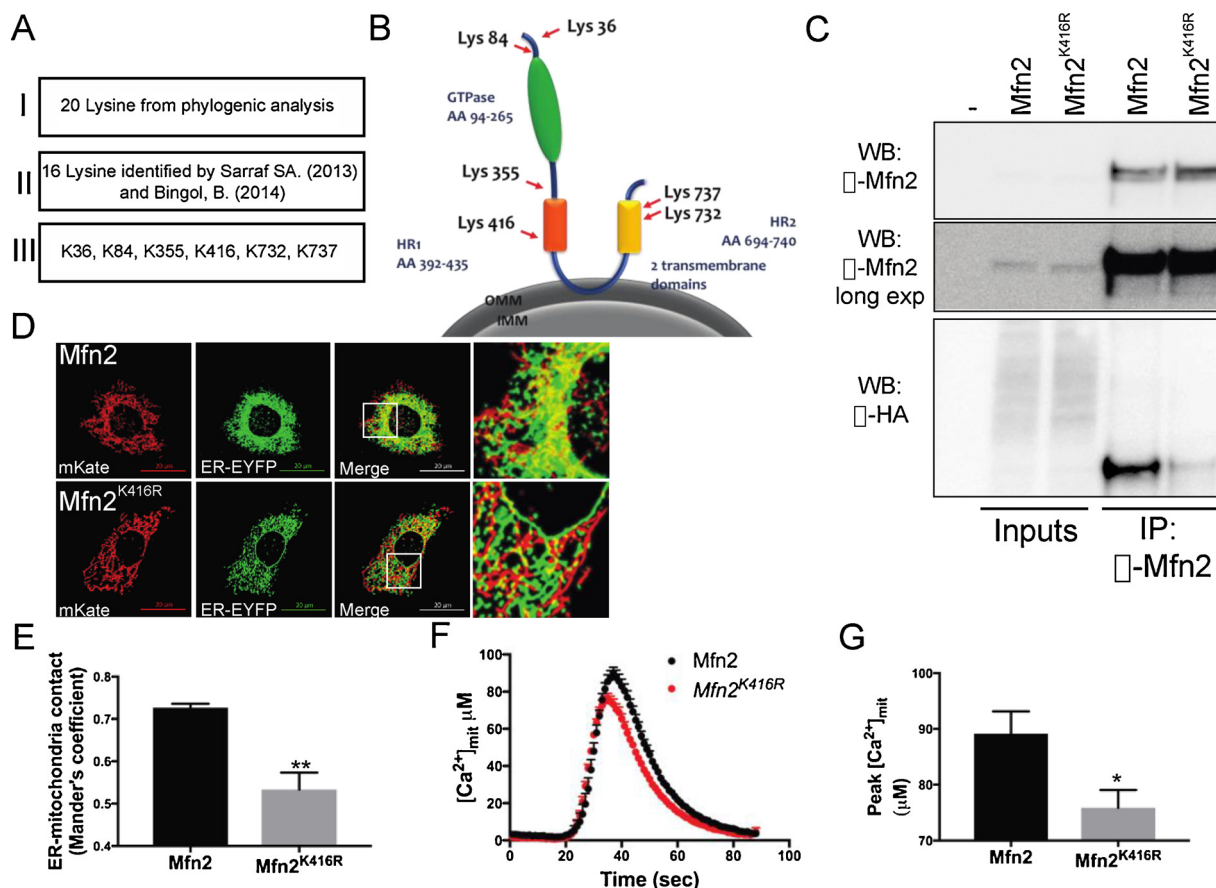


**Fig. 3.** Ubiquitination of Lysine 416 in the HR1 Mfn2 domain control physical and functional ER-mitochondria interaction.

(A) Panel shows a diagram of the *modus operandi* to identify the lysine residues (Lys, K) that are ubiquitinated by Parkin (see text) (B) Schematic representation of Mfn2 protein based on [4]. Residues K36 and K84 are located at the N-terminal of the protein, before the GTPase domain. Residue K355 is positioned between the GTPase and HR1 domain. Residue K416 is within the HR1 domain. Residues K732 and K737 are in the HR2 domain. (C) *Mfn2* KO MEFs were transfected with the indicated plasmids and in combination with HA-Ub and lysed after 24 h. Protein lysates were subjected to IP by using  $\alpha$ -Mfn2 antibody. WB analysis on the pulled down sample was performed by using  $\alpha$ -Mfn2 or  $\alpha$ -HA antibody. (-) identify samples incubated without antibody (negative control). Inputs and IP eluate represent 2% and 100% of the protein lysates, respectively. (D) *Mfn2* KO MEFs were transfected with the indicated plasmids. Mitochondria and ER were probed using organelles targeted fluorescence probes (mitoKate and ER-YFP respectively). Yellow spots represents area of organelle tethering. Panels on the right show enlarged views of the boxed areas. The scale bar is 20  $\mu$ m. (E) Graph bar indicates mean  $\pm$  SEM of percentage of ER co-localizing with mitochondria (degree of tethering) by using Mander's coefficient of co-localization upon volume-rendered 3D reconstruction of z-axis stacks of confocal images (n = 4, 15 cells per experiment). Unpaired Two-tailed t-test p value = 0.0029. (F) Mean  $\pm$  SEM of [Ca<sup>2+</sup>]<sub>mit</sub> from nine independent experiments where *Mfn2* KO MEFs were transfected with the indicated plasmids and mtAEQ. (G) Average  $\pm$  SEM of peak [Ca<sup>2+</sup>]<sub>mit</sub> in nine independent experiments performed as in G (Unpaired Two-tailed t-test p value = 0.0186) (For interpretation of the references to colour in this figure legend, the reader is referred to the web version of this article.)

[27,35], fly homologue Marf/dMfn [19] and human Mfn2 [21,35,36]. We therefore thought it was reasonable to hypothesize that the site of ubiquitination may be evolutionary conserved among species. Indeed, multiple sequence alignments using MultAlin revealed a high degree of homology between human, mouse and dMfn protein sequence. This phylogenetic analysis identified twenty Lysine residues (K) that are conserved between these species (arrowheads Supplementary Fig. 3A–B). Two independent studies also identified by using a mass spectrometry approach, a number of Lysine residues that are ubiquitinated upon Parkin overexpression [37,38]. We matched the residues

identified by these works with ours, and we identified six Lysine residues that are likely to represent good candidates for Parkin-dependent ubiquitination of Mfn2 (Fig. 3A). As illustrated, K36 and K84 are located at the N-terminal of the protein, before the GTPase domain, K355 is positioned between the GTPase and HR1 domain, K416 is within the HR1 domain and K732 and K737 are in the HR2 domain (Fig. 3B). We proceeded by generating non-ubiquitinatable mutants for each domain, and in this case for K36, K416 and K737 by substituting Lysine with Arginine (R), a common procedure to impair ubiquitination [39]. We expressed Flag-tagged mutants dMfn<sup>K36R</sup>, dMfn<sup>K416R</sup> and dMfn<sup>K737R</sup> in

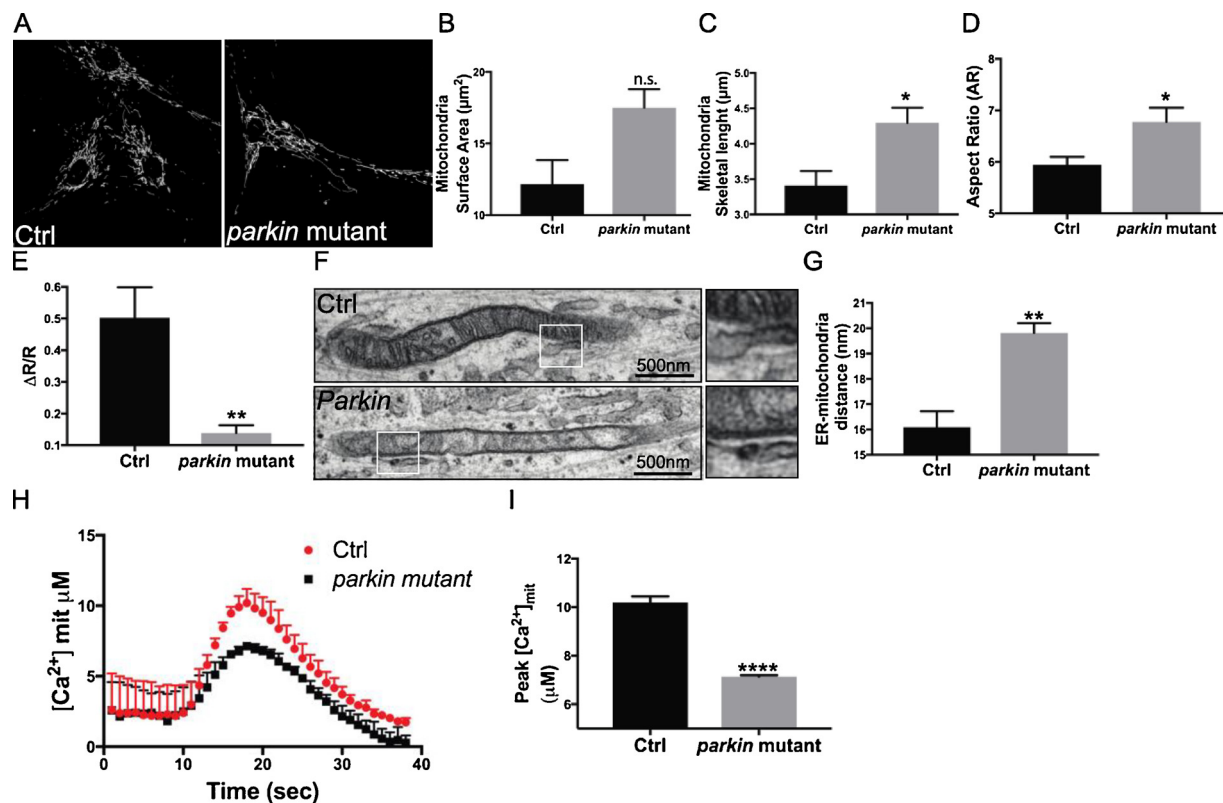


**Fig. 4.** ER-mitochondria physical and functional interaction is impaired in *parkin* mutant fibroblasts.

(A) Representative images of confocal acquisition of human fibroblast of the indicated genotypes generated from skin biopsy loaded with 1 μM of Tetramethylrhodamine methyl ester (TMRM). The 60 z-axis images separated by 0.2 μm were analyzed using Volocity 6.3 software, to obtain analysis of the mitochondrial volume, surface area (B) (unpaired Two-tailed *t*-test *p* value = 0.0655), skeletal length (C) (unpaired Two-tailed *t*-test *P* value = 0.0401) and the aspect ratio (D) (unpaired Two-tailed *t*-test *P* value = 0.05) calculated as described in materials and methods. Graph bars represent mean ± SEM of *n* = 3 replicates. (E) Human fibroblast of the indicated genotypes were infected with the FEMP probe. FRET ratio ( $\Delta R/R$ ) was calculated as described in materials and methods. Graph bar indicates mean ± SEM. *n* = 3; unpaired Two-tailed *t*-test *p* value = 0.0065 (F) Representative TEM images of human fibroblast of the indicated genotypes. (G) Mean ± SEM of mitochondria-ER distance calculated in four independent experiments as in F. Unpaired Two-tailed *t*-test *p* value = 0.0074. *n* = 3. (H) Mean ± SEM of [Ca<sup>2+</sup>]<sub>mit</sub> from four independent experiments of human fibroblast of the indicated genotypes, transfected with mtAEQ. Cells were perfused with a mixture of 0.1 μM ATP and 0.1 μM histamine. (I) Average ± SEM of peak [Ca<sup>2+</sup>]<sub>mit</sub> in four independent experiments performed as in H. Unpaired Two-tailed *t*-test *p* value < 0.0001.

S2R+ *Drosophila* cells. Western blotting analysis of dMfn by using anti Flag antibody revealed a single band of the predicted size of unmodified dMfn (~90 KDa) and a number of higher molecular weight bands which corresponds to mono and poly ubiquitinated forms of dMfn, as previously described [19]. Interestingly, expression of non-ubiquitinatable mutant dMfn<sup>K416R</sup> failed to reproduce the predicted pattern of ubiquitination (Supplementary Fig. 3C). Confocal microscopy analysis confirmed the mitochondrial subcellular localization of mutant dMfn<sup>K416R</sup> (Supplementary Fig. 3D), which indicated that impaired ubiquitination could not be due to misplacement of the protein. We next analysed the pattern of ubiquitination of non-ubiquitinatable mutant Mfn2<sup>K416R</sup> in MEFs. To do that, we transfected *Mfn2* KO MEFs with Myc-tagged form of wild type Mfn2 (Mfn2) or the non-ubiquitinatable mutant (Mfn2<sup>K416R</sup>) and HA-Ub. Western blotting analysis of wild type Mfn2 and Mfn2<sup>K416R</sup> by using anti Mfn2 antibody revealed a single band of the predicted size of Mfn2 (~86 KDa). To assess whether Mfn2 was ubiquitin modified, immunoprecipitates of Mfn2 were prepared by using anti Mfn2 antibody and WB analysis was performed with antibody against HA on the pulled down samples. We observed a clear reduction of ubiquitinated forms in the non-ubiquitinatable mutant Mfn2<sup>K416R</sup> (Fig. 3C), further supporting the notion that K416 in the HR1 Mfn2 domain is a genuine Parkin-dependent Mfn2 ubiquitination site.

To directly demonstrate the physiological significance of impaired MFN ubiquitination and ER-mitochondria miscommunication, we next

evaluated whether non-ubiquitinatable mutant Mfn2<sup>K416R</sup> is incompetent in promoting ER-mitochondria physical and functional interaction. To this aim, we expressed Mfn2<sup>K416R</sup> or wild type Mfn2 in *Mfn2* KO MEFs and measured ER-mitochondria physical interaction as previously described. Remarkably, we observed a reduction in ER-mitochondria contacts in *Mfn2* KO MEFs reconstituted with non-ubiquitinatable mutant Mfn2<sup>K416R</sup> (Fig. 3D–E). To evaluate the functional counterpart of ER-mitochondria physical interaction, we next measured ER-mitochondria Ca<sup>2+</sup> transfer in *Mfn2* KO MEFs reconstituted with non-ubiquitinatable mutant Mfn2<sup>K416R</sup>. In *Mfn2* KO cells expressing mutant Mfn2<sup>K416R</sup>, mitochondrial Ca<sup>2+</sup> uptake following ATP-generated InsP<sub>3</sub> signaling is significantly diminished (Fig. 3F–G).

Thus, ubiquitination of Lysine 416 in the HR1 Mfn2 domain controls physical and functional ER-mitochondria interaction.

#### 2.4. ER-mitochondria physical and functional interaction is impaired in *parkin* mutant fibroblasts

Our results strongly indicate a causal link between impaired ubiquitination of Mfn2 and physical and functional ER-mitochondria miscommunication, specifically in the context of Parkin deficiency. Although the exact cause for dopaminergic neurons loss in PD patients is unknown, these cells are highly susceptible to perturbations in Ca<sup>2+</sup> homeostasis and lipid transfer, both affected upon impaired ER-mitochondrial juxtaposition [40,41]. An elegant study has shown that the

vulnerability of dopaminergic neurons depends on their reliance on a specific subtype of voltage dependent L-type  $\text{Ca}^{2+}$  channels that require  $\text{Ca}^{2+}$  to maintain their autonomous pacemaking activity and which expression is age dependent. Blocking these channels has a neuroprotective effect because it allows neurons to “rejuvenate” and go back to a  $\text{Ca}^{2+}$  independent mechanism to generate their pacemaking activity [42]. This work highlighted the importance of age-dependent  $\text{Ca}^{2+}$  homeostasis regulation for the survival of dopaminergic neurons, and led us to the intriguing hypothesis that ER-mitochondria miscommunication might also add to the disease onset. With that in mind, we conducted a study to analyse mitochondria morphology and ER-mitochondria physical and functional interaction in a characterized clinical case of PD patient associated with a *parkin*-mutant. We used four sets of techniques, namely live cell confocal imaging of organelle morphology, electron microscopy, FRET based measurement of ER-mitochondria physical proximity and Aequorin based measurement of ER-mitochondria  $\text{Ca}^{2+}$  transfer, to assess the shape of mitochondria, and ER-mitochondria physical and functional interaction in fibroblasts coming from skin biopsy of *parkin* patient with compound heterozygous (R275 W and exon 3 deletion) *parkin* mutations. We started by investigating mitochondrial morphology in primary fibroblasts culture coming from skin biopsy of *parkin* patient and age matched control. Primary fibroblasts were loaded with membrane potential independent mitochondrial dye Mitotracker red (Molecular Probes) that allows qualitative *in vivo* imaging assessment of mitochondria morphology by confocal microscopy (Fig. 4A). Mitochondria morphology was analysed by Volocity software (PerkinElmer) upon three-dimensional (3D) reconstruction and volume rendering of confocal stacks. Mitochondrial surface area (Fig. 4B), skeletal length (Fig. 4C), diameter (Supplementary Fig. 4A), aspect ratio (AR, Fig. 4D) and volume (Supplementary Fig. 4B) were measured from three independent clones coming from *parkin* patient skin biopsy and age matched control. We found increased mitochondrial surface area as well as mitochondrial skeletal length and AR in cells coming from *parkin* mutant patient compared to control (Fig. 4B–D), clearly indicating altered mitochondrial morphology in primary fibroblasts deriving from *parkin* patient. We next measured ER-mitochondria proximity by using the FEMP probe as previously done [29]. *Parkin* patient cells expressing the FEMP probe measured a decrease in the FEMP FRET ratio compared to control cells, supporting the knowledge that ER-mitochondria distance is increased in *parkin* patient (Fig. 4E). To extend these observations we compared our previous finding with electron microscopy (EM) analysis of control and *parkin* fibroblasts. We measured the average distance between mitochondria and the juxtaposing ER and we found a significant increase in ER-mitochondria distance (i.e. MERCs width) in *parkin* deficient patient cells (Fig. 4F–G). We finally evaluated the functional counterpart of ER-mitochondria structural alteration of *parkin* patient cells, by looking at ER-mitochondria  $\text{Ca}^{2+}$  transfer. To this aim, we infected primary fibroblasts with mitochondrially targeted  $\text{Ca}^{2+}$  sensor Aequorin, and we measured mitochondrial  $\text{Ca}^{2+}$  uptake following ATP/histamine-generated  $\text{InsP}_3$  signalling. We found a significant decrease in mitochondrial  $\text{Ca}^{2+}$  transient upon ATP/histamine stimulation in *parkin* fibroblasts, (Fig. 4H–I), whether cytosolic  $\text{Ca}^{2+}$  transient was unaffected (Supplementary Fig. 4C–D). These results are indicative of aberrant ER-mitochondria  $\text{Ca}^{2+}$  flux in *parkin* patient cells and functionally correlates to defective ER-mitochondria physical interaction.

### 2.5. Expression of ER-mitochondria synthetic tether rescues the locomotor defect of a *Drosophila* model of Parkinson's disease

One of the most important functions of ER-mitochondria cross talk includes coordinating  $\text{Ca}^{2+}$  transfer and elegant studies have shown that artificial tether between the ER and mitochondria can be used to modulate  $\text{Ca}^{2+}$  transfer [43,44]. Starting from the rational that normalization of interorganelle contacts and ER-mitochondria  $\text{Ca}^{2+}$  transfer could be beneficial in PD models of aberrant  $\text{Ca}^{2+}$  homeostasis,

we investigated the effect of expressing an ER-mitochondria synthetic linker in *Drosophila* PINK1 KO, a well-established *in vivo* model of PD that is deficient for Parkin function [19,45]. This is also presumably a good *in vivo* model of aberrant  $\text{Ca}^{2+}$  homeostasis, since a number of studies have previously shown impaired  $\text{Ca}^{2+}$  handling in cellular models lacking PINK1 [46,47]. We generated two *Drosophila* transgenic lines that allow visualising *in vivo* in the adult wing ER-mitochondria contacts through expression of a synthetic tether construct driven by a neuron-specific driver. The construct was created by Csordás et al. [43] and encodes monomeric red fluorescent protein (mRFP) fused to the OMM-targeting sequence (MTS) of mAKAP1 at the N-terminus and fused to the ER-targeting sequence (ERTS) of  $\gamma\text{UBC6}$  at the C-terminus (Supplementary Fig. 5A). We cloned the construct for the synthetic linker into a fly vector and generated two “tethering” lines by random insertion in a wild type (*white1118*) background under expression of the GAL4-UAS system. These lines expressed mild (TM, Tether Mild) to high (TH, Tether High) levels of the tethering construct. We expressed the TM “tethering” line in wild type (*white1118*)<sup>-</sup> and PINK1 mutant (KO) flies (PINK1<sup>B9</sup>). To assess that the construct was appropriately expressed, and to visualize *ex vivo* ER-mitochondrial contacts in the fly, we took advantage of a recently described model, which allows imaging of sensory neurons in the translucent fly wing [48]. We fixed flies of the desired age in PFA, detached the wing and measured ER-mitochondria contact sites by imaging at confocal microscope of the red fluorescent signal in the L1 vein neuron bundle. In order to activate neuronal expression of the UAS tether lines we crossed these lines with nSyb-Gal4 (neuronal Synaptobrevin) expressing flies. We observed well-defined and easily quantifiable red fluorescent spots throughout the L1 vein that perfectly matched the pattern seen when expressing only mito-GFP or ER-GFP in the wing neurons (Supplementary Fig. 5B). Interestingly, we observed a reduced expression of the tethering probe (i.e. reduction in the RFP signal) in PINK1 KO flies (Fig. 5A–B), indicative of a previously described impairment in the mitochondrial protein import machinery of the PINK1 deficient flies [49]. Next we used a well-established locomotor assay to evaluate *in vivo* the physiological relevance of expressing the synthetic ER-mitochondria linker. In such assay, 10 flies for each strain were collected in a vertical plastic tube positioned with a line drawn at 6 cm from the bottom of the tube and under a light source. After tapping the flies to the bottom of the tube, the flies that successfully climbed above the mark after 10 s were counted (Fig. 5C). As already reported, PINK1<sup>B9</sup> mutant (PINK1 KO) flies performed poorly in the climbing assay compared to wild type (Ctrl) flies (Fig. 5D). Remarkably, climbing performance of PINK1 KO flies was significantly improved upon expression of the synthetic ER-mitochondria linker TM (Fig. 5D), sustaining the hypothesis that *in vivo* genetic normalization of ER-mitochondria tethering is beneficial in ameliorating the locomotor impairment associated to PINK1 deficiency. Of note, expression of the TH (tether high) synthetic tethering construct resulted lethal in wild type but not in PINK1 KO background, where it did not ameliorate the climbing performance of PINK1 flies (Fig. 5E) further corroborating the hypothesis that fine tuning ER-mitochondria interaction by expression of the synthetic linker has physiological implications *in vivo*. Intriguingly, TH expression did not impact eggs to pupae viability (Fig. 5F), but impaired adults/pupae ratio (Fig. 5G) indicating an age dependent lethality that occurs when pupae become adults.

### 3. Discussion

Parkin, a protein which mutations have been linked to the onset of a rare autosomal recessive form of familial PD, is an E3 ubiquitin ligase that belongs to the Ring-between-RING (RBR) type of E3 ubiquitin ligases, also known as RING/HECT hybrids [50]. By mediating the covalent attachment of the highly conserved 76-amino acid protein ubiquitin on target proteins, Parkin controls a fundamental post-translational modification (PTM) that is required for proteasome-dependent protein degradation. Parkin is predominantly localized in the

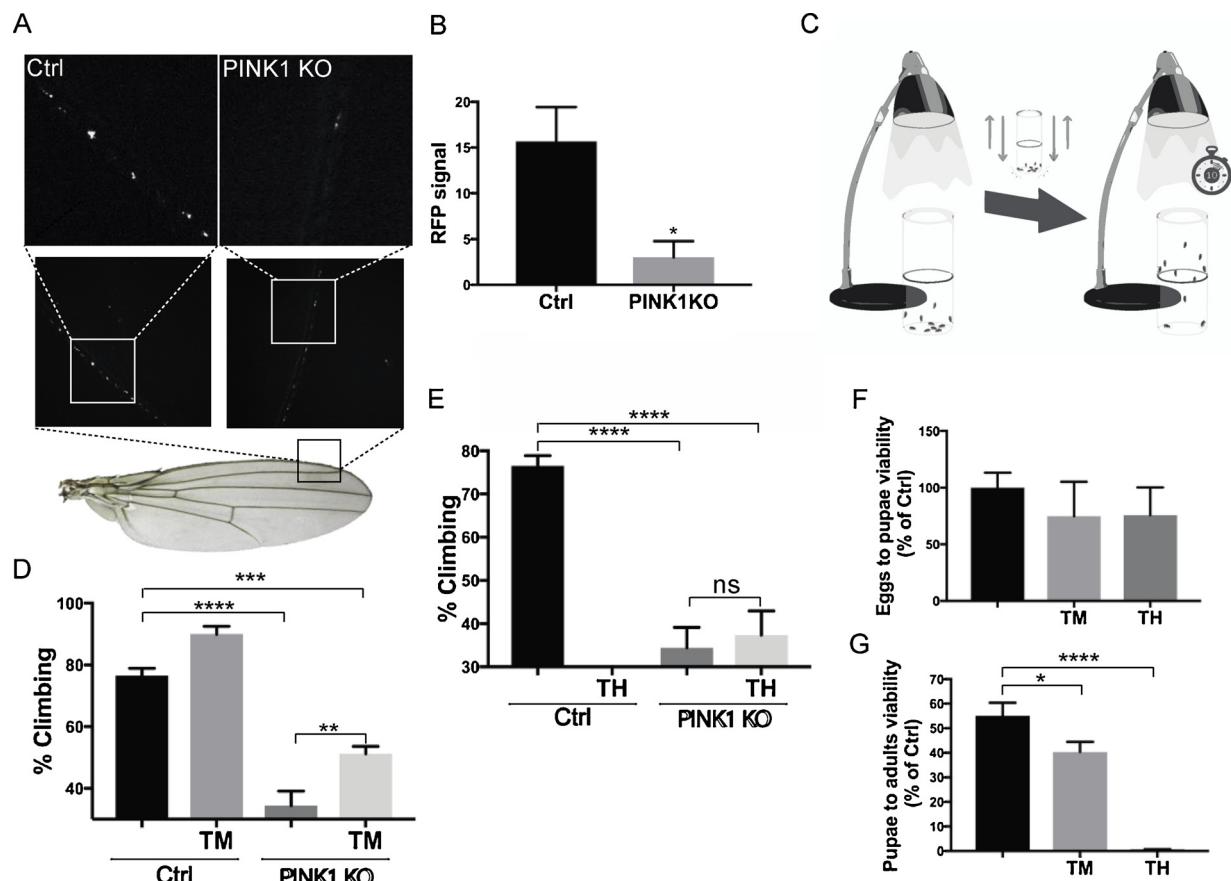


Fig. 5. Expression of ER-mitochondria synthetic tether rescues the locomotor defect of a *Drosophila* model of Parkinson's Disease.

(A) Representative images of TM (tether mild) "tethering" line in wild type (*white1118*)<sup>-</sup> and PINK1 mutant (KO) background (PINK1<sup>B9</sup>). The down panels shown enlarge views of the 150 nm length along the L1 vein neural bundle from the intersection of the L2 vein to proximal side of the wing flies. (B) RFP signal in the wing of flies of the indicated genotype was quantified as described in materials and methods. Graph bar indicates mean ± SEM of the number of RFP spots. n = 3. Unpaired Two-tailed *t*-test P value = 0.0381 (C) Schematic representation of the climbing assay. 10 flies were put into a tube in a dark room. A light was put on the top of the tube. After tapping the flies at the bottom of the tube, the number of flies that successfully climbed above the 6-cm mark after 10 s was noted. (D) Graph bars represents means ± SEM of percentage (%) of climbing of flies of the indicated genotype. TM (tether mild) "tethering" line in wild type (*white1118*)- and PINK1 mutant (KO) background (PINK1<sup>B9</sup>). n = 5, 10 flies per experiment. One way ANOVA, p value < 0.0001. One way ANOVA, p value < 0.0001. Tukey's multiple comparison test (Ctrl vs Ctrl + TM p value = 0.0377; Ctrl vs PINK1 KO p value < 0.0001; Ctrl vs PINK1 KO + TM, p value = 0.0001; Ctrl + TM vs PINK1 KO, p value < 0.0001; Ctrl + TM vs PINK1 KO + TM, p value < 0.0001, PINK1 KO vs PINK1 KO + TM, p = 0.0055). (E) Graph bar represents means ± SEM of percentage (%) of climbing of flies of the indicated genotype. TH (tether high) "tethering" line in wild type (*white1118*)- and PINK1 mutant (KO) background (PINK1<sup>B9</sup>) n = 5, 10 flies per experiment. One way ANOVA, p value < 0.0001. Tukey's multiple comparison test (Ctrl vs Ctrl + TH p value < 0.0001; Ctrl vs PINK1 KO p value < 0.0001; Ctrl vs PINK1 KO + TH, p value < 0.0001; Ctrl + TH vs PINK1 KO, p value < 0.0001; Ctrl + TH vs PINK1 KO + TH, p value < 0.0001, PINK1 KO vs PINK1 KO + TH, p value = 0.9293). (F) Graph bar indicates means ± SEM of egg to pupae ratio (% of Ctrl) calculated as described in materials and methods. (n = 3). (G) Graph bar indicates means ± SEM of adults to pupae ratio. n = 3. One way ANOVA, p value < 0.0001. Tukey's multiple comparison test (Ctrl vs TM p value = 0.0284; Ctrl vs TH p value < 0.0001; TM vs TH, p value < 0.0001).

cytosol, but it can translocate to depolarized mitochondria where it promotes polyubiquitination of outer mitochondrial membrane resident proteins, which is a prerequisite for mitochondria quality control or mitophagy, a well characterized cellular process that leads to the elimination of a selective subset of damaged mitochondria via autophagy [18]. In a number of cellular models, Parkin promotes the ubiquitination of Marf/dMfn (fly homologue of mammalian Mitofusins) [19] and both Mitofusin 1 (Mfn1) and Mitofusin 2 (Mfn2) [21,22]. Ubiquitination of Mitofusins leads to proteasome- and p97-dependent degradation of the proteins [21]. However, recent studies reported proteasome-independent-mediated ubiquitinations by Parkin, which do not result in degradative ubiquitination. For example, in 2006 two groups independently observed that Parkin catalyzes the formation of multiple monoubiquitination *in vitro* [51,52]. Additional study propounded that Parkin activation results in the formation of K63-linked ubiquitin chains, which does not result in decreased levels of the target protein [53]. Similarly it was demonstrated that Parkin can form linear ubiquitination of NF-κB essential modulator (NEMO) causing the

activation of NF-κB pro-survival pathway [50]. All these observations suggest that Parkin may act like a multi-functions ubiquitin protein ligase capable of both mediating degradative ubiquitination (proteasomal or autophagy-dependent degradation) [19,21,22,54,55], as well as regulative ubiquitination (non degradative ubiquitination) [50–51,52,53,56–57,58,59]. Not surprisingly, Parkin exists in an inactive state that resembles that of a coiled snake and its activity is finely regulated and repressed by mechanisms of autoinhibition under normal conditions [60,61].

Parkin targets Mitofusins, large GTPase proteins that are required on adjacent mitochondria to promote tethering and fusion of the outer mitochondrial membrane. In mammals Mfn2 also regulates ER-mitochondrial tethering [7–10,29]. ER-mitochondria physical interaction is a structural feature that is indispensable for Ca<sup>2+</sup> cross talk, phospholipid biosynthesis, autophagosome formation, DRP1 mediated mitochondrial fission and a number of additional physiological signaling pathways that are essential for cell survival [12,13,40,62–65]. Starting from the observation that Parkin downregulation in MEFs results in

decreased ubiquitinated forms of Mfn2, as also observed in *Drosophila* cells [19], HeLa and human neuroblastoma cells [21,22], we addressed the effect of Parkin downregulation on ER-mitochondria physical and functional communication. By using four independent approaches (namely live cell confocal imaging of organelle morphology, electron microscopy, FRET based measurement of ER-mitochondria physical proximity and Aequorin based measurement of ER-mitochondria  $\text{Ca}^{2+}$  transfer) we showed that Parkin downregulation induced a decrease in ER-mitochondria physical and functional interaction, confirming previous findings [14]. We also found that Charcot Marie Tooth type 2A disease-associate Mfn2 mutants, P251A and P280H, failed to be ubiquitinated and are incompetent in promoting ER-mitochondria interaction. These observations prompted us to investigate whether ubiquitination of Mfn2 might operate as a functional PTM that is required on juxtaposing ER-mitochondria to promote organelle physical interaction. To prove this hypothesis, we engaged on a bioinformatics and a mass spectrometry-based analysis to identify the site/s of Parkin dependent ubiquitination on Mfn2 molecule. We identified lysine 416 localized in the HR1 domain of Mfn2. We generated a non-ubiquitinatable K416 mutant, which failed to be ubiquitinated and was also incompetent in promoting ER-mitochondria physical interaction. The non ubiquitinatable mutant not only altered physical contacts formation, but also impaired the functionality of ER-mitochondria communication, reducing mitochondrial  $\text{Ca}^{2+}$  uptake upon treatment that generated ER  $\text{Ca}^{2+}$  release. Of note, no changes in the steady state levels of non ubiquitinatable mutant Mfn2<sup>K416R</sup> was observed, supporting the intriguing hypothesis that ubiquitination of Mfn2 on a specific lysine residue rather than Mfn2 steady state levels is crucial for proper ER-mitochondria interaction.

Aberrations in ER-mitochondria juxtaposition have been described in cellular models of a number of neurodegenerative diseases, including Parkinson's disease [14–16,66]. One of the most important functions of ER-mitochondria cross talk includes coordinating  $\text{Ca}^{2+}$  transfer and a number of studies have also shown impaired  $\text{Ca}^{2+}$  homeostasis in cellular models lacking PINK1 or Parkin [14,46,47,67–69]. Although it is not clear why dopaminergic neurons specifically degenerate in PD, it is tempting to hypothesize that this could be due to impaired  $\text{Ca}^{2+}$  cross talk at ER-mitochondria interface. Supporting this hypothesis we found that primary fibroblasts coming from skin biopsy of *parkin* patient display structural and functional ER-mitochondria miscommunication. Starting from the rational that normalization of ER-mitochondria  $\text{Ca}^{2+}$  transfer could be beneficial, we investigated the effect of expressing an ER-mitochondria synthetic linker in a well-established *in vivo Drosophila* model of PINK1 loss of function. PINK1 mutant (KO) flies have a very obvious phenotype characterized by male sterility, degeneration of thorax muscle, degeneration of dopaminergic neurons, locomotor defects, reduction in lifespan and mitochondrial dysfunction [23–25]. We demonstrated that expression of the mild tether (TM) induced a significantly improvement in the climbing performance of PINK1 KO flies, supporting the notion that ER-mitochondria cross talk normalization could be effective in ameliorating some of the phenotypes that are associated to PD neurodegeneration, and may hold substantial therapeutic implication for this disorder.

Altogether, these results led us to envision a model where Parkin dependent ubiquitination of Mfn2 is required on healthy mitochondria to mediate ER-mitochondria crosstalk (Fig. 6(a) upper representation). This model does not exclude the existence of a parallel stress induced pathways (like those generated by intoxicating substances), which promotes Parkin-dependent ubiquitination of Mfn2, and additional OMM resident proteins, to promote mitophagy (Fig. 6(b) lower representation).

## 4. Materials and methods

### 4.1. Cell culture

*Drosophila* S2R+ cells grow at 25 °C without  $\text{CO}_2$ , as semi-adherent monolayer in tissue culture flasks. The complete medium for SR2+ cells is Schneider's *Drosophila* Medium (Gibco) containing 10% heat-inactivated fetal bovine serum (FBS). Transfection was performed using Effectene Transfection Reagent (QIAGEN) following manufacturer instruction. 5 h after the transfection medium was removed and change with fresh medium and after 72 h the cells were used to the indicated experiments.

The mouse embryonic fibroblasts (MEFs) grow in Dulbecco's modified Eagle medium (DMEM) (Gibco) with addition of 1% penicillin/streptomycin, 1% non-essential amino acids solution, L-glutamine and 10% FBS at 37 °C with 5%  $\text{CO}_2$  atmosphere.

Mfn2 KO MEFs were provided by Dr. Luca Scorrano, Department of Biology, University of Padova. *Parkin*<sup>FLX/FLX</sup> MEF were obtained from Dr. Ted Dawson, Johns Hopkins University [31]. TransFectin™ Lipid Reagent (Bio-Rad) or GenJet™ In Vitro DNA Transfection Reagent (SigmaGen laboratories) were used for the transfection following the manufacturer's instruction. The medium was changed after 5 h and the experiments performed after 24 h/48 h from the transfection.

Human fibroblasts from skin biopsy were obtained from B.A., a 55-year old man who was diagnosed with PD at the age of 28 and presented an excellent response to a combination of levodopa and dopamine agonists until 2008. He then started complaining about motor fluctuations and involuntary movements and more recently developed pathological gambling, excessive impulsivity, aggressiveness and substance abuse (mainly cocaine). Cognitive testing in 2016 showed abnormalities in frontal executive and attention domains. His MRI revealed modest cortical and subcortical atrophy. Cells were grown in Dulbecco's modified Eagle medium (DMEM) (Gibco) with addition of 1% penicillin/streptomycin, 1% non-essential amino acids solution, L-glutamine and 10% FBS at 37 °C with 5%  $\text{CO}_2$  atmosphere. Cells were used between passage P = 4 to P = 7 and transfection was performed using Lipofectamine Transfection Reagent (Invitrogen) achieving a maximal efficiency of transfection of 5%. For calcium measurement experiments, human fibroblasts were seeded onto 13 mm-diameter glass coverslips and maintained at 37 °C in a humidified incubator. After 24 h, cells were infected with lentiviral (LV) particles using the minimal dilution adequate for obtaining ≈70% of infected cells.  $\text{Ca}^{2+}$  measurements were performed 96 h after plating as described.

HEK-293 T cells to generate Lentiviral (LV) particles were grown in Dulbecco's modified Eagle's medium/High-Glucose (Euroclone), supplemented with 10% fetal bovine serum (Euroclone), 100 U/ml penicillin and 100 µg/ml streptomycin (Euroclone), and maintained at 37°C in a humidified incubator with 5%  $\text{CO}_2$

### 4.2. Lentiviral production and cell transduction

$[\text{Ca}^{2+}]_{\text{cyt}}$  and  $[\text{Ca}^{2+}]_{\text{mit}}$  fluctuations analysis were performed by transducing human fibroblasts with a third generation lentivirus-based system that allow the expression of a chimeric construct encoding the  $\text{Ca}^{2+}$ -probe aequorin (AEQ) tagged with the influenza virus hemagglutinin (HA) epitope, and linked to sequences addressing the protein to the bulk cytosol (AEQcyt [70]) and mitochondrial matrix (AEQmit [71]), respectively. The transgene plasmids (pLV-AEQmit and pLV-AEQcyt) codifying for AEQmit and AEQcyt were generated by using an AEQ mutant with reduced  $\text{Ca}^{2+}$  affinity allowing  $[\text{Ca}^{2+}]$  measurements up to hundreds of µM [72], while a chimeric construct of WT AEQ was used to generate the lentiviral vector for AEQcyt [73].

To obtain lentiviral particles, HEK-293 T cells were seeded onto 100 mm-diameter Petri dishes at ~40% confluence. 24 h after plating, cells were co-transfected, by means of calcium-phosphate procedure, with one of the transgene plasmids (pLV-AEQmit or pLV-AEQcyt) and



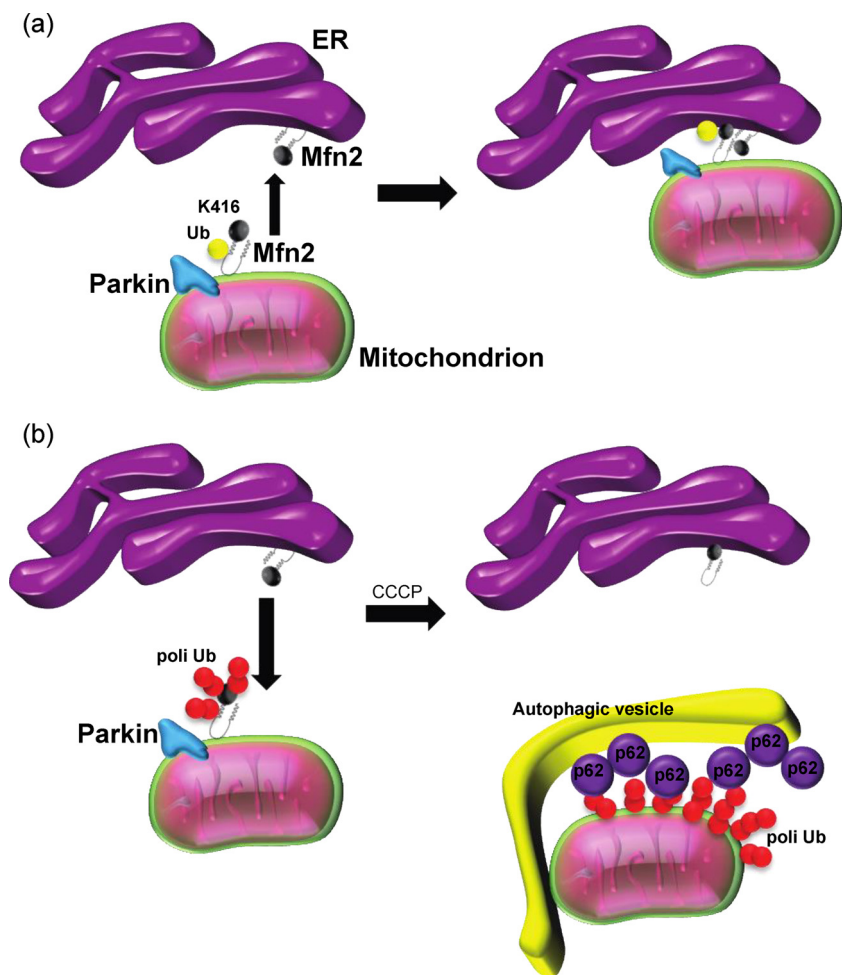


**Fig. 6.** Regulation of ER-mitochondria interaction by Parkin via Mfn2: a schematic representation.

Parkin ubiquitinates Mfn2 on lysine K416. This event is a prerequisite for ER-mitochondria physical and functional interaction (a). This model does not exclude the existence of a parallel pathway, which promotes Parkin-dependent ubiquitination of Mfn2, and additional OMM resident proteins, to promote mitophagy (b).

**Table 1**

Primers used for Site directed mutagenesis. Underscores indicate mismatch.

Constructs	Primers
Myc-Mfn2 <sup>P251A</sup>	Forward: 5'-GCGTCTCTCCCGGGCAAACATCTTCATC-3' Reverse: 5'-GATGAAGATGTTT <u>GC</u> CGGGGAGAGACGC-3'
Myc-Mfn2 <sup>R280H</sup>	Forward: 5'-CAGCACATGGAGCA <u>TT</u> TGTACCAGCTTCC-3' Reverse: 5'-GGAAGCTGGTACAATGCTCCATGTGCTG-3'
Myc-Mfn2 <sup>K416R</sup>	Forward: 5'-GAGCTCTTGGCTCAAGACTAT <u>AGG</u> CTCCGAATTAAGCAGATTACG-3' Reverse: 5'-CGTAATCTGCTTAATTCCGGAG <u>CT</u> TAGTCTTGAGCCAAGAGCTC-3'
MFN <sup>P251A</sup> Flag	Forward: 5'-TCGCAGAAGCTAAGCAAG <u>GCC</u> AACATCTTCATCCTGAAC-3' Reverse: 5'-GTTCAGGATGAAGATGTT <u>GGC</u> CTTGCTTAGCTTCTGCGA-3'
MFN <sup>R280H</sup> Flag	Forward: 5'-AAGTCTCAGCACACGGAA <u>CA</u> CTGCATCGACTTCCTCACC-3' Reverse: 5'-GGTGAGGAAGTCGATGCAG <u>TG</u> TTCCGTGTGCTGAGACTT-3'
MFN <sup>K36R</sup> Flag	Forward: 5'-TTGTGCGCGCC <u>AGG</u> AGGAGGATCAACGATATC-3' Reverse: 5'-GATATCGTTGAT <u>TC</u> CTCTCTCTGGCGCGCACAAA-3'
MFN <sup>K416R</sup> Flag/MFN <sup>K416R</sup> GFP	Forward: 5'-GGTTACGCGGGAAAT <u>GAG</u> GATGAGGATCCACAACATGGTTCG-3' Reverse: 5'-CGACCATGTTGTGGAT <u>CCT</u> CATCCTCATTTCCCGGTAACC-3'
MFN <sup>K737R</sup> Flag	Forward: 5'-AAGCTGCTCAGGAAT <u>AGG</u> GCCGGTTGGTTGGAC-3' Reverse: 5'-GTCCAACCAACCGGC <u>CT</u> ATTCTGAGCAGCTT-3'

the packaging plasmids pMDLg/pRRE, pMD2.VSVG, pRSV-Rev. After 10 h, the transfection medium was replaced with fresh culture medium. After 72 h, the HEK-293 T culture medium was collected and viral particles were harvested by ultracentrifugation (50,000 × g, 2 h) and resuspended in phosphate buffered saline (PBS; 140 mM NaCl, 2 mM KCl, 1.5 mM KH<sub>2</sub>PO<sub>4</sub>, 8 mM Na<sub>2</sub>HPO<sub>4</sub>, pH 7.4). Lentiviral stock infectivity was estimated by anti-HA immunocytochemistry as described

in Lazzari et al. [74]. All procedures for the production and use of lentiviral particles were performed in a biosafety level-2 environment.

#### 4.3. Measurements of mitochondrial and cytosolic Ca<sup>2+</sup> fluxes

Cells were incubated (1 h, 37°C, 5% CO<sub>2</sub>) with the prosthetic group coelenterazine (5 μM, Santa Cruz Biotechnology, cat. n. sc-205904) in

CaCl<sub>2</sub>-containing Krebs-Ringer buffer (KRB-CaCl<sub>2</sub>, 125 mM NaCl, 1 mM Na<sub>3</sub>PO<sub>4</sub>, 1 mM MgSO<sub>4</sub>, CaCl<sub>2</sub> 1 mM, 5.5 mM glucose, 5 mM KCl, 20 mM HEPES, pH 7.4) and then transferred to the recording chamber—equipped with a perfusion system—located into the luminometer. For the measurements of [Ca<sup>2+</sup>]<sub>cyt</sub> and [Ca<sup>2+</sup>]<sub>mit</sub>, after a 30 s-perfusion step with KRB-CaCl<sub>2</sub>, fibroblasts were stimulated with a mixture of 100 μM ATP and 100 μM histamine dissolved in KRB-CaCl<sub>2</sub>. The experiments were terminated by cell permeabilization with digitonin (100 μM, Sigma) in Ca<sup>2+</sup>-rich solution (10 mM CaCl<sub>2</sub> in H<sub>2</sub>O). AEQ light emission was collected by means of an in-house built luminometer, equipped with a low-noise photo-multiplier coupled by an A/D board to a computer-assisted acquisition system, with a 1 Hz sampling rate [75]. This allowed the calibration of the recorded light signal to the total AEQ content. Conversion of light signal into Ca<sup>2+</sup> concentration was performed as described in Brini et al. [70] and Montero et al. [76].

#### 4.4. Molecular biology

pEYFP-ER (ER YFP), mRFP, pCB6-Myc-Mfn2 (Mfn2 WT) were previously described (de Brito and Scorrano [8]). pcDNA 3.1 CRE (CRE), pcDNA 3.1 (Empty vector) and pcDNA 3.1 mitoKate were available in our lab. Site directed mutagenesis was performed from Myc-Mfn2 using QuikChange II XL Site-Directed Mutagenesis Kit (Agilent) to obtain Myc-Mfn2<sup>P251A</sup> (Mfn2<sup>P251A</sup>), Myc-Mfn2<sup>R280H</sup> (Mfn2<sup>R280H</sup>) and Myc-Mfn2<sup>K416R</sup> (Mfn2<sup>K416R</sup>) (primers in Table 1). pAct-PPA Marf-Flag (MFN) and pAct-PPA Marf GFP (MFN GFP) constructs were previously generated [19] and were available in the lab. Site directed mutagenesis was performed to generate MFN<sup>P251A</sup> Flag, MFN<sup>R280H</sup> Flag, MFN<sup>K36R</sup> Flag, MFN<sup>K416R</sup> Flag, MFN<sup>K737R</sup> Flag, MFN<sup>K416R</sup> GFP (primers in Table 1) using QuikChange II XL Site-Directed Mutagenesis Kit (Agilent). HA-Ubiquitin (HA-Ub) was obtained from Addgene. FRET based Mito-ER Linker probe (FEMP) and mitochondrial low-affinity aequorin (mtAEQ mut) were previously described [29,72].

#### 4.5. Parkin siRNA and MFN RNAi treatment

Parkin siRNA was transfected using Oligofectamine™ reagent (Invitrogen) and 100 nM of siRNA for each treatment following manufacturer instructions. The same amount of scrambled siRNA was used as control. For Parkin knockdown, cells were incubated with siRNA for at least 48 h. For RNA interference, cells were transfected with Parkin siRNA HSS107593 (Invitrogen).

Double-stranded RNAs (dsRNAs) were prepared using the MEGAscript kit (Ambion) according to the manufacturer's instructions. Primers used to generate dsRNAs contained a T7 promoter sequence at the 5' end (MFN forward primer 5'-GGAACCTCTTATTCTCTAT-3' and reverse primer 5'-GGTTTGCTTGGCCCAACAT-3'). A total of 1 million S2R+ cells were plated on a six-well plate and treated with 15 μg dsRNA probe in serum-free medium. One hour after probe treatment, complete medium was added to the wells, and cells were cultured for 2 days before being transfected.

#### 4.6. RNA isolation and Real time PCR

Parkin<sup>Flx/Flx</sup> MEF cells were transfected with the pcDNA 3.1-CRE (CRE) or empty vector (CTRL) and after 48 h total RNA was extracted from the cells with TRIzol™ Reagent (Invitrogen™) according to the manufacturer's instructions. Two hundred and fifty ng of RNA was reverse transcribed with SensiFAST™ cDNA Synthesis Kit (Bioline). Briefly, GoTaq qPCR Master mix containing SYBR green fluorescent dye (Promega) was mixed with 1 μl cDNA and 0.2 μM primers: *Parkin* forward primer 5'-AGGAATGCGTGTGCAAATG-3', reverse primer 5'-CTGTAGGCCTGAGAAGTGGC-3'; *mRPL13A* forward primer 5'-TGA AGCCTACCAGAAAGTTTC-3', reverse primer 5'-CCAGGAGTCCGTTGGTCTTG-3' in a final volume of 10 μl. Each cycle consisted of denaturation at 95 °C for 15 s, annealing at 60 °C for 60 s and extension at

95 °C for 15 s. Reactions were carried out on the 7900 HT Fast Real-time PCR System (Applied Biosystems). Quantification of gene expression (Relative level) was performed according to the 2<sup>-ΔCT</sup> method using *mRPL13A* gene as internal control. Reactions were run in triplicate (technical replicates) and three independent experiments were performed.

#### 4.7. Immunoblotting

MEFs were washed with phosphate-buffered saline (PBS) and scraped off using plastic cell scraper in PBS. The cells were centrifuged at 3000 rpm at 4 °C for 5 min. The supernatant was discarded and the pellet resuspended in appropriate volume of modified RIPA buffer (50 mM Tris-HCl, pH 7.4; 1% TritonX; 0.5% Na-deoxycholate; 0.1% SDS; 150 mM NaCl; 2 mM EDTA; 50 mM NaF), upon addition of fresh protease Inhibitor Cocktails (PIC), 50 μM MG132 and 10 mM N-Ethylmaleimide (NEM; a deubiquitinase inhibition). The cells were incubated in ice for 30 min. and vigorously mixed every 10 min. and were centrifuged at 4000 rpm for 10 min. at 4 °C and the supernatant was transferred to new tube.

SR2+ cells protein lysate was obtained following incubation with a buffer composed of: 50 mM Tris-HCl, 150 mM NaCl, 1% Triton X, 2 mM EGTA, 1 mM MgCl<sub>2</sub> with in addition 10% glycerol, PIC (100X), 10 mM NEM and 50 μM MG132. Cells were centrifuged at 4000 rpm for 10 min. at 4 °C and the supernatant was transferred to new tube.

Protein content was quantified using the Pierce™ BCA Protein Assay Kit (Thermo Scientific™).

NuPAGE™ LDS Sample Buffer (4X) (Invitrogen™) and 2-Mercaptoethanol (SIGMA) were added to the samples and proteins were boiled at 95 °C for 10 min.. Proteins were loaded in ExpressPlus™ PAGE Gel, 10 × 8, 8% (GenScript) or NuPAGE™ 3–8% Tris-Acetate Protein Gels, 1.0 mm (Invitrogen™) and separated using a constant voltage of 100 mV for the appropriate time. After electrophoresis run, proteins were transferred from the gel matrix to Polyvinylidene difluoride (PVDF) membrane (Thermo Fisher Scientific) applying a constant voltage of 100 mV for 2 h at 4 °C. The membrane was saturated upon incubation with 5% milk in T-BST (mixture of tris-buffered saline and Tween 20) for 1 h. Proteins were probed using the following antibodies: α-Flag (1:1000; Cell Signaling Technology: 2368S), α-Mfn2 (1:1000; Abnova: H0000927-M03), α-PINK1 (1:500; Novus Biologicals: BC100-494), α-HA (1:1000; Cell Signaling Technology: 3724).

#### 4.8. Immunoprecipitation (IP)

MEFs (about 500 000 cells) were plated in a 100 mm dish and the day after were transfected with the Mfn2 WT or the Mfn2 mutants and HA-Ub. 12 or 24 h later, cells were lysed with a buffer composed of: 50 mM Tris-HCl, 150 mM NaCl, 1% Triton X, 2 mM EGTA, 1 mM MgCl<sub>2</sub> with in addition 10% glycerol, PIC (100X), 10 mM NEM and 50 μM MG132. Protein extract (250 μg-1 mg) was incubated with 10 μl of protein A agarose beads (Roche), previously balanced in lysis buffer, for 30 min. at 4 °C on the wheel (pre-cleaning). In parallel 30 μl of balanced beads were incubated with 1 μg of α-Mfn2 (Abcam: ab56889) or without the antibody (negative control) for 1 h and half at 4 °C on wheel in 70 μl of lysis buffer. Pre-cleaning beads were centrifuged at 4000 rpm for 5 min. and the supernatant was incubated overnight at 4 °C with antibody-conjugated beads. The day after the mix was centrifuged and the supernatant was discarded. Beads were washed 3 times for 10 min. at 4 °C with lysis buffer and boiled for 10 min. at 95 °C in 30–50 μl Laemmli loading buffer 2X (Laemmli 4X: Tris HCL 300 μM, pH 6.8; SDS 300 μM; Sucrose 1,4 M; Beta mercaptoethanol 8%; + Bromophenol blue). Supernatant was recovered upon maximum speed centrifugation and analyzed by western blotting in NuPAGE™ 3–8% Tris-Acetate Protein Gels.

#### 4.9. Imaging acquisition and processing

MEFs or S2R + cells were plated on 24 mm round glass coverslips and co-transfected with mitoKate or mito-RFP and ER-YFP and the indicated plasmids for 48–72 h before imaging. Images were acquired using an UPlanSApo 60X/1.35 objective (iMIC Adromeda) upon excitation with 561 and 488 lasers. The percentage of ER that colocalize with mitochondria was measured with Mander's coefficient of colocalization (JACoP), following 3D volume rendered reconstruction of 60 z-axis images separated by 0.2  $\mu\text{m}$  (software: imageJ, plug in: volumeJ).

For FRET imaging about 1200–1800 MEFs cells were seeded on 384 well plate (Perkin Elmer). After 12 h cells were transfected with FEMP probe and the indicated plasmids (ratio 1:3) using Genjet in Vitro DNA Transfection Reagent and analyzed using Perkin Elmer Operetta High-Content Imaging System objective 20X after 12 or 24 h. FEMP probe is targeted to the mitochondrial outer membrane (OMM) (targeting sequence mAKAP1 connected to YFP fluorescent protein) and ER (targeting sequence Sac1 connected to CFP fluorescent protein) and contains a self-leaving Tav2A peptide, which undergoes autocleavage releasing YFP and CFP. FRET intensity is inversely proportional to the distance between the two fluorophores that are appropriately targeted to the two compartments. In the FEMP probe, OMM and ER targeting sequence are coupled with the two components of the FKBP-FRP heterodimerization system that allows covalent linkage between ER and mitochondria upon rapamycin administration. ER-mitochondria juxtaposition can therefore be correlated to FRET intensity and rapamycin treatment allows heterodimerization between adjacent FKBP and FRB domains to maximize FRET intensity. The basal FRET level (FRET basal) was obtained using ex 410–430 and em 460–500 for CFP and ex 490–510 and em 520–560 for YFP while  $\text{YFP}_{\text{FRET}}$  was obtained using ex 410–430 and em 520–560. The maximum FRET intensity (FRETmax) was measured after treatment with 100  $\mu\text{M}$  Rapamycin for 15 min, on fixed cells in PBS (1% Formaldehyde for 10 min.). The images were analyzed using Perkin Elmer Harmony 3.5 image software. The YFP channel was used to mark the ROI (Fcell) and a second bonder, around each ROI, was plotted to measure and subtract the background intensity (Fbg). FRETbasal and FRETmax were calculated as:  $\text{FYFPFRET}_{\text{cell}}/\text{FCFP}_{\text{cell}} - \text{Fbg}$ . The FRET Ratio ( $\Delta\text{R}/\text{R}$ ) is  $(\text{FRET}_{\text{max}} - \text{FRET}_{\text{basal}})/\text{FRET}_{\text{basal}}$ . For FRET imaging of the human fibroblasts about 1800 cells were seeded on 384 well plate (Perkin Elmer). After 24 h cells were transfected with FEMP using Transfection Reagent PEI and analyzed using Perkin Elmer Operetta High-Content Imaging System objective 20X after 12 h.

Human fibroblast from skin biopsy (50.000 cells) were plated on 24 mm round glass coverslips and after 12 h for mitochondria analysis the cells were treated with 1  $\mu\text{M}$  of Tetramethylrhodamine methyl ester (TMRM) and 10 nM cyclosporin H in HBSS for 20 min. at 37 °C or transfected with ER-YFP for 12 h with PEI for ER analysis. Images were acquired using an UPlanSApo 40X/1.00 objective (iMIC Adromeda) upon excitation with 561 or 488 lasers. The 60 z-axis images separated by 0.2  $\mu\text{m}$  were analysis using Volocity 6.3 software to obtain quantitative analysis of the mitochondrial volume, surface area, skeletal length, skeletal diameter. The number of cells per genotype that have been assessed for morphological analysis is minimum 200 per genotype and the average number of mitochondria that have been analysed is 50 per cell. The aspect ratio (AR) was calculated by dividing the mitochondrial skeletal length by the mitochondrial skeletal diameter.

#### 4.10. Bioinformatic analysis

Protein sequences of MFN2\_HUMAN (O95140), MFN2\_MOUSE (Q80U63) and MARF\_DROME (Q7YU24) were obtained from database Protein (UniProt). The alignment was performed using MultAlin software.

#### 4.11. Aequorin measurement

MEFs were grown on 13 mm round glass coverslips at 50–60% of confluence and co-transfected with the indicated constructs and mitochondrial low affinity aequorin (mtAEQ mut). Cells were incubated for 1.5 h at 37 °C in DMEM 1% FBS after being reconstituted with 5  $\mu\text{M}$  coelenterazine wt (invitrogene). To monitor mitochondrial  $\text{Ca}^{2+}$  transients, cells were perfused with Krebs Ringer buffer (KRB: 125 mM NaCl, 5 mM KCl, 1 mM  $\text{Na}_3\text{PO}_4$ , 1 mM  $\text{MgSO}_4$ , 5.5 mM glucose, 20 mM HEPES, pH 7.4, 37 °C, 1 Mm  $\text{CaCl}_2$ ) for 20–30 s with or without 200  $\mu\text{M}$  ATP. At the end of each experiment, the cells are perfused with milliQ  $\text{H}_2\text{O}_2$  containing 10 mM  $\text{CaCl}_2$  and 100  $\mu\text{M}$  digitonin to calibrate the luminescence signal in  $\text{Ca}^{2+}$  values. The rate of  $\text{Ca}^{2+}$  uptake is calculated as  $\text{Ca}^{2+}$  uptake speed in  $\mu\text{M}/\text{s}$  at the half of peak upon treatment with 200  $\mu\text{M}$  ATP.

#### 4.12. Electron microscopy

Cells cultured in 24 well plate were fixed in 2% paraformaldehyde, 2.5% gluteraldehyde for 1 h/overnight. After rinsing in 0.1 M cacodylate buffer with 1% tannic acid, samples were post-fixed in 1:1 2%  $\text{OsO}_4$  and 0.2 M cacodylate buffer for 1 h. Samples were rinsed, dehydrated in an ethanol, and embedded by using Epon. Ultrathin sections were examined using a transmission electron microscope. The number of contacts that have been analysed for ultrastructure is a minimum of 200 contacts per condition.

#### 4.13. Fly stocks and breeding condition

Fly lines were grown on standard cornmeal medium and were maintained at 23 °C, 70% relative humidity, on a 12-h light:12-h dark cycle. The UAS mitoGFP/TM6B and UAS KDELGFP/TM6B were obtained from the lab of Prof. Daga, Department of Pharmaceutical and Pharmacological Sciences, University of Padova. The mito-ER syntetic linker, created by Csordás, consists of a monomeric fluorescent protein (mRFP) fused to the OMM targeting sequence of mAKAP1 at the N terminus and fused to the ER targeting sequence of yUBC6 at the C terminus [43]. The construct was cloned into a fly vector (pUAST) and two fly lines expressing different levels of the tethering construct were generated by random insertion into a *white1118*<sup>-</sup> background or PINK1 mutant (KO) background (PINK1<sup>B9</sup>/FM7): UAS-mito-mRFP-ER<sup>TH</sup>/TM6B (TH, high expression of tether) and UAS-mito-mRFP-ER<sup>TM</sup>/TM6B (TM, mild expression of tether). In order to activate neuronal expression of the tethering construct, flies were crossed with nSyb-Gal4/TM6B, neuronal Synaptobrevin-expressing flies obtained from the Bloomington stock center. PINK1 mutant (KO) flies (PINK1B9/FM7) [24] were a kind gift of Dr. Alexander Whitworth.

#### 4.14. Mounting and imaging of fly wing

Flies at 3–5 days of age were fixed with 4% of paraformaldehyde (PFA) for 2 h at room temperature on a rotating wheel and then washed 3 times for 10 min with PBS. The whole wings were cut with Castro-Viejo Scissors, mounted on 24 mm round glass coverslips with a small amount of ProLong™ Gold Antifade Mountant and subsequently covered with another 12 mm round glass coverslip which was fixed with nail polish. The images were acquired using an UPlanSApo 20X/0.75 objective (iMIC Adromeda) after the excitation with a 561 laser. The quantification of the RFP signal was performed counting the spots using ImageJ along 150  $\mu\text{m}$  of length of the L1 vein neural bundle [48] from the intersection of the L2 vein to proximal side of the wing flies.

#### 4.15. Climbing assay

The climbing test was performed at 3 days of age at the same time of the day with male flies of the indicated genotypes. 10 flies for each

genotype were transferred in a plastic cylinder of 12 cm of length and 5 cm of diameter, marked with a line at 6 cm from the bottom of the tube. Flies were tapped to the bottom of the tube and the number of flies that successfully climbed across the 6 cm line in 10 s was counted. Fifteen separate and consecutive trials were performed for each experiment, and the results were averaged. 50 flies for each genotype were analyzed. The results were expressed as percentage of climbing flies.

#### 4.16. Eggs-to-adults viability

The assay was performed to analyze eggs-to-adults viability of the tethering TM and TH flies compared to WT flies. For each lines (WT, WT TM and WT TH) 10 virgin females were crossed with 10 males nSyb-Gal4/TM6B on a plate with sugar yeast fruit medium. The day after, adults were removed and after 3 days eggs were counted. Next the medium with eggs was added to the tube with standard cornmeal medium. After 5 and 10 days from egg laying, the number of pupae and the number of male adults were counted. To analyze the eggs-to-pupae viability the number of pupae was divided by the number of eggs for each genotype and the resulting value was normalized to control (WT). In order to address the larvae-to-adults viability, the number of male adults was divided by the total number of pupae and expressed as percentage.

#### 4.17. Statistics

Data were presents as mean  $\pm$  SEM from at least three independent experiments. Statistical significance was determined using Unpaired *t*-test and *p* values are indicated (GraphPad software).

#### Author contribution

VB and EM designed, performed and interpreted experiments; CP performed calcium measurement experiments in patient fibroblasts; JC performed some of the western blotting; SVS designed and performed *in vivo* experimental work in flies and data analysis; MG performed some of the FEMP experiments and analysed FRET data analysis; DO performed calcium measurement experiments in MEFs; VD generated the tethering *Drosophila* fly lines; FC performed electron microscopy acquisition and provide technical support; ET and VP generated and maintained primary human fibroblasts from skin biopsy; CA, AA, AB and MB critically read the manuscript and conceptually contributed to manuscript content. EZ conceived and supervised the project, designed and interpreted experiments and wrote the manuscript.

#### Declaration of interests

None.

#### Acknowledgements

This work was supported by grants from Italian Ministry of Health “Ricerca Finalizzata” [GR-2011-02351151], Rita Levi Montalcini “Brain Gain” program and Michael J. Fox RRIA 2014 [Grant ID 9795] to E.Z. We also thank PISCOPIA-MARIE CURIE fellowship for the support. We would like to acknowledge Francesco Boldrin from the EM facility for their help and technical support. We are grateful to Emilie Schrepfer for her help with the graphical modelling of Fig. 6. We are also deeply grateful to Professor Luca Scorrano for his intellectual contribution and for critically reading the manuscript.

#### Appendix A. Supplementary data

Supplementary material related to this article can be found, in the online version, at doi:<https://doi.org/10.1016/j.phrs.2018.09.006>.

#### References

- [1] B. Thomas, M.F. Beal, Parkinson's disease, *Hum. Mol. Genet* 16 (2007) R183–194, <https://doi.org/10.1093/hmg/ddm159> Spec No. 2.
- [2] V. Bogaerts, J. Theuns, C. van Broeckhoven, Genetic findings in Parkinson's disease and translation into treatment: a leading role for mitochondria? *Genes Brain Behav.* 7 (2008) 129–151, <https://doi.org/10.1111/j.1601-183X.2007.00342.x>.
- [3] J. Bereiter-Hahn, M. Voth, Dynamics of mitochondria in living cells: shape changes, dislocations, fusion, and fission of mitochondria, *Microsc. Res. Technol.* 27 (1994) 198–219, <https://doi.org/10.1002/jemt.1070270303>.
- [4] M. Rojo, F. Legros, D. Chateau, A. Lombes, Membrane topology and mitochondrial targeting of mitofusins, ubiquitous mammalian homologs of the transmembrane GTPase Fzo, *J. Cell Sci.* 115 (2002) 1663–1674.
- [5] E.D. Wong, et al., The dynamin-related GTPase, Mgm1p, is an intermembrane space protein required for maintenance of fusion competent mitochondria, *J. Cell. Biol.* 151 (2000) 341–352.
- [6] S. Cipolat, O. Martins de Brito, B. Dal Zilio, L. Scorrano, OPA1 requires mitofusin 1 to promote mitochondrial fusion, *Proc. Natl. Acad. Sci. U. S. A.* 101 (2004) 15927–15932, <https://doi.org/10.1073/pnas.0407043101>.
- [7] Y. Chen, et al., Mitofusin 2-containing mitochondrial-reticular microdomains direct rapid cardiomyocyte bioenergetic responses via interorganelle Ca(2+) crosstalk, *Circ. Res.* 111 (2012) 863–875, <https://doi.org/10.1161/CIRCRESAHA.112.266585>.
- [8] O.M. de Brito, L. Scorrano, Mitofusin 2 tethers endoplasmic reticulum to mitochondria, *Nature* 456 (2008) 605–610.
- [9] P. Cosson, A. Marchetti, M. Ravazzola, L. Orci, Mitofusin-2 independent juxtaposition of endoplasmic reticulum and mitochondria: an ultrastructural study, *PLoS One* 7 (2012) e46293, <https://doi.org/10.1371/journal.pone.0046293>.
- [10] R. Filadi, et al., Mitofusin 2 ablation increases endoplasmic reticulum-mitochondria coupling, *Proc. Natl. Acad. Sci. U. S. A.* 112 (2015) E2174–2181, <https://doi.org/10.1073/pnas.1504880112>.
- [11] A.A. Rowland, G.K. Voeltz, Endoplasmic reticulum-mitochondria contacts: function of the junction, *Nat. Rev. Mol. Cell Biol.* 13 (2012) 607–625, <https://doi.org/10.1038/nrm3440>.
- [12] R. Rizzuto, et al., Close contacts with the endoplasmic reticulum as determinants of mitochondrial Ca<sup>2+</sup> responses, *Science* 280 (1998) 1763–1766.
- [13] J.E. Vance, Phospholipid synthesis in a membrane fraction associated with mitochondria, *J. Biol. Chem.* 265 (1990) 7248–7256.
- [14] T. Cali, D. Ottolini, A. Negro, M. Brini, Enhanced Parkin levels favor ER-mitochondria crosstalk and guarantee Ca(2+) transfer to sustain cell bioenergetics, *Biochim. Biophys. Acta* 1832 (2013) 495–508, <https://doi.org/10.1016/j.bbdis.2013.01.004>.
- [15] D. Ottolini, T. Cali, A. Negro, M. Brini, The Parkinson disease-related protein DJ-1 counteracts mitochondrial impairment induced by the tumour suppressor protein p53 by enhancing endoplasmic reticulum-mitochondria tethering, *Hum. Mol. Genet* 22 (2013) 2152–2168, <https://doi.org/10.1093/hmg/ddt068>.
- [16] T. Cali, D. Ottolini, A. Negro, M. Brini, Alpha-synuclein controls mitochondrial calcium homeostasis by enhancing endoplasmic reticulum-mitochondria interactions, *J. Biol. Chem.* 287 (2012) 17914–17929, <https://doi.org/10.1074/jbc.M111.302794>.
- [17] A.V. Panov, et al., Early mitochondrial calcium defects in Huntington's disease are a direct effect of polyglutamines, *Nat. Neurosci.* 5 (2002) 731–736, <https://doi.org/10.1038/nn884>.
- [18] D. Narendra, A. Tanaka, D.F. Suen, R.J. Youle, Parkin is recruited selectively to impaired mitochondria and promotes their autophagy, *J. Cell. Biol.* 183 (2008) 795–803.
- [19] E. Ziviani, R.N. Tao, A.J. Whitworth, *Drosophila* parkin requires PINK1 for mitochondrial translocation and ubiquitinates mitofusin, *Proc. Natl. Acad. Sci. U. S. A.* 107 (2010) 5018–5023, <https://doi.org/10.1073/pnas.0913485107>.
- [20] A.C. Poole, et al., The PINK1/Parkin pathway regulates mitochondrial morphology, *Proc. Natl. Acad. Sci. U. S. A.* 105 (2008) 1638–1643.
- [21] A. Tanaka, et al., Proteasome and p97 mediate mitophagy and degradation of mitofusins induced by Parkin, *J. Cell. Biol.* 191 (2010) 1367–1380.
- [22] M.E. Gegg, et al., Mitofusin 1 and mitofusin 2 are ubiquitinated in a PINK1/Parkin-dependent manner upon induction of mitophagy, *Hum. Mol. Genet* 19 (2010) 4861–4870, <https://doi.org/10.1093/hmg/ddq419>.
- [23] I.E. Clark, et al., *Drosophila* pink1 is required for mitochondrial function and interacts genetically with Parkin, *Nature* 441 (2006) 1162–1166.
- [24] J. Park, et al., Mitochondrial dysfunction in *Drosophila* PINK1 mutants is complemented by Parkin, *Nature* 441 (2006) 1157–1161.
- [25] Y. Yang, et al., Mitochondrial pathology and muscle and dopaminergic neuron degeneration caused by inactivation of *Drosophila* Pink1 is rescued by parkin, *Proc. Natl. Acad. Sci. U. S. A.* 103 (2006) 10793–10798.
- [26] N. Exner, et al., Loss-of-function of human PINK1 results in mitochondrial pathology and can be rescued by Parkin, *J. Neurosci.* 27 (2007) 12413–12418, <https://doi.org/10.1523/JNEUROSCI.0719-07.2007>.
- [27] F. Anton, G. Dittmar, T. Langer, M. Escobar-Henriques, Two deubiquitylases act on mitofusin and regulate mitochondrial fusion along independent pathways, *Mol. Cell.* 49 (2013) 487–498, <https://doi.org/10.1016/j.molcel.2012.12.003>.
- [28] V. Debattisti, D. Pendin, E. Ziviani, A. Daga, L. Scorrano, Reduction of endoplasmic reticulum stress attenuates the defects caused by *drosophila* mitofusin depletion, *J. Cell. Biol.* 204 (2014) 303–312, <https://doi.org/10.1083/jcb.201306121>.
- [29] D. Naon, et al., Critical reappraisal confirms that Mitofusin 2 is an endoplasmic reticulum-mitochondria tether, *Proc. Natl. Acad. Sci. U. S. A.* 113 (2016) 11249–11254, <https://doi.org/10.1073/pnas.1606786113>.

- [30] J.H. Shin, et al., PARIS (ZNF746) repression of PGC-1 $\alpha$  contributes to neurodegeneration in Parkinson's disease, *Cell* 144 (2011) 689–702, <https://doi.org/10.1016/j.cell.2011.02.010>.
- [31] R. Von Coelln, et al., Loss of locus coeruleus neurons and reduced startle in parkin null mice, *Proc. Natl. Acad. Sci. U. S. A.* 101 (2004) 10744–10749, <https://doi.org/10.1073/pnas.0401297101>.
- [32] S. Zuchner, et al., Mutations in the mitochondrial GTPase mitofusin 2 cause Charcot-Marie-Tooth neuropathy type 2A, *Nat. Genet.* 36 (2004) 449–451, <https://doi.org/10.1038/ng1341>.
- [33] H. Chen, et al., Mitofusins Mfn1 and Mfn2 coordinately regulate mitochondrial fusion and are essential for embryonic development, *J. Cell. Biol.* 160 (2003) 189–200, <https://doi.org/10.1083/jcb.200211046>.
- [34] S. Mattie, J. Riemer, J.G. Wideman, H.M. McBride, A new mitofusin topology places the redox-regulated C terminus in the mitochondrial intermembrane space, *J. Cell. Biol.* 217 (2018) 507–515, <https://doi.org/10.1083/jcb.201611194>.
- [35] M.M. Cohen, G.P. LeBoucher, N. Livnat-Levanon, M.H. Glickman, A.M. Weissman, Ubiquitin-proteasome-dependent degradation of a mitofusin, a critical regulator of mitochondrial fusion, *Mol. Biol. Cell* 19 (2008) 2457–2464, <https://doi.org/10.1091/mbc.E08-02-0227>.
- [36] A. Rakovic, et al., Mutations in PINK1 and Parkin impair ubiquitination of mitofusins in human fibroblasts, *PLoS One* 6 (2011) e16746, <https://doi.org/10.1371/journal.pone.0016746>.
- [37] B. Bingol, et al., The mitochondrial deubiquitinase USP30 opposes Parkin-mediated mitophagy, *Nature* 510 (2014) 370–375, <https://doi.org/10.1038/nature13418>.
- [38] S.A. Sarraf, et al., Landscape of the PARKIN-dependent ubiquitylome in response to mitochondrial depolarization, *Nature* 496 (2013) 372–376, <https://doi.org/10.1038/nature12043>.
- [39] G. Xu, S.R. Jaffrey, Proteomic identification of protein ubiquitination events, *Biotechnol. Genetic Eng. Rev.* 29 (2013) 73–109, <https://doi.org/10.1080/02648725.2013.801232>.
- [40] S. Paillusson, et al., There's something wrong with my MAM; The ER-mitochondria axis and neurodegenerative diseases, *Trends Neurosci.* 39 (2016) 146–157, <https://doi.org/10.1016/j.tins.2016.01.008>.
- [41] M. Krots, et al., Mitochondria-associated membranes as hubs for neurodegeneration, *Acta Neuropathol.* 131 (2016) 505–523, <https://doi.org/10.1007/s00401-015-1528-7>.
- [42] C.S. Chan, et al., 'Rejuvenation' protects neurons in mouse models of Parkinson's disease, *Nature* 447 (2007) 1081–1086, <https://doi.org/10.1038/nature05865>.
- [43] G. Csordas, et al., Structural and functional features and significance of the physical linkage between ER and mitochondria, *J. Cell. Biol.* 174 (2006) 915–921, <https://doi.org/10.1083/jcb.200604016>.
- [44] G. Csordas, et al., Imaging interorganelle contacts and local calcium dynamics at the ER-mitochondrial interface, *Mol. Cell.* 39 (2010) 121–132, <https://doi.org/10.1016/j.molcel.2010.06.029>.
- [45] D.P. Narendra, et al., PINK1 is selectively stabilized on impaired mitochondria to activate Parkin, *PLoS Biol.* 8 (2010) e1000298, <https://doi.org/10.1371/journal.pbio.1000298>.
- [46] B. Heeman, et al., Depletion of PINK1 affects mitochondrial metabolism, calcium homeostasis and energy maintenance, *J. Cell Sci.* 124 (2011) 1115–1125, <https://doi.org/10.1242/jcs.078303>.
- [47] A. Sandebring, et al., Parkin deficiency disrupts calcium homeostasis by modulating phospholipase C signalling, *FEBS J.* 276 (2009) 5041–5052, <https://doi.org/10.1111/j.1742-4658.2009.07201.x>.
- [48] A. Vagnoni, S.L. Bullock, A simple method for imaging axonal transport in aging neurons using the adult *Drosophila* wing, *Nat. Protoc.* 11 (2016) 1711–1723, <https://doi.org/10.1038/nprot.2016.112>.
- [49] S. Gehrke, et al., PINK1 and Parkin control localized translation of respiratory chain component mRNAs on mitochondria outer membrane, *Cell Metab.* 21 (2015) 95–108, <https://doi.org/10.1016/j.cmet.2014.12.007>.
- [50] A.K. Muller-Rischart, et al., The E3 ligase Parkin maintains mitochondrial integrity by increasing linear ubiquitination of NEMO, *Mol. Cell.* 49 (2013) 908–921, <https://doi.org/10.1016/j.molcel.2013.01.036>.
- [51] N. Matsuda, et al., Diverse effects of pathogenic mutations of Parkin that catalyze multiple monoubiquitylation in vitro, *J. Biol. Chem.* 281 (2006) 3204–3209, <https://doi.org/10.1074/jbc.M510393200>.
- [52] C. Hampe, H. Ardila-Osorio, M. Fournier, A. Brice, O. Corti, Biochemical analysis of Parkinson's disease-causing variants of Parkin, an E3 ubiquitin-protein ligase with monoubiquitylation capacity, *Hum. Mol. Genet.* 15 (2006) 2059–2075, <https://doi.org/10.1093/hmg/ddl131>.
- [53] K.L. Lim, et al., Parkin mediates nonclassical, proteasomal-independent ubiquitination of synphilin-1: implications for Lewy body formation, *J. Neurosci.* 25 (2005) 2002–2009, <https://doi.org/10.1523/JNEUROSCI.4474-04.2005>.
- [54] L. Glauser, S. Sonnay, K. Stafa, D.J. Moore, Parkin promotes the ubiquitination and degradation of the mitochondrial fusion factor mitofusin 1, *J. Neurochem.* 118 (2011) 636–645, <https://doi.org/10.1111/j.1471-4159.2011.07318.x>.
- [55] A.C. Poole, R.E. Thomas, S. Yu, E.S. Vincow, L. Pallanck, The mitochondrial fusion-promoting factor mitofusin is a substrate of the PINK1/Parkin pathway, *PLoS One* 5 (2010) e10054, <https://doi.org/10.1371/journal.pone.0010054>.
- [56] I.H. Henn, et al., Parkin mediates neuroprotection through activation of I $\kappa$ B kinase/nuclear factor- $\kappa$ B signaling, *J. Neurosci.* 27 (2007) 1868–1878, <https://doi.org/10.1523/JNEUROSCI.5537-06.2007>.
- [57] L. Fallon, et al., A regulated interaction with the UIM protein Eps15 implicates parkin in EGF receptor trafficking and PI(3)K-Akt signalling, *Nat. Cell Biol.* 8 (2006) 834–842, <https://doi.org/10.1038/ncb1441>.
- [58] E.W. Doss-Pepe, L. Chen, K. Madura, Alpha-synuclein and Parkin contribute to the assembly of ubiquitin lysine 63-linked multiubiquitin chains, *J. Biol. Chem.* 280 (2005) 16619–16624, <https://doi.org/10.1074/jbc.M413591200>.
- [59] L. Salmena, P.P. Pandolfi, Changing venues for tumour suppression: balancing destruction and localization by monoubiquitylation, *Nat. Rev. Cancer* 7 (2007) 409–413, <https://doi.org/10.1038/nrc2145>.
- [60] K.K. Dove, R.E. Klevit, Structural biology: Parkin's serpentine shape revealed in the year of the snake, *Curr. Biol.: CB* 23 (2013) R691–693, <https://doi.org/10.1016/j.cub.2013.07.039>.
- [61] T. Wauer, D. Komander, Structure of the human Parkin ligase domain in an auto-inhibited state, *EMBO J.* 32 (2013) 2099–2112, <https://doi.org/10.1038/emboj.2013.125>.
- [62] M. Hamasaki, et al., Autophagosomes form at ER-mitochondria contact sites, *Nature* 495 (2013) 389–393, <https://doi.org/10.1038/nature11910>.
- [63] D. De Stefani, A. Raffaello, E. Teardo, I. Szabo, R. Rizzuto, A forty-kilodalton protein of the inner membrane is the mitochondrial calcium uniporter, *Nature* 476 (2011) 336–340, <https://doi.org/10.1038/nature10230>.
- [64] J.R. Friedman, et al., ER tubules mark sites of mitochondrial division, *Science* 334 (2011) 358–362, <https://doi.org/10.1126/science.1207385>.
- [65] Y. Kirichok, G. Kravinsky, D.E. Clapham, The mitochondrial calcium uniporter is a highly selective ion channel, *Nature* 427 (2004) 360–364, <https://doi.org/10.1038/nature02246>.
- [66] T. Cali, D. Ottolini, M. Brini, Calcium and endoplasmic reticulum-mitochondria tethering in neurodegeneration, *DNA Cell Biol.* 32 (2013) 140–146, <https://doi.org/10.1089/dna.2013.2011>.
- [67] S. Gandhi, et al., PINK1-associated Parkinson's disease is caused by neuronal vulnerability to calcium-induced cell death, *Mol. Cell.* 33 (2009) 627–638, <https://doi.org/10.1016/j.molcel.2009.02.013>.
- [68] S. Gandhi, et al., Dopamine induced neurodegeneration in a PINK1 model of Parkinson's disease, *PLoS One* 7 (2012) e37564, <https://doi.org/10.1371/journal.pone.0037564>.
- [69] C.A. Gautier, et al., Regulation of mitochondrial permeability transition pore by PINK1, *Mol. Neurodegener.* 7 (2012) 22, <https://doi.org/10.1186/1750-1326-7-22>.
- [70] M. Brini, et al., Transfected aequorin in the measurement of cytosolic Ca<sup>2+</sup> concentration ([Ca<sup>2+</sup>]<sub>i</sub>). A critical evaluation, *J. Biol. Chem.* 270 (1995) 9896–9903.
- [71] R. Rizzuto, A.W. Simpson, M. Brini, T. Pozzan, Rapid changes of mitochondrial Ca<sup>2+</sup> revealed by specifically targeted recombinant aequorin, *Nature* 358 (1992) 325–327, <https://doi.org/10.1038/358325a0>.
- [72] J.M. Kendall, G. Sala-Newby, V. Ghalaut, R.L. Dormer, A.K. Campbell, Engineering the CA(2<sup>+</sup>)-activated photoprotein aequorin with reduced affinity for calcium, *Biochem. Biophys. Res. Commun.* 187 (1992) 1091–1097.
- [73] D. Lim, et al., Calcium signalling tollkitts in astrocytes and spatio-temporal progression of Alzheimer's disease, *Curr. Alzheimer Res.* 13 (2016) 359–369.
- [74] C. Lazzari, et al., Cellular prion protein is implicated in the regulation of local Ca<sup>2+</sup> movements in cerebellar granule neurons, *J. Neurochem.* 116 (2011) 881–890, <https://doi.org/10.1111/j.1471-4159.2010.07015.x>.
- [75] D. Ottolini, T. Cali, M. Brini, Methods to measure intracellular Ca(2<sup>+</sup>) fluxes with organelle-targeted aequorin-based probes, *Methods Enzymol.* 543 (2014) 21–45, <https://doi.org/10.1016/B978-0-12-801329-8.00002-7>.
- [76] M. Montero, et al., Monitoring dynamic changes in free Ca<sup>2+</sup> concentration in the endoplasmic reticulum of intact cells, *EMBO J.* 14 (1995) 5467–5475.

## Research Article

# Alpha-Synuclein Preserves Mitochondrial Fusion and Function in Neuronal Cells

Gaia Faustini <sup>1</sup>, Elena Marchesan,<sup>2</sup> Laura Zonta,<sup>2</sup> Federica Bono,<sup>3</sup> Emanuela Bottani,<sup>1</sup> Francesca Longhena <sup>1</sup>, Elena Ziviani,<sup>2</sup> Alessandra Valerio,<sup>1</sup> and Arianna Bellucci <sup>1,3</sup>

<sup>1</sup>Department of Molecular and Translational Medicine, University of Brescia, Viale Europa, 11, 25123 Brescia, Italy

<sup>2</sup>Department of Biology, University of Padova, Via Ugo Bassi, 58b, 35131 Padova, Italy

<sup>3</sup>Laboratory of Preventive and Personalized Medicine, University of Brescia, Viale Europa, 11, 25123 Brescia, Italy

Correspondence should be addressed to Arianna Bellucci; [arianna.bellucci@unibs.it](mailto:arianna.bellucci@unibs.it)

Received 23 July 2019; Revised 12 September 2019; Accepted 28 October 2019; Published 23 November 2019

Guest Editor: Roberta Cascella

Copyright © 2019 Gaia Faustini et al. This is an open access article distributed under the Creative Commons Attribution License, which permits unrestricted use, distribution, and reproduction in any medium, provided the original work is properly cited.

Dysregulations of mitochondria with alterations in trafficking and morphology of these organelles have been related to Parkinson's disease (PD), a neurodegenerative disorder characterized by brain accumulation of Lewy bodies (LB), intraneuronal inclusions mainly composed of  $\alpha$ -synuclein ( $\alpha$ -syn) fibrils. Experimental evidence supports that  $\alpha$ -syn pathological aggregation can negatively impinge on mitochondrial functions suggesting that this protein may be crucially involved in the control of mitochondrial homeostasis. The aim of this study was to assay this hypothesis by analyzing mitochondrial function and morphology in primary cortical neurons from C57BL/6JOLAHsd  $\alpha$ -syn null and C57BL/6J wild-type (wt) mice. Primary cortical neurons from mice lacking  $\alpha$ -syn showed decreased respiration capacity measured with a Seahorse XFe24 Extracellular Flux Analyzer. In addition, morphological Airyscan superresolution microscopy showed the presence of fragmented mitochondria while real-time PCR and western blot confirmed altered expression of proteins involved in mitochondrial shape modifications in the primary cortical neurons of  $\alpha$ -syn null mice. Transmission electron microscopy (TEM) studies showed that  $\alpha$ -syn null neurons exhibited impaired mitochondria-endoplasmic reticulum (ER) physical interaction. Specifically, we identified a decreased number of mitochondria-ER contacts (MERCs) paralleled by a significant increase in ER-mitochondria distance (i.e., MERC length). These findings support that  $\alpha$ -syn physiologically preserves mitochondrial functions and homeostasis. Studying  $\alpha$ -syn/mitochondria interplay in health and disease is thus pivotal for understanding their involvement in PD and other LB disorders.

## 1. Introduction

The pathological aggregation of  $\alpha$ -synuclein ( $\alpha$ -syn) and its deposition in proteinaceous inclusions named Lewy bodies (LB) is the key pathological hallmark of LB disorders such as Parkinson's disease (PD). This is the most common neurodegenerative movement syndrome and is characterized by a progressive loss of dopaminergic neurons of the nigrostriatal system.

The aggregation of pathological  $\alpha$ -syn is thought to be the major agent of PD pathophysiology [1], but mitochondrial deficits have been largely described as crucial pathogenic events in the pathogenesis of PD [2]. Indeed, a bidirectional interplay between  $\alpha$ -syn and mitochondrial dysfunction has

been described, since  $\alpha$ -syn aggregates may negatively impinge on mitochondrial homeostasis and dynamics, while mitochondrial dysfunctions severely affect  $\alpha$ -syn deposition [3].

It has been reported that a fraction of soluble  $\alpha$ -syn directly interacts with mitochondria-associated endoplasmic reticulum (ER) membranes (MAM) [4], influencing mitochondrial fusion and fission. Interestingly,  $\alpha$ -syn aggregation produces mitochondrial fragmentation or mitochondrial respiration failure and death in cell-based models of PD [5–7]. Furthermore, mitochondrial protein import and protein degradation may impact on  $\alpha$ -syn and mitochondrial physiological functions, but their reciprocal modulation is still to be elucidated [8]. On the other hand, a protective role of  $\alpha$ -syn was identified in neurons exposed to oxidative stress

[9], while the effect of several neurotoxins on mitochondria deficiency is thought to be mediated, at least in part, by  $\alpha$ -syn aggregation [3, 10]. For instance, elevated levels of  $\alpha$ -syn promote the toxic action of 1-methyl-4-phenyl-1,2,3,6-tetrahydropyridine (MPTP), which inhibits mitochondrial complex I [11], that is deficient in PD brains [12, 13]. Contrariwise,  $\alpha$ -syn-deficient mice exposed to rotenone exhibited a pronounced degeneration of dopamine neurons exceeding that observed in wild type (wt) mice [14], even if silencing  $\alpha$ -syn was reported to prevent neuron degeneration in an *in vitro* model [15]. These findings fit with the hypothesis that alterations of  $\alpha$ -syn may contribute to bioenergetics defects inducing mitochondrial dysfunctions and PD onset. This notwithstanding,  $\alpha$ -syn deficiency *per se* may also negatively impinge on mitochondrial homeostasis [16], supporting that the metabolism and function of healthy neurons may depend on the expression levels and conformation of  $\alpha$ -syn and on the critical interplay between  $\alpha$ -syn and mitochondria, with imbalances in their reciprocal modulation leading to neuronal impairment [3].

The aim of this study was to assay the relevance of  $\alpha$ -syn function on mitochondrial homeostasis by assessing whether primary cortical neurons, produced from C57BL/6J OlaHsd mice carrying a spontaneous deletion of  $\alpha$ -syn locus ( $\alpha$ -syn null) [17], may present alterations of mitochondrial function and morphology when compared to those of C57BL/6J wt animals.

The Oxygen Consumption Rate (OCR) of cortical neurons from wt or  $\alpha$ -syn null mice was evaluated by a Seahorse-based analysis both in basal condition and after exposure to the Complex I inhibitor rotenone. Mitochondria morphology was studied by using both Airyscan super-resolution microscopy on mito-YFP-transfected neurons and transmission electron microscopy (TEM). Finally, the expression of proteins mediating mitochondria fusion and fission was also evaluated by real-time polymerase chain reaction (PCR) and western blotting (WB). These studies revealed a reduced mitochondrial respiration of  $\alpha$ -syn null neurons and an increased susceptibility to rotenone administration. These cells also exhibited an increased mitochondrial fragmentation and alterations in the key proteins mediating mitochondrial fission and fusion, such as mitofusin (Mfn1) and the dynamin-like GTPase Opa1. Finally, TEM studies showed that the primary cortical neurons from  $\alpha$ -syn null mice exhibited a decreased number of mitochondria-ER contacts (MERCs) and a significant increase in ER-mitochondria distance.

Our findings strongly support that, by orchestrating mitochondrial fusion and functions and preserving MERCs,  $\alpha$ -syn physiologically acts as a determining regulator of mitochondrial homeostasis.

## 2. Materials and Methods

**2.1. Animals.** C57BL/6J wt (Charles River, Wilmington, MA) and C57BL/6J OlaHsd (Harlan Olac Bicester, UK) mice were bred in our animal house facility at the Department of Molecular and Translational Medicine of University of Brescia, Brescia, Italy. Animals were maintained under a 12 h

light-dark cycle at a room temperature (rt) of 22°C and had ad libitum food and water. All experiments were made in accordance to Directive 2010/63/EU of the European Parliament and of the Council of 22 September 2010 on the protection of animals used. All experimental and surgical procedures for the preparation of primary cortical neuronal cell cultures from 18-day embryos were conformed to the National Research Guide for the Care and Use of Laboratory Animals and were approved by the Animal Research Committees of the University of Brescia (Protocol Permit 719/2015-PR). All achievements were made to minimize animal suffering and to reduce the number of animals used.

**2.2. Primary Cortical Neurons.** Primary cortical neurons were dissected from C57BL/6J wt control mice and C57BL/6J OlaHsd  $\alpha$ -syn null mice, carrying a spontaneous deletion of the  $\alpha$ -syn locus [17], at embryonic day 18 according to previously described protocols [18]. After dissociation with Accumax (Sigma-Aldrich, Milan, Italy), the single cells were resuspended in a Neurobasal medium (Thermo Fisher Scientific, Massachusetts, USA) containing 100  $\mu$ g/ml penicillin, 100  $\mu$ g/ml streptomycin (Sigma-Aldrich, Milan, Italy), 2 mM glutamine (EuroClone, Milan, Italy), and 1% B27 supplement (Thermo Fisher Scientific) and then centrifuged. Cell counts and viability assays were performed using the Trypan Blue exclusion test. Neurons were seeded onto glass coverslips in 24-well plates for imaging analyses, Seahorse XFe24-well plates for energetic analyses, 24-well plates for TEM analyses or Petri dishes coated with 10-12  $\mu$ g/ml poly-D-lysine for quantitative analyses. Cells were maintained at 37°C under a humidified atmosphere of 5% CO<sub>2</sub> in the Neurobasal medium for 8-10 days *in vitro* (DIV).

**2.3. Cortical Neuron Respirometry Analysis.** Seahorse XF Cell Culture Microplates (Seahorse Biosciences, Agilent Technologies, USA) were used to seed 45,000 cortical neurons per well. At day 8, cells were treated with 100 nM rotenone, which was directly added in the cell culture media for 1 h and analyzed the following day. The medium was replaced with freshly prepared Seahorse XF Base Media (25 mM glucose, 0.25 mM sodium pyruvate, and 1 mM L-glutamine, pH 7.4) in a non-CO<sub>2</sub> incubator for 1 h prior to the assay, then loaded on a Seahorse XF24 Extracellular Flux Analyzer (Seahorse Biosciences). The XF Cell Mito Stress Test (Agilent technologies) was performed, after 3 cycles of basal condition, sequentially injecting 1  $\mu$ M oligomycin, 0.5  $\mu$ M carbonyl cyanide-4-(trifluoromethoxy)phenylhydrazone (FCCP), and 0.5  $\mu$ M rotenone plus 0.5  $\mu$ M antimycin A. Oxygen Consumption Rate and Extracellular Acidification Rate (ECAR) were measured every three cycles of 3 min mix after the injection.

Normalization was performed by using the Bio-Rad DC™ protein assay kit (Bio-Rad Laboratories, California, USA).

Basal respiration was measured as the last rate before the first injection minus the nonmitochondrial respiration rate deriving from the rotenone/antimycin injection. Maximal respiration was considered the maximum rate measurement after the FCCP injection minus the nonmitochondrial respiration rate. The ATP-linked respiration was calculated as the

subtraction of the last measurement before oligomycin injection and the minimum rate after oligomycin injection.

**2.4. Mitochondrial Isolation and Seahorse Analysis.** Liver, cortex, and midbrain tissues were explanted from two-month-old mice after cervical dislocation. After five washes with MIB1 buffer (210 mM D-mannitol, 70 mM sucrose, 5 mM HEPES, 1 mM EGTA and 0.5% free fatty acid BSA), tissues were homogenate and centrifuged at 600g for 10 min at 4°C. The supernatant was then centrifuged at 7000g for 10 min at 4°C. After washing the pellet with MIB1 by centrifugation at 7000g for 10 min at 4°C, the pellet was resuspended in MAS1 (220 mM D-mannitol, 70 mM sucrose, 2 mM HEPES, 1 mM EGTA, 0.2% free fatty acid BSA, 10 mM KH<sub>2</sub>PO<sub>4</sub>, 5 mM MgCl<sub>2</sub>, 10 mM glutamate, 5 mM malate, and 10 mM succinate, pH 7.2).

The total mitochondrial extract was quantified by using the Bio-Rad DC™ protein assay kit and 7 μg per well was loaded in the 24-well Seahorse plate and centrifuged at 600g for 20 min at 4°C.

The XF Cell Mito Stress Test was performed, after one cycle of basal condition, sequentially injecting 4 mM ADP, 2.5 μg/ml oligomycin, 4 μM FCCP, and 4 μM rotenone plus 4 μM antimycin A.

Basal respiration was measured as the first basal rate minus the nonmitochondrial respiration rate deriving from the rotenone/antimycin injection. State III was calculated as the measurement after the ATP injection minus the nonmitochondrial respiration rate, State IV<sub>0</sub> as the measurement after oligomycin minus the last rate, and State III<sub>u</sub> as the measurement after FCCP injection minus the last rate.

**2.5. Mito-Yellow Fluorescent Protein (YFP) Transfection and Immunofluorescence Staining.** For imaging analysis, 80,000 primary cortical neurons were seeded onto poly-D-lysine-coated glass coverslips in 24-well plates. At 8 days of differentiation, neurons were transfected with pEYFP-Mito (Catalog #6115-1, Clontech) by using Lipofectamine 3000 (Life Technologies, California, USA), according to the manufacturer's instructions.

Fixed neurons were permeabilized in PBS 0.1 M supplemented with 20% methanol and 0.1% Triton X-100, incubated for 1 h at rt in blocking solution (2% Normal Goat Serum (NGS), 3% Bovine Serum Albumin (BSA), and 0.1% Triton-X100 in PBS 0.1 M), and then with the primary antibody (Microtubule-Associated Protein 2 (MAP-2), Merck Millipore, Burlington, Massachusetts, USA) in blocking solution overnight at 4°C. Neurons were washed with 0.1% Triton X-100 PBS 0.1 M and incubated with the fluorochrome-conjugated secondary antibody (goat anti-mouse cy3, Jackson ImmunoResearch, Cambridge, UK) in 0.1% Triton X-100 PBS 0.1 M plus 1 mg/ml BSA for 1 h at rt. After three washes in 0.1% Triton X-100 PBS, cells were mounted onto superfrost slides using a VECTASHIELD mounting medium for fluorescence (Vector Laboratories, Burlingame, CA) and observed by means of a Zeiss confocal laser microscope LSM 880 (Carl Zeiss, Oberkochen, Germany) with Airyscan superresolution and z-stack with the height of the sections

scanning  $\cong 1 \mu\text{m}$ . Images (1024 × 1024 pixels) were then reconstructed using Zen lite 2.3 (Carl Zeiss).

**2.6. Quantification of Mitochondrial Morphology.** The number of mitochondria and the total area of mitochondria per neuron were analyzed by using the macro of ImageJ Software designed by Dagda et al. [19] with minor modification to differentially analyze cell bodies and dendrites. All the z-stack images were processed to maximum intensity projection. The acquisition parameters during confocal imaging were maintained constant for all the image settings used for the analysis.

The interconnectivity between mitochondria was analyzed using the mitochondrial network analysis (MiNA) toolset [20].

**2.7. Real-Time PCR.** Total RNA was extracted from wt and  $\alpha$ -syn null cortical neurons using an RNA extraction kit (RNeasy Mini Kit, Qiagen, Hilden, GE) according to the manufacturer's recommendations. Two micrograms of RNA was retrotranscribed by using a QuantiTect Reverse Transcription Kit (Qiagen) according to the manufacturer's instructions. Real-time PCR was performed by using a SYBR Green Master Mix (Applied Biosystems, Foster City, USA) and the following primer pairs: Mfn1 for ACAAGCTTGCTGTCATTGGG Mfn1 rev TCGACACTCAGGAAGCAGTT; Mfn2 for ATATAGAGGAAGGTCTGGGCCG, Mfn2 rev CCGCATAGATACAGGAAGAAGGG; Opa1 rev GTCATTGTCGGAGCAGGAATC, Opa1 for TTCACTAAGGATTG GCAGACTT; and GAPDH for TCAACAGCAACTCCACTCTT, GAPDH rev CCAGGGTTTCTTACTTACTCCTTGG.

The ViiA7 Real-Time PCR system (Life Technologies, Grand Island, NY, USA) was used for 40 cycles of 95°C for 15 s and 60°C for 1 min. mRNA expression was normalized to glyceraldehyde 3-phosphate dehydrogenase (GAPDH) gene expression.

**2.8. Western Blot Analysis.** Total proteins were extracted with a Radioimmunoprecipitation Assay (RIPA) buffer made up with 50 mM Tris-HCl pH 7.4, 150 mM NaCl, NP-40 1%, sodium deoxycholate 0.1%, sodium dodecyl sulfate (SDS) 0.1%, 1 mM NaF, and 1 mM NaVO<sub>4</sub> plus complete protease inhibitor mixture (Roche Diagnostics, Mannheim, Germany). Protein concentration in the samples was measured by using the Bio-Rad protein assay kit. Equal amounts of proteins (30 μg) were run on 10% polyacrylamide gels and transferred onto polyvinylidene fluoride (PVDF) membrane. Densitometric analysis of the bands was performed by using ImageJ software and all bands were normalized to Tom20 levels as a control of equal loading of samples in the total protein extracts. For densitometry analysis of bands, each experimental condition was performed in quadruplicate and the resulting data were subjected to statistical analysis. The primary antibodies used for western blot analysis were the following: Opa1 (1:1000; Abcam; ab42364), Mfn2 (1:1000; Abnova; H00009927-M03) and Tom20 (1:1000; Santa Cruz; sc-11415). Secondary antibodies used were sheep anti-mouse or donkey anti-rabbit HRP (GE Healthcare, Chicago, USA).



**2.9. Transmission Electron Microscopy Ultrastructural Morphological Analysis.** For ultrastructural morphological analysis, cortical neurons were fixed with Immunofix (BioOptica, Milan, Italy) for 1 hour. After rinsing in 0.1 M cacodylate buffer with 1% tannic acid, samples were postfixed in 1 : 1 2% OsO<sub>4</sub> and 0.2 M cacodylate buffer for 1 h. Samples were rinsed, dehydrated in ethanol and embedded in Epon resin. Ultrathin sections were imaged on a Tecnai-20 electron microscope (Philips-FEI).

**2.10. Analysis of TEM Mitochondria-ER Contacts.** The number of mitochondria-ER contacts has been analysed for ultrastructure in a minimum of 250 contacts per condition. Morphometric measurements were carried out using ImageJ. For calculations of the mitochondria-ER distance,  $n > 5$  mitochondria per image in 60 images per condition were considered and a minimum distance of ER located in a 40 or 10 nm radius from the considered mitochondria was computed.

### 3. Results and Discussion

The aggregation of  $\alpha$ -syn has been repeatedly associated with mitochondrial dysfunctions [16], but the physiological role of  $\alpha$ -syn in mitochondrial function still needs to be elucidated in order to achieve extensive comprehension of  $\alpha$ -syn/mitochondria interplay.

To probe whether  $\alpha$ -syn can physiologically influence mitochondrial function, we examined both mitochondrial respiration and morphology in primary cortical neurons derived from C57BL/6J wt and C57BL6J<sup>OlaHsd</sup>  $\alpha$ -syn null mice.

In particular, mitochondrial respiration of murine primary cortical neurons of wt and  $\alpha$ -syn null mice was analyzed by using the Seahorse XFe24 Extracellular Flux Analyzer measuring the OCR and the ECAR (Figure 1(a)). The ATP synthase inhibitor oligomycin, the mitochondrial oxidative phosphorylation uncoupler FCCP and the Complex I inhibitor rotenone plus the complex III inhibitor antimycin A were sequentially injected to evaluate basal respiration, ATP production and maximal respiration of primary neuronal cells.

Interestingly, we found that  $\alpha$ -syn null neurons exhibited a significant decrease in basal respiration when compared to that of wt control cells. Maximal respiration (i.e., mitochondrial energetic reserve capability) and ATP production were also reduced in the cortical neurons lacking  $\alpha$ -syn (Figure 1(b)). These findings support that the absence of  $\alpha$ -syn compromises the OCR both in basal conditions and in response to FCCP, which, by stimulating the respiratory chain to run at maximum capacity, allows estimating the energetic reserve capability of the cell.

By analyzing OCR, we also found that the  $\alpha$ -syn null neurons, which were subjected to 1 h rotenone pretreatment, exhibited a significant decrease in basal respiration, maximal respiration and ATP production after the 24 h washout, when compared to untreated  $\alpha$ -syn null neurons. This finding is in line with evidence supporting that  $\alpha$ -syn-deficient mice are more sensitive to rotenone and show a more marked

degeneration of dopaminergic neurons upon exposure to this neurotoxin (Dauer et al., PNAS, 2002). Conversely, the OCR profile of wt neurons was not affected by 1 h rotenone pretreatment, supporting that these cells displayed a better resilience within our experimental paradigm. This observation supports that in  $\alpha$ -syn null neurons, the functional activity of mitochondria resulted in more vulnerability to the 1 h Complex I inhibition achieved by rotenone pretreatment.

We examined the ECAR profile, an indirect but reliable index of cellular glycolytic rate [21], in basal conditions and in response to mitochondrial respiratory chain inhibitors in wt and  $\alpha$ -syn null neurons (Figure 1(a)). We found that the absence of  $\alpha$ -syn reduced the basal and oligomycin-stimulated ECAR profile when compared to that of wt neurons, regardless of rotenone pretreatment.

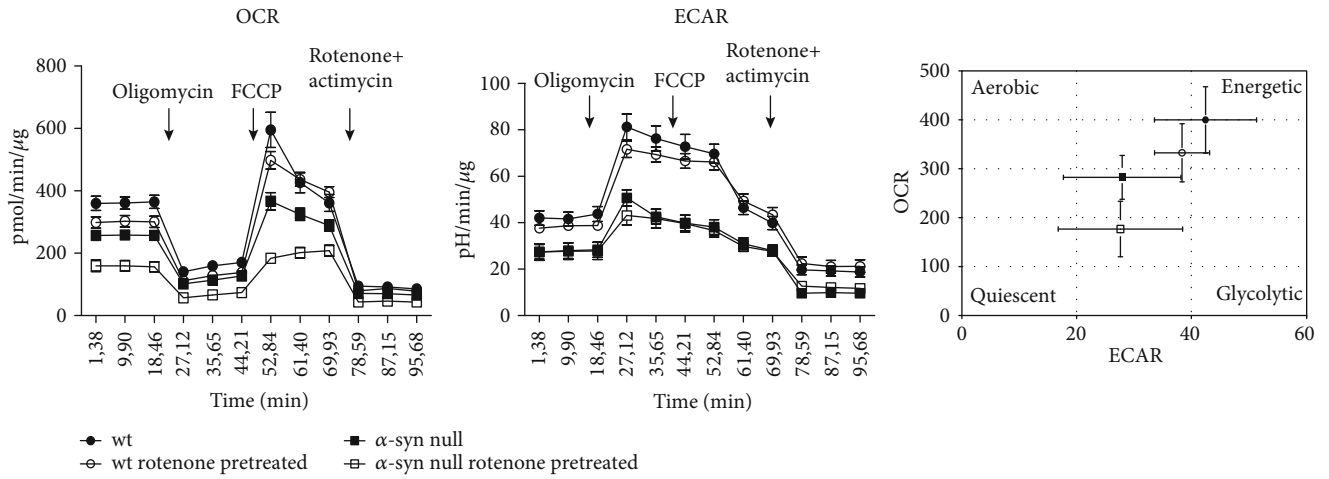
While rotenone is known to inhibit neuronal OCR and enhance ECAR when measured during its infusion [22], we found that 1 h rotenone pretreatment *per se* did not affect ECAR and OCR in wt neuronal cells. This could be explained by the recovery of neuronal bioenergetic capacity during the 24 h washout period. The combined evaluation of the OCR and ECAR parameters in basal conditions, as shown in the energy map (Figure 1(a)), indicated that wt neurons have higher bioenergetics capacity, whereas  $\alpha$ -syn null neurons have a more quiescent metabolic phenotype.

Finally, we analyzed mitochondrial OCR also in mitochondria purified from liver, cortices, and midbrain of adult wt and  $\alpha$ -syn null mice, but we did not detect any difference in respiration or ATP production (Figures 1(c) and 1(d)). This may possibly be ascribed to the fact that  $\alpha$ -syn is enriched in neurons. Therefore,  $\alpha$ -syn absence would not affect mitochondrial respiration in peripheral tissues and its effect may be hardly detectable in brain mitochondrial preparations due to the presence of mitochondria deriving from glial cells, which do not normally express the protein [23–25]. Contrariwise, the expression of  $\alpha$ -syn in neurons is elevated, especially at synaptic sites [26], where mitochondria are also abundant [27]. This supports that  $\alpha$ -syn may affect mitochondrial homeostasis and impinge on respiration exclusively in neuronal cells.

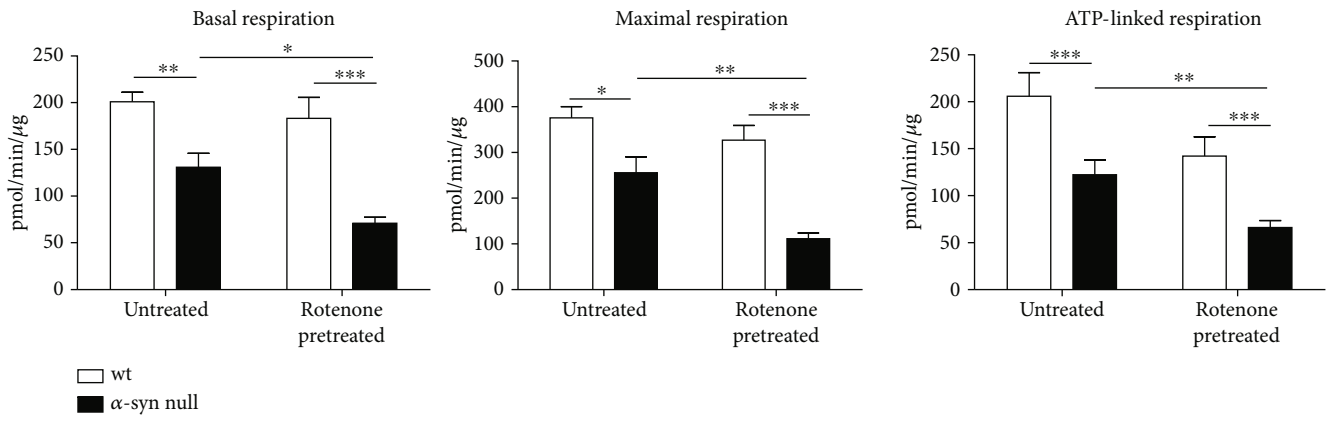
Collectively, these findings support that  $\alpha$ -syn null neurons exhibit a reduced respiration and are also less energetic, thus supporting that  $\alpha$ -syn plays a relevant role in orchestrating mitochondrial functions and energy production.

It has been found that, in the presence of  $\alpha$ -syn aggregates, neurons show fragmented mitochondria [28, 29]. Considering that  $\alpha$ -syn aggregation may mimic a loss of function of the protein [30], we analyzed the morphology of mitochondria in the MAP-2-immunolabelled cortical neurons from wt and  $\alpha$ -syn null mice which had been transfected with mito-YFP construct (Supplementary Figure 1) to discriminate mitochondria within the cell soma and dendrites (Figure 2). These areas were separately examined, as dendrites were acquired by standard confocal microscopy, while cell somas were acquired by Airyscan superresolution microscopy to allow a better visualization of mitochondrial morphology.

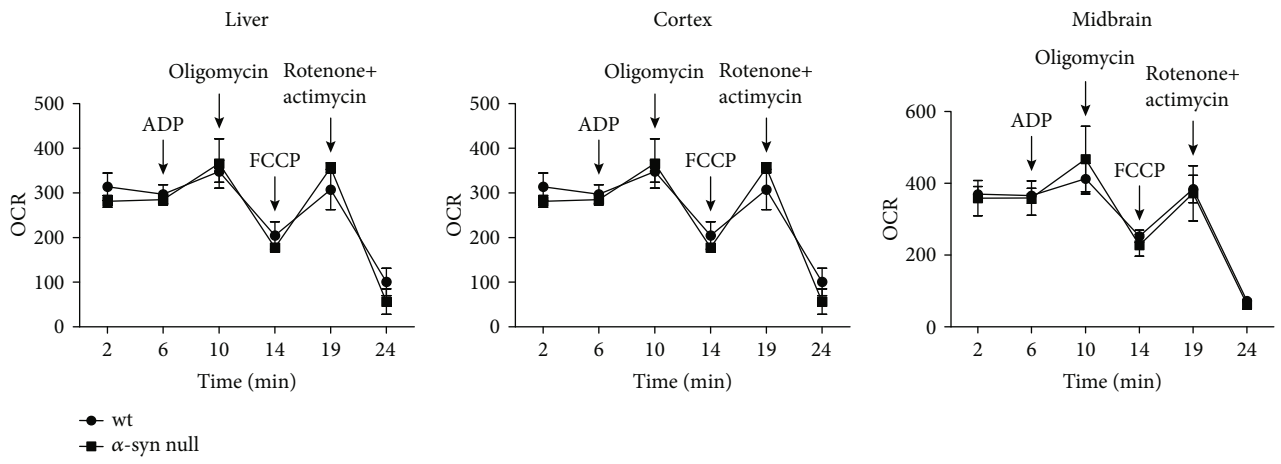
By analyzing the dendrites of  $\alpha$ -syn null neurons, we found a decrease in the number of mitochondria, which also



(a)



(b)



(c)

FIGURE 1: Continued.

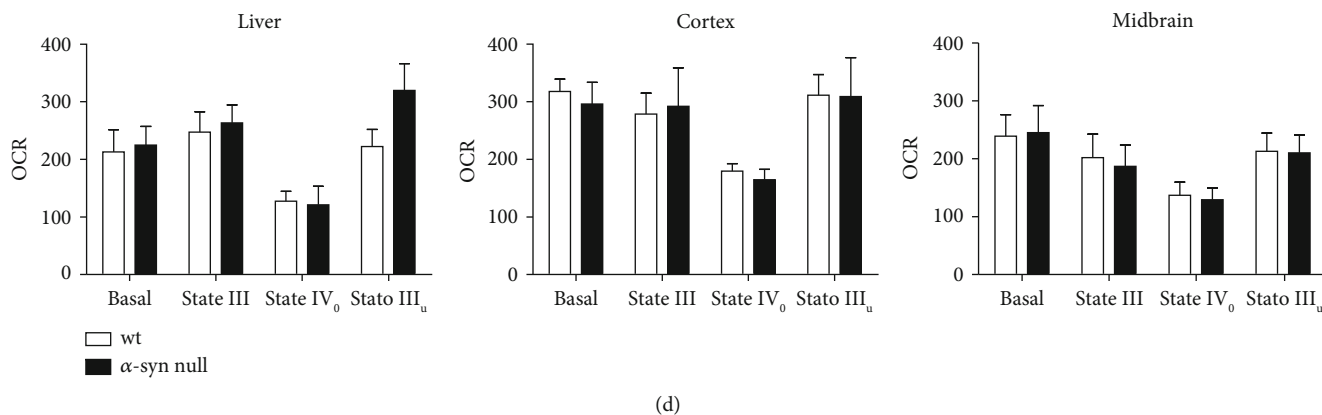


FIGURE 1: Seahorse-based mitochondrial respiration assay on primary cortical neurons or mitochondria purified from wt or  $\alpha$ -syn null mice. (a) The two graphs show time-dependent changes in OCR and ECAR measured sequentially injecting oligomycin, FCCP, and rotenone plus antimycin A on primary cortical neurons of wt and  $\alpha$ -syn null mice in basal conditions or after rotenone exposure. Basal OCR and ECAR values (before oligomycin injection) were plotted in the energy map to illustrate the difference in the cell metabolic profile. (b) Basal respiration (first injection minus the rotenone/antimycin injection), maximal respiration (rate after the FCCP injection minus the nonmitochondrial respiration rate), and ATP production (measurement before oligomycin injection and after the oligomycin injection) showed a decreased respiration of  $\alpha$ -syn null cortical neurons that are significantly affected by rotenone treatment. (c) OCR of mitochondria purified from the liver, cortices, and midbrains was measured sequentially injecting ADP, oligomycin, FCCP, and rotenone plus antimycin A. Note the absence of changes between C57BL/6J wt and C57BL/6J OlaHsd  $\alpha$ -syn null mice. (d) The basal respiration, the State III, the State IV<sub>0</sub>, and the State III<sub>u</sub> did not show differences in the OCR of liver, cortex, and midbrain extracts between wt and  $\alpha$ -syn null mice. \* $P < 0.05$ , \*\* $P < 0.01$ , and \*\*\* $P < 0.001$ , two-way ANOVA+Bonferroni's postcomparison test. Data are presented as mean  $\pm$  standard error of the mean (SEM) ( $n = 12$ ).

exhibited a reduction in the mean area when compared to those of wt neurons (Figure 2(a)). This is in line with previous studies showing increased mitochondrial fragmentation after  $\alpha$ -syn silencing in HeLa cells [31]. Moreover, the number of interconnections between mitochondria, analyzed by using the MiNA toolset, was also significantly decreased in  $\alpha$ -syn null neurons. The reduction of mitochondrial contacts and mitochondrial mean area may be indicative of mitochondrial fission/reduced fusion [32, 33] occurring in the absence of  $\alpha$ -syn.

Interestingly, when we analyzed mitochondria number and morphology in the cell bodies, we found that  $\alpha$ -syn null neurons exhibited an increased number of mitochondria, whose mean area only showed a trend toward size reduction, which however did not show significant results with respect to wt cells (Figure 2(b)). Moreover, the absence of  $\alpha$ -syn did not result in a decrease of mitochondria interconnections in cell bodies. These findings suggest that  $\alpha$ -syn null neurons may present an impairment of mitochondrial transport along processes, which may show mitochondrial fission as a consequence of this process [34, 35].

Mitochondrial fragmentation may be associated with changes in the expression of fusion and fission proteins [35]. While mitochondrial fusion is considered a prosurvival mechanism [36], fission/fragmentation is often an index of mitochondria damage.

We thus analyzed the expression levels of genes involved in mitochondrial shape modifications: Mfn1, Mfn2, Opa1, and Drp1 (Figure 3(a)). In the cortical neurons of  $\alpha$ -syn null mice, we observed decreased levels of Mfn1, which is involved in the fusion of the outer mitochondrial membrane, but no changes in the expression of the fission protein Drp1

or in Opa1 and Mfn2. This finding supports that, by modulating Mfn1 expression,  $\alpha$ -syn may ensure mitochondrial fusion but does not seem to affect proteins controlling the fission, stability, or formation of these organelles. This is in line with evidence indicating that  $\alpha$ -syn aggregation inhibits mitochondrial fusion through a Drp1-independent pathway [37].

The absence of Mfn2 changes was confirmed by western blot analysis (Figure 3(b)), which showed an interesting increase in the ratio between the short and long forms of Opa1, which is crucially involved in control of mitochondrial morphology. This observation supports that the absence of  $\alpha$ -syn can promote mitochondrial fission also by reducing long Opa1, which is relevant for conferring fusion competences [38]. On the other hand, an increased short Opa1 generation can promote fragmentation [39].

Since the presence of wt  $\alpha$ -syn was previously observed in MAM [4] and mitofusins are known to be involved in mediating MERCs [40–42], we also analyzed mitochondria-ER interactions by TEM (Figure 4). Indeed, Mfn2 is known to have a key role in the mitochondria-ER tethering but is also known to form homo- or heterodimerization with Mfn1. By localizing to MAM [4],  $\alpha$ -syn absence could modify Mfn2 localization, thus consequently influencing mitochondria-ER interaction. The results of this part of the study showed a decreased number of MERCs in the  $\alpha$ -syn null neurons when compared to that of wt neurons that still significantly decreased when normalized on the number of mitochondria. In parallel, we observed an increased distance between mitochondria and the ER. MERCs are relevant for ensuring mitochondrial biogenesis, dynamics, and inheritance and  $\text{Ca}^{2+}$  release from ER at MERC controls

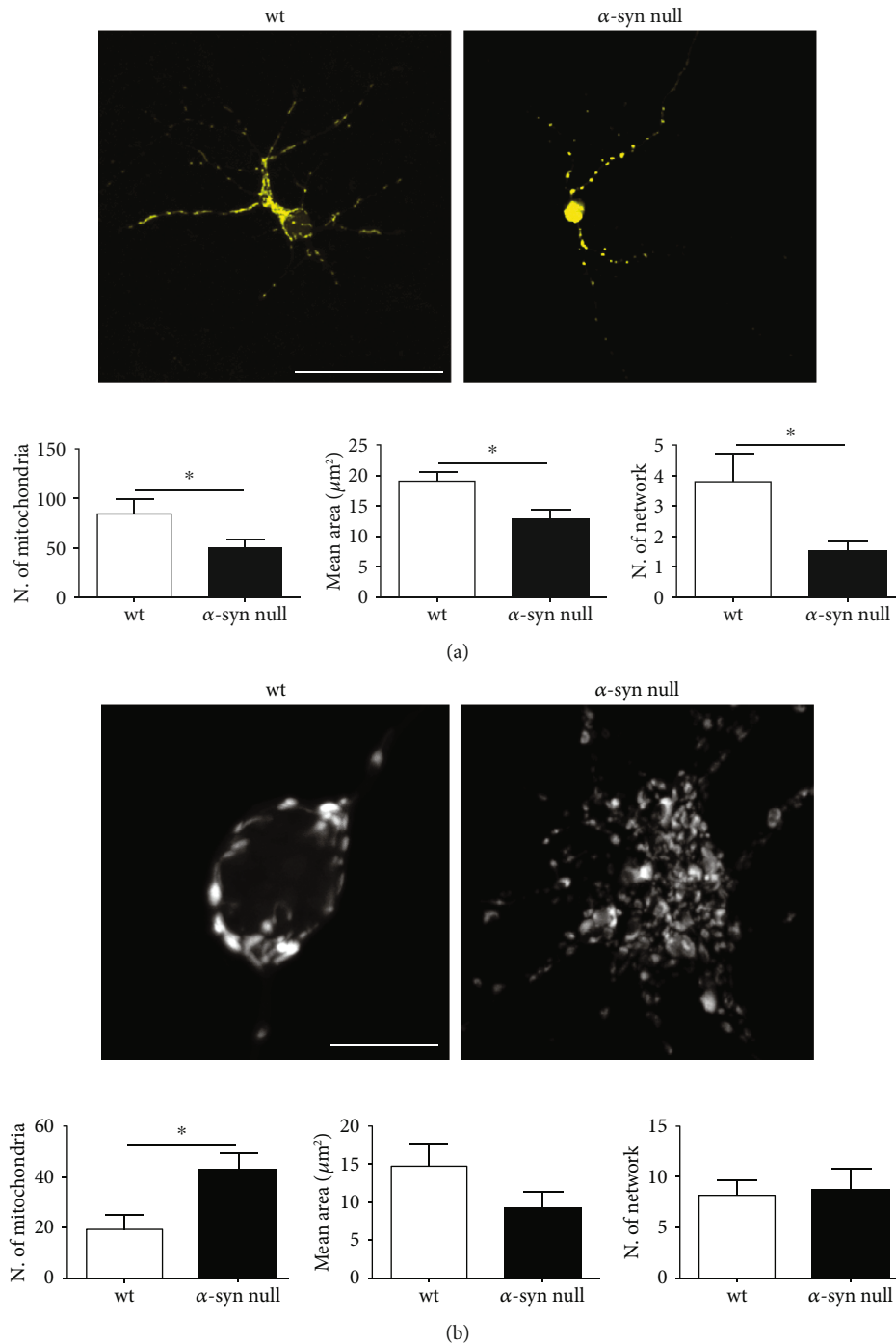


FIGURE 2: Mitochondrial morphology in mito-YFP transfected primary cortical neurons of wt and  $\alpha$ -syn null mice. (a) Representative images of maximum intensity projections of primary cortical neurons from wt and  $\alpha$ -syn null mice transfected with mito-YFP construct at 8 DIV. The morphological analysis showed decreased number of mitochondria exhibiting also reduction in the mean area and in the number of interconnections in those of  $\alpha$ -syn null mice when compared to wt neurons. (b) Maximum intensity projection of Airyscan superresolution microscopy showed an increased number of mitochondria in the cell body of  $\alpha$ -syn null neurons which did not exhibit reductions in the mean area or in their interconnections when compared to those of wt mice. \* $P < 0.05$ , unpaired two-tailed  $t$ -test. Data are presented as mean  $\pm$  SEM ( $n = 30$ ). Scale bar:  $a = 50 \mu\text{m}$  and  $b = 10 \mu\text{m}$ .

mitochondrial function, division, and regulation of apoptosis [43]. Our data confirm and extend previous studies showing alterations in MAM structure due to  $\alpha$ -syn mutations [4] and the disruption of ER-mitochondrial contacts caused by  $\alpha$ -syn overexpression [44], which may coincide

with a loss of  $\alpha$ -syn function. Further research is required to assess whether the reduction of MERCs and increased mitochondria-ER distance observed in the  $\alpha$ -syn null mice might play a causal role in the altered mitochondrial function and dynamics.

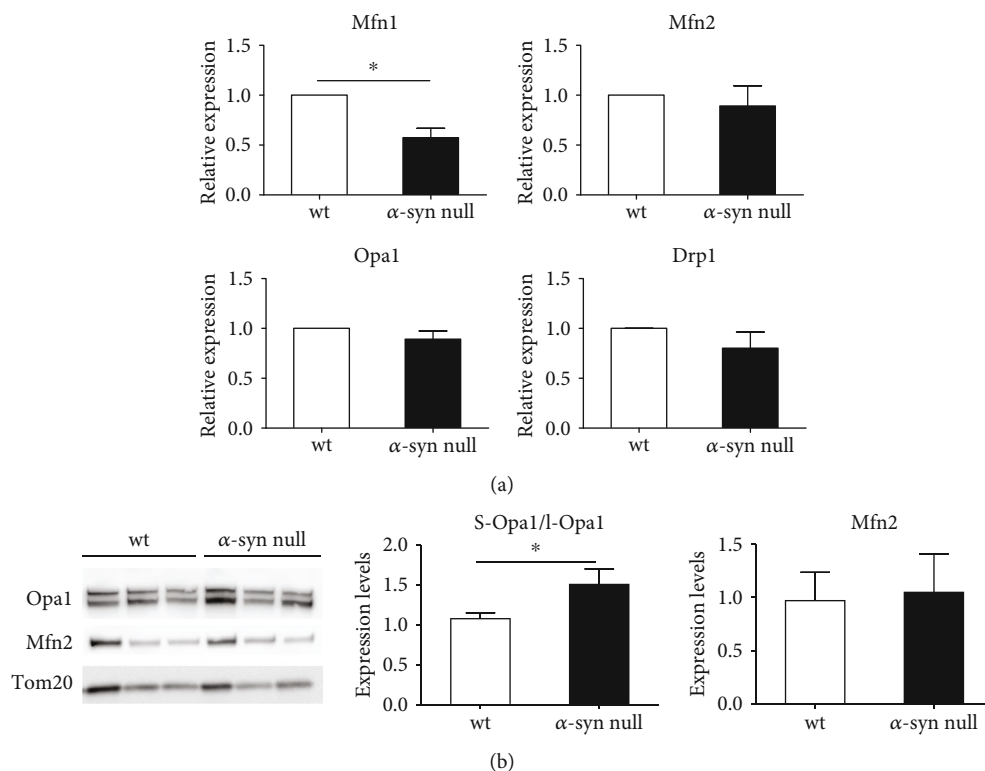


FIGURE 3: Expression levels of mitochondrial proteins involved in shape modification. (a) Relative expression of Mfn1, Mfn2, Opa1, and Drp1 was evaluated by using real-time PCR on primary cortical neuron extracts of wt and  $\alpha$ -syn null mice. Note the statistically significant reduction of Mfn1 in the primary cortical neurons from  $\alpha$ -syn null mice. (b) Western blot analysis revealed increased ratio between the short and long forms of Opa1 in the absence of  $\alpha$ -syn which did not exhibit alterations in the levels of Mfn2. \* $P < 0.05$ , unpaired two-tailed  $t$ -test. Data are presented as mean  $\pm$  SEM ( $n = 8$ ).

#### 4. Conclusions

Collectively, the results of this study support that  $\alpha$ -syn plays a physiological and essential role in the control of mitochondrial respiration capacity and homeostasis.

Alpha-synuclein aggregation and mitochondrial defects are believed to be central in the pathogenesis of neurodegeneration in PD [3, 10, 45, 46]. This is clearly reinforced by the fact that mutations of  $\alpha$ -syn or mitochondria-associated genes can cause the onset of familial early-onset parkinsonism [47, 48]. Interestingly, recent evidence pointed out that  $\alpha$ -syn localizes in and affects MAM function [4, 16, 49] and that the N-terminus of  $\alpha$ -syn, a region exhibiting high affinity for biological membranes [50], can control mitochondrial membrane permeability [51]. Moreover,  $\alpha$ -syn can interact with Complex I modulating its activity [52], while  $\alpha$ -syn overexpression induces mitochondrial fission by interacting with mitochondrial membranes [5]. The  $\alpha$ -syn-mediated control of mitochondrial homeostasis, which is not altered by the A30P variant, is selectively disrupted by the A53T mutation [45]. Consistently, A53T transgenic mice show a marked reduction of the  $\text{Na}^+$ - $\text{Ca}^{2+}$  exchanger 3 (NCX3) accompanied by mitochondrial  $\text{Ca}^{2+}$  overload, events which have been proposed to be central for neurodegeneration of dopaminergic neurons in this mouse line [53]. These studies, strongly supporting a role for  $\alpha$ -syn in mitochondrial homeostasis, fail to provide information on the physiological

role of  $\alpha$ -syn on morpho-functional aspects of mitochondrial biology. In line with the Complex I deficit previously described by Devi and colleagues [52], electron transport chain impairment, with no changes in mitochondrial number, has been demonstrated in mice lacking  $\alpha$ -syn [54]. Nevertheless, a complete characterization of the physiological effects of  $\alpha$ -syn on mitochondrial morphology and activity in pure neuronal preparations have never been investigated before, with the exception of a single study that however failed to detect differences in mitochondrial bioenergetics between wt and  $\alpha$ -syn ko mice [55].

Remarkably, our results are partially in line with those described by Pathak et al. as when we analyzed mitochondria purified by cortical tissues, we also failed to detect functional differences. Differently from their findings on primary hippocampal neurons prepared from  $\alpha$ -syn ko pups, when we analyzed primary cortical neurons from  $\alpha$ -syn null mouse embryos, we found that they exhibited significant reduction in basal and maximal respirations as well as ATP production when compared to those from wt mouse embryos. Moreover,  $\alpha$ -syn null neurons resulted in more vulnerability to rotenone treatment, supporting that the effect of this toxin is influenced by the presence of  $\alpha$ -syn. The functional impairments were accompanied by marked reduction of MERCs as well as by mitochondrial morphology alterations supportive of the occurrence of fragmentations within dendrites and reduction of mitochondria transport. Remarkably, the expression of  $\alpha$ -

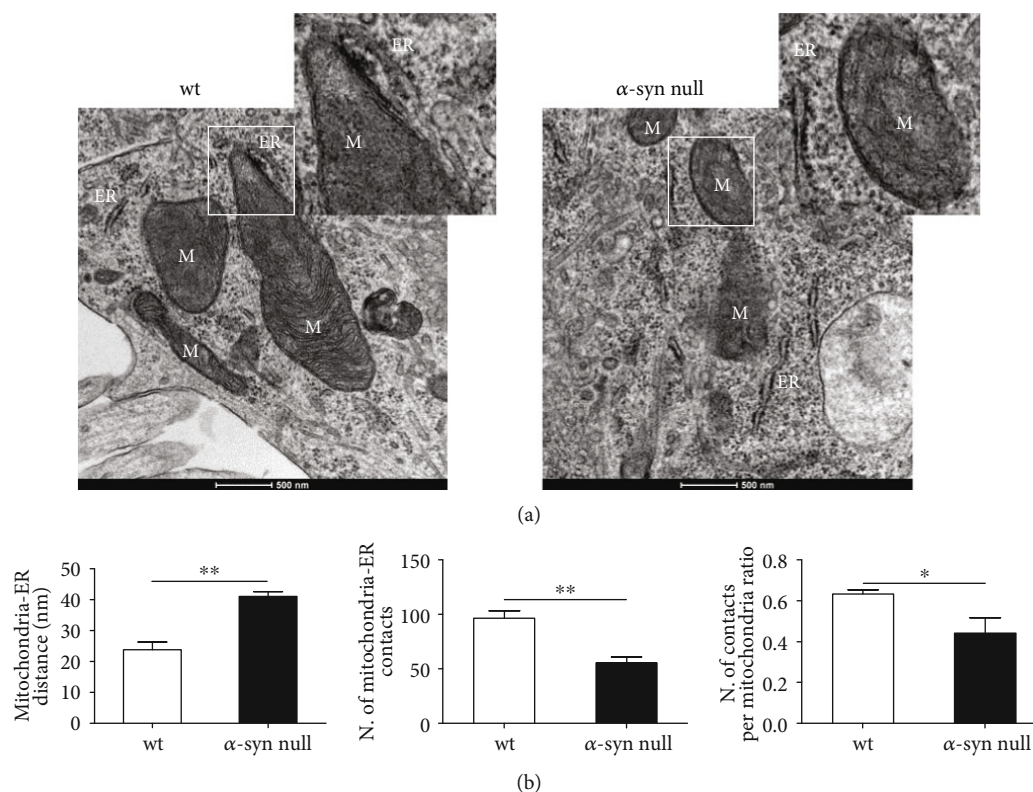


FIGURE 4: TEM-based morphological analysis of mitochondria-ER interaction of primary cortical neurons of wt and  $\alpha$ -syn null mice. (a) Representative images of TEM showing the mitochondria-ER interactions in primary cortical neurons of wt and  $\alpha$ -syn null mice. ER = endoplasmic reticulum; M = mitochondria. Scale bar: 500 nm. (b) The image analysis showed an increased distance between mitochondria and ER, a decreased number of MERCs, and a decreased ratio in the number of contacts per mitochondria in  $\alpha$ -syn null neurons when compared to wt neurons. \* $P < 0.05$  and \*\* $P < 0.01$ , unpaired two-tailed  $t$ -test. Data are presented as mean  $\pm$  SEM ( $n = 5$ ).

syn can vary between diverse brain areas and different neuronal populations [56], thus supporting that the protein may differentially impinge on mitochondrial functions in hippocampal or cortical neurons. Therefore, the discrepancies between our findings and those described by Pathak et al. can be the result of different factors: (a) we analyzed different neuronal subpopulations (whole cortices vs. hippocampi); (b) these were prepared at different time points (embryos vs. pups); and (c) we used different strains and experimental models (C57BL/6J  $\alpha$ -syn null vs. C57BL/6N  $\alpha$ -syn ko mice).

Notably, our results sound in agreement with multiple evidence supporting that  $\alpha$ -syn overexpression and mutations can influence mitochondrial homeostasis and fragmentation as well as ER-mitochondrial interaction [4, 5, 46, 52]. However, the physiological effect  $\alpha$ -syn on mitochondria function, morphology, and interaction with ER had been only partially addressed up to date [4, 5, 37, 57]. Our results support that  $\alpha$ -syn can physiologically affect the mitochondrial functional profile, preserves mitochondrial fusion and transport, and contributes to ensure MERCs in neuronal cells. When considering the central role that  $\alpha$ -syn aggregation plays in PD, these observations support that the absence of the protein in C57BL/6JolaHsd null neurons may mimic the effects derived from  $\alpha$ -syn insoluble inclusion formation, which, by sequestering the protein, may reduce its functional

profile [3, 30, 46]. This process may severely alter mitochondrial and mitochondria/ER dynamics, thus promoting neuronal damage and degeneration.

## Data Availability

The datasets used and/or analyzed during the current study are available from the corresponding author on reasonable request.

## Conflicts of Interest

The authors declare that there is no conflict of interest regarding the publication of this paper.

## Acknowledgments

We are grateful to Fondazione Cariplo (2014-0769 to A.B. and 2016-1006 to A.V.); the University of Brescia (BIOMANE); MIUR (PNR 2015-2020 PerMedNet); and the Michael J. Fox Foundation for Parkinson's Research, NY, USA (Target Advancement Program, grant ID #10742.01). E.B. was supported by a fellowship by Fondazione Umberto Veronesi.

## Supplementary Materials

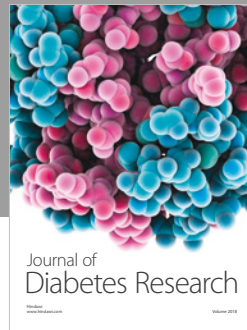
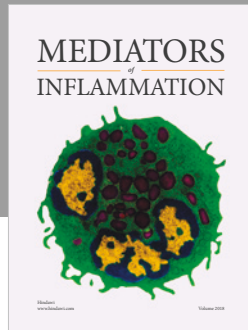
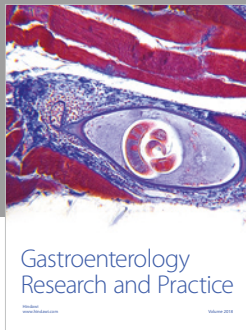
Supplementary Figure 1: representative photomicrographs showing MAP-2-labelled neurons transfected with mito-YFP construct of wt and  $\alpha$ -syn null mice. Scale bar: 20  $\mu$ m. (*Supplementary Materials*)

## References

- [1] M. Goedert, R. Jakes, and M. G. Spillantini, "The synucleinopathies: twenty years on," *Journal of Parkinson's Disease*, vol. 7, no. s1, pp. S51–S69, 2017.
- [2] F. Gao, J. Yang, D. Wang et al., "Mitophagy in Parkinson's disease: pathogenic and therapeutic implications," *Frontiers in Neurology*, vol. 8, p. 527, 2017.
- [3] G. Faustini, F. Bono, A. Valerio, M. Pizzi, P. Spano, and A. Bellucci, "Mitochondria and  $\alpha$ -synuclein: friends or foes in the pathogenesis of Parkinson's disease?," *Genes*, vol. 8, no. 12, p. 377, 2017.
- [4] C. Guardia-Laguarta, E. Area-Gomez, C. Rub et al., " $\alpha$ -synuclein is localized to mitochondria-associated ER membranes," *The Journal of Neuroscience*, vol. 34, no. 1, pp. 249–259, 2014.
- [5] K. Nakamura, V. M. Nemani, F. Azarbal et al., "Direct membrane association drives mitochondrial fission by the Parkinson disease-associated protein  $\alpha$ -synuclein," *Journal of Biological Chemistry*, vol. 286, no. 23, pp. 20710–20726, 2011.
- [6] V. Tapias, X. Hu, K. C. Luk, L. H. Sanders, V. M. Lee, and J. T. Greenamyre, "Synthetic alpha-synuclein fibrils cause mitochondrial impairment and selective dopamine neurodegeneration in part via iNOS-mediated nitric oxide production," *Cellular and Molecular Life Sciences*, vol. 74, no. 15, pp. 2851–2874, 2017.
- [7] X. Wang, K. Becker, N. Levine et al., "Pathogenic alpha-synuclein aggregates preferentially bind to mitochondria and affect cellular respiration," *Acta Neuropathologica Communications*, vol. 7, no. 1, p. 41, 2019.
- [8] J. Lautenschlager and G. S. Kaminski Schierle, "Mitochondrial degradation of amyloidogenic proteins — A new perspective for neurodegenerative diseases," *Progress in Neurobiology*, vol. 181, article 101660, 2019.
- [9] S. Menges, G. Minakaki, P. M. Schaefer et al., "Alpha-synuclein prevents the formation of spherical mitochondria and apoptosis under oxidative stress," *Scientific Reports*, vol. 7, no. 1, article 42942, 2017.
- [10] M. Zaltieri, F. Longhena, M. Pizzi, C. Missale, P. Spano, and A. Bellucci, "Mitochondrial Dysfunction and  $\alpha$ -Synuclein Synaptic Pathology in Parkinson's Disease: Who's on First?," *Parkinson's Disease*, vol. 2015, Article ID 108029, 10 pages, 2015.
- [11] L. K. Song, K. L. Ma, Y. H. Yuan et al., "Targeted overexpression of  $\alpha$ -Synuclein by rAAV2/1 vectors induces progressive nigrostriatal degeneration and increases vulnerability to MPTP in mouse," *PLoS One*, vol. 10, no. 6, article e0131281, 2015.
- [12] I. H. Flones, E. Fernandez-Vizarrá, M. Lykouri et al., "Neuronal complex I deficiency occurs throughout the Parkinson's disease brain, but is not associated with neurodegeneration or mitochondrial DNA damage," *Acta Neuropathologica*, vol. 135, no. 3, pp. 409–425, 2018.
- [13] W. D. Parker Jr., J. K. Parks, and R. H. Swerdlow, "Complex I deficiency in Parkinson's disease frontal cortex," *Brain Research*, vol. 1189, pp. 215–218, 2008.
- [14] W. Dauer, N. Kholodilov, M. Vila et al., "Resistance of  $\alpha$ -synuclein null mice to the parkinsonian neurotoxin MPTP," *Proceedings of the National Academy of Sciences of the United States of America*, vol. 99, no. 22, pp. 14524–14529, 2002.
- [15] A. D. Zharikov, J. R. Cannon, V. Tapias et al., "shRNA targeting  $\alpha$ -synuclein prevents neurodegeneration in a Parkinson's disease model," *The Journal of Clinical Investigation*, vol. 125, no. 7, pp. 2721–2735, 2015.
- [16] C. Guardia-Laguarta, E. Area-Gomez, E. A. Schon, and S. Przedborski, "A new role for  $\alpha$ -synuclein in Parkinson's disease: alteration of ER-mitochondrial communication," *Movement Disorders*, vol. 30, no. 8, pp. 1026–1033, 2015.
- [17] C. G. Specht and R. Schoepfer, "Deletion of the alpha-synuclein locus in a subpopulation of C57BL/6J inbred mice," *BMC Neuroscience*, vol. 2, no. 1, p. 11, 2001.
- [18] L. Navarria, M. Zaltieri, F. Longhena et al., "Alpha-synuclein modulates NR2B-containing NMDA receptors and decreases their levels after rotenone exposure," *Neurochemistry International*, vol. 85-86, pp. 14–23, 2015.
- [19] R. K. Dagda, S. J. Cherra 3rd, S. M. Kulich, A. Tandon, D. Park, and C. T. Chu, "Loss of PINK1 function promotes mitophagy through effects on oxidative stress and mitochondrial fission," *Journal of Biological Chemistry*, vol. 284, no. 20, pp. 13843–13855, 2009.
- [20] A. J. Valente, L. A. Maddalena, E. L. Robb, F. Moradi, and J. A. Stuart, "A simple ImageJ macro tool for analyzing mitochondrial network morphology in mammalian cell culture," *Acta Histochemica*, vol. 119, no. 3, pp. 315–326, 2017.
- [21] J. Zhang, E. Nuebel, D. R. Wisidagama et al., "Measuring energy metabolism in cultured cells, including human pluripotent stem cells and differentiated cells," *Nature Protocols*, vol. 7, no. 6, pp. 1068–1085, 2012.
- [22] S. Giordano, M. Dodson, S. Ravi et al., "Bioenergetic adaptation in response to autophagy regulators during rotenone exposure," *Journal of Neurochemistry*, vol. 131, no. 5, pp. 625–633, 2014.
- [23] D. W. Miller, J. M. Johnson, S. M. Solano, Z. R. Hollingsworth, D. G. Standaert, and A. B. Young, "Absence of  $\alpha$ -synuclein mRNA expression in normal and multiple system atrophy oligodendroglia," *Journal of Neural Transmission*, vol. 112, no. 12, pp. 1613–1624, 2005.
- [24] H. J. Lee, J. E. Suk, E. J. Bae, and S. J. Lee, "Clearance and deposition of extracellular  $\alpha$ -synuclein aggregates in microglia," *Biochemical and Biophysical Research Communications*, vol. 372, no. 3, pp. 423–428, 2008.
- [25] N. Braidy, W. P. Gai, Y. H. Xu et al., "Uptake and mitochondrial dysfunction of alpha-synuclein in human astrocytes, cortical neurons and fibroblasts," *Translational Neurodegeneration*, vol. 2, no. 1, p. 20, 2013.
- [26] A. Bellucci, N. B. Mercuri, A. Venneri et al., "Review: Parkinson's disease: from synaptic loss to connectome dysfunction," *Neuropathology and Applied Neurobiology*, vol. 42, no. 1, pp. 77–94, 2016.
- [27] P. J. Hollenbeck, "Mitochondria and neurotransmission: evacuating the synapse," *Neuron*, vol. 47, no. 3, pp. 331–333, 2005.
- [28] C. Perier and M. Vila, "Mitochondrial biology and Parkinson's disease," *Cold Spring Harbor Perspectives in Medicine*, vol. 2, no. 2, article a009332, 2012.
- [29] J. H. Martinez, F. Fuentes, V. Vanasco et al., "Alpha-synuclein mitochondrial interaction leads to irreversible translocation

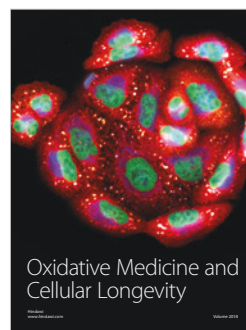
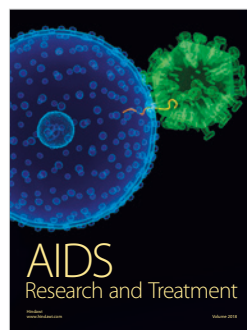
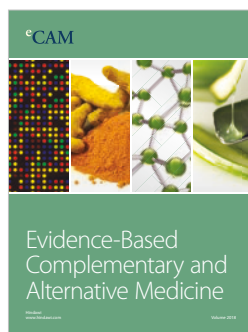
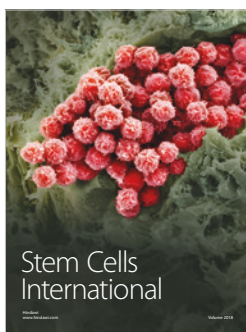
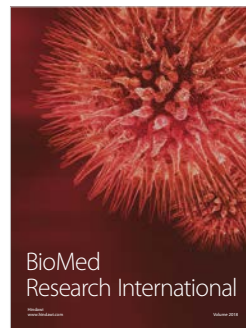
- and complex I impairment,” *Archives of Biochemistry and Biophysics*, vol. 651, pp. 1–12, 2018.
- [30] T. J. Collier, D. E. Redmond Jr., K. Steece-Collier, J. W. Lipton, and F. P. Manfredsson, “Is alpha-synuclein loss-of-function a contributor to Parkinsonian pathology? Evidence from non-human primates,” *Frontiers in Neuroscience*, vol. 10, p. 12, 2016.
- [31] T. Cali, D. Ottolini, A. Negro, and M. Brini, “ $\alpha$ -synuclein controls mitochondrial calcium homeostasis by enhancing endoplasmic reticulum-mitochondria interactions,” *Journal of Biological Chemistry*, vol. 287, no. 22, pp. 17914–17929, 2012.
- [32] S. A. Detmer and D. C. Chan, “Functions and dysfunctions of mitochondrial dynamics,” *Nature Reviews Molecular Cell Biology*, vol. 8, no. 11, pp. 870–879, 2007.
- [33] S. L. Archer, “Mitochondrial dynamics—mitochondrial fission and fusion in human diseases,” *The New England Journal of Medicine*, vol. 369, no. 23, pp. 2236–2251, 2013.
- [34] H. Chen and D. C. Chan, “Mitochondrial dynamics—fusion, fission, movement, and mitophagy—in neurodegenerative diseases,” *Human Molecular Genetics*, vol. 18, no. R2, pp. R169–R176, 2009.
- [35] F. Burte, V. Carelli, P. F. Chinnery, and P. Yu-Wai-Man, “Disturbed mitochondrial dynamics and neurodegenerative disorders,” *Nature Reviews Neurology*, vol. 11, no. 1, pp. 11–24, 2015.
- [36] D. Tondera, S. Grandemange, A. Jourdain et al., “SLP-2 is required for stress-induced mitochondrial hyperfusion,” *The EMBO Journal*, vol. 28, no. 11, pp. 1589–1600, 2009.
- [37] F. Kamp, N. Exner, A. K. Lutz et al., “Inhibition of mitochondrial fusion by  $\alpha$ -synuclein is rescued by PINK1, Parkin and DJ-1,” *The EMBO Journal*, vol. 29, no. 20, pp. 3571–3589, 2010.
- [38] H. Lee, S. B. Smith, and Y. Yoon, “The short variant of the mitochondrial dynamin OPA1 maintains mitochondrial energetics and cristae structure,” *Journal of Biological Chemistry*, vol. 292, no. 17, pp. 7115–7130, 2017.
- [39] T. MacVicar and T. Langer, “OPA1 processing in cell death and disease – the long and short of it,” *Journal of Cell Science*, vol. 129, no. 12, pp. 2297–2306, 2016.
- [40] V. Basso, E. Marchesan, C. Peggion et al., “Regulation of ER-mitochondria contacts by Parkin via Mfn2,” *Pharmacological Research*, vol. 138, pp. 43–56, 2018.
- [41] N. Ilacqua, M. Sanchez-Alvarez, M. Bachmann, V. Costiniti, M. A. Del Pozo, and M. Giacomello, “Protein localization at mitochondria-ER contact sites in basal and stress conditions,” *Frontiers in Cell and Development Biology*, vol. 5, p. 107, 2017.
- [42] W. Wang, Q. Xie, X. Zhou et al., “Mitofusin-2 triggers mitochondria  $\text{Ca}^{2+}$  influx from the endoplasmic reticulum to induce apoptosis in hepatocellular carcinoma cells,” *Cancer Letters*, vol. 358, no. 1, pp. 47–58, 2015.
- [43] A. A. Rowland and G. K. Voeltz, “Endoplasmic reticulum-mitochondria contacts: function of the junction,” *Nature Reviews Molecular Cell Biology*, vol. 13, no. 10, pp. 607–615, 2012.
- [44] S. Paillusson, P. Gomez-Suaga, R. Stoica et al., “ $\alpha$ -synuclein binds to the ER-mitochondria tethering protein VAPB to disrupt  $\text{Ca}^{2+}$  homeostasis and mitochondrial ATP production,” *Acta Neuropathologica*, vol. 134, no. 1, pp. 129–149, 2017.
- [45] V. M. Pozo Devoto, N. Dimopoulos, M. Alloatti et al., “ $\alpha$ Synuclein control of mitochondrial homeostasis in human-derived neurons is disrupted by mutations associated with Parkinson’s disease,” *Scientific Reports*, vol. 7, no. 1, article 5042, 2017.
- [46] M. Vicario, D. Cieri, M. Brini, and T. Cali, “The close encounter between alpha-synuclein and mitochondria,” *Frontiers in Neuroscience*, vol. 12, p. 388, 2018.
- [47] S. Fujioka and Z. K. Wszolek, “Clinical aspects of familial forms of frontotemporal dementia associated with parkinsonism,” *Journal of Molecular Neuroscience*, vol. 45, no. 3, pp. 359–365, 2011.
- [48] A. H. Schapira and P. Jenner, “Etiology and pathogenesis of Parkinson’s disease,” *Movement Disorders*, vol. 26, no. 6, pp. 1049–1055, 2011.
- [49] C. Guardia-Laguarta, E. Area-Gomez, E. A. Schon, and S. Przedborski, “Novel subcellular localization for  $\text{I}\pm$ -synuclein: possible functional consequences,” *Frontiers in Neuroanatomy*, vol. 9, p. 17, 2015.
- [50] A. Bellucci, L. Navarria, M. Zaltieri, C. Missale, and P. Spano, “Alpha-synuclein synaptic pathology and its implications in the development of novel therapeutic approaches to cure Parkinson’s disease,” *Brain Research*, vol. 1432, pp. 95–113, 2012.
- [51] J. Shen, T. Du, X. Wang et al., “ $\alpha$ -synuclein amino terminus regulates mitochondrial membrane permeability,” *Brain Research*, vol. 1591, pp. 14–26, 2014.
- [52] L. Devi, V. Raghavendran, B. M. Prabhu, N. G. Avadhani, and H. K. Anandatheerthavarada, “Mitochondrial import and accumulation of alpha-synuclein impair complex I in human dopaminergic neuronal cultures and Parkinson disease brain,” *Journal of Biological Chemistry*, vol. 283, no. 14, pp. 9089–9100, 2008.
- [53] R. Sirabella, M. J. Sisalli, G. Costa et al., “NCX1 and NCX3 as potential factors contributing to neurodegeneration and neuroinflammation in the A53T transgenic mouse model of Parkinson’s Disease,” *Cell Death & Disease*, vol. 9, no. 7, p. 725, 2018.
- [54] C. E. Ellis, E. J. Murphy, D. C. Mitchell et al., “Mitochondrial lipid abnormality and electron transport chain impairment in mice lacking alpha-synuclein,” *Molecular and Cellular Biology*, vol. 25, no. 22, pp. 10190–10201, 2005.
- [55] D. Pathak, A. Berthet, J. T. Bendor et al., “NCX1 and NCX3 as potential factors contributing to neurodegeneration and neuroinflammation in the A53T transgenic mouse model of Parkinson’s Disease,” *Cell Death & Disease*, vol. 9, no. 7, article 725, 2017.
- [56] K. Taguchi, Y. Watanabe, A. Tsujimura, and M. Tanaka, “Brain region-dependent differential expression of alpha-synuclein,” *Journal of Comparative Neurology*, vol. 524, no. 6, pp. 1236–1258, 2016.
- [57] Y. X. Gui, X. Y. Wang, W. Y. Kang et al., “Extracellular signal-regulated kinase is involved in alpha-synuclein-induced mitochondrial dynamic disorders by regulating dynamin-like protein 1,” *Neurobiology of Aging*, vol. 33, no. 12, pp. 2841–2854, 2012.





**Hindawi**

Submit your manuscripts at  
[www.hindawi.com](http://www.hindawi.com)



## Mitochondrial quality control beyond PINK1/Parkin

Sophia von Stockum, Elena Marchesan and Elena Ziviani

Neurons strictly rely on proper mitochondrial function and turnover. They possess a high energy requirement which is mostly fueled by mitochondrial oxidative phosphorylation. Moreover the unique morphology of neurons implies that mitochondria need to be transported along the axons to sites of high energy demand. Finally, due to the non-dividing state of neurons, cellular mitosis cannot dilute dysfunctional mitochondria, which can produce harmful by-products such as reactive oxygen species (ROS) and thus a functioning mechanism of quality control (QC) is essential. The critical impact of mitochondria on neuronal function and viability explains their involvement in several neurodegenerative diseases such as Parkinson's disease (PD) [1].

Mitophagy, a selective form of autophagy, is employed by cells to degrade dysfunctional mitochondria in order to maintain a healthy mitochondrial network, a process also called mitochondrial QC. In order for mitophagy to take place it essentially requires molecules that on the one hand sense the dysfunctional mitochondria and on the other hand tag the latter for autophagic degradation. Most studies on mitophagy are focused on a canonical pathway including the PD-related proteins PINK1 and Parkin. PINK1 is a kinase that recruits the

E3 ubiquitin ligase Parkin to depolarized mitochondria, where it ubiquitinates several target proteins on the outer mitochondrial membrane (OMM) leading to their proteasomal degradation and serving as a signal to recruit the autophagic machinery [1] (Figure 1, upper left corner). A large number of studies on PINK1/Parkin mitophagy are based on treatment of cell lines with the uncoupler CCCP collapsing the mitochondrial membrane potential ( $\Delta\Psi_m$ ), as well as overexpression of Parkin, conditions that are far from physiological [1]. Furthermore, Parkin translocation to mitochondria in neuronal cells occurs only under certain stimuli and is much slower, possibly due to their metabolic state and low endogenous Parkin expression [2]. Thus, in recent years several studies have highlighted pathways of mitophagy induction that are independent of PINK1 and/or Parkin and could act in parallel or addition to the latter. We want to discuss what is known about these QC mechanisms and hypothesize on their role in neuronal physiology and neurodegeneration.

Alternative mitophagy pathways can basically branch into or parallel the PINK1/Parkin pathway at any point ranging from Parkin translocation to autophagosome formation. However, most studies are focused on two steps: ubiquitination of OMM proteins by E3 ubiquitin ligases

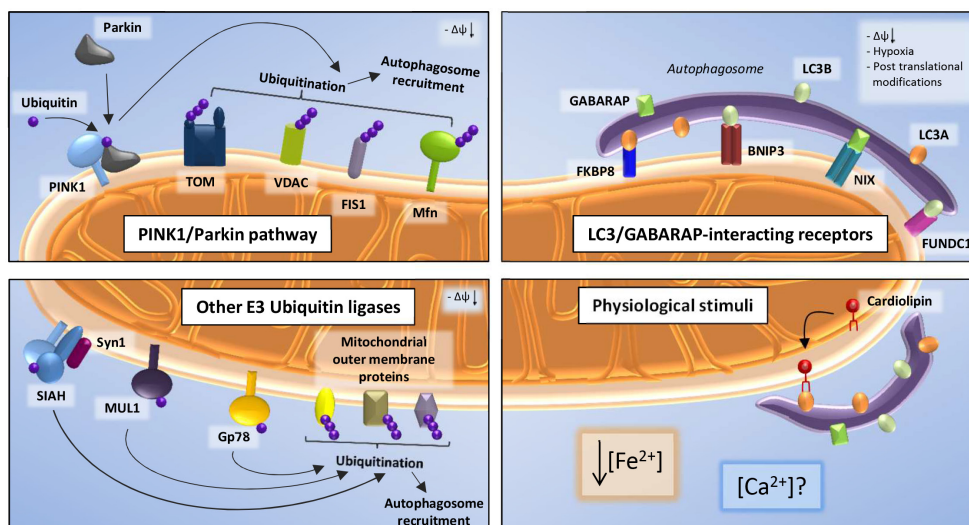


**Figure 1: Upon loss of transmembrane potential, the kinase PINK1 accumulates on the OMM and recruits the E3 ubiquitin ligase Parkin.** Parkin-mediated ubiquitination on several mitochondrial proteins leads to the clearance of dysfunctional mitochondria (upper left). Following additional conditions (i.e. hypoxia, post translational modification), LC3-II and GABARAP, components of the autophagosomal membrane, can interact with OMM mitophagy receptors such as FKBP8, BNIP3, NIX and FUNDC1, thus inducing mitophagy (upper right). Mitochondrial recruitment of LC3 can also be mediated by Cardiolipin; moreover, calcium ( $[Ca^{2+}]$ ) and iron ( $[Fe^{2+}]$ ) levels could play a role in PINK1/Parkin-independent mitophagy (lower right). Finally, E3 Ubiquitin ligases other than Parkin, such as Gp78, MUL1 and SIAH1 contribute to ubiquitination of OMM target proteins (lower left).

other than Parkin, or involvement of OMM mitophagy receptors that target mitochondria to autophagosomes independently of Parkin-induced ubiquitination. These receptors directly interact with LC3-II and GABARAP, components of the autophagosomal membrane, through a specific binding motif, the LC3-interacting region (LIR). A few examples of these receptors are FKBP8, a member of the FK506-binding protein family, recruiting LC3A to damaged mitochondria in response to depolarization [3], BNIP3 and NIX, pro-apoptotic members of the Bcl2-family, and FUNDC1 which target mitochondria to autophagosomes interacting directly with LC3B and GABARAP in response to hypoxia or phosphorylation of the receptor itself [4] (Figure, upper right corner). Another non-protein molecule that can directly interact with LC3-II is the inner mitochondrial membrane (IMM) phospholipid Cardiolipin (CL), which contains a LIR motif. When CL is externalized from the IMM to the OMM in response to depolarization, it can recruit LC3, thus inducing mitophagy [5] (Figure, lower right corner).

Additionally, E3 Ubiquitin ligases other than Parkin, such as Gp78, MUL1 and SIAH1 have been reported to contribute to ubiquitination of OMM target proteins such as the mitochondrial fusion protein Mitofusin (Mfn). Gp78 ubiquitinates Mfn1 and Mfn2 inducing their proteasomal degradation, thereby regulating mitochondrial dynamics, mobility and mitophagy [6]. MUL1 was also shown to ubiquitinate Mfn in *Drosophila* and to regulate mitophagy [4]. SIAH1 acts in a complex together with PINK1 and synphilin-1 that promotes mitophagy in the absence of Parkin. PINK1 can recruit synphilin-1 to the mitochondria, which in turn recruits SIAH1, subsequently ubiquitinating mitochondrial proteins, leading to LC3 recruitment (Figure, lower left corner). Interestingly, PINK1 PD-related mutants do not form this complex pointing at a possible involvement of this pathway in the disease [7].

How these different mitophagy pathways are regulated and differentially activated under physiological conditions and which role they play in neuronal function and neurodegeneration still needs investigation. Several studies have convincingly shown that elimination of dysfunctional mitochondria is taking place in brains and neurons as measured e.g. by co-localization of mitochondria with autophagosomes or by measurement of mitochondrial mass in the presence of lysosomal inhibitors [2]. As mentioned above, PINK1 and Parkin certainly play a role in this but might not be the only actors. It is still unclear which physiological stimuli trigger mitophagy induction *in vivo*. Recently, an iron chelator was identified as an inducer of PINK1/Parkin-independent mitophagy without collapsing  $\Delta\Psi_m$  [8] hinting to iron depletion as a novel physiological stimulus, although the proper mechanism needs investigation. This could be particularly relevant in PD and other neurodegenerative diseases,

since impaired iron metabolism through its link to ROS production and iron-sulfur cluster biosynthesis was associated with neuronal pathology [8]. CL externalization has been shown to induce mitophagy in primary cortical neurons and in response to PD-inducing toxins [5], hinting to the importance of this pathway in neuronal life and death. It is tempting to speculate that also  $Ca^{2+}$  signals that play a crucial role in neuronal function and survival might be a physiological mitophagy inducer, as e.g. FKBP8 contains a  $Ca^{2+}$ /Calmodulin binding domain and its PPIase activity is sensitive to  $Ca^{2+}$  [3]. It is very probable that different mitophagy pathways amplify the regulatory potential of neurons to act to different physiological stimuli and cell type-specific requirements and that alterations in any of these pathways may result in neurodegeneration.

**Elena Ziviani:** Department of Biology, University of Padova, Padova, Italy; Istituto IRCCS San Camillo, Lido di Venezia, Venezia, Italy

**Correspondence to:** Elena Ziviani, **email** elena.ziviani@unipd.it

**Keywords:** mitochondria; mitophagy pathways; quality control; neurodegeneration; neuroscience

**Received:** December 20, 2017

**Published:** January 02, 2018

## REFERENCES

1. von Stockum S, et al. *Neurobiol Dis.* 2016; 90:58-67.
2. Cummins N, et al. *Cell Mol Life Sci.* 2017 Oct 30. <https://dx.doi.org/10.1007/s00018-017-2692-9>. [Epub ahead of print]
3. Bhujabal Z, et al. *EMBO Rep.* 2017; 18:947-961.
4. Georgakopoulos ND, et al. *Nat Chem Biol.* 2017; 13:136-146.
5. Chu CT, et al. *Nat Chem Biol.* 2013; 15:1197-1205.
6. Fu M, et al. *Mol Biol Cell.* 2013; 24:1153-62.
7. Szargel R, et al. *Hum Mol Genet.* 2016; 25:3476-3490.
8. Allen GF, et al. *EMBO Rep.* 2013; 14:1127-35.

**Copyright:** von Stockum et al. This is an open-access article distributed under the terms of the Creative Commons Attribution License 3.0 (CC BY 3.0), which permits unrestricted use, distribution, and reproduction in any medium, provided the original author and source are credited.